GROUND MOTIONS DUE TO LARGE MAGNITUDE SUBDUCTION ZONE EARTHQUAKES

WA-RD 450.1

Research Report
December 1998

Washington State Department of Transportation

Washington State Transportation Commission
Planning and Programming Service Center
in cooperation with the U.S. Department of Transportation
Federal Highway Administration

Research Report
Research Project T9903, Task 67
Ground Motion Subzone

GROUND MOTIONS DUE TO LARGE MAGNITUDE SUBDUCTION ZONE EARTHQUAKES

by

Steven L. Kramer
John R. Kiely Professor of Civil Engineering
Department of Civil Engineering
University of Washington

Walter J. Silva
Senior Seismologist
Pacific Engineering & Analysis

David A. Baska
Research Assistant
Department of Civil Engineering
University of Washington

Washington State Transportation Center (TRAC)
University of Washington, Box 354802
University District Building
1107 NE 45th Street, Suite 535
Seattle, Washington 98105-4631

Washington State Department of Transportation
Technical Monitor
Tony Allen
State Geotechnical Engineer

Prepared for

Washington State Transportation Commission
Department of Transportation
and in cooperation with
U.S. Department of Transportation
Federal Highway Administration

December 1998

TECHNICAL REPORT STANDARD TITLE PAGE

1. REPORT NO.	2. GOVERNMENT ACCESSION NO.	3. RECIPIENT'S CATALOG NO.
WA-RD 450.1		

4. TITLE AND SUBTITLE	5. REPORT DATE
GROUND MOTIONS DUE TO LARGE MAGNITUDE SUBDUCTION ZONE EARTHQUAKES	December 1998
	6. PERFORMING ORGANIZATION CODE
7. AUTHOR(S)	8. PERFORMING ORGANIZATION REPORT NO.
Steven L. Kramer, Walter J. Silva, David A. Baska	
9. PERFORMING ORGANIZATION NAME AND ADDRESS	10. WORK UNIT NO.
Washington State Transportation Center (TRAC) University of Washington, Box 354802 University District Building; 1107 NE 45th Street, Suite 535 Seattle, Washington 98105-4631	11. CONTRACT OR GRANT NO. T9903, Task 65
12. SPONSORING AGENCY NAME AND ADDRESS	13. TYPE OF REPORT AND PERIOD COVERED
Washington State Department of Transportation Transportation Building, MS 7370 Olympia, Washington 98504-7370	Research report
	14. SPONSORING AGENCY CODE

15. SUPPLEMENTARY NOTES

This study was conducted in cooperation with the U.S. Department of Transportation, Federal Highway Administration.

16. ABSTRACT

The notion that the Cascadia subduction zone (CSZ) has produced very large earthquakes in the past, and that it can be expected to produce very large earthquakes again, is now widely accepted in the seismological and engineering communities. Because no records of ground shaking or damage exist for historical CSZ earthquakes, it is difficult to evaluate their potential effects on bridges, buildings, embankments, and other structures. However, recent advances in engineering seismology now allow the numerical simulation of earthquakes, including fault rupture, the propagation of seismic waves from the fault to the site of interest, and amplification of the resulting rock motions by shallow soil and rock layers beneath the site.

Rock outcrop motions were simulated for three CSZ earthquake scenarios: magnitude 8.0, 8.5, and 9.0 earthquakes. The magnitude 8.0 earthquake was assumed to result from rupture of the portion of the CSZ adjacent to the northern part of the state; the larger magnitude earthquakes were associated with rupture on a portion of the CSZ extending along the entire length of the state. Thirty different simulations of each earthquake scenario were analyzed. For each, rock outcrop motions were computed at each of 13 locations within Washington state. Site response analyses were then performed for 15 soil profiles at the 13 locations.

The rock outcrop motions showed amplitudes, frequency contents, and durations that were significantly different than the ground motions that civil structures are commonly designed for in Washington state. Peak accelerations and spectral acceleration at T=0.3 sec were all considerably lower than the values on which most current design procedures are based. Spectral accelerations for T=1.0 sec were less than those on which current design procedures are based for M_W=8.0 earthquakes, but they were comparable for M_W=9.0 earthquakes and, at some sites, for M_W=8.5 earthquakes. CSZ ground motions have strong long-period (low frequency) components and thus should be more damaging to structures with long natural periods. Finally, the durations of CSZ ground motions are much longer than those of the motions on which current design procedures are based. This aspect of CSZ motions may be quite significant for reinforced concrete structures and potentially liquefiable soil deposits in which the accumulation of damage depends on the number of load or stress reversals that occur during earthquake shaking.

17. KEY WORDS	18. DISTRIBUTION STATEMENT
earthquake, response spectra, Cascadia subduction zone, Green's function, seismic design	No restrictions. This document is available to the public through the National Technical Information Service, Springfield, VA 22616

19. SECURITY CLASSIF. (of this report)	20. SECURITY CLASSIF. (of this page)	21. NO. OF PAGES	22. PRICE
None	None	182	

DISCLAIMER

The contents of this report reflect the views of the authors, who are responsible for the facts and the accuracy of the data presented herein. The contents do not necessarily reflect the official views or policies of the Washington State Transportation Commission, Department of Transportation, or the Federal Highway Administration. This report does not constitute a standard, specification, or regulation.

TABLE OF CONTENTS

LIST OF FIGURES

LIST OF TABLES

EXECUTIVE SUMMARY

The notion that the Cascadia subduction zone (CSZ) has produced very large earthquakes in the past, and that it can be expected to produce very large earthquakes again, is now widely accepted in the seismological and engineering communities. There remains, however, considerable uncertainty about the potential magnitude, location, and effects of future CSZ earthquakes. Seismologists and earthquake engineers currently believe that earthquakes of a magnitude of up to 8.5 or 9.0 could occur on the CSZ.

Because no records of ground shaking or damage exist for historical CSZ earthquakes, it is difficult to evaluate their potential effects on bridges, buildings, embankments, and other structures. However, recent advances in engineering seismology now allow the numerical simulation of earthquakes, including fault rupture, the propagation of seismic waves from the fault to the site of interest, and amplification of the resulting rock motions by shallow soil and rock layers beneath the site. This research project was intended to use state-of-the-art numerical procedures to simulate potential Cascadia subduction zone earthquakes and to evaluate their potential effects on civil structures.

Rock outcrop motions were simulated for three CSZ earthquake scenarios: a magnitude 8.0 earthquake, a magnitude 8.5 earthquake, and a magnitude 9.0 earthquake. The magnitude 8.0 earthquake was assumed to result from rupture of the portion of the CSZ adjacent to the northern part of the state; the larger magnitude earthquakes were associated with rupture on a portion of the CSZ extending along the entire length of the state. Thirty different simulations of each earthquake scenario, representing different earthquake nucleation points, rupture patterns, and other variables, were analyzed. For each, rock outcrop motions were computed at each of 13 locations within Washington state. Site response analyses were then performed for 15 soil profiles at the 13 locations.

The rock outcrop motions showed amplitudes, frequency contents, and durations that were significantly different than the ground motions that civil structures are com-

monly designed for in Washington state. The amplitudes of the computed peak rock outcrop motions varied with magnitude and distance from the CSZ; amplitudes were higher for the larger magnitude earthquakes and also higher near the Pacific coast than farther inland. Peak accelerations and spectral acceleration at T=0.3 sec, however, were all considerably lower than the values on which most current design procedures are based. Spectral accelerations for T=1.0 sec were less than those on which current design procedures are based for M_w=8.0 earthquakes, but they were comparable for M_w=9.0 earthquakes and, at some sites, for M_w=8.5 earthquakes. The observations regarding spectral accelerations reflect the significant differences between frequency contents of CSZ ground motions and the motions on which current design procedures are based: CSZ ground motions have considerably stronger long-period (low frequency) components and thus should be expected to be more damaging to structures with long natural periods. Finally, the durations of CSZ ground motions are much longer than those of the motions on which current design procedures are based. This aspect of CSZ motions may be quite significant for reinforced concrete structures and potentially liquefiable soil deposits in which the accumulation of damage depends on the number of load or stress reversals that occur during earthquake shaking.

INTRODUCTION AND RESEARCH APPROACH

The research described in this report was meant to evaluate the potential effects of great subduction earthquakes on transportation structures in western Washington state. The results of the research will allow WSDOT to identify structures that may be particularly susceptible to the effects of subduction earthquakes and to evaluate the potential for damage to structures that were not designed with consideration of subduction earthquakes.

THE PROBLEM

The notion that the Cascadia subduction zone has produced very large earthquakes in the past, and that it can be expected to produce very large earthquakes again, is now widely accepted in the seismological and engineering communities. There remains, however, considerable uncertainty about the potential magnitude, location, and effects of future Cascadia subduction zone earthquakes.

Earthquake damage to bridges and other transportation facilities depends on the nature of the ground motions they are subjected to. At a particular site, earthquake ground motions are influenced by the source mechanism of the earthquake, the travel path between the source and the site, and the local soil/rock conditions at the site. Engineers charged with designing new structures and evaluating the seismic vulnerability of existing structures need to know the anticipated ground motion characteristics of earthquakes produced by all potentially damaging seismic sources. Before this research project, estimates of ground motions from great subduction zone earthquakes that explicitly considered source, travel path, and local site effects in Washington state were not available. As a result, reliable evaluations of the engineering implications of great subduction earthquakes were not possible. This situation led to great difficulty in considering subduction earthquake potential in the earthquake-resistant design of transportation structures and facilities.

RESEARCH OBJECTIVES

This research project was intended to investigate the nature of strong ground motion produced by great subduction earthquakes in the Cascadia subduction zone. Specifically, the main objectives of the research were as follows:

1. Use recently developed, state-of-the-art analytical tools to model great Cascadia subduction zone earthquakes of three different magnitudes.

2. Use equivalent linear and nonlinear ground response analyses to evaluate the resulting ground surface motions for 13 sites with 15 different soil profiles distributed throughout Washington state.

3. Evaluate the potential effects of great subduction zone earthquakes on the seismic design of new structures and on the seismic vulnerability of older structures that were not designed with consideration of subduction earthquakes.

Realization of these objectives was meant to improve ground motion estimates for use in the design of new structures and the evaluation of existing structures in Washington state, and reduce uncertainty over the possible effects of subduction zone earthquakes.

BACKGROUND

The Cascadia subduction zone extends from the southern part of British Columbia to the northern part of California just off the coast of the North American continent, as illustrated in Figure 1. The Cascadia subduction zone involves the Juan de Fuca plate system—which includes the Gorda, Explorer, and Juan de Fuca plates—and the North American plate. The Cascadia subduction zone is approximately 1,000 km long, with a locked zone width of 90 km (Hyndman and Wang, 1995). The Juan de Fuca plate is subducting beneath the North American plate as it moves in a generally north-east direction. The Cascadia subduction zone trench, which forms the western border of the continental margin, lies at the boundary between the Juan de Fuca and North American plates. From this boundary, the subducting portion of the Juan de Fuca plate dips at an angle of 10° to 20° as far east as the Puget Sound Basin and at an angle of 15° to 20° under southwestern Washington (McCrumb et al., 1989). Beneath the Cascade Range,

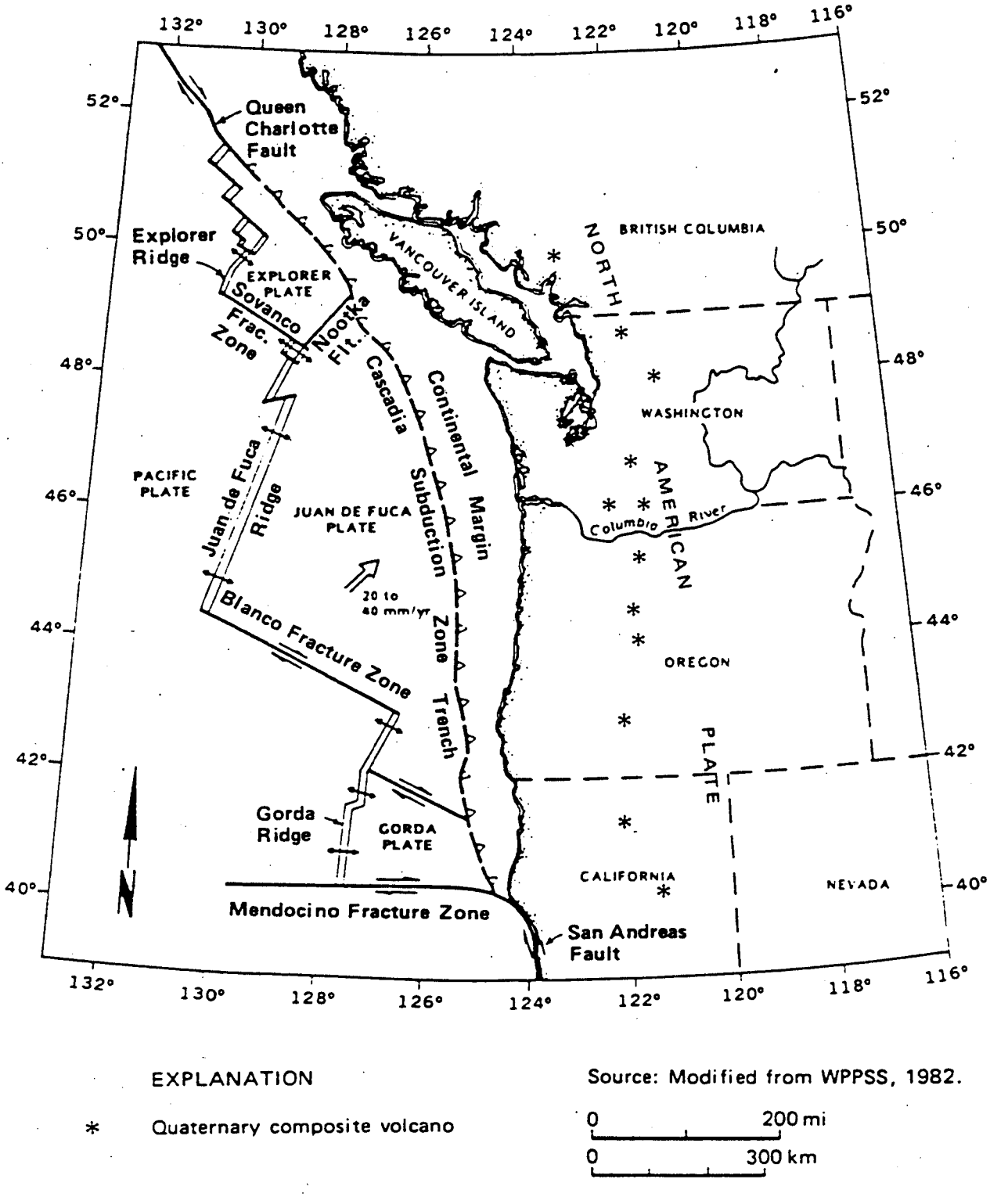

Figure 1. Tectonic plates of the Pacific Northwest and the Cascadia subduction zone (after McCrumb et al., 1989)

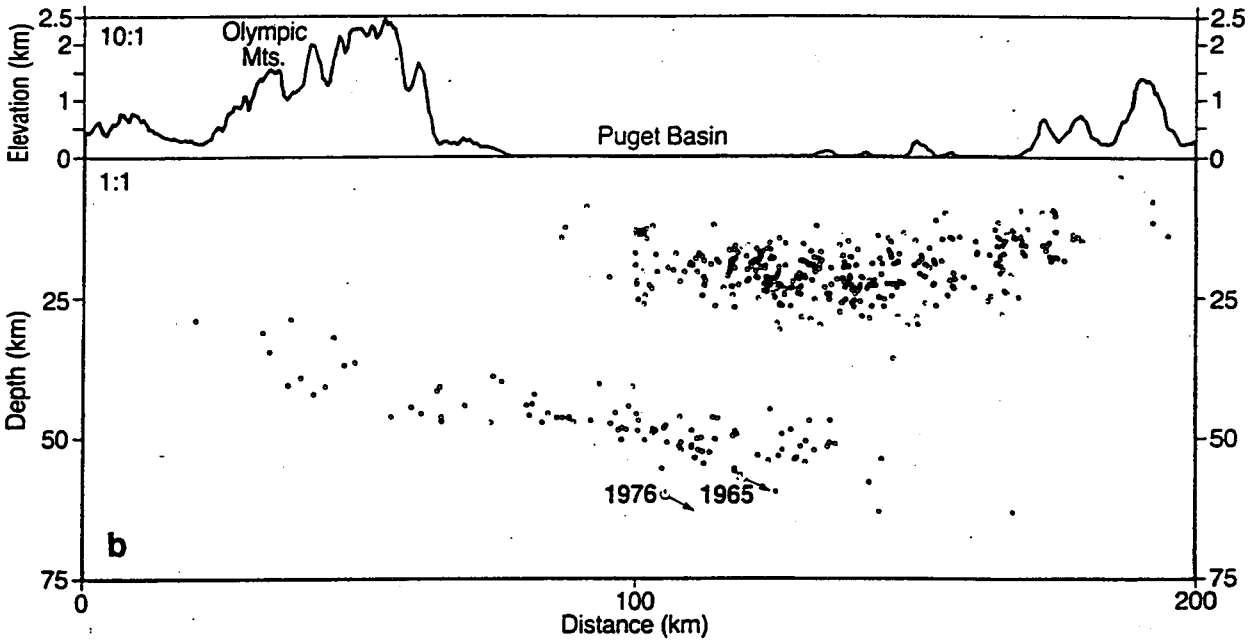

Figure 2. Typical cross-section through northwest Washington state showing hypocenters of earthquakes since 1970. Shallow and deep zones of seismicity are clearly apparent (after Ludwin et al., 1991).

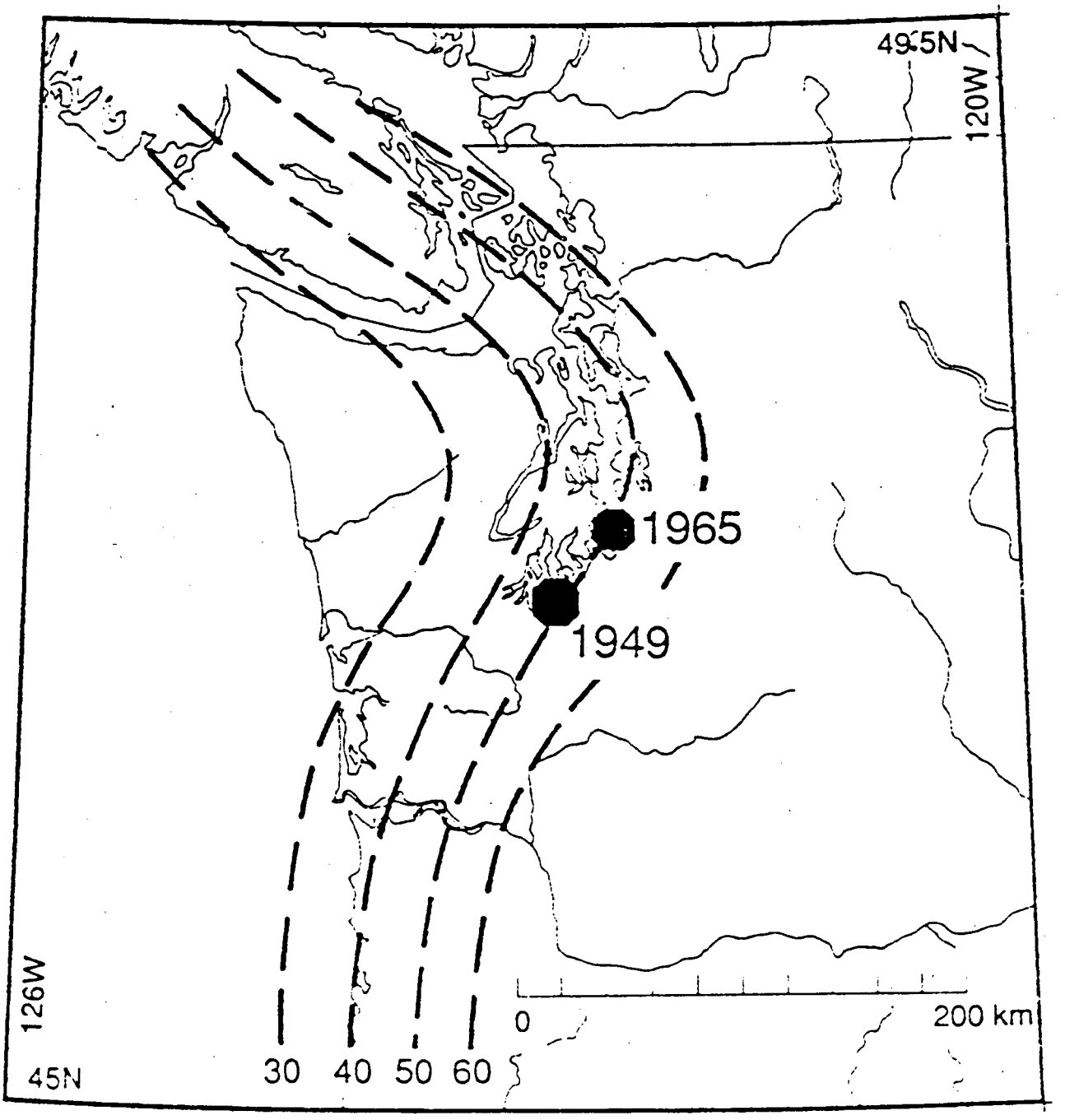

Figure 3. Contours of depth to the subducting Juan de Fuca slab (in kilometers) (after McCrumb et al., 1991).

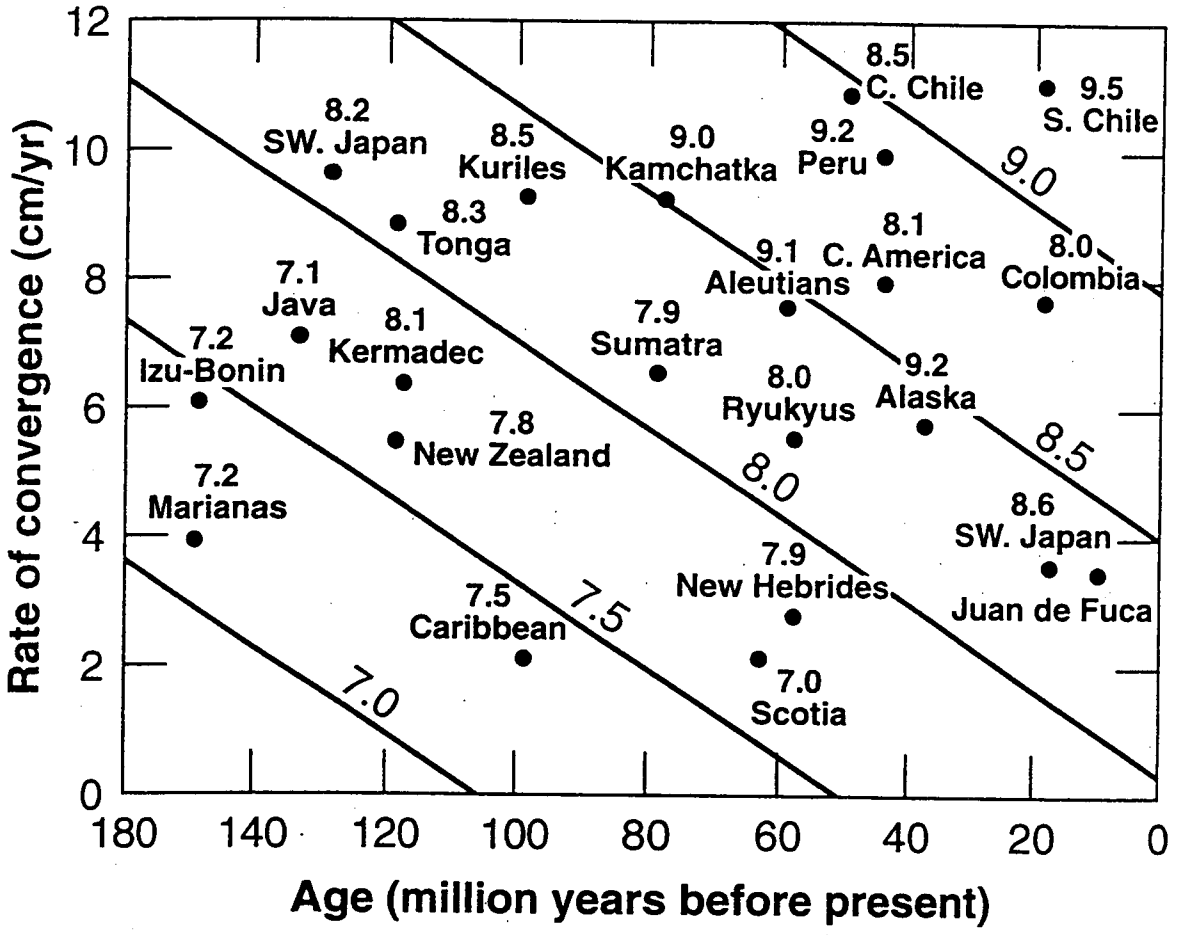

Figure 4. Effects of age and rate of convergence on subduction zone earthquake magnitude. Age and rate conditions for Cascadia subduction zone are labelled as Juan de Fuca (after Heaton and Kanamori, 1984).

the Juan de Fuca plate dips more steeply at angles of 30° to 50°. A cross-section of the Cascadia subduction zone is shown in Figure 2. Figure 3 presents contours of depth to the top of the subducting Juan de Fuca plate inferred from earthquake hypocenter distributions.

Estimated rates for subduction of the Juan de Fuca plate under the North American plate have been determined from magnetic reversal data. Such data indicate that approximately 43 km of new oceanic crust has formed from the Juan de Fuca ridge since the last magnetic reversal, Brunhes-Matuyama, which occurred about 700,000 years ago. This and other data suggest an average convergence rate of 3 to 4 cm/year over the past 5 million years (Heaton and Kanamori, 1984). The Cascadia subduction zone is also relatively young, at least in comparison to other subduction zones around the world. Heaton and Kanamori (1984) compared the age and rate of convergence of the Cascadia subduction zone with those of other subduction zones, giving consideration to the maximum earthquake magnitudes produced by the other subduction zones. As illustrated in Figure 4, available data suggest a general trend toward larger magnitudes with increasing convergence rate and decreasing age. On the basis of the maximum earthquake magnitudes produced by other subduction zones, the length and width of the Cascadia subduction zone suggest a maximum magnitude between 8.5 and 9.0 (Hyndman and Wang, 1995).

Because current paleoseismological and other studies (e.g. Atwater, 1987; Rodgers, 1988) indicate that large magnitude megathrust earthquakes have occurred along the Cascadia subduction zone off the coasts of northern California, Oregon, and Washington, the likelihood of additional great subduction zone earthquakes in the future is considered high. Given that there is written evidence of such events within the last 300 years in the Pacific Northwest, consideration of the possible effects of large subduction zone earthquakes on transportation structures in Washington state motivated the research described in this report.

APPROACH

Until recently, ground motions due to such large subduction zone events could only be evaluated with empirical estimates of ground motions based on data recorded in other, more active subducting regions of the world. In the last few years, however, a cost effective and accurate numerical approach that can account for the unique source, crustal path, and site conditions found in Washington state has been developed, validated, and applied to a large number of projects to develop ground motions for engineering design. This model was used to develop rock outcrop motions corresponding to three possible subduction earthquake magnitudes—M_w = 8.0, M_w = 8.5, and M_w = 9.0— for each of 13 sites in Washington state. Equivalent linear and nonlinear ground response analyses were then performed to compute ground surface motions. Because the rupture scenarios (hypocenter location and slip distribution) of such large earthquakes cannot be predicted, motions for 30 different scenarios were produced for each earthquake.

Finite Source RVT Model

Subduction zone earthquakes were simulated with a stochastic finite source ground motion model. In this approach, a seismic source (fault) is divided into a number of small elements that are assumed to rupture in a predetermined sequence. The motion produced by the rupture of each small element is described by a Brune ω-square point-source model (Brune, 1970; 1971). The effects of these motions at a site of interest are then obtained by summing, with appropriate time delays, the effects caused by the rupture of each small element. This general approach is referred to as a Green function approach (Hartzell, 1978; Irikura, 1983).

Source Parameters

The first step in modeling Cascadia subduction zone earthquakes is definition of the geometry of the Cascadia subduction zone. The Cascadia subduction zone geometry of Hyndman and Wang (1995) was used for this project. In this model, the locked zone (or potential rupture surface) is approximately 90 km wide, with the downdip extent constrained by a

zone of aseismic plastic flow that occurs at temperatures of above 350 to 450°C. With an average dip of 10°, the potential rupture surface spans a depth range of about 9 to 24 km and dips down to the east. The width of the potential rupture surface varies along the strike, with the westward boundary extending closer to the coast along Washington and northern California. Because the finite-fault simulation is more straightforward to implement for rectangular rupture surfaces, the down-dip edge was approximated by a straight line generally midway between the 350 to 450°c isotherms. The isotherms and modeled rupture surface are shown in Figure 5.

Modeling individual Cascadia subduction zone earthquakes required definition of both the size and location of the rupture surface and, for the Green function approach, specification of rupture scenarios. Earthquake magnitude can be correlated to rupture area. Because the width of the seismogenic portion of the Cascadia subduction zone is limited to 90 km, different magnitude earthquakes are associated with different rupture lengths. Rupture lengths were estimated using the empirical relationship

$$\log(A) = M_w - 4.0 \qquad (1)$$

where A is the rupture area in km^2. This relation results from regression based on subduction zone data, as well as the crustal earthquake data of Wells and Coppersmith (1994). In the regression, the coefficient of unity applied to M_w implies a constant static stress drop of about 30 bars (Silva et al., 1997). This is consistent with the general observation of constant static stress drop for earthquakes based on aftershock locations (Wells and Coppersmith, 1994). Using Equation 1 and a 90-km width produced the rupture lengths shown in Table 1.

Table 1. Assumed length and width of rupture zones for Cascadia subduction zone earthquakes.

M_w	Width (km)	Length (km)
8.0	90	111
8.5	90	351
9.0	90	1111

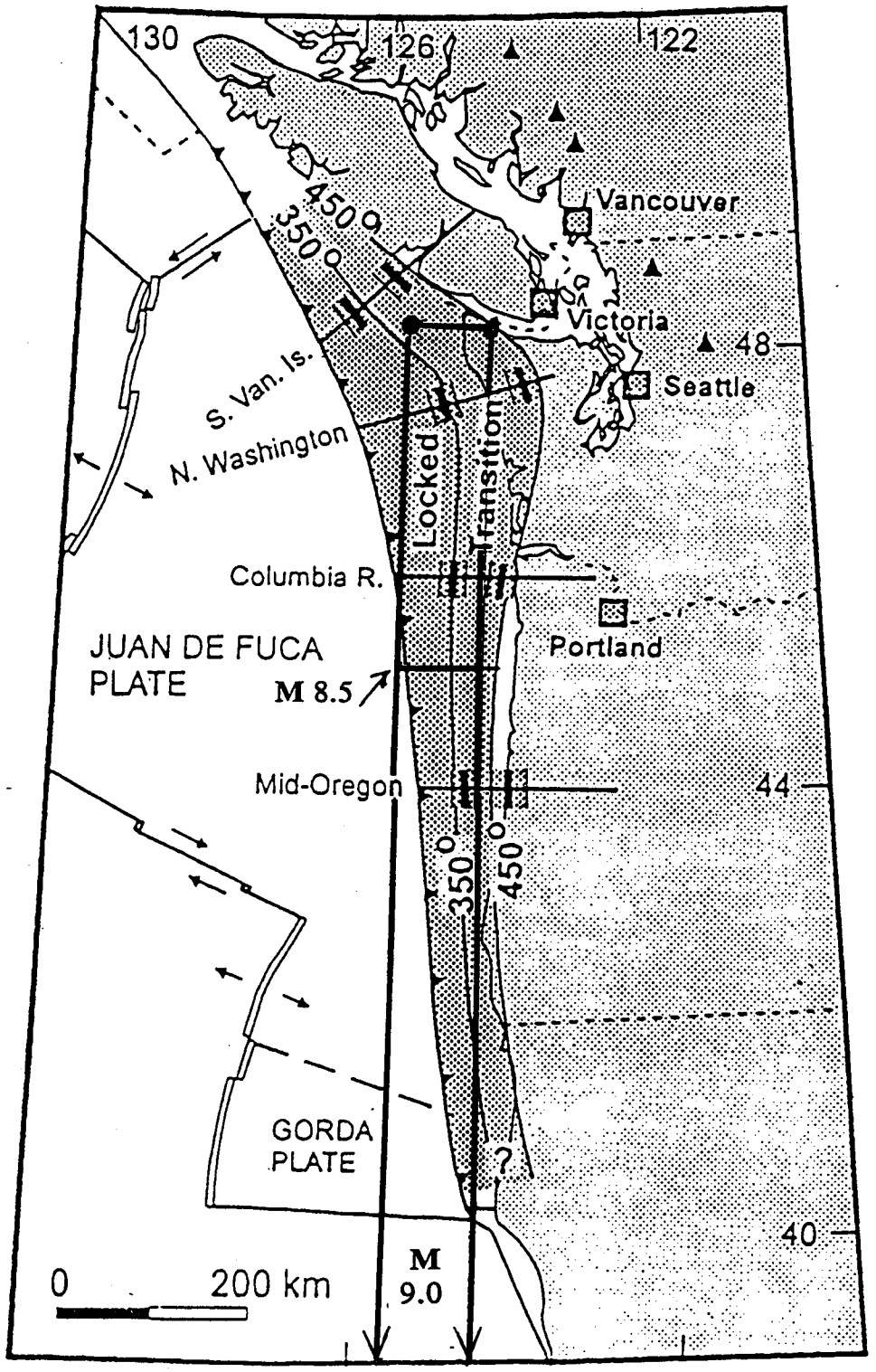

Figure 5. The widths of the locked and transition zones from thermal analyses (thick short lines) compared to those from the current deformation (stippled areas). The bands on the thermal results (350 and 450°C) indicate the estimated uncertainties. Surface projections of the M 8.5 (351 x 90 km^2) and M 9.0 (1,111 x 90 km^2) rupture surfaces. (Figure adopted from Hyndman and Wang, 1995).

Because the length of the M_w = 8.0 event is considerably shorter than the north-south length of Washington state, rock motions were computed for two M_w = 8.0 scenarios. The first assumed rupture along a 111-km length in the northern part of the state, and the second assumed a similar rupture in the southern part of the state. For each site, the response to rupture in the more heavily populated northern part of the state is presented in this report.

Simulation of future earthquakes, particularly in areas of sparse seismicity, is complicated by lack of knowledge about where the rupture will initiate and how the rupture process will proceed. Any single realization of a particular earthquake scenario must therefore be regarded as approximate. For engineering purposes, estimates of the mean and variance of the expected response are most useful. To estimate the mean and variance of ground response for this project, the location of the nucleation point (hypocenter) and slip characteristics (distribution of asperities, or strong points, along the fault) were randomized to produce 30 rupture examples for each Cascadia subduction zone scenario earthquake.

To generate random nucleation points for subduction zone earthquakes, which generally rupture in the updip direction, a nucleation zone was defined within the lower half of the rupture surface and the central 80 percent of the potential rupture surface. The end constraints were used to prevent rupture from initiating too close to the ends of the rupture surface (Silva, 1992). The nucleation initiation points were assumed to occur randomly within the nucleation zone. Random slip models were generated with a method that preserved statistics of asperity characteristics (e.g., size and location) based on an analysis of variance of slip models inferred from recordings of about 10 large earthquakes (Silva et al., 1997). Examples showing contours of slip displacement for four randomly generated slip models for each earthquake are shown in Figures 6, 7, and 8 for **M** 8.0, 8.5, and 9.0, respectively. The random locations of the nucleation points are not shown but control the effects of directivity on the motions. The effects of directivity are most pronounced at the longer periods (> 1 sec) for response spectra (Silva, 1992) and affect durations of time histories over all periods. Rupture toward a site (for long rupture

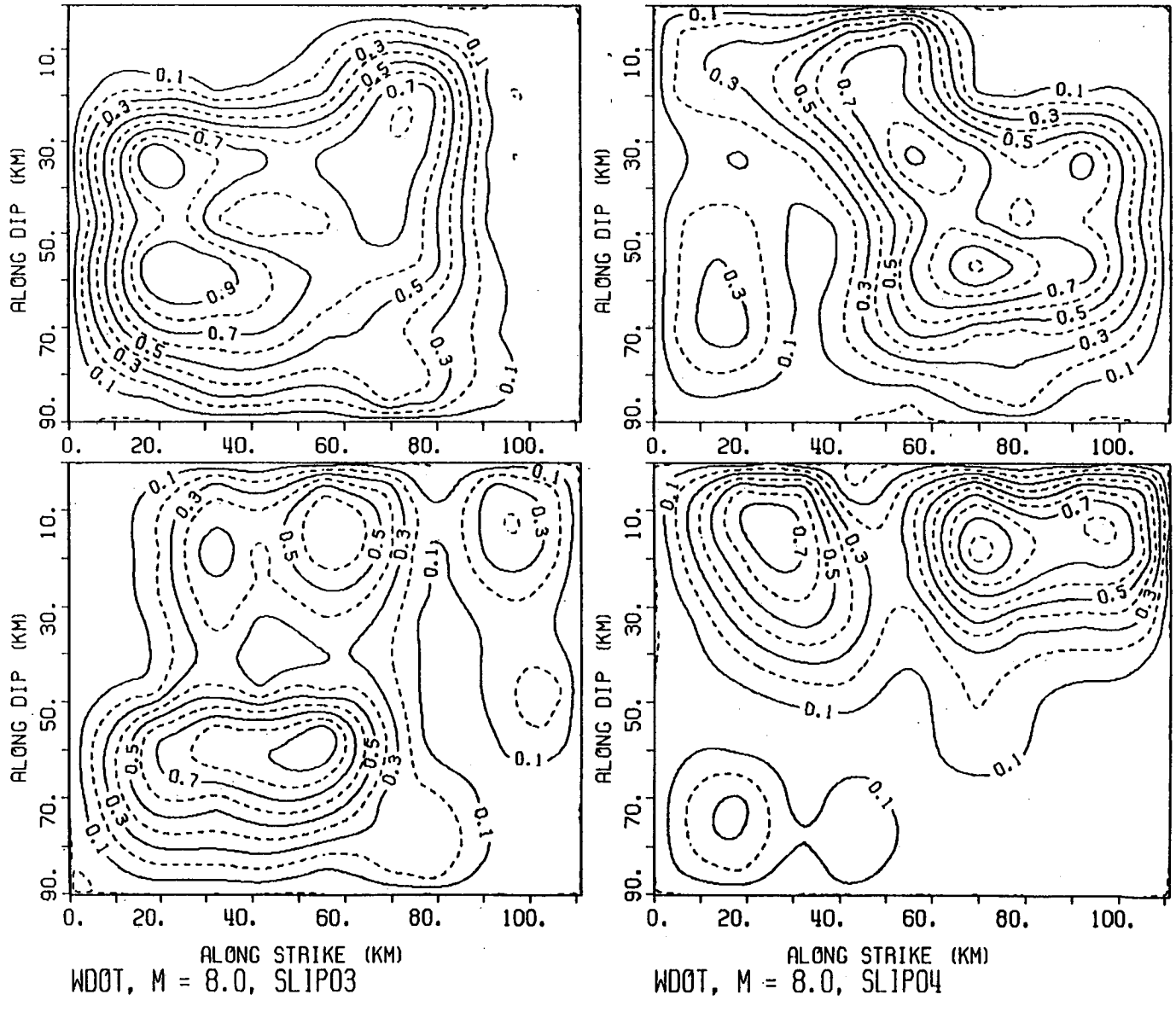

Figure 6. First four slip models for the M 8.0 Cascadia subduction zone source. Slip is normalized to a maximum of 1. The average slip is about 4m.

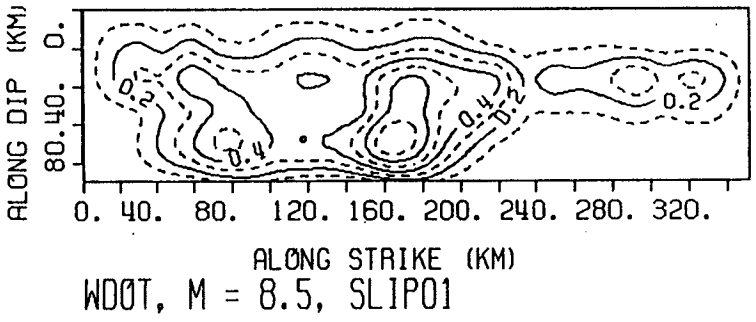

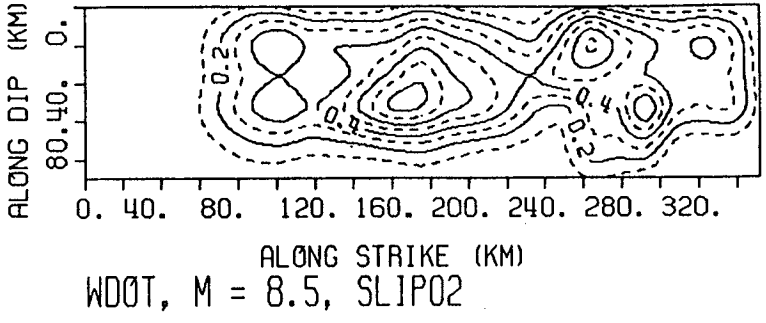

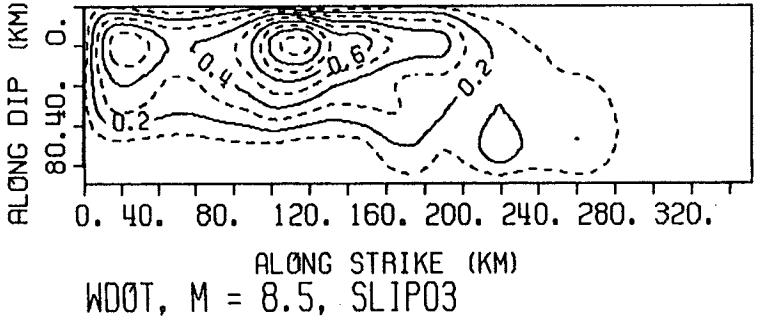

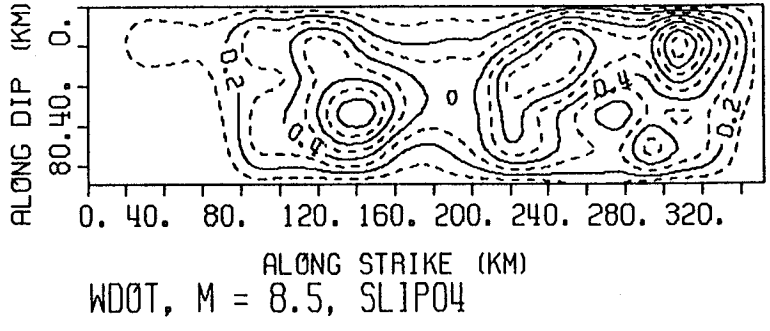

Figure 7. First four slip models for the M 8.5 Cascadia subduction zone source. Slip is normalized to a maximum of 1. The average slip is about 7m.

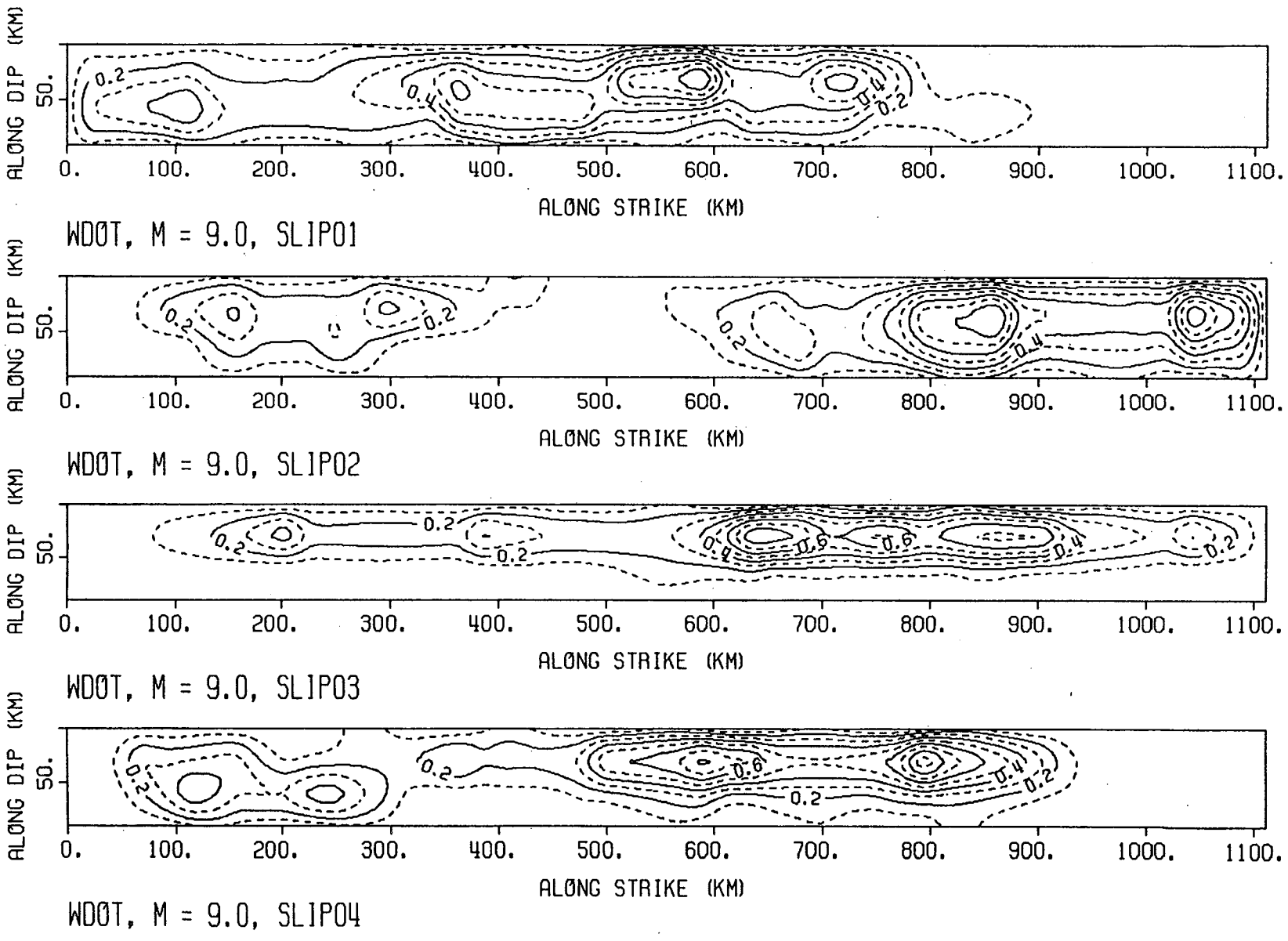

Figure 8. First four slip models for the M 9.0 Cascadia subduction zone source. Slip is normalized to a maximum of 1. The average slip is about 13m.

surfaces) generally results in shorter levels of significant acceleration, velocity, and displacement than does rupture away from a site. On the other hand, the locations of asperities or regions of high slip generally elevate motions over a very wide period range when they are close to a site. Variability in nucleation point and asperity location result in large variations in motions, particularly for sites located near large ruptures (Roblee et al., 1996).

Point-Source Ground Motion Model

The finite-source code is an extension of the simple single-corner-frequency ω-square ground motion model and consists of the sum of a suite of point-source models appropriately distributed along a rupture surface. Because the point-source ground motion model is a vital component of the finite-source model and because it uses the same propagation and site parameters as the finite-source model, it is described in detail in the following paragraphs.

The conventional stochastic ground motion point-source ground motion model uses an ω-square source model (Brune, 1970, 1971) with a single corner frequency and a constant stress drop (Boore, 1983; Atkinson, 1984). Random vibration theory is used to relate RMS (root-mean-square) values to peak values of acceleration (Boore, 1983), and to relate oscillator response (Boore and Joyner, 1984; Toro, 1985; Silva and Lee, 1987) computed from the power spectra to expected peak time domain values (Boore, 1983).

In the ω-square model, the shape of the acceleration spectral density, a(f), is given by

$$a(f) = C \frac{f^2}{1+\left(\frac{f}{f_0}\right)^2} \frac{M_0}{R} P(f) A(f) e^{-\frac{\pi f R}{B_0 Q(f)}} \qquad (2)$$

where

$$C = \left(\frac{1}{\rho_0 \beta_0^3}\right) \bullet (2) \bullet (0.55) \bullet \left(\frac{1}{\sqrt{2}}\right) \bullet \pi$$

M_0 = seismic moment

R = hypocentral distance

β_0 = shear-wave velocity at the source

ρ_0 = density at the source

$Q(f)$ = frequency dependent quality factor (crustal damping)

$A(f)$ = crustal amplification

$P(f)$ = high-frequency truncation filter

f_0 = source corner frequency

The constant, C, contains source region density (ρ_0) and shear-wave velocity (β_0) terms and accounts for the free-surface effect (factor of 2), the source radiation pattern averaged over a sphere (0.55) (Boore, 1986), and the partition of energy into two horizontal components (0.7071).

Source scaling is provided by specifying two independent parameters, the seismic moment (M_0) and the high-frequency stress parameter, or stress drop ($\Delta\sigma$). The seismic moment is related to magnitude through the definition of moment magnitude M_w by the relation (Hanks and Kanamori, 1979)

$$\log M_0 = 1.5\, M_w + 16.05 \tag{3}$$

The stress drop ($\Delta\sigma$) relates the corner frequency f_0 to M_0 through the relation (Brune, 1970; 1971)

$$f_0 = \beta_0\, (\Delta\sigma / 8.44\, M_0)^{1/3} \tag{4}$$

The stress drop is sometimes referred to as the high frequency stress parameter (Boore, 1983) (or simply the stress parameter) because it directly scales the Fourier amplitude spectrum for frequencies above the corner frequency (Silva, 1991; Silva and Darragh 1995). High (> 1 Hz) frequency model predictions are therefore very sensitive to this parameter (Silva, 1991;

EPRI, 1993), and the interpretation of the parameter being a stress drop or simply a scaling parameter depends upon how well real earthquake sources (on average) obey the ω-square scaling (Equation 4) and how well they are fit by the single-corner-frequency model. If earthquakes truly have single-corner-frequency ω-square sources, the stress drop in Equation 4 is a physical parameter, and its value has a physical interpretation related to the forces (stresses) accelerating the relative slip across the rupture surface. High stress drop sources produce smaller source (fault rupture) areas than low stress drop sources (Brune, 1970) for the same earthquake magnitude. Otherwise, the stress drop must simply be interpreted as a high frequency scaling or fitting parameter. The spectral shape of the single-corner-frequency ω-square source model is then described by the two free parameters M_0 and $\Delta\sigma$. The corner frequency increases with the shear-wave velocity and with increasing stress drop, both of which may be region-dependent.

The crustal amplification function accounts for the increase in wave amplitude as seismic energy travels through lower-velocity crustal materials from the source to the surface. The amplification depends on average crustal and near surface shear-wave velocity and density (Boore, 1986).

The P(f) filter is used to model the observation that acceleration spectral density appears to fall off rapidly beyond some region- or site-dependent maximum frequency (Hanks, 1982; Silva and Darragh, 1995). This observed phenomenon truncates the high frequency portion of the spectrum, along with the source corner frequency, and is responsible for the band-limited nature of the stochastic model. This spectral fall-off at high frequency has been attributed to near-site attenuation (Hanks, 1982; Anderson and Hough, 1984) or to source processes (Papageorgiou and Aki, 1983) or perhaps to both effects. In the Anderson and Hough (1984) attenuation model, adopted here, the form of the P(f) filter is taken as

$$P(f, r) = e^{-\pi\kappa(r)f} \tag{5}$$

In Equation 3.35, $\kappa(r)$ is a site and distance dependent parameter that represents the effect of intrinsic attenuation upon the wavefield as it propagates through the crust from source to

receiver. The parameter $\kappa(r)$ depends on epicentral distance, r, and on both the shear-wave velocity, β, and quality factor (Q_S) averaged over a depth, H, beneath the site (Hough et al., 1988). At zero epicentral distance, $\kappa(r)$ is given by

$$\kappa(0) = \frac{H}{\overline{\beta}\,\overline{Q_S}} \tag{6}$$

and is referred to simply as κ.

The overbars in Equation 6 indicate averaging of the quantities over the depth, H. The value of kappa at zero epicentral distance is attributed to attenuation in the very shallow crust directly below the site (Hough and Anderson, 1988; Silva and Darragh, 1995). The intrinsic attenuation along this part of the path is not thought to be frequency dependent and is modeled using a frequency independent, but site and crustal region dependent, constant value of κ (Hough et al., 1988; Rovelli et al., 1988). This zero epicentral distance κ was used in this study.

The crustal path attenuation from the source to just below the site is modeled with the frequency-dependent quality factor Q(f). Thus the distance component of the original $\kappa(r)$ (Equation 5) is accommodated by Q(f) and R in the last term of Equation 2:

$$\kappa(r) = \frac{H}{\overline{\beta}\,\overline{Q_S}} + \frac{R}{\overline{\beta}_0\,\overline{Q}(f)} \tag{7}$$

The Fourier amplitude spectrum given by Equation 2 represents the stochastic ground motion model based on a Brune source spectrum with a single corner frequency. It is a point source, and models direct shear-waves in a homogeneous half-space (with effects of a velocity gradient captured by the A(f) filter). For horizontal motions, vertically propagating shear-waves are assumed. Validations produced with incident inclined SH-waves accompanied by raytracing to find appropriate incidence angles leaving the source showed little reduction in uncertainty in comparison to results produced with vertically propagating shear-waves.

Equation 2 represents an elegant ground motion model that accommodates source and wave propagation physics, as well as propagation path and site effects, with an attractive simplicity. The model is appropriate for an engineering characterization of ground motion because it captures the general features of strong ground motion in terms of peak acceleration and spectral composition with a minimum of free parameters (Boore, 1983; McGuire et al., 1984; Boore, 1986; Silva and Green, 1988; Silva et al., 1990; Schneider et al., 1993; Silva and Darragh, 1995). An additional important aspect of the stochastic model that employs a simple source description is that the region-dependent parameters may be evaluated by observations of small local or regional earthquakes. Region-specific seismic hazards can then be evaluated for areas that have sparse strong motion data with relatively simple spectral analyses of weak motion (Silva, 1992).

Factors such as surface topography, finite and propagating seismic sources, laterally varying near-surface velocity and Q gradients, and random inhomogeneities along the propagation path affect strong ground motions but are not included in the point source model. While some or all of these factors are generally present in any observation of ground motion and may exert controlling influences in some cases, the simple stochastic point-source model appears to be robust in predicting median or average properties of ground motion (Boore 1983, 1986; Schneider et al., 1993; Silva, 1992; Silva et al., 1997). For this reason it represents a powerful predictive and interpretative tool for engineering characterization of strong ground motion.

Finite-Source Ground Motion Model

Close to the source of large earthquakes, effects such as rupture propagation, directivity, and source-receiver geometry can violate the basic assumptions of the point source model. To accommodate these effects, a methodology that combines the aspects of finite-earthquake-source modeling techniques (Hartzell, 1978; Irikura 1983) with the stochastic point-source ground motion model has been developed to produce response spectra and time histories appropriate for engineering design (Silva et al., 1990; Silva and Stark, 1993; Schneider et al., 1993; Silva et al.,

1997). The approach is very similar to the empirical Green function methodology introduced by Hartzell (1978) and Irikura (1983). In this case, however, the stochastic point-source is substituted for the empirical Green function.

As a result of a recent Department of Energy supported study (Silva et al., 1997), in which 15 earthquakes were modeled at over 500 sites with both the point- and finite-source stochastic models, these are now the most thoroughly validated models available to characterize strong ground motions for engineering design.

Use of the stochastic point-source as a Green function is motivated by its demonstrated success in modeling ground motions in general and strong ground motions in particular (Boore, 1983, 1986; Silva and Stark, 1993; Schneider et al., 1993; Silva and Darragh, 1995; Silva et al., 1997), as well as the benefits of using a model that is truly site- and region-specific. The necessity for having available regional and site-specific recordings or for modifying possibly inappropriate empirical Green functions is eliminated.

For the finite-source characterization, a rectangular fault is discretized into a number subfaults of moment M_0^s The empirical relationship of Equation 1 is used to assign areas to both the target earthquake (if its rupture surface is not fixed) and to the subfaults.

The subevent magnitude, M_S, is taken to be 6.4 for large subduction earthquakes of $M_w >$ 7.5. The number of subfaults is determined as the ratio of the target event area to the subfault area. To produce the proper seismic moment for the entire earthquake, the total number of subevents is assumed to be the ratio of the target event moment to the subevent moment. Rupture is assumed to continue for a time duration, or rise time

$$\log \tau = 0.33 \log M_0 - 8.54 \tag{8}$$

which results from a fit to the rise times inferred from modeling 15 large earthquakes (Silva et al., 1997). The ratio of target-to-subevent rise times is given by

$$\frac{\tau}{\tau^s} = 10^{0.5(M-Ms)} \tag{9}$$

and determines the number of subevents to sum in each subfault. This approach is referred to as the constant-rise-time model and results in a variable slip velocity for nonuniform slip distributions. Alternatively, one can assume a constant slip velocity, resulting in a variable-rise-time model for heterogeneous slip distributions.

To introduce heterogeneity of the earthquake source process into the stochastic finite-fault model, the location of the subevents within each subfault (Hartzell, 1978) and the subevent rise time are randomized. The stress drop of the stochastic point-source Green function is taken to be 30 bars, consistent with the static value based on the **M** 5.0 subevent area, using the equation (Brune, 1970, 1971)

$$\Delta\sigma = \frac{7}{16}\left(\frac{M_e}{R_e^3}\right) \tag{10}$$

where R_e is the equivalent circular radius of the rectangular sub-event.

Different values of slip are assigned to each subfault as relative weights so that asperities or non-uniform slip can be incorporated into the methodology. To produce slip distributions for future earthquakes, random slip models are generated on the basis of a statistical asperity model with parameters calibrated to the published slip distributions. This approach has been validated by comparing the modeling uncertainty and bias estimates for the Loma Prieta and Whittier Narrows earthquakes based on motion at each site averaged over 30 random slip models to the bias and uncertainty estimates based on the published slip model. The results show nearly identical bias and uncertainty estimates, suggesting that averaging the motions over random slip models produces as accurate a prediction at a site as a single motion computed using the "true" slip model, which is determined by inversion of actual recordings.

The rupture velocity is assumed to be depth independent at a value of 0.8 times the shear-wave velocity, generally at the depth of the dominant slip. This value is based on a number of studies of source rupture processes that also suggest that rupture velocity is non-uniform. To capture the effects of non-uniform rupture velocity, a random component (20 percent) is added.

The radiation pattern is computed for each subfault, a random component is added, and the RMS is applied to the motions computed at the site.

The ground-motion time history at the receiver is computed by summing the contributions from each subfault associated with the closest Green function, transforming to the frequency domain, and convolving with the Green function spectrum (Equation 2). The locations of the Green functions are generally taken at the center of each subfault for small subfaults or at a maximum separation of about 5 to 10 km for large subfaults. As a final step, the individual contributions associated with each Green function are summed in the frequency domain and multiplied by the RMS radiation pattern. Then the resultant power spectrum at the site is computed. The appropriate duration used in the RVT computations for PGA, PGV, and oscillator response is computed by transforming the summed Fourier spectrum into the time domain and computing the 5 to 75 percent Arias intensity (Ou and Herrmann, 1990).

As with the point-source model, crustal response effects are accommodated through the amplification factor (A(f)) or by using vertically propagating shear waves through a vertically heterogeneous crustal structure. Propagation path damping, through the Q(f) model, is incorporated from each fault element to the site. Near-surface crustal damping is incorporated through the κ operator. To model crustal propagation path effects, the method of Ou and Herrmann (1990) is applied from each subfault to the site.

Time histories may be computed in the process as well by simply adding phase spectra appropriate to the subevent earthquakes. The phase spectra can be extracted from recordings made close to earthquakes of a size comparable to that of the subevent. Transforming the Fourier spectrum computed at the site into the time domain results in a computed time history that then includes all of the aspects of rupture propagation and source size, as well as region-specific propagation path and site effects. For fixed fault size, mechanism, and moment, the specific source parameters for the finite-fault are slip distribution, location of nucleation point, and site azimuth. The propagation path and site parameters remain identical for both the point- and finite-source models.

Propagation Path and Site Parameters

The regional model of Cohee et al. (1991) shown in Table 2 was used to model crustal velocity structure. To simulate motions appropriate for input at the base of soil columns, a soft rock profile was placed upon the regional Cohee et al. (1991) crustal model. This soft rock profile is based on statistical analyses of shear-wave velocities measured at soft rock sites. For this profile, the shear-wave velocity at the surface is about 300m/sec, but these surficial layers were removed to a depth corresponding to a shear-wave velocity of 838 m/sec. This is considered appropriate for engineering bedrock and will result in motions suitable as outcropping rock at the base of soil profiles.

To obtain a κ value appropriate for the Cohee et al. (1991) crustal model, the empirical relation

$$\log \kappa = 2.22 - 1.09 \log (V_s), \tag{11}$$

Table 2. Soft rock profile for computation of rock outcrop motions. The upper five layers are assumed to lie on top of the regional crustal model of Cohee et al. (1991).

Thickness (m)	V_s (m/sec)	Density (Mg/m^3)
5.8	838.2	2.0
6.7	966.2	2.0
8.2	1,127.7	2.0
9.1	1,274.0	2.1
11.6	1,438.6	2.1
3,000	1,500.0	2.3
16,500	3,800.0	2.7
17,500	4,300.0	2.8
Infinite	4,650.0	3.1

where V_s is the average shear-wave velocity (ft/sec) over the top 100 ft, produced a κ value of 0.03 sec. This empirical relation is based on κ values measured at strong motion recording sites, with shear-wave velocities determined by borehole methods. To accommodate uncertainty in κ, the values were randomized with a lognormal distribution of $\sigma_{\ln \kappa} = 0.3$ (EPRI, 1993).

For the regional crustal Q(f) model, values of Q_o=263 and h=0.49 were selected on the basis of recent work of Atkinson (1996); these are appropriate values for lower crustal earthquakes that occur in and offshore of western Canada and northwest Washington. To accommodate uncertainty in the Q(f) model, Q_0 was randomized with $\sigma_{\ln Qo} = 0.3$. This results in mean $\pm 2\sigma$ values for Q_o of about 150 and 500, which are typical values of western and eastern North America, respectively. This is considered to reflect an acceptable range in Q(f) because the model is not well constrained, and the extent of the rupture zone is large.

Site-Specific Ground Response Models

Seismic ground response is well known to be strongly influenced by local site conditions. The general effects can be shown theoretically and have been observed empirically in many earthquakes. For a particular site, the effects of local soil conditions can be predicted by ground response analyses. Depending on the site topography and subsurface conditions, one-, two-, or three-dimensional ground response analyses may be required. In practice, however, one-dimensional analyses are most commonly used.

One-dimensional ground response analyses were performed for each instance of each Cascadia subduction zone earthquake scenario for 15 different soil profiles. Given the number of soil profiles (15), the number of earthquake scenarios (3), the number of simulations of each scenario (30), and the fact that the sites were analyzed with both equivalent linear and nonlinear analyses, a total of 2,700 ground response analyses were performed.

Ground Response Sites and Characterization

A total of 15 soil profiles, representing 13 different locations within Washington state, were identified, investigated, and characterized for ground response analysis. The sites and

profiles were selected in consultation with WSDOT engineers from the Bridge and Structures office and the Materials Laboratory. Site selection involved a variety of factors, including geologic conditions, locations of constructed facilities, population density, and the availability of subsurface information. Though the amount and quality of available subsurface information varied widely for the different sites, the information was interpreted consistently at all sites. This process was accomplished with the understanding that the goal was to produce a generalized model that would represent a range of similar geologic conditions rather than to precisely characterize conditions at one particular site.

The primary soil properties for which characterization was required included shear modulus, damping ratio, density, strength, and (where appropriate) liquefaction resistance. A consistent hierarchy of evaluation procedures was used for each of these properties. First, actual measurements were used whenever available. Measured quantities included shear wave velocities (by downhole or seismic cone), soil density, and shear strength (by triaxial or direct shear testing). When direct measurements were not available, properties were estimated by correlation with other parameters such as standard penetration resistance, plasticity index, overconsolidation ratio, and undrained strength. Finally, when neither direct measurements nor correlations were available, properties were estimated on the basis of anticipated geology; all characterizations of anticipated geology were reviewed by geologists from the WSDOT Materials Laboratory. A brief description of the correlations used in this project is presented in Appendix A.

The 15 ground response profiles are listed in Table 3 below; their locations are illustrated in Figure 9. The profiles cover a range of soil conditions, from soft clays and silts to dense sands and gravels, and they cover a wide geographic area in western Washington. One ground response site is located east of the Cascades to quantify the anticipated low level of shaking that would occur in that part of the state. Shear wave velocity profiles for each of the ground response profiles are illustrated in Appendix B.

Table 3. Names, locations, and surficial soil description of ground response profiles.

Name	Map Location	Location	Description
Alaskan Way Viaduct I	AW1	Seattle	20 ft loose sand over very dense sandy gravel and gravelly sand
Alaskan Way Viaduct II	AW2	Seattle	60 ft loose sand over very dense sandy gravel and gravelly sand
Andresen Road	AR	Vancouver	40 ft loose to medium dense sand over sandy clay over dense, gravelly and silty sands
Black Diamond Road	BD	Port Angeles	200 ft dense silty sand with gravel over dense silty gravel with sand
Bone River	BR	Raymond	85 ft soft silt and silty clay over stiff clayey and sandy silt
Capitol Boulevard	CB	Olympia	205 ft dense silty sand over dense sandy gravel
Coldwater Creek	CC	Mt. St. Helens	100 ft loose sand, sandy clay, and silty sand
I5/NE 99th Street	INE	Vancouver	5 ft very soft silt over 15 ft loose sand over medium dense silty sand
I405/SR522	ISR	Woodinville	75 ft loose sand and silt with organics over stiff clayey and sandy silt
Kent Valley	KV	Kent	50 ft loose to medium dense sands over dense gravelly sand
Mercer Slough I	MS1	Bellevue	30 ft very soft peat over dense sand
Mercer Slough II	MS2	Bellevue	60 ft very soft peat over 40 ft soft clay over dense sand
Nooksack River	NR	Nooksack	20 ft medium dense sand and sandy gravel over 170 ft soft silty clay and sandy clay
North Ferndale	NF	Ferndale	15 ft loose gravelly, silty sand over 60 ft soft silty clay
Yakima	YA	Yakima	70 ft dense gravel

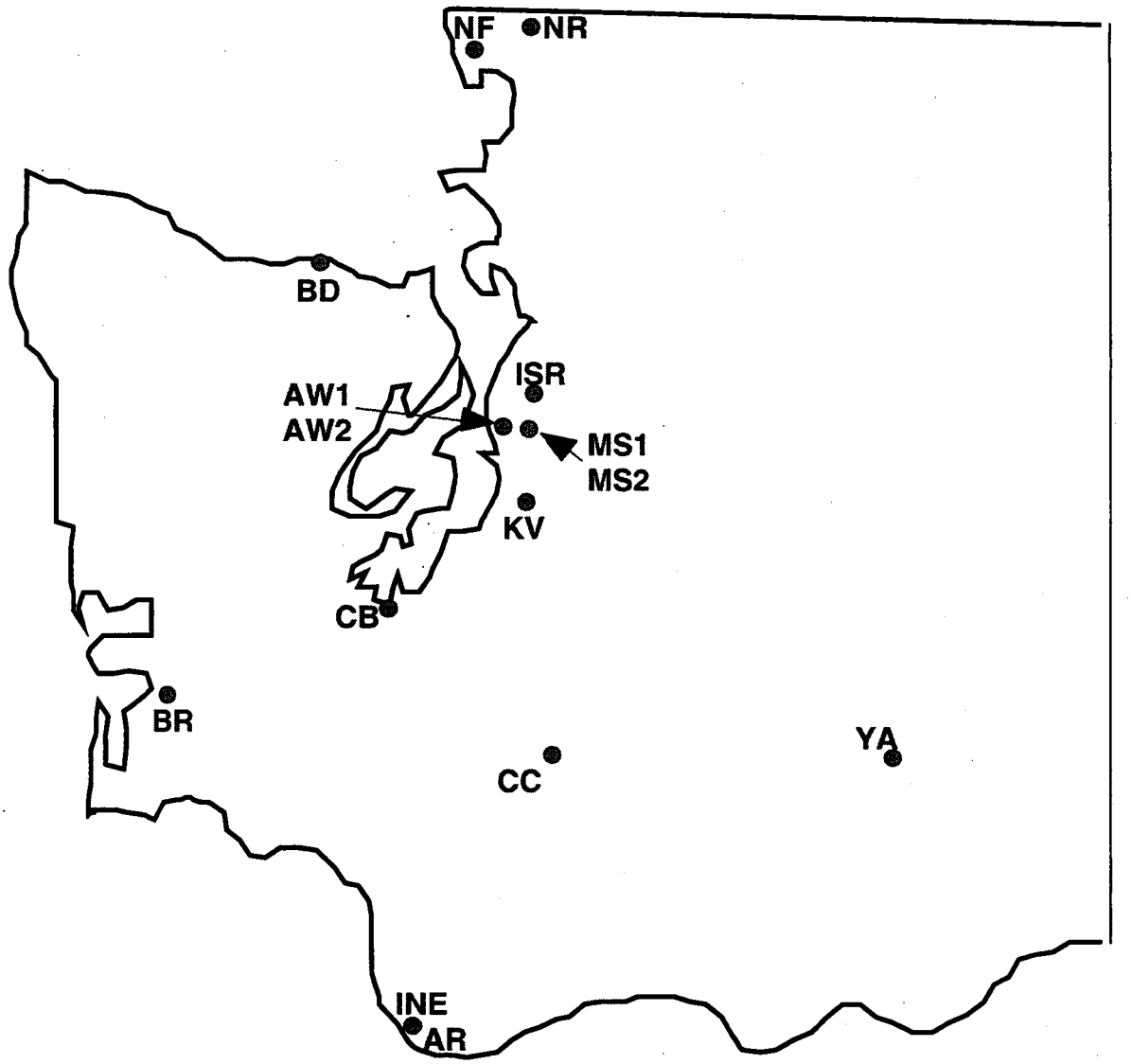

Figure 9. Locations of ground response analysis sites.

Equivalent Linear Model

Seismic ground response can be computed very efficiently using an equivalent linear approach. This approach, which has been commonly used in geotechnical earthquake engineering for some 25 years, approximates the nonlinear response of soils by iterating toward strain-compatible shear modulus and damping values. The approach allows computations to be per-

formed in the frequency domain where very high frequencies that do not influence civil structures can be easily neglected. It must be recognized, however, that the equivalent linear approach produces linear analyses in which the stiffness and damping characteristics of the soil remain constant throughout the duration of an earthquake. The equivalent linear model has been incorporated into several computer programs for seismic ground response analysis. The most commonly used of these is SHAKE (Schnabel et al., 1972), which considers one-dimensional ground response. In this research, an updated version called SHAKE91 was used for equivalent linear ground response analysis.

Nonlinear Model

Under cyclic loading, soils exhibit nonlinear, inelastic stress-strain behavior. Their stiffness changes throughout the loading process and can both increase and decrease at different times during loading. This aspect of soil behavior can only be captured by nonlinear ground response models.

Nonlinear ground response analyses were performed with the program WAVE (Horne, 1996; Horne and Kramer, 1997). WAVE uses an explicit finite difference solution of the wave equation to compute one-dimensional ground response. Nonlinear stress-strain behavior is specified in terms of nonlinear backbone curves, and inelastic response under cyclic loading conditions is modeled with the Cundall-Pyke hypothesis (Pyke, 1979). WAVE uses a solution algorithm that provides second-order accuracy at the cost of increased computation time. WAVE is able to perform effective stress analyses by using an energy-based model for pore pressure generation and an explicit finite difference solution of the one-dimensional diffusion equation for pore pressure redistribution and dissipation.

FINDINGS

The primary purpose of this project was to evaluate the potential consequences of subduction earthquakes in western Washington. The ground motion simulations and site-specific ground response analyses indicated a range of ground motion levels and characteristics for the different sites within western Washington. The results of the analyses can be interpreted in different ways; in this report, the results are presented in terms of their potential for structural and geotechnical damage.

The potential of an earthquake ground motion to cause damage can be characterized in a number of ways. A variety of ground motion parameters have been used to characterize ground motion potential; some of these are widely used and recognized, and others are just as valuable, though less widely used. In this report, the potential consequences of subduction earthquakes are characterized by the following ground motion parameters:

- peak acceleration
- spectral acceleration (T=0.3 sec, T=1.0 sec)
- peak velocity
- duration
- Arias intensity
- response spectrum intensity

ROCK OUTCROP MOTIONS

The finite-source model was used to predict suites of rock outcrop motions at each of the 13 ground response sites. These predictions indicate the expected nature of rock outcrop motions at these sites (even though rock does not outcrop at or near all of them) and were used as input to the site-specific ground response analyses. Important characteristics of the rock outcrop motions can be described by peak acceleration and spectral acceleration values.

The rock outcrop motions illustrate the important effects of source, path, and site characteristics on earthquake ground motions. For a given earthquake scenario, the amplitude, frequency content, and duration of the resulting ground motion are strongly influenced by factors such as nucleation point location, rupture pattern, asperity distribution, and others. The inability to predict such factors is the reason that multiple instances of each earthquake scenario were incorporated into the analyses. For example, consider the suite of 30 rock outcrop motions computed for the Alaskan Way Viaduct site (downtown Seattle) for a M_w=8.5 earthquake. Figures 10, 11, and 12 illustrate the computed time histories of acceleration, velocity, and displacement, respectively. Even a brief visual examination of these time histories demonstrates the wide range of possible ground motions that can be produced by a given scenario earthquake. The computed response spectra for each of the 30 motions are shown in Figure 13; the response spectra are plotted together in Figure 14(a), and mean and mean ± one standard deviation spectra are plotted in Figure 14(b).

Peak Acceleration

The peak acceleration of an earthquake ground motion is simply defined as the maximum absolute value of acceleration. Peak acceleration is probably the most commonly used ground motion parameter in earthquake engineering practice. It provides a good description of the amplitude of the higher-frequency components of a ground motion. Many design procedures, including those of AASHTO, are strongly influenced by peak accelerations. Computed peak rock outcrop accelerations for the sites analyzed in this investigation are summarized in Table 4. The spatial distribution of computed rock outcrop peak acceleration is shown in Figure 15. The values, computed for the M_w=9.0 events, show a general decrease in amplitude from west to east.

The computed rock outcrop peak acceleration values were relatively low because of the significant distance between the ground response sites and the Cascadia subduction zone. As would be expected, the westernmost sites were generally subjected to the greatest peak accelerations and the easternmost to the smallest. The Andresen Road site experienced one of

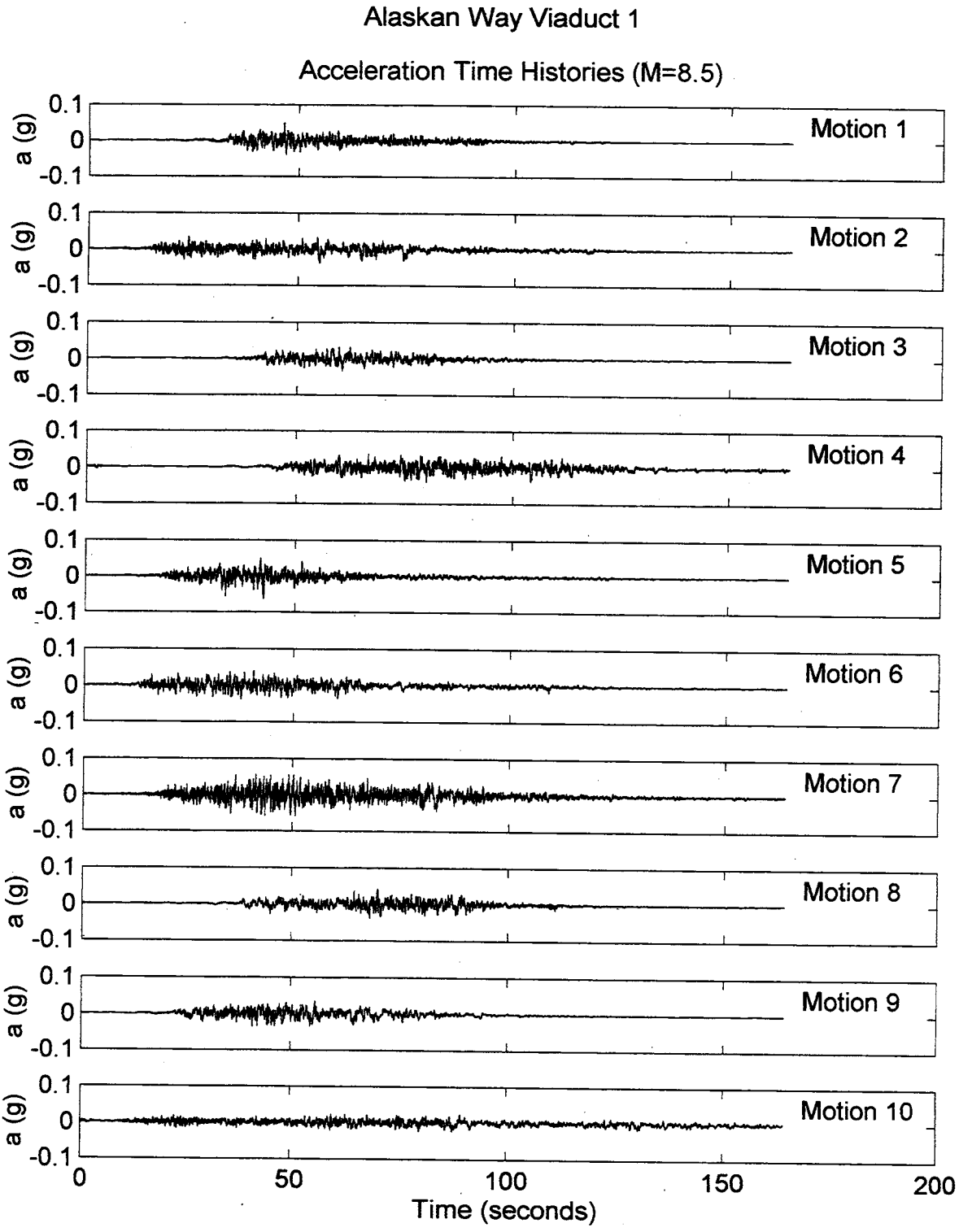

Figure 10. Computed time histories of rock outcrop acceleration at Alaskan Way Viaduct site for M_w = 8.5 Cascadia subduction zone earthquake.

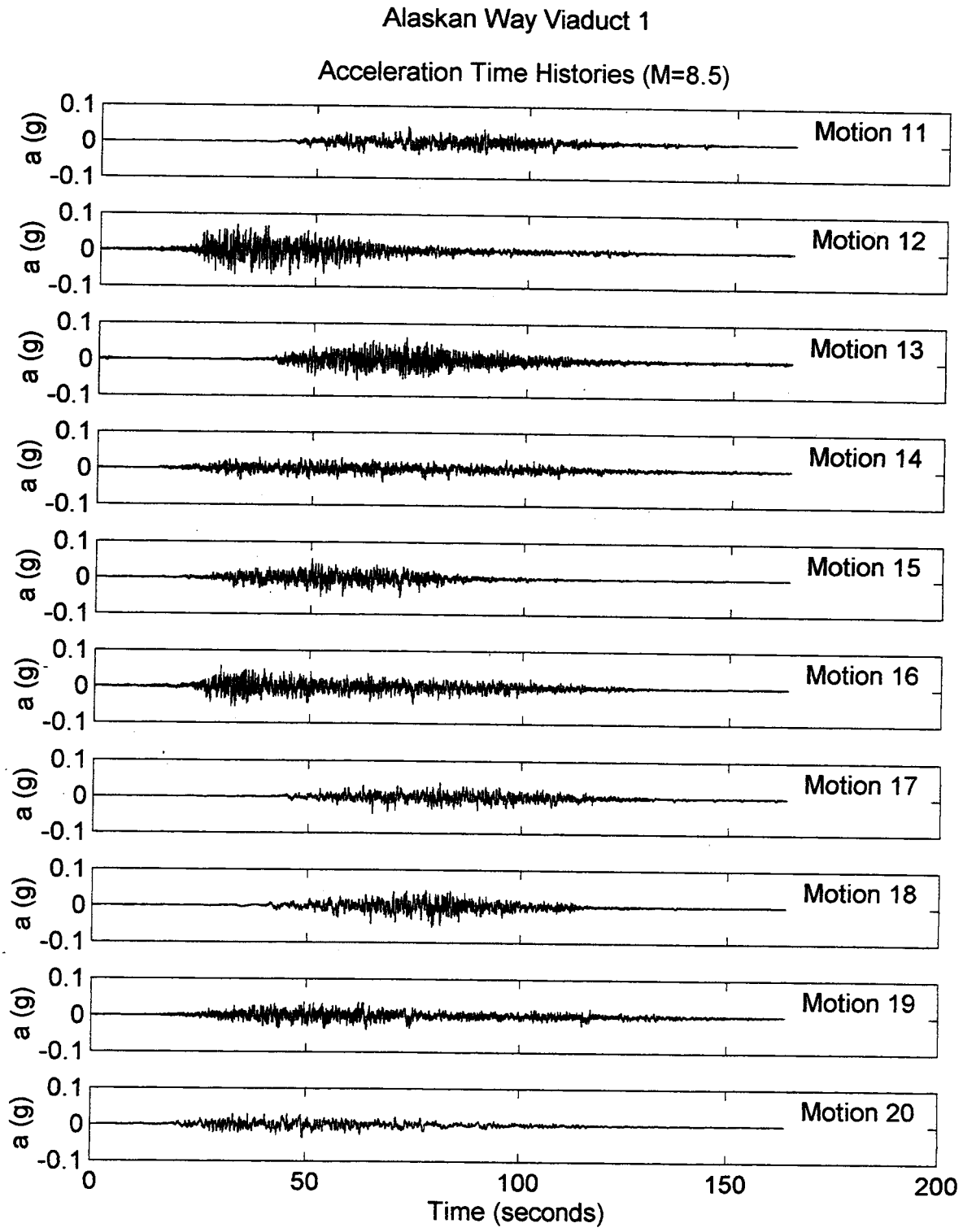

Figure 10. Computed time histories of rock outcrop acceleration at Alaskan Way Viaduct site for M_w = 8.5 Cascadia subduction zone earthquake (continued).

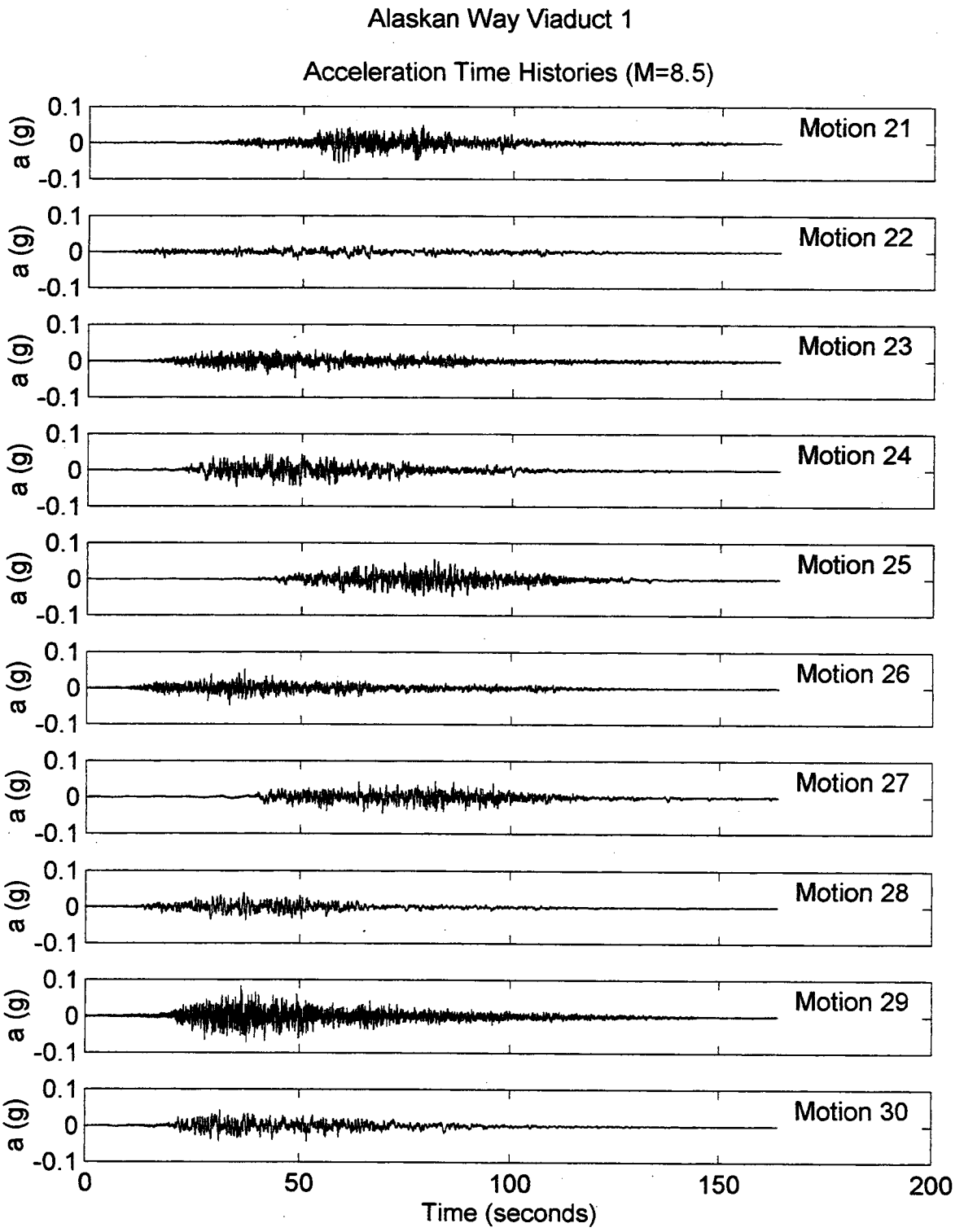

Figure 10. Computed time histories of rock outcrop acceleration at Alaskan Way Viaduct site for $M_W = 8.5$ Cascadia subduction zone earthquake (continued).

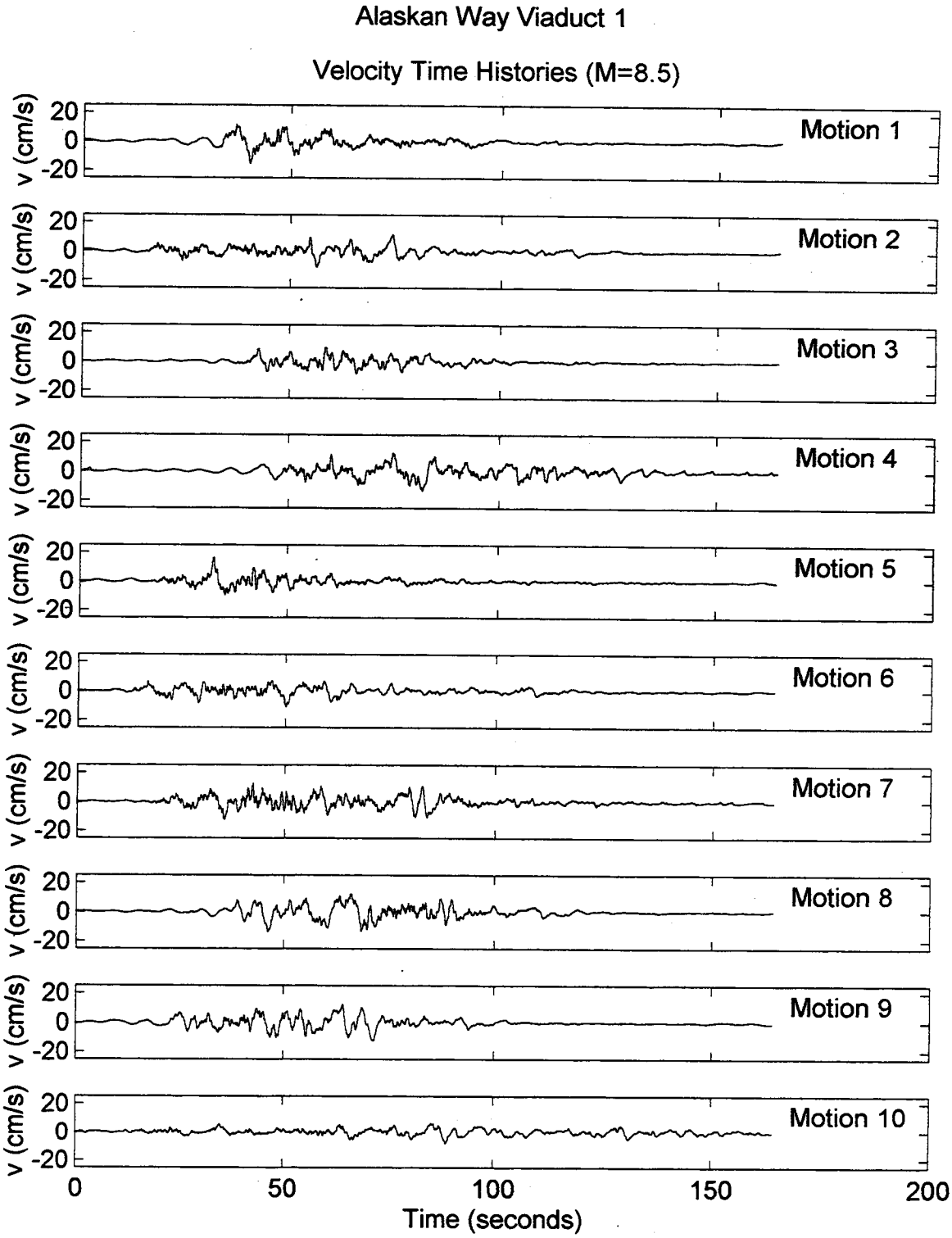

Figure 11. Computed time histories of rock outcrop velocity at Alaskan Way Viaduct site for $M_W = 8.5$ Cascadia subduction zone earthquake.

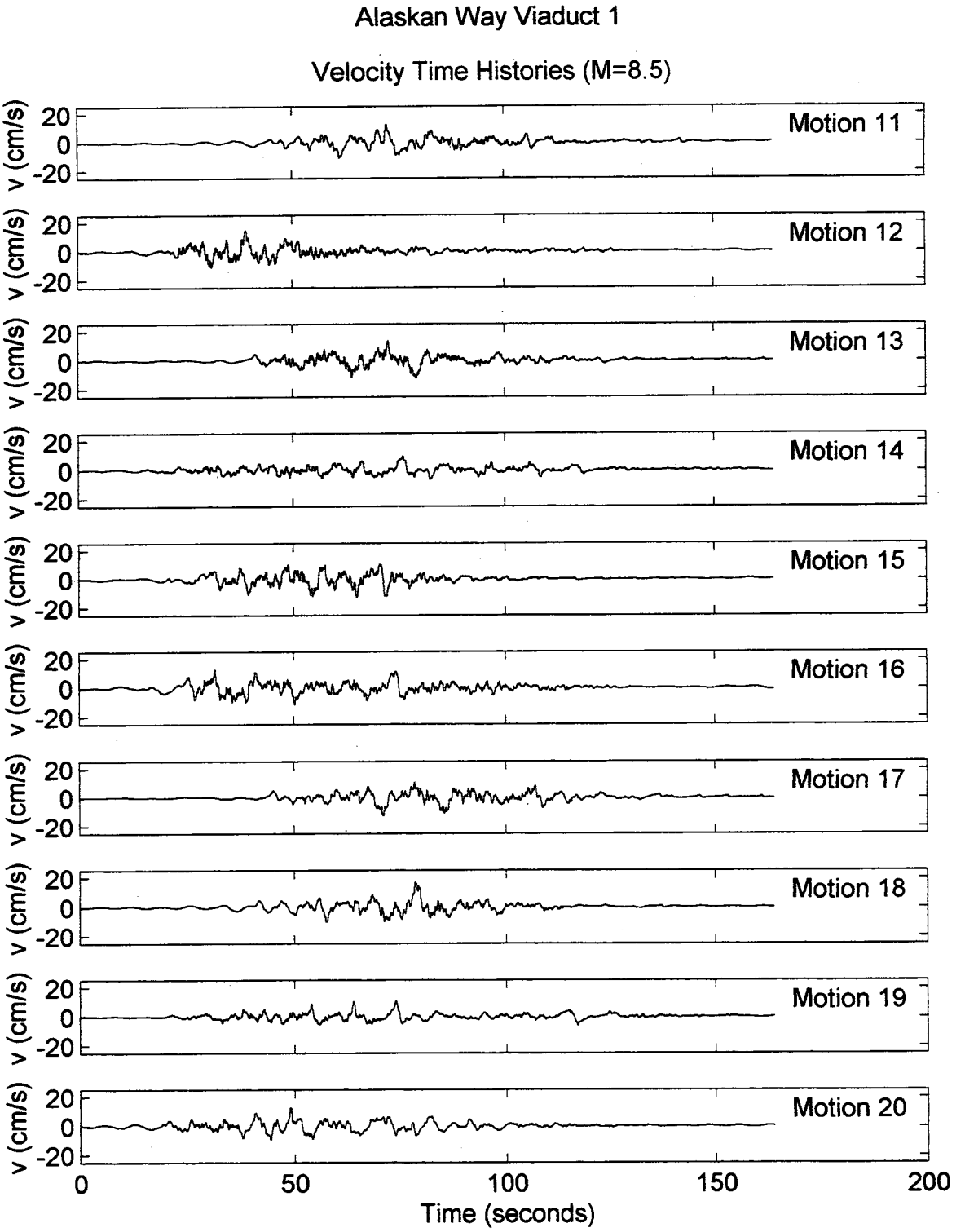

Figure 11. Computed time histories of rock outcrop velocity at Alaskan Way Viaduct site for $M_W = 8.5$ Cascadia subduction zone earthquake (continued).

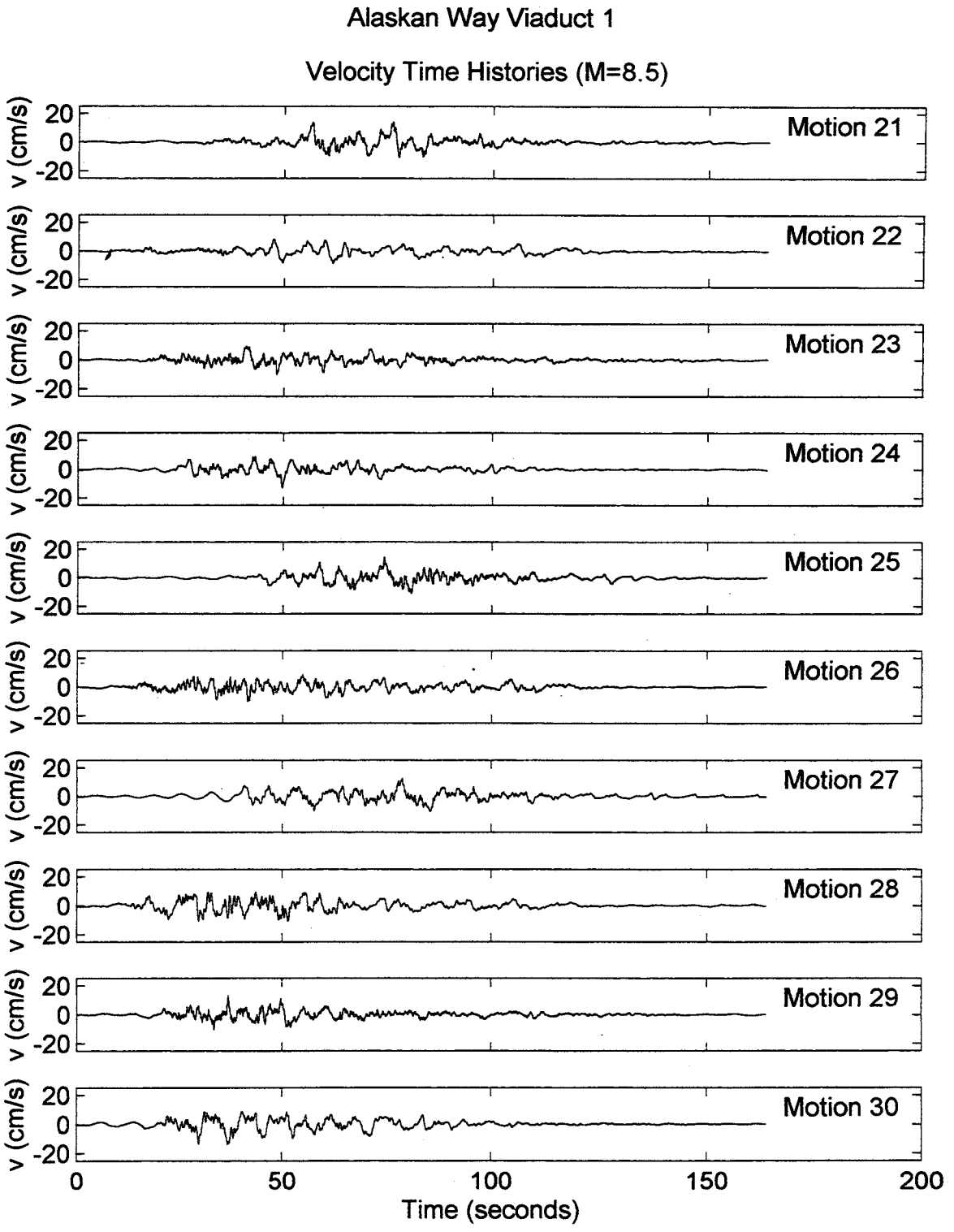

Figure 11. Computed time histories of rock outcrop velocity at Alaskan Way Viaduct site for $M_W = 8.5$ Cascadia subduction zone earthquake (continued).

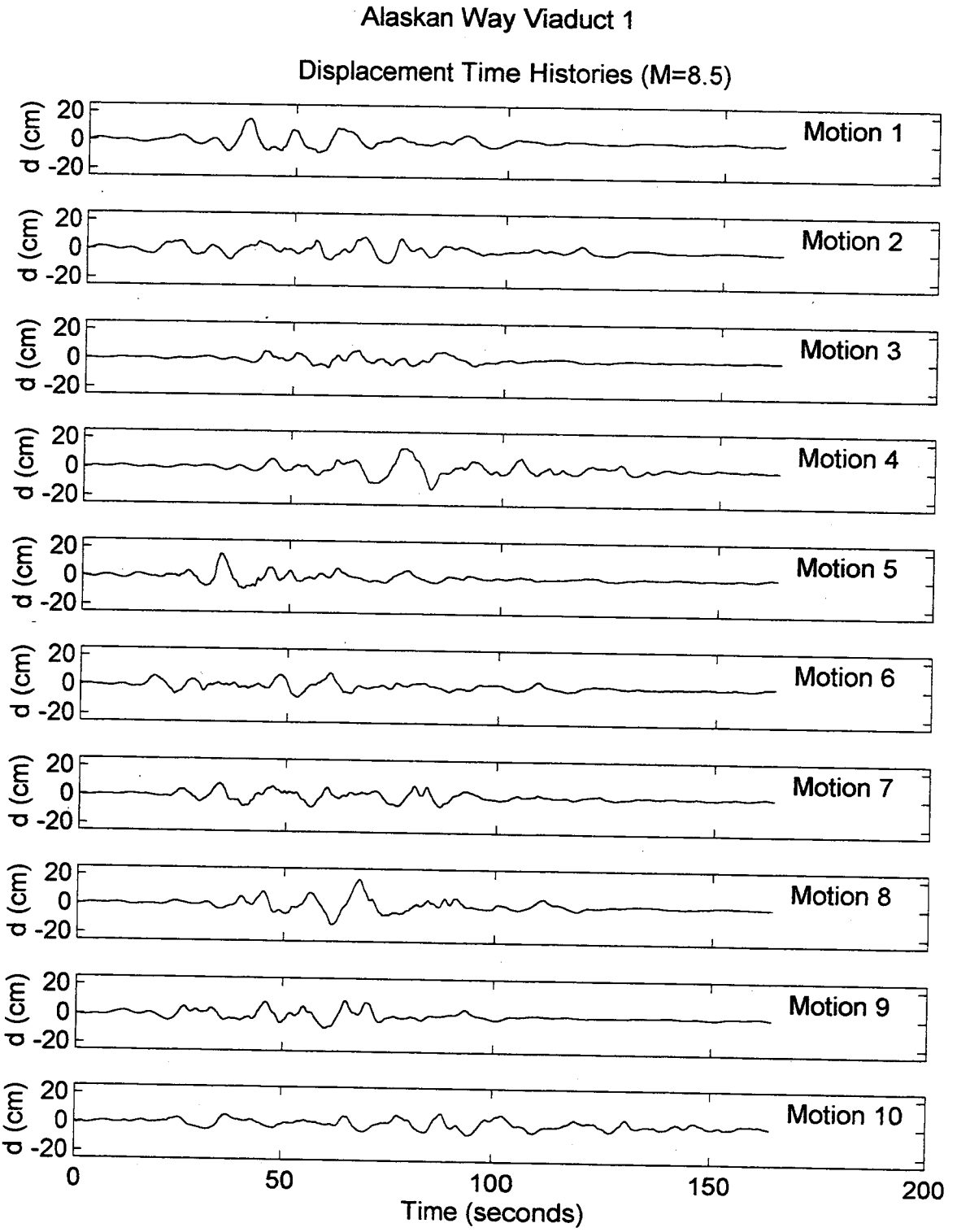

Figure 12. Computed time histories of rock outcrop displacement at Alaskan Way Viaduct site for $M_w = 8.5$ Cascadia subduction zone earthquake.

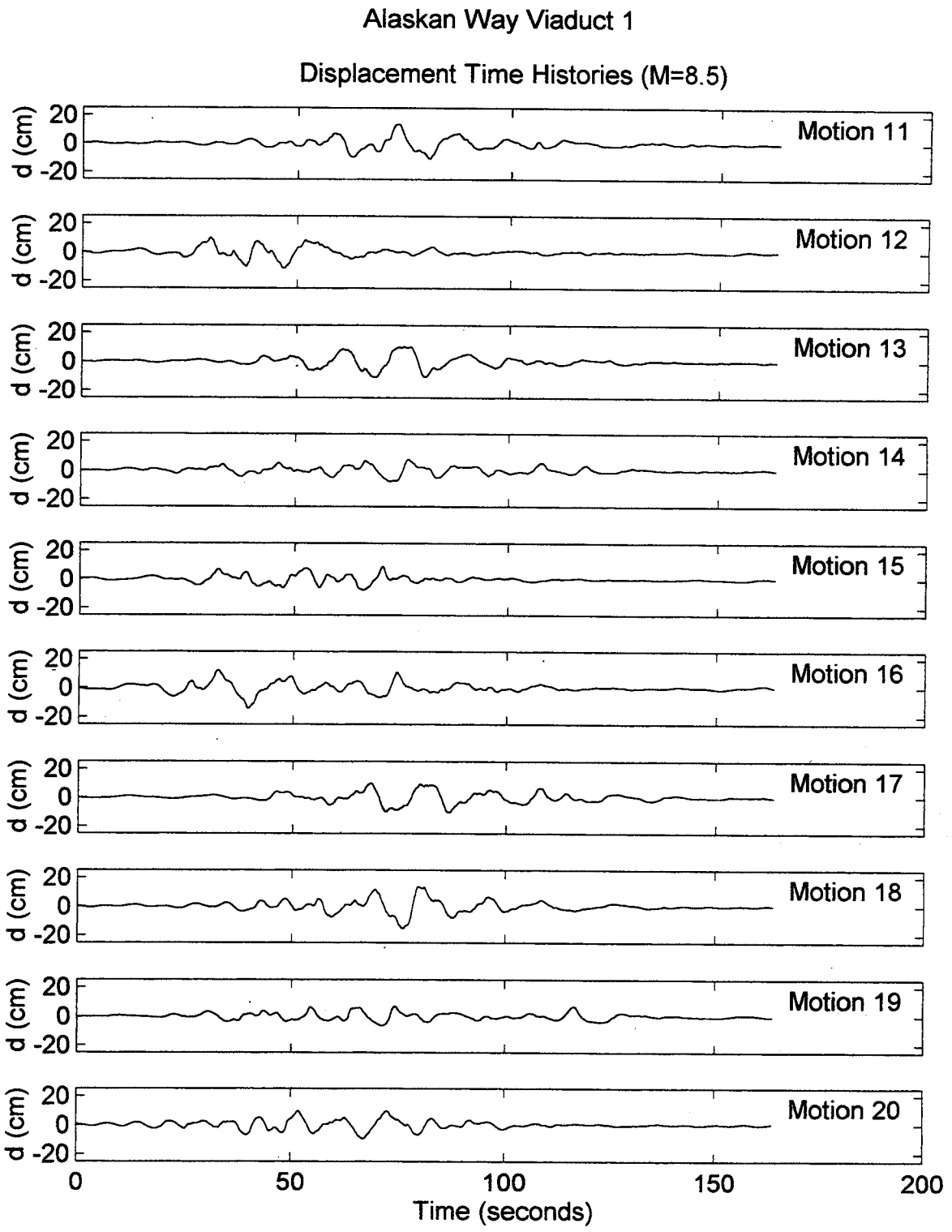

Figure 12. Computed time histories of rock outcrop displacement at Alaskan Way Viaduct site for M_w = 8.5 Cascadia subduction zone earthquake (continued).

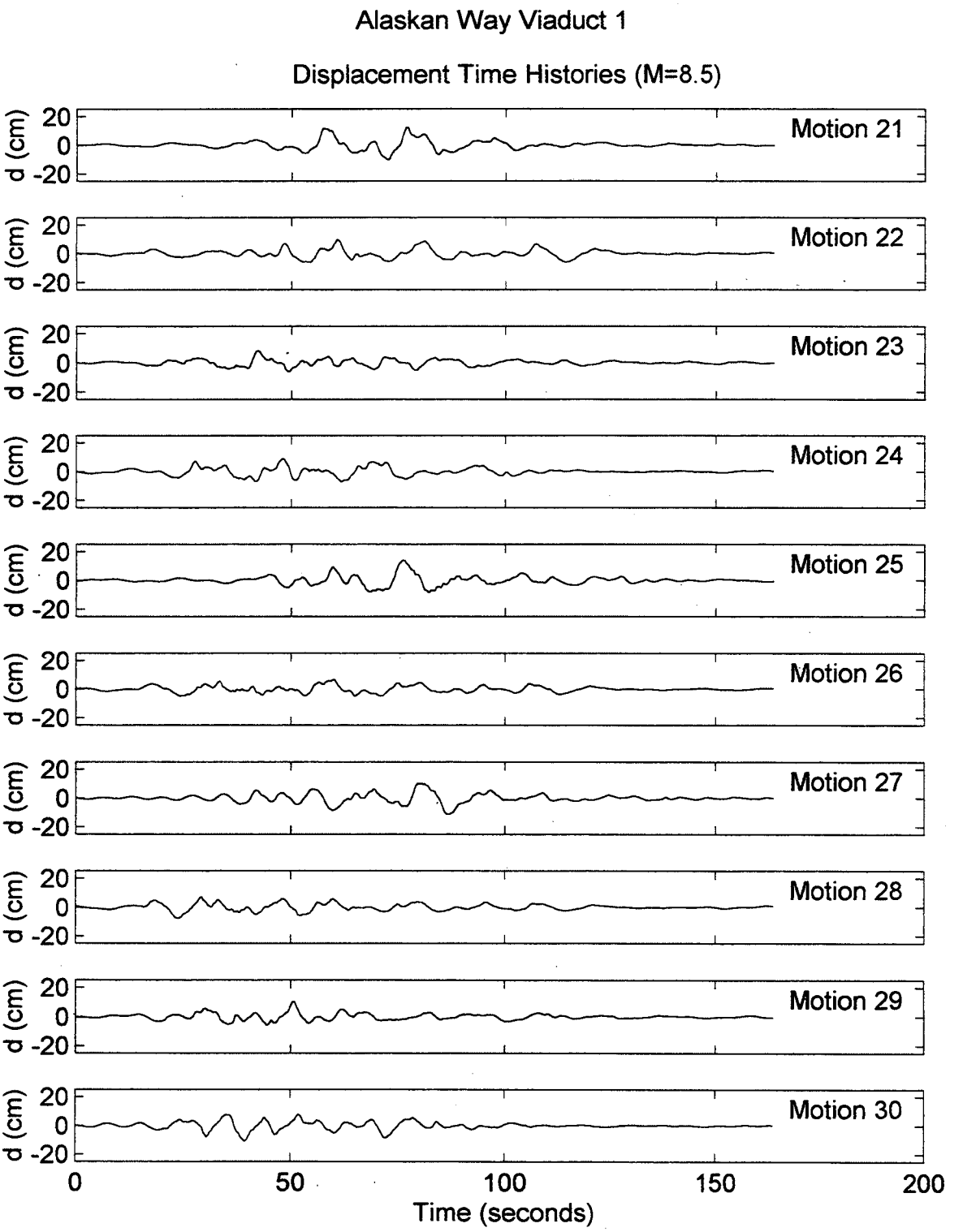

Figure 12. Computed time histories of rock outcrop displacement at Alaskan Way Viaduct site for M_W = 8.5 Cascadia subduction zone earthquake (continued).

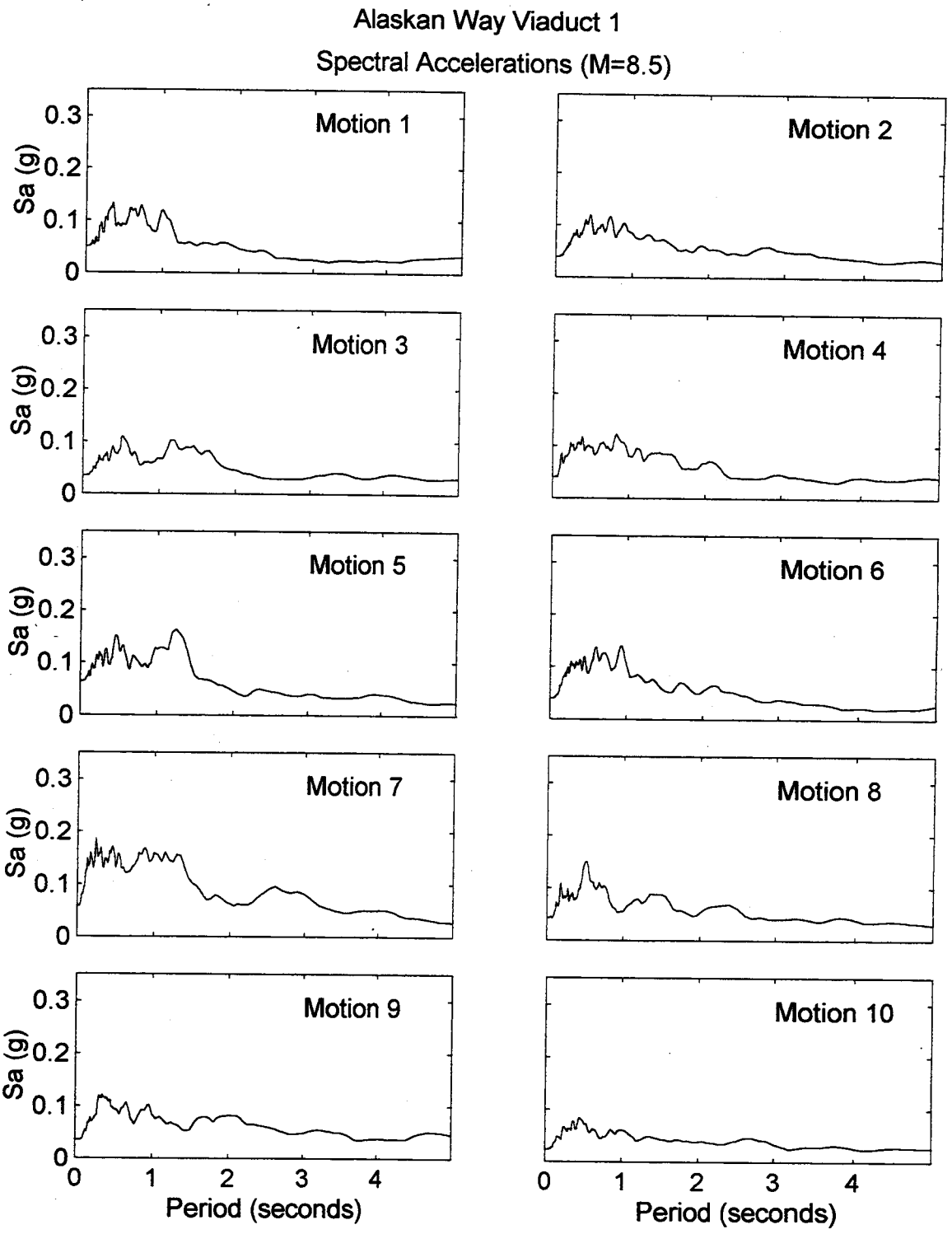

Figure 13. Computed rock outcrop response spectra at Alaskan Way Viaduct site for M_W = 8.5 Cascadia subduction zone earthquake.

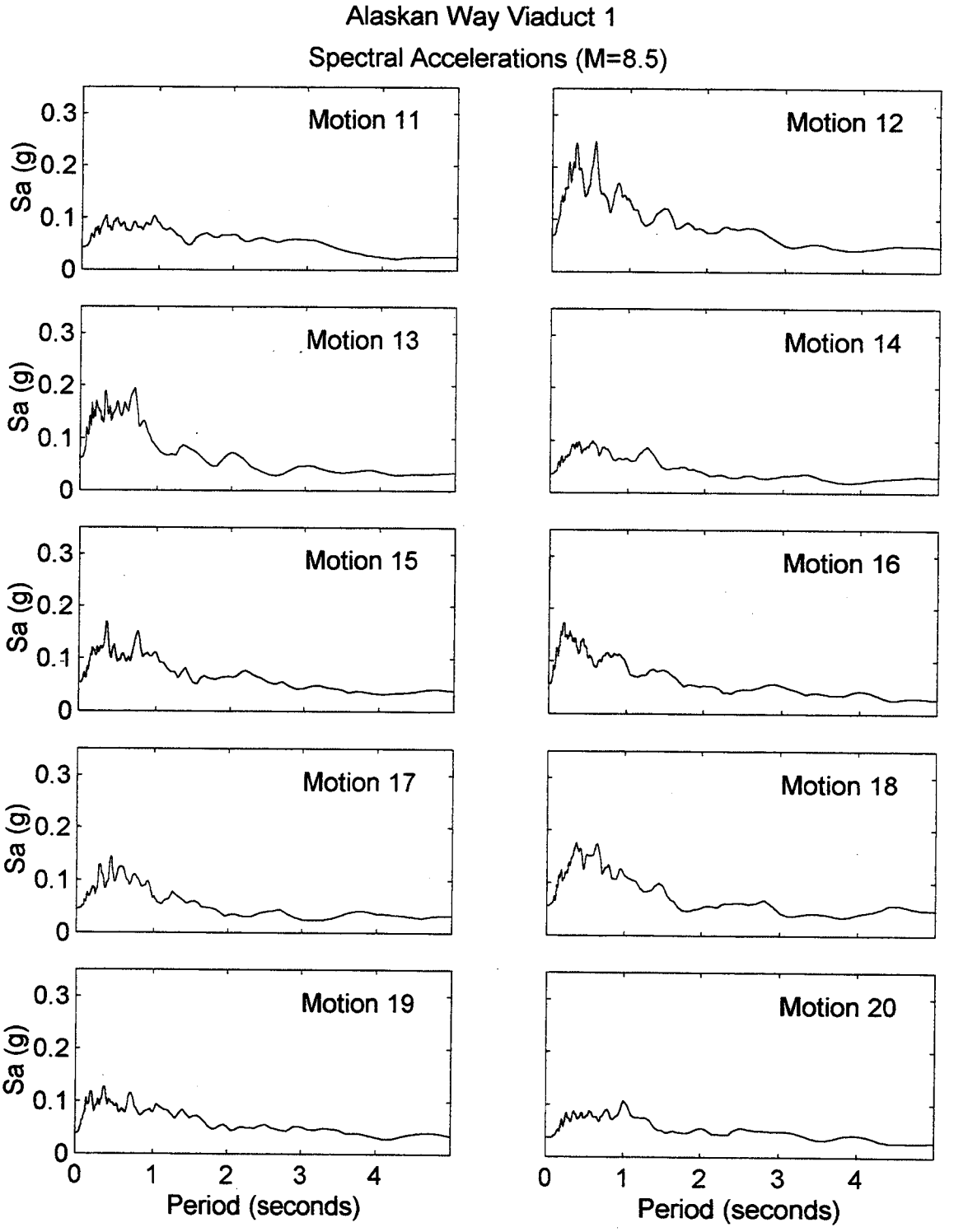

Figure 13. Computed rock outcrop response spectra at Alaskan Way Viaduct site for $M_W = 8.5$ Cascadia subduction zone earthquake (continued).

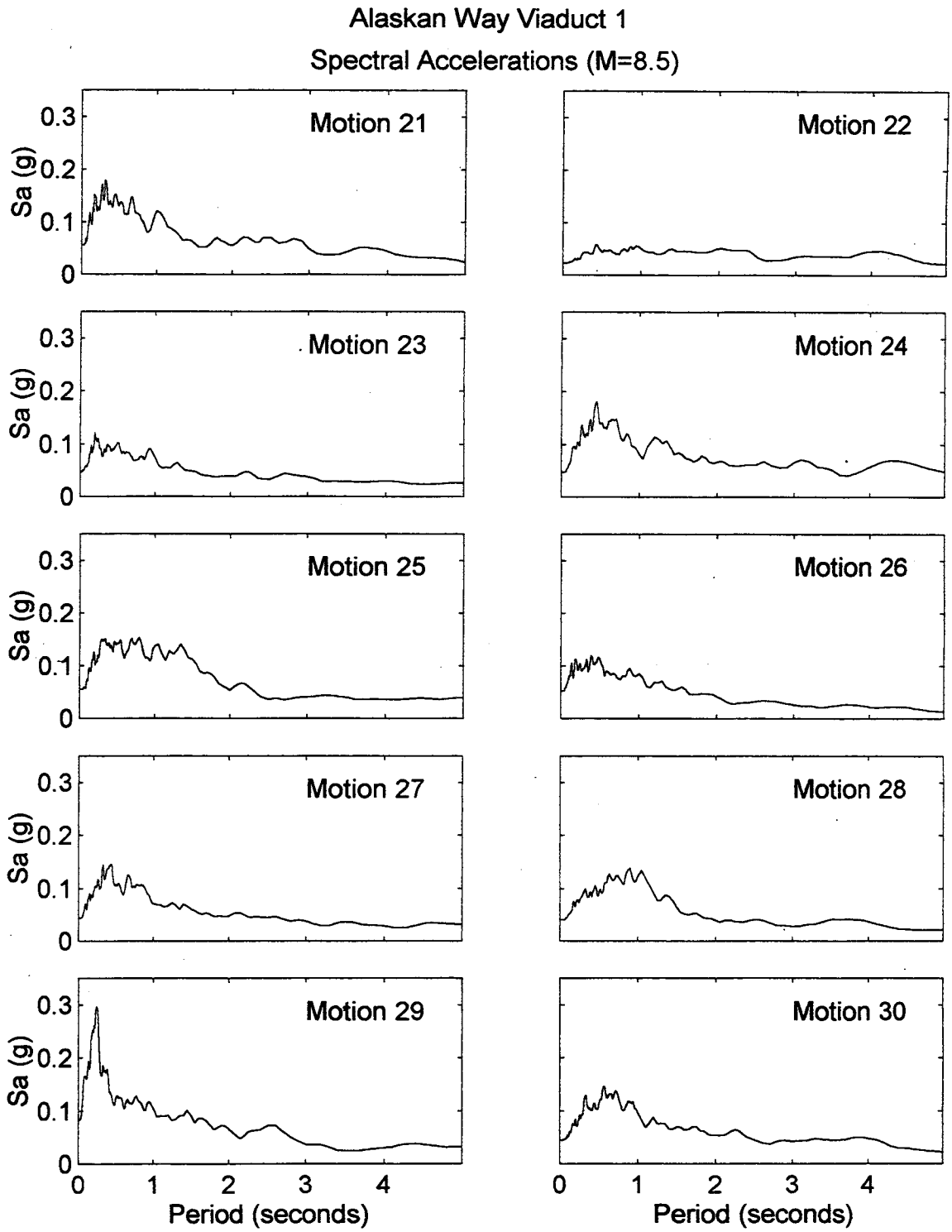

Figure 13. Computed rock outcrop response spectra at Alaskan Way Viaduct site for $M_W = 8.5$ Cascadia subduction zone earthquake (continued).

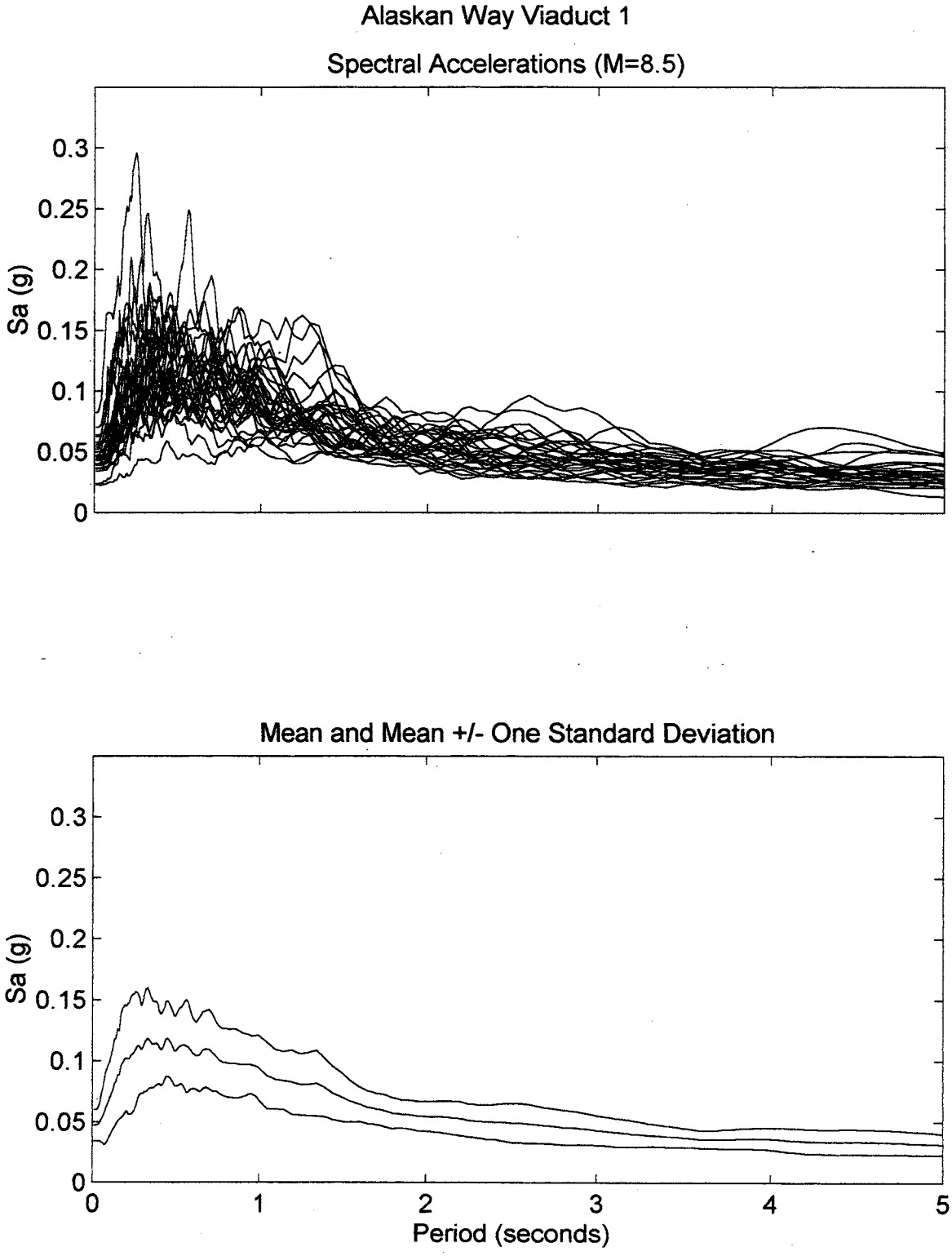

Figure 14. (a) Computed rock outcrop response spectra at Alaskan Way Viaduct site for 30 realizations of the $M_W = 8.5$ Cascadia subduction zone earthquake, and (b) corresponding mean and mean ± one standard deviation rock outcrop response spectra.

Table 4. Computed median (coefficient of variation of ln (a_{max})) of peak rock outcrop accelerations, and USGS- and WSDOT-mapped peak rock outcrop accelerations with 10 percent probability of exceedance in 50 yrs. All accelerations expressed as fractions of gravity.

Site	M_w=8.0	M_w=8.5	M_w=9.0	USGS	Higgins
AWV I	.0315 (-.0650)	.0454 (-.0898)	.0430 (-.1165)	0.321	0.27
AWV II	.0315 (-.0650)	.0454 (-.0898)	.0430 (-.1165)	0.321	0.27
Andresen Rd.	.0143 (.0557)	.0586 (-.1030)	.0750 (-.1229)	0.186	0.16
Bl. Diam. Rd.	.0733 (-.1157)	.0800 (-.1391)	.0776 (-.1742)	0.279	0.16
Bone River	.0541 (-.0908)	.2121 (-.1826)	.1224 (-.1421)	0.272	0.11
Capitol Blvd.	.0383 (-.0797)	.0762 (-.0908)	.0730 (-.1222)	0.259	0.25
Coldwater Cr.	.0186 (-.0650)	.0506 (-.0850)	.0551 (-.1134)	0.192	0.20
I5/NE 99th St.	.0140 (-.0586)	.0581 (-.1040)	.0768 (-.1272)	0.191	0.16
I405/SR522	.0279 (-.0749)	.0401 (-.0830)	.0382 (-.1141)	0.295	0.26
Kent Valley	.0278 (-.0746)	.0442 (-.0794)	.0421 (-.1095)	0.322	0.26
Mercer Slough I	.0278 (-.0723)	.0424 (-.0863)	.0400 (-.1155)	0.325	0.26
Mercer Slough II	.0278 (-.0723)	.0424 (-.0863)	.0400 (-.1155)	0.325	0.26
Nooksack R.	.0229 (-.0756)	.0257 (-.0869)	.0272 (-.1380)	0.201	0.21
N. Ferndale	.0261 (-.0744)	.0304 (-.0906)	.0313 (-.1390)	0.230	0.21
Yakima	.0092 (-.0542)	.0194 (-.0660)	.0206 (-.0857)	0.098	0.10

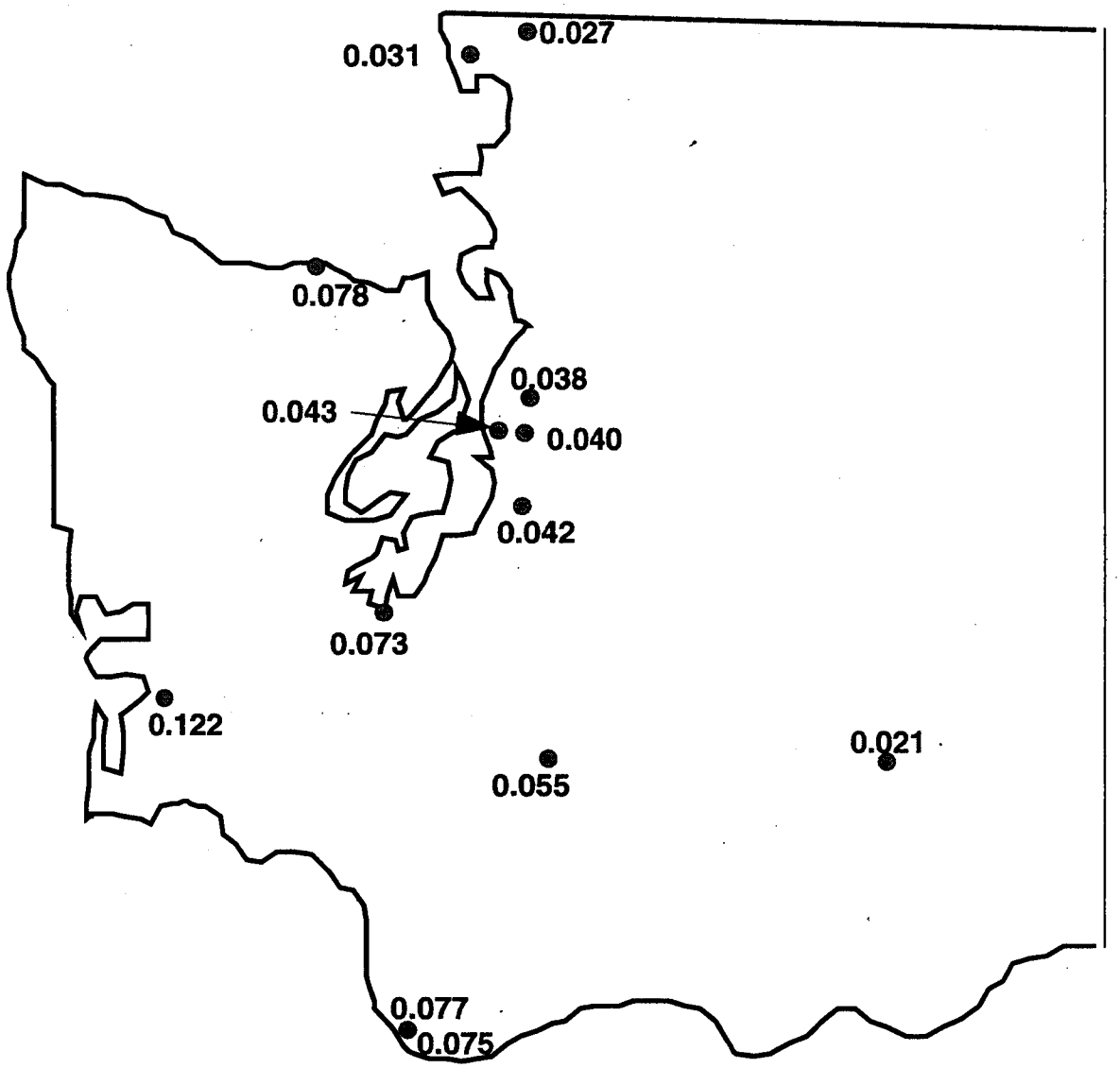

Figure 15. Computed median peak rock outcrop accelerations for M_w=9.0 earthquakes.

the lowest peak accelerations in the M_W=8.0 earthquake because that earthquake was assumed to occur in the northern part of the state. For the M_W=8.5 and M_W=9.0 earthquakes, which would rupture along the entire length of the state, the Andresen Road site would experience much higher peak accelerations.

Table 4 also illustrates the considerable variability in peak acceleration within each group of 30 ground motion simulations. Peak accelerations tend to be lognormally distributed, so the coefficient of variation is taken as $cov = \sigma_{ln(amax)} / \overline{ln_{(amax)}}$. The coefficient of variation for peak acceleration ranged from 20 percent to 29 percent for the M_W=8.0 events, 24 percent to 31 percent for the M_W=8.5 events, and 35 percent to 40 percent for the M_W=9.0 events.

Peak rock outcrop accelerations can also be compared with peak accelerations that have various probabilities of exceedance in a given period of time. Most bridge and building codes implicitly base designs on ground motions that have a 10 percent probability of exceedance in a 50-year period, or a return period of 475 yrs. The U.S. Geological Survey recently released the data upon which its most recent ground motion maps are based, digitized on a grid of 0.1° latitude and longitude. The USGS accelerations correspond to soft rock conditions that are similar to those of the rock outcrop motions computed during this research. The rock outcrop accelerations shown in Table 4 at the ground response analysis sites were significantly smaller than the USGS mapped accelerations, which have a 10 percent probability of exceedance in 50 years. Higgins et al. (1988) developed a seismic zonation map for Washington State that expressed recommended design criteria in terms of velocity-related acceleration coefficients. These coefficients, also shown in Table 4 and labeled as Higgins, are larger than the computed rock outcrop accelerations. These results suggest that current design procedures are conservative with respect to the higher frequency components of Cascadia subduction zone earthquakes. When the ground motion parameters computed in this study are compared with those reported by USGS and Higgins et al. (1988), it is important to recognize that the computer motions correspond to specific Cascadia subduction zone scenario earthquakes. The USGS and Higgins et al. (1988) parameters, on the other hand, consider all significant seismic sources and their respective seismicities. Because Cascadia subduction zone earthquakes occur relatively infrequently, they have little influence on the USGS and Higgins et al. (1988) parameters, which are dominated by events from other sources.

Note also that the M_w=8.5 accelerations exceed the M_w=9.0 accelerations at the three sites (Bone River, Black Diamond, and Capitol Blvd) closest to the Cascadia subduction zone. This apparent anomaly results from the large difference in source lengths for the M_w=8.5 and M_w-9.0 events. Because the M_w=8.5 events all occur adjacent to the state of Washington, all hypocenters are relatively close to these three sites; hence, all 30 simulations produce relatively strong motions. For the M_w=9.0 events, however, hypocenters may be located adjacent to Oregon and northern California as well as Washington. As a result, some of the 30 simulations will represent distant events that lower the median value of acceleration. For the same hypocentral distance, however, the procedures used in this research produce stronger motions for M_w=9.0 than for M_w=8.5 events.

Spectral Accelerations

Response spectra are commonly used to describe the potential effects of earthquake ground motions on structures with different dynamic characteristics. Furthermore, the design of bridges and other structures is often specified in terms of design response spectra in various codes and regulations. Thus, comparison of the response spectra for Cascadia subduction zone earthquakes with commonly used design spectra should offer insight into the relative hazards posed by Cascadia subduction zone earthquakes.

Response spectra were computed for each of the rock outcrop motions generated by the finite source model. Spectral ordinates for each site are presented in Table 5 (T=0.3 sec) and Table 6 (T=1.0 sec). Response spectral ordinates were normally distributed.

As shown in Table 5, the spectral accelerations for T=0.3 sec were generally considerably lower than the USGS values. In only one case, the Bone River site for M_w=9.0, was the T=0.3 sec spectral acceleration from a CSZ earthquake expected to exceed half the corresponding USGS spectral acceleration. At longer periods, spectral accelerations from the CSZ earthquakes were larger relative to the USGS spectral accelerations. As indicated in Table 6, spectral

Table 5. Computed mean (standard deviation) rock outcrop spectral accelerations (T = 0.3 sec) for each ground response site, and USGS spectral acceleration (T = 0.3 sec) values. All accelerations expressed as fractions of gravity.

Site	M_w=8.0	M_w=8.5	M_w=9.0	USGS
AWV I	0.072 (0.31)	0.111 (0.34)	0.046 (2.02)	0.606
AWV II	0.072 (0.31)	0.111 (0.34)	0.046 (2.02)	0.606
Andresen Rd.	0.030 (0.33)	0.142 (0.42)	0.191 (0.39)	0.395
Bl. Diam. Rd.	0.169 (0.34)	0.202 (0.34)	0.209 (0.47)	0.567
Bone River	0.129 (0.29)	0.516 (0.33)	0.316 (0.38)	0.596
Capitol Blvd.	0.087 (0.35)	0.187 (0.25)	0.188 (0.43)	0.507
Coldwater Ck.	0.041 (0.37)	0.115 (0.32)	0.133 (0.32)	0.393
I5/NE 99th St.	0.027 (0.33)	0.140 (0.35)	0.189 (0.40)	0.406
I405/SR522	0.063 (0.37)	0.096 (0.32)	0.096 (0.43)	0.583
Kent Valley	0.063 (0.32)	0.110 (0.35)	0.101 (0.38)	0.605
Mercer Slough I	0.063 (0.30)	0.103 (0.34)	0.095 (0.40)	0.609
Mercer Slough II	0.063 (0.30)	0.103 (0.34)	0.095 (0.40)	0.609
Nooksack R.	0.049 (0.35)	0.061 (0.41)	0.068 (0.54)	0.400
N. Ferndale	0.055 (0.33)	0.071 (0.37)	0.078 (0.53)	0.427
Yakima	0.018 (0.39)	0.041 (0.44)	0.044 (0.45)	0.198

Table 6. Computed mean (standard deviation) rock outcrop spectral accelerations (T = 1.0 sec) for each ground response site, and USGS spectral acceleration (T = 1.0 sec) values. All accelerations expressed as fractions of gravity.

Site	M_w=8.0	M_w=8.5	M_w=9.0	USGS
AWV I	0.050 (0.42)	0.094 (0.29)	0.093 (0.33)	0.212
AWV II	0.050 (0.42)	0.094 (0.29)	0.093 (0.33)	0.212
Andresen Rd.	0.027 (0.22)	0.114 (0.29)	0.151 (0.25)	0.164
Bl. Diam. Rd.	0.105 (0.35)	0.137 (0.34)	0.143 (0.40)	0.224
Bone River	0.079 (0.33)	0.281 (0.26)	0.204 (0.36)	0.274
Capitol Blvd.	0.062 (0.27)	0.144 (0.28)	0.139 (0.30)	0.204
Coldwater Ck.	0.036 (0.31)	0.097 (0.22)	0.115 (0.30)	0.149
I5/NE 99th St.	0.028 (0.29)	0.111 (0.33)	0.146 (0.29)	0.173
I405/SR522	0.048 (0.40)	0.082 (0.28)	0.085 (0.36)	0.206
Kent Valley	0.050 (0.28)	0.090 (0.23)	0.089 (0.29)	0.211
Mercer Slough I	0.048 (0.35)	0.086 (0.31)	0.085 (0.33)	0.213
Mercer Slough II	0.048 (0.35)	0.086 (0.31)	0.085 (0.33)	0.213
Nooksack R.	0.039 (0.33)	0.060 (0.35)	0.064 (0.42)	0.143
N. Ferndale	0.045 (0.29)	0.061 (0.39)	0.070 (0.44)	0.165
Yakima	0.020 (0.40)	0.044 (0.39)	0.049 (0.33)	0.079

accelerations for T=1.0 sec were much closer to the USGS spectral accelerations. At some sites, the mean+σ (mean-plus-one-standard-deviation) values were greater than the USGS values.

Comparison with USGS Ground Motion Parameters

The computed ground motion parameters generally show significantly lower amplitudes than those obtained from recent USGS maps. To understand and properly interpret the relative values from this study and the USGS work, it is important to understand the basis for each type of analysis. The analyses of this study, which have been described in previous portions of this report, fall under the heading of deterministic analyses. The USGS values, on the other hand, were determined through probabilistic seismic hazard analysis (PSHA). The following paragraphs provide a brief description of the basic assumptions and processes of each approach.

Deterministic Approach

The deterministic approach seeks to establish one or more earthquake scenarios and compute the anticipated ground motions corresponding to those scenarios. In a deterministic seismic hazard analysis (DSHA), the scenario is generally described in terms of some magnitude and distance, M and R. In the present study, the different magntiudes were deterministically selected; for each magnitude, 30 different slip models and nucleation points were selected by assuming that earthquakes were equally likely to occur at any location within the source zone. As a result, some of the 30 motions had high slip zones located relatively near the individual sites, and others were located far away.

Probabilistic Approach

The USGS ground motion parameters were obtained from a PSHA. PSHAs attempt to characterize uncertainties in the most significant variables that determine ground motion levels and then use those variables to objectively compute probabilities of exceeding specific ground motion levels. In most PSHAs, including those on which the USGS maps are based, there are three primary sources of uncertainty:

1. **Size**. The size of an earthquake is generally described in terms of magnitude. In a PSHA, historical seismicity data is used to develop a probability distribution, $f_M(m)$, for earthquake magnitude. This is usually a bounded exponential distribution to account for the fact that small earthquakes occur much more frequently than large earthquakes, though other models may also be used.
2. **Location**. The location of an earthquake relative to the site of interest is described in terms of source-to-site distance. This can be measured in different ways, but the measurement is taken to be consistent with that implied by the attenuation relationship used in the analysis. The geometry of the source zone (relative to the site) allows development of a probability distribution, $f_R(r)$, for source-to-site distance.
3. **Effects**. The effects of an earthquake can be described in terms of ground motion parameters, e.g. peak acceleration or spectral acceleration. For a given magnitude and distance (M and R), an attenuation relationship can be used to predict ground motion parameter values. Typical attenuation relationships assume lognormally distributed parameters and therefore predict median parameter values. All attenuation relationships include standard error estimates (referred to as σ-values) which characterize the uncertainty in the predicted parameter. Because the σ-values are obtained from regression analyses involving empirical data from many different earthquakes, they include the effects of two types of uncertainty - intra-event uncertainty (which describes the "scatter" in measured motions from a single event) and inter-event uncertainty (which accounts for scatter resulting from the use of data from different events). Large σ-values denote high uncertainty in parameter prediction as illustrated below.

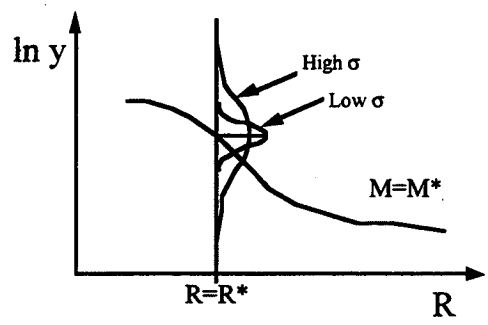

The uncertainty can also be characterized by a ground motion randomness variable, ε, taken as the number of (logarithmic) standard deviations by which the (logarithmic) ground motion exceeds the (logarithmic) mean. Uncertainty in effects can then be characterized by a probability distribution, $f_\varepsilon(\varepsilon)$.

By summing contributions from all possible magnitudes, distances, and ground motion effects, each weighted according to their respective probabilities, the mean annual rate of exceedance (reciprocal of return period) of a given parameter value, y^*, can be computed for a single source as

$$\lambda(y^*) = \nu \iiint P\left[Y > y^* | m,r,\varepsilon\right] f_m(m)\, f_r(r)\, f_\varepsilon(\varepsilon)\, dm\, dr\, d\varepsilon$$

where ν is the total activity rate of the source. Repeating this process for different values of y^* allows development of a seismic hazard curve from which the return period for any value of the ground motion parameter of interest can be determined. The USGS maps have been prepared for return periods of 475 yrs (i.e. 10% probability of exceedance in 50 yrs).

In a PSHA, the annual rate of exceeding a certain ground motion level due to all possible combinations of M, R, and ε are considered. The calculations include the probabilities of each combination of M, R, and ε occurring. For example, the probability of exceeding y^* given the occurrence of a magnitude M^* earthquake occurring at a distance R^* would be given by the area below the probability distributions exceeding y^* in the figure below; clearly the probability is much higher for the high σ curve than for the low σ curve. This illustrates the effect of σ on

ground motion levels in a PSHA - higher σ values lead to higher conditional probabilities and, ultimately, to higher ground motion parameter values for a given return period. The attenuation relationship used to model CSZ subduction events in the USGS PSHA had a σ-value of 0.625, which is quite high because it must reflect the paucity of empirical data on subduction earthquakes in this and other areas.

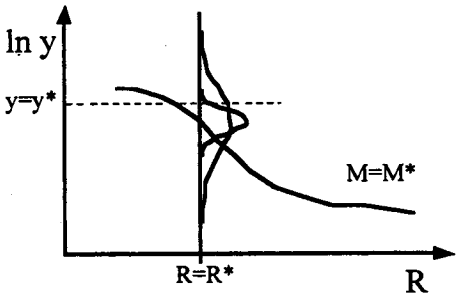

Disaggregation

As a result of the integrative nature of PSHAs, the ground motion parameter value corresponding to a particular return period is not associated with any particular values of *M*, *R*, or ε. Instead, it results from the combined effects of a wide range of possible *M*, *R*, and ε values.

Through the process of disaggregation, however, it is possible to determine the combination of *M*, *R*, and ε that contribute most strongly to the ground motion parameter. USGS has published disaggregations for some of their maps, however, the disaggregations show only the contributions of *M* and *R* (not ε). For example, the USGS PSHA produced a peak acceleration value with a 2% probability of exceedance in 50 years (2,375-year return period) in Aberdeen, Washington of 0.531g. Disaggregation with respect to *M* and *R* shows the relative contribution of various combinations of *M* and *R* to this peak acceleration; the contributions (in percent) are indicated in Table 7. The table clearly shows that the peak acceleration is dominated by events of magnitude 8.0 - 8.5 at distances less than 25 km. The same attenuation relationship used in the USGS mapping project, an average event in this range (i.e. $M = 8.25$, $R = 12.5$ km) produces

Table 7. Disaggregation of USGS mapped value of peak acceleration with 2 percent probability of exceedance in 50 years with respect to magnitude and disturbance.

Distance (km)	Magnitude								
	<5.0	<5.5	<6.0	<6.5	<7.0	<7.5	<8.0	<8.5	<9.0
<25	0.000	0.508	0.487	1.624	0.952	0.000	0.000	67.621	16.759
<50	0.000	0.261	0.306	0.801	0.540	0.000	0.000	4.157	0.000
<75	0.000	0.316	0.432	1.334	0.922	0.000	0.000	0.788	0.000
<100	0.000	0.101	0.168	0.687	0.558	0.000	0.000	0.203	0.000
<125	0.000	0.016	0.033	0.159	0.145	0.000	0.000	0.037	0.000
<150	0.000	0.002	0.004	0.024	0.027	0.000	0.000	0.013	0.000
<175	0.000	0.000	0.000	0.003	0.003	0.000	0.000	0.004	0.000
<200	0.000	0.000	0.000	0.001	0.001	0.000	0.000	0.001	0.000

a median peak acceleration of 0.27 g. This peak acceleration is consistent with the peak accelerations computed in this study *for the same range of magnitude and distance.* The USGS mapped value of 0.531 g, however, corresponds to $\varepsilon = 1.1$ (i.e. is 1.1 logarithmic standard deviations above the logarithmic mean, or median peak acceleration). This occurs because larger magnitude earthquakes tend to contribute more and more as the peak acceleration value in the PSHA progresses toward higher return periods. However, if the magnitude distribution limits the participation of higher magnitude events, the peak acceleration value will be farther from the median peak acceleration for that magnitude (i.e., a greater number of standard deviations from the logarithmic mean). Thus, high ε-values are associated with high peak acceleration values.

Discussion

As the preceding paragraphs indicate, there are several reasons why the computed ground motion parameter values presented in this report do not coincide with those obtained from USGS

maps. As a result, direct comparison of the parameter values is not appropriate. These reasons include:

1. The parameters computed in this research project were obtained from deterministic analyses. For each of three earthquake magnitudes, 30 different slip models and hypocentral locations were assumed prior to ground motion simulation. The PSHA on which the USGS ground motion parameters are based consider thousands of possible earthquake scenarios.
2. The parameters computed in this research project are based on interplate subduction zone earthquakes only. The USGS PSHA included intraplate and crustal sources in addition to the interplate source. The contributions of each of these additional sources tend to increase the PSHA-computed ground motion parameters.
3. The average distance of the 30 realizations of each earthquake magnitude analyzed in this research was considerably larger than the distance associated with the dominant event in the USGS PSHA. This fact tends to decrease the mean values of the computed ground motion parameters relative to the USGS mapped parameters.
4. The USGS PSHA results are strongly dependent upon the large standard error in the attenuation relationship used in those analyses. This standard error includes contributions from both intra-event and inter-event uncertainties. The deterministic analyses conducted in this research represent intra-event uncertainties in an approximate way and do not include inter-event uncertainties.
5. The USGS mapped parameter values implicitly include the large uncertainty in ground motion effects that exists for subduction earthquakes. Though ε-values were not de-aggregated by USGS, the mapped peak acceleration values appear to be more than one (large) standard deviation above the (logarithmic) mean values.

It is important to recognize that the ground motion parameters computed by the deterministic simulations described in this report are consistent with the attenuation relationship that forms the backbone of the USGS PSHA.

GROUND SURFACE MOTIONS

The characteristics of earthquake ground surface motions are strongly influenced by the nature of the local soil conditions. Soil deposits can amplify, or de-amplify, different components of an earthquake motion and thereby produce motions with characteristics that are significantly different than the motions that would be observed at a rock outcrop. The computed ground surface motions at sites with the previously discussed soil conditions are described in the following sections. These motions reflect the locations of the sites, as did the previously described rock outcrop motions, but also reflect the effects of the soil conditions at each site.

Peak Acceleration

Peak ground surface accelerations may be amplified or de-amplified by local soil deposits. The nature of the amplification depends on the thickness and stiffness of the soil deposit, and on the characteristics of the input motion. Computed peak acceleration values for the soil profiles analyzed in this investigation are summarized in Table 8.

The computed peak ground surface accelerations reflected the amplification characteristics of the individual soil profiles. Peak ground surface accelerations were generally greater than the previously described peak rock outcrop accelerations by an amount that varied for each soil profile. However, the peak ground surface accelerations remained relatively low.

Spectral Accelerations

Spectral accelerations may be particularly sensitive to local soil conditions. The results of the ground response analyses were used to compute spectral accelerations (5 percent damping) for periods of 0.3 sec and 1.0 sec. Computed spectral acceleration values for the soil profiles analyzed in this investigation are presented in Tables 9 and 10. Spectral accelerations were observed to be normally distributed.

Table 8. Computed median (coefficient of variation of ln (a_{max})) peak ground surface accelerations for each ground response profile. All accelerations expressed as fractions of gravity.

	Equivalent Linear Analysis			Nonlinear Analysis		
Name	M_w=8.0	M_w=8.5	M_w=9.0	M_w=8.0	M_w=8.5	M_w=9.0
AWV I	0.062 (-0.081)	0.081 (-0.137)	0.078 (-0.154)	0.109 (-0.095)	0.149 (-0.124)	0.146 (-0.137)
AWV II	0.045 (-0.066)	0.058 (-0.052)	0.057 (-0.065)	0.062 (-0.058)	0.084 (-0.081)	0.083 (-0.088)
Andresen Rd.	0.027 (-0.101)	0.106 (-0.139)	0.133 (-0.141)	0.040 (-0.082)	0.124 (-0.098)	0.148 (-0.090)
Bl. Diam. Rd.	0.072 (-0.083)	0.077 (-0.090)	0.074 (-0.121)	0.088 (-0.067)	0.100 (-0.098)	0.103 (-0.119)
Bone River	0.039 (-0.034)	0.037 (-0.028)	0.040 (-0.047)	0.044 (-0.075)	0.108 (-0.103)	0.063 (-0.101)
Capitol Blvd.	0.066 (-0.117)	0.120 (-0.086)	0.116 (-0.124)	0.099 (-0.079)	0.154 (-0.076)	0.154 (-0.083)
Coldwater Cr.	0.034 (-0.114)	0.088 (-0.086)	0.100 (-0.117)	0.045 (-0.074)	0.092 (-0.065)	0.096 (-0.071)
I5/NE 99th St.	0.045 (-0.067)	0.080 (-0.059)	0.080 (-0.058)	0.041 (-0.076)	0.128 (-0.092)	0.152 (-0.083)
I405/SR522	0.039 (-0.071)	0.052 (-0.080)	0.052 (-0.098)	0.044 (-0.054)	0.061 (-0.069)	0.055 (-0.076)
Kent Valley	0.042 (-0.073)	0.063 (-0.070)	0.062 (-0.093)	0.058 (-0.059)	0.081 (-0.064)	0.076 (-0.085)
Mercer Slough I	0.025 (-0.073)	0.034 (-0.064)	0.028 (-0.076)	0.076 (-0.059)	0.068 (-0.048)	0.067 (-0.093)
Mercer Slough II	0.018 (-0.063)	0.025 (-0.045)	0.020 (-0.066)	0.074 (-0.056)	0.093 (-0.053)	0.085 (-0.099)
Nooksack R.	0.045 (-0.069)	0.051 (-0.074)	0.053 (-0.113)	0.063 (-0.094)	0.071 (-0.068)	0.070 (-0.128)
N. Ferndale	0.039 (-0.072)	0.045 (-0.081)	0.044 (-0.112)	0.054 (-0.051)	0.061 (-0.067)	0.063 (-0.089)
Yakima	0.012 (-0.081)	0.027 (-0.104)	0.028 (-0.110)	0.024 (-0.103)	0.048 (-0.127)	0.051 (-0.126)

Table 9. Computed mean (standard deviation) ground surface spectral accelerations (T = 0.3 sec) for each ground response site. All accelerations expressed as fractions of gravity.

	Equivalent Linear Analysis			Nonlinear Analysis		
Site	M_w=8.0	M_w=8.5	M_w=9.0	M_w=8.0	M_w=8.5	M_w=9.0
AWV I	0.137 (0.310)	0.205 (0.400)	0.195 (0.520)	0.211 (0.327)	0.302 (0.348)	0.318 (0.431)
AWV II	0.066 (0.260)	0.085 (0.140)	0.080 (0.230)	0.113 (0.283)	0.157 (0.204)	0.158 (0.266)
Andresen Rd.	0.056 (0.340)	0.198 (0.340)	0.271 (0.320)	0.059 (0.220)	0.192 (0.297)	0.247 (0.312)
Bl. Diam. Rd.	0.128 (0.200)	0.140 (0.240)	0.145 (0.340)	0.148 (0.196)	0.167 (0.222)	0.169 (0.254)
Bone River	0.071 (0.350)	0.039 (0.100)	0.059 (0.440)	0.066 (0.182)	0.167 (0.299)	0.096 (0.219)
Capitol Blvd.	0.182 (0.390)	0.311 (0.210)	0.315 (0.290)	0.199 (0.231)	0.326 (0.181)	0.324 (0.247)
Coldwater Cr.	0.068 (0.380)	0.170 (0.300)	0.192 (0.280)	0.103 (0.330)	0.197 (0.213)	0.227 (0.225)
I5/NE 99th St.	0.102 (0.210)	0.132 (0.300)	0.114 (0.290)	0.076 (0.250)	0.228 (0.206)	0.266 (0.192)
I405/SR522	0.062 (0.210)	0.077 (0.230)	0.077 (0.210)	0.080 (0.238)	0.096 (0.167)	0.099 (0.222)
Kent Valley	0.103 (0.230)	0.144 (0.280)	0.140 (0.260)	0.113 (0.212)	0.145 (0.200)	0.156 (0.231)
Mercer Slough I	0.026 (0.270)	0.035 (0.230)	0.030 (0.230)	0.079 (0.165)	0.073 (0.151)	0.073 (0.233)
Mercer Slough II	0.019 (0.260)	0.026 (0.190)	0.021 (0.240)	0.078 (0.167)	0.097 (0.134)	0.092 (0.207)
Nooksack R.	0.046 (0.240)	0.052 (0.210)	0.051 (0.270)	0.078 (0.167)	0.086 (0.209)	0.091 (0.264)
N. Ferndale	0.069 (0.190)	0.076 (0.210)	0.082 (0.270)	0.055 (0.200)	0.060 (0.183)	0.060 (0.250)
Yakima	0.034 (0.530)	0.085 (0.050)	0.095 (0.560)	0.116 (0.414)	0.234 (0.380)	0.249 (0.329)

Table 10. Computed mean (standard deviation) ground surface spectral accelerations (T = 1.0 sec) for each ground response site. All accelerations expressed as fractions of gravity.

	Equivalent Linear Analysis			Nonlinear Analysis		
Site	M_w=8.0	M_w=8.5	M_w=9.0	M_w=8.0	M_w=8.5	M_w=9.0
AWV I	0.073 (0.260)	0.116 (0.330)	0.122 (0.370)	0.138 (0.413)	0.262 (0.305)	0.267 (0.393)
AWV II	0.159 (0.270)	0.185 (0.190)	0.187 (0.210)	0.159 (0.201)	0.218 (0.133)	0.220 (0.141)
Andresen Rd.	0.040 (0.350)	0.172 (0.330)	0.254 (0.330)	0.043 (0.256)	0.231 (0.346)	0.321 (0.280)
Bl. Diam. Rd.	0.165 (0.220)	0.201 (0.190)	0.270 (0.210)	0.124 (0.161)	0.136 (0.169)	0.143 (0.210)
Bone River	0.072 (0.290)	0.050 (0.200)	0.086 (0.300)	0.058 (0.190)	0.122 (0.172)	0.096 (0.146)
Capitol Blvd.	0.129 (0.350)	0.302 (0.270)	0.301 (0.300)	0.239 (0.155)	0.347 (0.135)	0.339 (0.159)
Coldwater Cr.	0.053 (0.430)	0.154 (0.270)	0.188 (0.350)	0.106 (0.340)	0.280 (0.175)	0.307 (0.244)
I5/NE 99th St.	0.052 (0.420)	0.200 (0.270)	0.190 (0.220)	0.041 (0.268)	0.244 (0.398)	0.331 (0.323)
I405/SR522	0.096 (0.390)	0.137 (0.260)	0.152 (0.340)	0.077 (0.247)	0.119 (0.218)	0.125 (0.240)
Kent Valley	0.088 (0.270)	0.131 (0.210)	0.138 (0.250)	0.080 (0.213)	0.124 (0.202)	0.123 (0.220)
Mercer Slough I	0.044 (0.180)	0.056 (0.200)	0.057 (0.280)	0.138 (0.145)	0.105 (0.152)	0.106 (0.226)
Mercer Slough II	0.031 (0.230)	0.038 (0.240)	0.038 (0.290)	0.123 (0.211)	0.159 (0.176)	0.144 (0.236)
Nooksack R.	0.100 (0.220)	0.114 (0.200)	0.117 (0.220)	0.142 (0.197)	0.167 (0.174)	0.186 (0.194)
N. Ferndale	0.135 (0.210)	0.155 (0.250)	0.174 (0.250)	0.079 (0.215)	0.089 (0.191)	0.097 (0.227)
Yakima	0.021 (0.330)	0.046 (0.350)	0.052 (0.310)	0.023 (0.391)	0.050 (0.380)	0.057 (0.333)

The computed ground surface spectral acclerations were both higher and lower than the corresponding bedrock spectral accelerations, depending on the amplification characteristics of the individual sites. At all sites, the T=0.3 sec spectral accelerations were significantly smaller than the USGS rock spectra. At a number of sites, however, the T=1.0 sec spectral accelerations for the M_w=8.5 and M_w=9.0 events were greater than the USGS rock spectral accelerations.

Computed response spectra with mean and mean ± one standard deviation spectra are presented for all profiles and all scenario earthquakes in Appendices C (equivalent linear) and D (nonlinear). Examination of the shapes of these spectra further verified the strong low-frequency (long period) components of the Cascadia subduction earthquakes. When normalized by peak acceleration, these spectra have very different shapes than the normalized spectra found in various codes.

Peak Velocity

The peak velocity of an earthquake ground motion is simply defined as the maximum absolute value of ground surface velocity. The use of peak velocity as a measure of ground motion amplitude is becoming increasingly common in earthquake engineering practice. It provides a good description of the amplitude of the intermediate frequency components of a ground motion. Computed peak velocity values for the soil profiles analyzed in this investigation are summarized in Table 11.

Peak ground surface velocity maps were not available, so comparison of the computed peak velocities from CSZ motions with other peak velocities was not straightforward. A general comparison could be made, however, by considering the peak velocites that would be expected from likely earthquakes in various parts of the state. The size and location of likely earthquakes could not be predicted with certainty, but deaggregated probabilistic seismic hazard analyses could be used to identify combinations of earthquake magnitude and distance that would produce the strongest contribution to seismic hazard at a particular location. Using USGS published deaggregation data (**http://geohazards.cr.usgs.gov:80/eq/html/deagg.shtml**) with common

predictive relationships allowed evaluation of ground motion parameters for likely earthquakes in different areas. The peak horizontal velocity predictive relationship of Joyner and Boore (1988) produced median peak velocities of 17 cm/sec, 30 cm/sec, and 30 cm/sec for Bellingham, Seattle, and Vancouver, respectively. The peak velocities from the CSZ motions were much closer to these peak velocities than the peak accelerations were to the USGS peak accelerations, further illustrating the relative strength of the lower frequency components of the CSZ motions. It is important to note that such comparisons were between hypothetical events that may have very different likelihoods of occurrence.

Duration

Large magnitude earthquakes are well known to produce ground motions of long duration. Consequently, great earthquakes on the Cascadia subduction zone would be expected to produce ground motions of significantly greater duration than shallow crustal earthquakes or deep intraplate earthquakes. Estimation of the duration of ground motions from subduction zone earthquakes was an important part of the research described in this report.

Ground motion duration can be characterized by absolute or relative measures. For earthquake engineering purposes, strong motion duration is most commonly characterized by the bracketed duration (Bolt, 1969), defined as the time between the first and last absolute exceedances of a threshold acceleration, usually taken to be 0.05g. Duration can also be characterized in a relative sense; this is most commonly accomplished with the Trifunac duration (Trifunac and Brady, 1975), defined as the period between which 5 percent and 95 percent of the integral of squared accelerations occur. The bracketed duration will have a value of zero for ground motions that do not exceed 0.05 g, but non-zero Trifunac durations can computed for any ground motion.

Bracketed durations and Trifunac durations are given below in Tables 12 and 13, respectively, for each of the ground response profiles. Durations computed from the nonlinear analyses are greater than those from the equivalent linear analyses as a result of the well known

Table 11. Computed median (coefficient of variation of ln (v_{max})) peak ground surface velocities in cm/sec for each ground response site.

	Equivalent Linear Analysis			Nonlinear Analysis		
Site	M_w=8.0	M_w=8.5	M_w=9.0	M_w=8.0	M_w=8.5	M_w=9.0
AWV I	8.763 (0.127)	13.759 (0.096)	11.548 (0.122)	11.586 (0.113)	18.298 (0.084)	16.515 (0.101)
AWV II	10.589 (0.111)	15.642 (0.082)	14.095 (0.110)	11.712 (0.107)	18.358 (0.081)	16.359 (0.102)
Andresen Rd.	5.187 (0.185)	15.917 (0.782)	19.893 (0.089)	5.553 (0.124)	17.181 (0.070)	20.680 (0.083)
Bl. Diam. Rd.	18.047 (0.123)	18.419 (0.089)	18.035 (0.127)	18.607 (0.088)	20.331 (0.099)	19.186 (0.127)
Bone River	15.651 (0.094)	29.798 (0.069)	21.154 (0.178)	17.400 (0.109)	48.321 (0.070)	26.050 (0.101)
Capitol Blvd.	11.339 (0.105)	20.325 (0.069)	18.613 (0.096)	14.462 (0.081)	25.766 (0.069)	23.742 (0.070)
Coldwater Cr.	6.038 (0.156)	15.327 (0.081)	15.007 (0.106)	8.173 (0.104)	17.783 (0.068)	17.484 (0.084)
I5/NE 99th St.	6.184 (0.152)	19.073 (0.082)	20.489 (0.063)	5.583 (0.118)	18.960 (0.090)	21.843 (0.088)
I405/SR522	12.405 (0.114)	17.399 (0.084)	15.086 (0.112)	15.325 (0.100)	21.789 (0.080)	18.951 (0.094)
Kent Valley	9.266 (0.134)	15.880 (0.070)	13.828 (0.113)	13.559 (0.088)	20.201 (0.070)	17.243 (0.098)
Mercer Slough I	14.882 (0.095)	22.192 (0.081)	18.642 (0.085)	37.800 (0.064)	43.927 (0.048)	38.869 (0.086)
Mercer Slough II	12.159 (0.111)	20.887 (0.085)	16.911 (0.099)	39.256 (0.051)	57.497 (0.053)	49.081 (0.082)
Nooksack R.	14.705 (0.126)	18.372 (0.106)	15.297 (0.163)	22.328 (0.076)	25.065 (0.074)	22.735 (0.122)
N. Ferndale	10.361 (0.113)	12.731 (0.108)	12.859 (0.174)	12.887 (0.089)	15.308 (0.079)	15.472 (0.136)
Yakima	3.595 (0.257)	6.994 (0.135)	6.642 (0.160)	3.945 (0.198)	7.596 (0.130)	7.211 (0.149)

Table 12. Computed median (coefficient of variation of ln (duration)) bracketed durations in seconds for each ground response site.

	Equivalent Linear Analysis			Nonlinear Analysis		
Site	M_w=8.0	M_w=8.5	M_w=9.0	M_w=8.0	M_w=8.5	M_w=9.0
AWV I	5.207 (0.806)	24.271 (0.321)	31.111 (0.474)	31.023 (0.069)	66.906 (0.056)	108.549 (0.077)
AWV II	0.093 (-0.096)	3.840 (1.047)	4.607 (1.141)	12.119 (0.371)	46.327 (0.197)	71.355 (0.213)
Andresen Rd.	0.045 (-0.074)	39.556 (0.139)	98.847 (0.070)	0.232 (-0.479)	61.388 (0.083)	143.304 (0.047)
Bl. Diam. Rd.	6.932 (0.481)	15.687 (0.389)	23.602 (0.443)	26.045 (0.114)	46.370 (0.087)	69.129 (0.210)
Bone River	0.013 (-0.001)	0.000 (0.000)	0.005 (-0.003)	0.262 (-0.457)	43.021 (0.088)	13.787 (0.703)
Capitol Blvd.	5.824 (0.736)	54.506 (0.060)	78.033 (0.093)	30.342 (0.082)	85.516 (0.037)	138.093 (0.048)
Coldwater Cr.	0.245 (-0.468)	35.228 (0.114)	50.525 (0.282)	0.477 (-1.034)	57.346 (0.058)	92.874 (0.115)
I5/NE 99th St.	0.181 (-0.236)	24.877 (0.269)	49.774 (0.180)	0.166 (-0.294)	64.935 (0.075)	150.213 (0.046)
I405/SR522	0.066 (-0.101)	1.313 (4.208)	4.237 (1.176)	0.131 (-0.223)	4.509 (0.887)	8.300 (0.913)
Kent Valley	0.162 (-0.259)	8.859 (0.596)	12.730 (0.690)	3.101 (1.210)	38.220 (0.199)	53.662 (0.301)
Mercer Slough I	0.000 (0.000)	0.000 (0.000)	0.000 (0.000)	22.322 (0.163)	25.044 (0.248)	28.236 (0.474)
Mercer Slough II	0.000 (0.000)	0.000 (0.000)	0.000 (0.000)	18.589 (0.228)	51.233 (0.078)	66.843 (0.284)
Nooksack R.	0.126 (-0.199)	0.469 (-0.964)	0.768 (-4.201)	3.930 (0.920)	16.024 (0.431)	18.775 (0.590)
N. Ferndale	0.138 (-0.207)	1.355 (3.568)	5.197 (1.049)	2.134 (1.686)	6.466 (0.824)	15.685 (0.691)
Yakima	0.000 (0.000)	0.034 (-0.051)	0.272 (-0.692)	0.000 (0.000)	2.402 (1.863)	4.835 (1.263)

Table 13. Computed median (coefficient of variation of ln (duration)) Trifunac durations in seconds for each ground response site.

	Equivalent Linear Analysis			Nonlinear Analysis		
Site	M_w=8.0	M_w=8.5	M_w=9.0	M_w=8.0	M_w=8.5	M_w=9.0
AWV I	32.21 (0.056)	60.15 (0.055)	102.65 (0.056)	37.09 (0.038)	70.20 (0.051)	119.12 (0.050)
AWV II	31.60 (0.060)	62.84 (0.054)	112.08 (0.060)	40.43 (0.039)	80.19 (0.044)	142.67 (0.046)
Andresen Rd.	30.44 (0.078)	59.82 (0.060)	122.15 (0.042)	35.23 (0.057)	70.24 (0.054)	145.93 (0.030)
Bl. Diam. Rd.	31.78 (0.055)	54.39 (0.083)	92.96 (0.071)	38.97 (0.055)	72.36 (0.068)	120.28 (0.058)
Bone River	29.45 (0.081)	58.81 (0.071)	127.40 (0.048)	36.29 (0.057)	78.69 (0.037)	158.18 (0.040)
Capitol Blvd.	31.73 (0.068)	62.47 (0.041)	106.87 (0.047)	39.02 (0.043)	78.16 (0.032)	135.35 (0.042)
Coldwater Cr.	31.17 (0.075)	63.09 (0.044)	119.46 (0.045)	35.44 (0.052)	74.27 (0.035)	148.99 (0.033)
I5/NE 99th St.	31.22 (0.075)	60.72 (0.063)	133.99 (0.034)	35.22 (0.055)	65.75 (0.056)	135.64 (0.035)
I405/SR522	32.17 (0.066)	61.67 (0.054)	118.58 (0.061)	40.13 (0.038)	77.28 (0.041)	147.71 (0.049)
Kent Valley	32.97 (0.058)	62.48 (0.049)	112.76 (0.056)	39.96 (0.039)	77.14 (0.039)	147.07 (0.046)
Mercer Slough I	34.15 (0.065)	64.31 (0.045)	133.87 (0.061)	36.87 (0.052)	74.57 (0.036)	147.75 (0.053)
Mercer Slough II	35.98 (0.058)	64.63 (0.048)	139.69 (0.058)	36.31 (0.046)	72.67 (0.038)	147.07 (0.054)
Nooksack R.	32.22 (0.068)	56.47 (0.081)	108.60 (0.082)	38.44 (0.060)	72.68 (0.061)	145.32 (0.062)
N. Ferndale	31.22 (0.073)	56.86 (0.084)	101.41 (0.071)	39.63 (0.056)	75.32 (0.062)	140.04 (0.059)
Yakima	33.31 (0.059)	64.09 (0.040)	137.03 (0.044)	47.51 (0.052)	72.91 (0.034)	148.22 (0.036)

tendency of equivalent linear analyses to overdamp the low-amplitude portions of ground motions. Because a large portion of the computer CSZ motions had relatively low amplitudes, the differences between the computed durations are significant.

Duration is the CSZ ground motion characteristic that is most distinctive with respect to the characteristics implicit in current seismic design requirements. Because great CSZ earthquakes involve rupture over very long distances, ground shaking is expected to continue for a very long period. This characteristic of CSZ earthquakes is reflected in the long bracketed durations listed in Table 12. At some of the soft sites, e.g., Mercer Slough and I405/522, ground surface accelerations were so low that the 0.05g threshold acceleration upon which bracketed duration was based was not exceeded or was exceeded by only a single pulse. However, these sites would experience low amplitude shaking that might last for very long durations, as indicated by the Trifunac durations shown in Table 13. Trifunac durations were on the order of 30 to 35 sec for M_w=8.0 events, 60 to 65 sec for M_w=8.5 events, and 85 to 105 sec for M_w=9.0 events.

On the basis of USGS deaggregation data and the predictive relationship of Chang and Krinitszky (1977), bracketed durations for likely earthquakes in Bellingham, Seattle, and Olympia are 20 sec, 27 sec, and 27 sec, respectively. Computed CSZ ground motion durations were significantly greater than these values.

Arias Intensity

The preceding ground motion parameters relate to ground motion amplitude (in different frequency ranges for peak acceleration and velocity) and ground motion duration. A single parameter that reflects the effects of the amplitude, frequency content, and duration of a ground motion is the Arias intensity (Arias, 1970). The Arias intensity, defined as

$$I_a = \frac{\pi - p_i}{2g} \int_0^\infty [a(t)]^2 dt$$

can easily be computed from an earthquake ground motion. Computed Arias intensities for each of the ground response profiles are given in Table 14.

On the basis of USGS deaggregation data and the predictive relationship of Campbell and Duke (1974), Arias intensities on shallow alluvium (<20 m thick) sites for likely earthquakes in Bellingham, Seattle, and Olympia are 253 cm/sec, 1,036 cm/sec, and 1,036 cm/sec, respectively. The computed CSZ Arias intensities were significantly lower than these values.

Response Spectrum Intensity

Because many structures have fundamental periods between 0.1 and 2.5 sec, Housner (1959) reasoned that response spectrum ordinates in this period range should provide an indication of their potential response. The response spectrum intensity was therefore defined as

$$SI(\xi) = \int_{0.1}^{2.5} PSV(\xi, T)dT$$

where PSV(ξ, T) is the pseudo-spectral velocity of an oscillator with natural period, T, and damping ratio, ξ. Computed response spectrum intensities, assuming 5 percent damping, for each of the ground response profiles are presented in Table 15.

On the basis of USGS deaggregation data and the predictive relationship of Von Thun et al. (1988), spectral intensities for likely earthquakes in Bellingham, Seattle, and Olympia are 70 cm, 115 cm, and 115 cm, respectively. The computed CSZ spectral intensities were lower than these values.

Table 14. Computed median (coefficient of variation ln (I_a)) Arias intensities in cm/sec for each ground response site.

	Equivalent Linear Analysis			Nonlinear Analysis		
Site	M_w=8.0	M_w=8.5	M_w=9.0	M_w=8.0	M_w=8.5	M_w=9.0
AWV I	0.1423 (-0.199)	0.3765 (-0.565)	0.5663 (-1.450)	0.4629 (-0.483)	1.3599 (1.236)	2.1075 (0.794)
AWV II	0.0887 (-0.111)	0.2468 (-0.177)	0.3772 (-0.430)	0.2741 (-0.182)	0.7512 (-0.825)	1.2059 (2.203)
Andresen Rd.	0.0299 (-0.158)	0.6413 (-1.105)	1.8236 (-0.722)	0.0676 (-0.177)	1.0101 (40.581)	2.683 (0.373)
Bl. Diam. Rd.	0.1979 (-0.218)	0.3599 (-0.308)	0.5338 (-0.910)	0.3168 (-0.252)	0.5473 (-0.444)	0.8547 (-3.383)
Bone River	0.0837 (-0.085)	0.1324 (-0.126)	0.2233 (-0.181)	0.0967 (-0.112)	0.7294 (-0.801)	0.5201 (-0.524)
Capitol Blvd.	0.1665 (-0.250)	0.9017 (-2.796)	1.2661 (2.257)	0.4305 (-0.398)	1.8863 (0.363)	2.7617 (0.408)
Coldwater Cr.	0.0431 (-0.188)	0.5114 (-0.557)	0.9244 (-6.360)	0.1094 (-0.184)	0.7929 (-1.120)	1.4467 (0.008)
I5/NE 99th St.	0.0866 (-0.150)	0.4464 (-0.460)	0.6977 (-1.048)	0.0667 (-0.163)	1.3052 (1.606)	3.3964 (0.324)
I405/SR522	0.0685 (-0.111)	0.1992 (-0.178)	0.3119 (-0.421)	0.1019 (-0.150)	0.2793 (-0.152)	0.4311 (-0.523)
Kent Valley	0.0741 (-0.140)	0.2725 (-0.242)	0.4221 (-0.603)	0.1621 (-0.166)	0.4881 (-0.364)	0.7572 (-1.467)
Mercer Slough I	0.0379 (-0.113)	0.1018 (-0.130)	0.1304 (-0.215)	0.4772 (-0.369)	0.5370 (-0.334)	0.7460 (-1.464)
Mercer Slough II	0.0215 (-0.090)	0.0592 (-0.111)	0.0679 (-0.145)	0.4159 (-0.281)	1.0291 (8.771)	1.3349 (1.515)
Nooksack	0.0880 (-0.147)	0.1725 (-0.182)	0.3015 (-0.450)	0.1633 (-0.119)	0.3342 (-0.190)	0.5787 (-0.648)
Nooksack R.	0.0812 (-0.118)	0.1673 (-0.209)	0.2422 (-0.510)	0.1739 (-0.128)	0.3314 (-0.217)	0.5046 (-0.790)
Yakima	0.0060 (-0.120)	0.0469 (-0.203)	0.0855 (-0.305)	0.0308 (-0.212)	0.1662 (-0.387)	0.2929 (-0.648)

Table 15. Computed median (coefficient of variation ln (SI)) response spectrum intensities in cm for each ground response site.

	Equivalent Linear Analysis			Nonlinear Analysis		
Site	M_w=8.0	M_w=8.5	M_w=9.0	M_w=8.0	M_w=8.5	M_w=9.0
AWV I	25.844 (0.067)	40.898 (0.059)	40.351 (0.096)	38.849 (0.071)	64.625 (0.054)	64.660 (0.080)
AWV II	37.646 (0.070)	58.631 (0.046)	59.104 (0.076)	45.526 (0.061)	73.220 (0.045)	74.768 (0.074)
Andresen Rd.	14.825 (0.103)	56.178 (0.063)	75.004 (0.064)	16.704 (0.083)	62.177 (0.055)	80.899 (0.055)
Bl. Diam. Rd.	63.488 (0.065)	75.499 (0.060)	73.915 (0.084)	63.625 (0.046)	74.676 (0.044)	74.060 (0.067)
Bone River	39.942 (0.042)	29.916 (0.042)	41.399 (0.053)	35.372 (0.035)	66.203 (0.039)	51.772 (0.040)
Capitol Blvd.	37.373 (0.064)	78.340 (0.045)	75.256 (0.067)	57.098 (0.047)	112.992 (0.039)	109.406 (0.048)
Coldwater Cr.	18.407 (0.104)	50.962 (0.057)	56.590 (0.078)	27.104 (0.074)	67.655 (0.047)	74.155 (0.065)
I5/NE 99th St.	19.338 (0.098)	70.161 (0.040)	74.421 (0.027)	16.631 (0.072)	67.556 (0.060)	85.784 (0.062)
I405/SR522	32.261 (0.069)	46.823 (0.052)	46.213 (0.078)	29.273 (0.062)	41.449 (0.046)	43.686 (0.066)
Kent Valley	32.971 (0.075)	56.905 (0.052)	54.940 (0.073)	51.113 (0.036)	74.118 (0.034)	73.051 (0.046)
Mercer Slough I	26.737 (0.066)	36.571 (0.052)	35.398 (0.084)	64.542 (0.035)	69.053 (0.037)	71.278 (0.062)
Mercer Slough II	17.670 (0.072)	23.454 (0.062)	21.912 (0.093)	64.268 (0.040)	82.959 (0.030)	81.729 (0.044)
Nooksack R.	46.206 (0.059)	57.242 (0.061)	59.201 (0.090)	50.933 (0.041)	57.730 (0.032)	62.929 (0.051)
N. Ferndale	41.806 (0.061)	53.126 (0.073)	57.209 (0.100)	52.733 (0.049)	65.434 (0.040)	67.951 (0.064)
Yakima	8.189 (0.149)	18.346 (0.084)	19.213 (0.104)	9.663 (0.133)	19.989 (0.085)	21.055 (0.105)

CONCLUSIONS

The research described in this report sheds considerable light on the engineering implications of great Cascadia subduction zone earthquakes for transportation structures and facilities in Washington state. The ground motion modeling used in this research is the most thoroughly validated that is currently available to seismologists and earthquake engineers. It is without doubt the most advanced that has yet been attempted in this region and provides, for the first time, an objective means for comparing hazards from great subduction earthquakes with hazards from other earthquakes. From the results of this work, the following conclusions can be drawn:

1. Great subduction earthquakes that occur on the Cascadia subduction zone can be expected to produce shaking that is felt over the entire western portion of Washington state and as far east as Yakima.

2. The level of ground shaking will be strongest on the Pacific coast and will generally become less intense to the east.

3. Great subduction earthquakes will produce ground shaking of extremely long duration. The duration will increase with increasing magnitudes, but strong ground motion can be expected to last over 90 seconds in a magnitude 9.0 earthquake.

4. Median ground motion amplitudes will be high along the Pacific coast, but will decrease to the east. Within the Puget Sound basin, median rock outcrop amplitudes will be relatively low except at low frequencies. In most cases, median ground motion amplitudes are significantly lower than the amplitudes on which modern earthquake-resistant design procedures are based.

5. While high and intermediate frequency components of ground motions, as characterized by parameters such as peak acceleration and T=0.3 sec spectral acceleration, are expected to be relatively low, the low-frequency components, as characterized by parameters such as peak displacement and T > 1.0 sec spectral acceleration, are likely to be large.

6. Current earthquake-resistant design procedures are likely to be conservative with respect to the median loading imposed on structures with relatively short natural periods by great Cascadia subduction zone earthquakes. Structures with long natural periods (T > 1 sec), on the other hand, may be subjected to median forces greater than those anticipated by current earthquake-resistant design procedures.

7. The results of deterministic simulations such as those performed in this study should only be compared with those of PSHAs with great care. There are several reasons why the numerical values of ground motion parameters produced by the deterministic analyses should not be expected to equal those produced by PSHAs.

8. Structures or soil deposits that are subject to cumulative damage from load or stress reversals may be significantly affected by the long duration shaking associated with great subduction earthquakes.

9. Structures supported on pile foundations extending through soft soils may be significantly affected by the large ground displacements that are expected to be produced by great subduction earthquakes.

RECOMMENDATIONS AND IMPLEMENTATION

Existing significant structures and sites of the types identified in the preceding section (Conclusions) as being particularly susceptible to damage from great subduction earthquakes should be reviewed in light of the anticipated ground shaking characteristics identified in this report. In many cases, current design requirements will be sufficient to mitigate damage from great Cascadia subduction zone earthquakes. In some cases, however, the motions transmitted to structures and sites by great subduction earthquakes may have greater damage potential than those associated with conventional earthquake-resistant design procedures. The need for remedial action in such cases should be evaluated on a case-by-case basis, given consideration of the relative likelihood of great subduction earthquakes.

The levels of loading imposed on new structures by great subduction earthquakes should be considered in their design. In many, but not all, cases, current design requirements will be sufficient to mitigate damage from great Cascadia subduction zone earthquakes. For cases in which they will not, the need for elevated design requirements should be evaluated with due consideration of the relative likelihood of great subduction earthquakes.

ACKNOWLEDGMENTS

The research described in this report was funded by the Washington State Department of Transportation. The research was conducted by the University of Washington Department of Civil Engineering and by Pacific Engineering & Analysis of El Cerrito, California. Pacific Engineering & Analysis was a subcontractor to the University of Washington. Professor Steven L. Kramer was the principal investigator for the University of Washington, and Dr. Walter J. Silva was the principal in charge for Pacific Engineering & Analysis. Mr. David A. Baska conducted the site response analyses described in the report.

The authors would like to acknowledge the assistance of several individuals. Myint Lwin of the WSDOT Bridge and Structures office, and Robert Kimmerling and Tony Allen of the WSDOT Materials Laboratory provided valuable advice and guidance during the initial site selection and subsurface characterization phases of the work. Keith Anderson of the WSDOT Research Office monitored project progress. Troy Parke, former graduate student at the University of Washington, contributed greatly to subsurface characterization and performed preliminary ground response analyses for several sites. John Horne of Clemson University provided advice on the use of the ground response analysis program WAVE. The authors are grateful for all of this assistance.

REFERENCES

Anderson, J. G. and S. E. Hough (1984). "A Model for the Shape of the Fourier Amplitude Spectrum of Acceleration at High Frequencies." *Bulletin of the Seismological Society of America,* 74(5), 1969-1993.

Arias, A. (1970) "A measure of earthquake intensity," in Seismic Design for Nuclear Power Plants, Hansen, R. J., ed. MIT Press, Cambridge, Massachusetts, 438-483.

Atkinson, G.M. (1984). "Attenuation of strong ground motion in Canada from a random vibrations approach." *Bull. Seism. Soc. Am.*, 74(5), 2629-2653.

Atkinson, G.M. (1996). "The high-frequency shape of the source spectrum for earthquakes in eastern and western Canada." *Bull. Seism. Soc. Am.* 86(1A), 106-112.

Atwater, B.R. (1987). "Evidence for great Holocene earthquakes along the outer coast of Washington State," *Science*, 236(4804), 942-944.

Bolt, B. A. (1969) "Duration of strong motion," *Proc. 4th World Conf. Earthquake Engrg.*, Santiago, Chile, 1304-1315. [3]

Boore, D.M. (1983). "Stochastic simulation of high-frequency ground motions based on seismological models of the radiated spectra." *Bull. Seism. Soc. Am.*, 73(6), 1865-1894.

Boore, D.M. (1986). "Short-period P- and S-wave radiation from large earthquakes: implications for spectral scaling relations." *Bull. Seism. Soc. Am.*, 76(1) 43-64.

Boore, D.M. and Joyner, W.B. (1984). "A note on the use of random vibration theory to predict peak amplitudes of transient signals." *Bull. Seism. Soc. Am.*, 74, 2035-2039.

Brune, J.N. (1970). "Tectonic stress and the spectra of seismic shear waves from earthquakes." *J. Geophys. Res.* 75, 4997-5009.

Brune, J.N. (1971). "Correction." *J. Geophys. Res.* 76, 5002.

Campbell, K.W. and Duke, C.M. (1974). Bedrock intensity, attenuation, and site factors from San Fernando earthquake records, Bulletin of the Seismological Society of America, Vol. 64, No. 1, pp. 173-185.

Chang, F. K. and Krinitzsky, E. L. (1977) "Duration, spectral content, and predominant period of strong motion earthquake records from western United States," U. S. Army Engineer Waterways Experiment Station, Misc. Paper 5-73-1, Vicksburg, Mississippi.

Cohee, B.P., P.G. Somerville and N.A. Abrahamson (1991). "Simulated ground motions for hypothesized M_w = 8 subduction earthquakes in Washington and Oregon." *Bull. Seism. Soc. Am.*, 81(1), 28-56.

Electric Power Research Institute (1993). "Guidelines for determining design basis ground motions." Palo Alto, Calif: Electric Power Research Institute, vol. 1-5, EPRI TR-102293. vol. 1: Methodology and guidelines for estimating earthquake ground motion in eastern North America. vol. 2: Appendices for ground motion estimation. vol. 3: Appendices for field investigations. vol. 4: Appendices for laboratory investigations. vol. 5: Quantification of seismic source effects.

Hanks, T.C. (1982). "f_{max}." *Bull. Seism. Soc. Am.*, 72, 1867-1879.

Hanks, T.C., and Kanamori, H. (1979). "A moment magnitude scale." *J. Geophys. Res.*, 84, 2348-2350.

Hartzell, S.H. (1978). "Earthquake aftershocks as Green's functions." *Geophys. Res. Letters*, 5, 1-4.

Heaton, T.H. and Kanamori, H. (1984). "Seismic potential associated with subduction in the northwestern United States," *Bulletin of the Seismological Society of America*, Vol. 73, No. 3, pp. 933-941. [4]

Higgins, J.D., Fragaszy, R.J., Beard, L.D. (1988). "Seismic zonation for highway bridge design," Final Report, Washington State Transportation Center, Washington State University, Pullman, Washington, 154 pp.

Horne, J.C. (1996). "Analysis of the effects of liquefaction and lateral spreading on pile foundations," Ph.D. Dissertation, University of Washington.

Horne, J.C. and Kramer, S.L. (1997). "Effects of liquefaction on pile foundations," Draft Research Report, Transportation Research Center, Washington State Department of Transportation, 115 pp.

Hough, S. E. and J. G. Anderson (1988). "High-Frequency Spectra Observed at Anza, California: Implications for Q Structure." *Bull. Seism. Soc. Am.*, 78(2), 692-707.

Hough, S.E., Anderson, J.G., Brune, J., Vernon III, F., Berger, J., Fletcher, J., Haar, L., Hanks, T., and Baker, L. (1988). "Attenuation near Anza, California." *Bull. Seism. Soc. Am.*, 78(2), 672-691.

Housner, G. W. (1959) "Behavior of structures during earthquakes," Journal of the Engineering Mechanics Division, ASCE, Vol. 85, No. EM14, 109-129.

Hyndman, R.D. and Wang, K. (1995). "The rupture zone of Cascadia great earthquakes from current deformation and the thermal regime." *J. Geophys. Res.*, 100(B11), 22,133-22,154.

Irikura, K. (1983). "Semi-empirical estimation of strong ground motions during large earthquakes." *Bull. Disaster Prevention Res. Inst.*, Kyoto Univ., 33, 63-104.

Joyner, W. B. and Boore, D. M. (1988) "Measurement, characterization, and prediction of strong ground motion," in Earthquake Engineering and Soil Dynamics II - Recent Advances in Ground-Motion Evaluation, ASCE Geotechnical Special Publication 20, pp. 43-102.

McCrumb, D.R., Galster, R.W., West, D.O., Crosson, R.S., Ludwin, R.S., Hancock, W.E., and Mann, L.V. (1989). "Tectonics, seismicity, and engineering seismology in Washington," Engineering Geology in Washington, Washington Division of Geology and Earth Resources Bulletin 78, Vol. 1, pp. 97-120.

McGuire, R. K., A. M. Becker, and N. C. Donovan (1984). "Spectral Estimates of Seismic Shear Waves." *Bull. Seism. Soc. Am.*, 74(4), 1427-1440.

Ou, G.B. and R. B. Herrmann (1990). "Estimation theory for strong ground motion." *Seism. Res. Letters.* 61.

Papageorgiou, A.S., and Aki, K. (1983). "A specific barrier model for the quantitative description of inhomogeneous faulting and the prediction of strong ground motion, part I, Description of the model." *Bull. Seism. Soc. Am.*, 73(4), 693-722.

Pyke, R.M. (1979). "Nonlinear soil models for irregular cyclic loadings," *Journal of the Geotechnical Engineering Division*, ASCE, Vol. 105, No. GT6, pp. 715-726. [6]

Roblee, C.J., W.J. Silva, G.R. Toro, and N. Abrahamson (1996) "Variability in Site-Specific Seismic Ground-Motion Predictions." Uncertainty in the Geologic Environment: From Theory to Practice, Proceedings of "Uncertainty '96" *ASCE* Specialty Conference, Edited by C.D. Shackelford, P.P. Nelson, and M.J.S. Roth, Madison, WI, Aug. 1-3, pp. 1113-1133.

Rogers, G.C. (1988). "Seismic potential of the Cascadia subduction zone," *Nature*, 343, 17.

Rovelli, A., Bonamassa, O. Cocco, M., Di Bona, M. and Mazza, S. (1988). "Scaling laws and spectral parameters of the ground motion in active extensional areas in Italy." *Bull. Seism. Soc. Am.*, 78(2), 530-560.

Schnabel, P.B., Lysmer, J., and Seed, H.B. (1972). "SHAKE: A computer program for earthquake response analysis of horizontally layered sites," Report No. EERC 72-12, Earthquake Engineering Research Center, University of California, Berkeley, California.

Schneider, J.F., W.J. Silva, and C.L. Stark (1993). "Ground motion model for the 1989 **M** 6.9 Loma Prieta earthquake including effects of source, path and site." *Earthquake Spectra*, 9(2), 251-287.

Silva, W. and Lee, K. (1987). "WES RASCAL code for synthesizing earthquake ground motions," Miscellaneous Paper S-73-1,Report 24, Waterways Experiment Station, U.S. Army Corps of Engineers, Vicksburg, Mississippi, 73 pp.

Silva, W. J. and R. K. Green (1988). "Magnitude and Distance Scaling of Response Spectral Shapes for Rock Sites with Applications to North American Environments." In *Proceedings: Workshop on Estimation of Ground Motion in the Eastern United States*, EPRI NP-5875, Electric Power Research Institute.

Silva, W. J., R. Darragh, C. Stark, I. Wong, J. C. Stepp, J. Schneider, and S-J. Chiou (1990). "A Methodology to Estimate Design Response Spectra in the Near-Source Region of Large Earthquakes Using the Band-Limited-White-Noise Ground Motion Model". *Procee. of the Fourth U.S. Conf. on Earthquake Engineering,* Palm Springs, California. 1, 487-494.

Silva, W.J. (1991). "Global characteristics and site geometry." Chapter 6 in *Proceedings: NSF/EPRI Workshop on Dynamic Soil Properties and Site Characterization.* Palo Alto, Calif.: Electric Power Research Institute, NP-7337.

Silva, W.J. (1992). "Factors controlling strong ground motions and their associated uncertainties." *Dynamic Analysis and Design Considerations for High Level Nuclear Waste Repositories, ASCE* 132-161.

Silva, W.J. and Stark, C.L. (1993) "Source, path, and site ground motion model for the 1989 **M** 6.9 Loma Prieta earthquake." CDMG draft final report.

Silva, W.J., and Darragh, R. (1995). "Engineering characterization of earthquake strong ground motion recorded at rock sites." Palo Alto, Calif:Electric Power Research Institute, TR-102261.

Silva, W.J., N. Abrahamson, G. Toro, C. Costantino (1997). "Description and validation of the stochastic ground motion model." *Submitted to Brookhaven National Laboratory, Associated Universities, Inc. Upton, New York.*

Toro, G.R. (1985). "Stochastic model estimates of strong ground motion." *Seismic Hazard Methodology for Nuclear Facilities in the Eastern United States,* Appendix B, edited by R.K. McGuire, Electric Power Res. Inst., EPRI P101-29.

Trifunac, M. D. and Brady, A. G. (1975) "A study of the duration of strong earthquake ground motion," *Bulletin of the Seismological Society of America*, 65, 581-626. [3]

Von Thun, J. L., Rochim, L. H., Scott, G. A., and Wilson, J. A. (1988) "Earthquake ground motions for design and analysis of dams," in Earthquake Engineering and Soil Dynamics II - Recent Advance in Ground-Motion Evaluation, ASCE Geotechnical Special Publication 20, 463-481.

Wells, D.L., Coppersmith, K.J. (1994). "New empirical relationships among magnitude, rupture length, rupture width, rupture area, and surface displacement." *Bull. Seism. Soc. Am.* 84(4), 974-1002.

APPENDIX A

MATERIAL PROPERTY CHARACTERIZATION

APPENDIX A

Material Property Characterization

The site-specific ground response analyses required characterization of the dynamic soil properties for each of the 15 ground response profiles that were analyzed. The nature and amount of soil property data that was available varied considerably from profile to profile. For some soil units, detailed information with measured properties were available; for others, only qualitative descriptions were available. This Appendix describes the procedures that were used to characterize the dynamic soil properties for the ground response analyses.

The specific procedures used to characterize dynamic soil properties depended on the available subsurface information, and on the type of soil being considered. In all cases, the most direct and reliable means of characterizing soil properties were used. Whenever available, direct measurements of the properties of interest were utilized. When direct measurements were not available, properties were obtained by correlation with other measured properties. In some cases, interpretative estimation based on geotechnical descriptions were used; these interpretations were submitted to the WSDOT Materials Laboratory for review and verification by staff engineers and geologists.

Shear Wave Velocity Measurements

The low-strain shear modulus, Gmax, can be computed from measured shear wave velocities and measured or estimated soil densities using the relationship

$$G_{max}=\rho V_s^2$$

where ρ is the density and V_s is the shear wave velocity of the soil. Consequently, shear wave velocity measurements are equivalent to direct measurements of Gmax. Shear wave velocities

were measured using downhole and seismic cone techniques at a number of the ground response analysis sites.

Standard Penetration Test Correlation

At sites for which shear wave velocity data were not available, the initial stiffness of coarse-grained soils was obtained by an SPT correlation procedure. First, measured SPT blow counts were corrected for energy and overburden pressure. Then G_{max} was estimated from the empirical relationship of Ohta and Goto (1976)

$$G_{max} = 20000(N_1)_{60}^{0.333}(\sigma_m^1)^{0.5}$$

where $(N_1)_{60}$ is the corrected SPT resistance and σ'_m is the mean principal effective stress in psf. The effect of effective overburden pressure was then removed by computing the modulus parameter

$$K_{2,max} = \frac{G_{max}}{1000(\sigma_m^1)^{0.5}}$$

$K_{2,max}$ values were computed and plotted against depth. For each coarse-grained unit, an average $K_{2,max}$ value was identified and used to compute a smooth variation of G_{max} with depth from

$$G_{max} = 1000K_{2,max}(\sigma_m^1)^{0.5}$$

Undrained Strength Correlation

The initial stiffness of fine-grained soils was estimated by correlation with undrained shear strength at sites where shear wave velocity measurements were not available. This correlation also depended on plasticity index which was either taken from Atterberg Limit

measurements or estimated from grain size characteristics and/or boring log descriptions. Using this approach, G_{max} was estimated from

$$G_{max} = s_u [G_{max}/s_u]$$

where s_u is the undrained strength of the soil and is obtained from Table A-1.

Interpretive Estimation

The final alternative for estimation of G_{max} was by estimating or extrapolating soil properties on the basis of interpreted geologic conditions. In certain situations, for example at depths below the bottom of exploratory borings or sounding but above bedrock, this was the only available alternative. Sources used in the estimation of soil and rock properties by this approach included Galster and Laprade (1991), Hall and Othberg (1974), and the experience of WSDOT Materials Laboratory engineers and geologists who reviewed all such interpretive estimates.

Table A-1. Values of $[G_{max}/s_u]$ (after Weiler, 1988).

Plasticity Index	OCR=1	OCR=2	OCR=5
15-20	1100	900	600
20-25	700	600	500
35-45	450	380	300

APPENDIX B

GROUND RESPONSE PROFILES

Table B-1. Soil Profile Data for Alaskan Way Viaduct I Site.

Depth (ft)	g (pcf)	PI	V_s (ft/sec)	V_s basis*	Model
0 - 20	110	0	490	V	Vucetic-Dobry
20 - 45	110	0	1250	V	Vucetic-Dobry
45 - 220	140	0	1700	V	Vucetic-Dobry
220 -	150	n.a.	2500	E	Rock

Groundwater level: 10 ft depth
Boring log depth: 222 ft

Table B-2. Soil Profile Data for Alaskan Way Viaduct II Site.

Depth (ft)	g (pcf)	PI	V_s (ft/sec)	V_s basis*	Model
0 - 30	110	0	610	V	Vucetic-Dobry
30 - 60	110	0	400	V	Vucetic-Dobry
60 - 85	140	0	1250	V	Vucetic-Dobry
85 - 260	140	0	1700	V	Vucetic-Dobry
260 -	150	n.a.	2500	E	Rock

Groundwater level: 10 ft depth
Boring log depth: 250 ft

* V = From shear wave velocity measurements
N = From SPT correlations
S = From s_u correlations
E = From expected geology

Table B-3. Soil Profile Data for Andresen Road Site.

Depth (ft)	g (pcf)	PI	V_s (ft/sec)	V_s basis*	Model
0 - 5	120	0	380	N,S	Vucetic-Dobry
5 - 15	120	0	510	N,S	Vucetic-Dobry
15 - 25	120	0	600	N,S	Vucetic-Dobry
25 - 35	120	0	670	S,E	Vucetic-Dobry
35 - 40	120	0	703	S,E	Vucetic-Dobry
40 - 55	120	15	540	S,E	Vucetic-Dobry
55 - 60	125	0	900	S,E	Vucetic-Dobry
60 - 70	125	0	930	S,E	Vucetic-Dobry
70 - 80	125	0	960	S,E	Vucetic-Dobry
80 -	150	n.a.	2500	E	Rock

Groundwater level: 0 ft depth
Boring log depth: 80 ft

Table B-4. Soil Profile Data for Black Diamond Site.

Depth (ft)	g (pcf)	PI	V_s (ft/sec)	V_s basis*	Model
0 - 5	135	0	400	N,S	Vucetic-Dobry
5 - 15	145	0	780	N,S	Vucetic-Dobry
15 - 25	145	0	920	N,S	Vucetic-Dobry
25 - 40	145	0	1040	N,S	Vucetic-Dobry
40 - 200	130	0	900	S,E	Vucetic-Dobry
200 -	150	n.a.	2500	E	Rock

Groundwater level: 100 ft depth
Boring log depth: 60 ft

* V = From shear wave velocity measurements
N = From SPT correlations
S = From s_u correlations
E = From expected geology

Table B-5. Soil Profile Data for Bone River Site.

Depth (ft)	g (pcf)	PI	V_s (ft/sec)	V_s basis*	Model
0 - 5	105	15	85	N,S	Vucetic-Dobry
5 - 10	105	0	390	N,S	Vucetic-Dobry
10 - 25	105	0	480	N,S	Vucetic-Dobry
25 - 30	105	0	530	N,S	Vucetic-Dobry
30 - 35	120	0	233	N,S	Vucetic-Dobry
35 - 45	120	0	252	S,E	Vucetic-Dobry
45 - 55	120	0	286	S,E	Vucetic-Dobry
55 - 60	120	0	309	S,E	Vucetic-Dobry
60 - 65	100	15	343	S,E	Vucetic-Dobry
65 - 70	100	15	354	S,E	Vucetic-Dobry
70 - 75	100	0	370	S,E	Vucetic-Dobry
75 - 80	115	0	352	S,E	Vucetic-Dobry
80 - 85	115	0	365	S,E	Vucetic-Dobry
85 - 90	115	0	860	S,E	Vucetic-Dobry
90 - 95	115	0	875	S,E	Vucetic-Dobry
95 - 100	115	0	887	S,E	Vucetic-Dobry
100 - 120	115	15	1100	S,E	Vucetic-Dobry
120 -	150	n.a.	2500	E	Rock

Groundwater level: 5 ft depth
Boring log depth: 120 ft

---

* V = From shear wave velocity measurements
N = From SPT correlations
S = From s_u correlations
E = From expected geology

Table B-6. Soil Profile Data for Capitol Boulevard Site.

Depth (ft)	g (pcf)	PI	V_s (ft/sec)	V_s basis*	Model
0 - 5	120	0	420	N,V	Vucetic-Dobry
5 - 10	120	0	550	N,V	Vucetic-Dobry
10 - 20	120	0	660	N,V	Vucetic-Dobry
20 - 25	120	0	730	N,V	Vucetic-Dobry
25 - 30	120	0	830	N,V	Vucetic-Dobry
30 - 35	120	0	880	N,V	Vucetic-Dobry
35 - 45	120	0	920	N,V	Vucetic-Dobry
45 - 65	120	0	1000	N,V	Vucetic-Dobry
65 - 115	120	0	1120	N,E	Vucetic-Dobry
115 - 165	120	0	1260	N,E	Vucetic-Dobry
165 - 185	120	0	1350	N,E	Vucetic-Dobry
185 - 195	120	0	1390	N,E	Vucetic-Dobry
195 - 205	120	0	1400	N,E	Vucetic-Dobry
205 - 300	140	0	2190	N,E	Vucetic-Dobry
300 -	150	n.a.	2500	E	Rock

Groundwater level: 205 ft depth
Boring log depth: 110 ft

* V = From shear wave velocity measurements
N = From SPT correlations
S = From s_u correlations
E = From expected geology

Table B-7. Soil Profile Data for Coldwater Creek Site.

Depth (ft)	g (pcf)	PI	V_s (ft/sec)	V_s basis*	Model
0 - 20	120	0	500	N,S	Vucetic-Dobry
20 - 40	120	0	810	N,S	Vucetic-Dobry
40 - 55	120	15	830	S,E	Vucetic-Dobry
55 - 80	125	0	830	S,E	Vucetic-Dobry
80 - 100	125	0	890	S,E	Vucetic-Dobry
100 -	150	n.a.	2500	E	Rock

Groundwater level: 0 ft depth
Boring log depth: 80 ft

* V = From shear wave velocity measurements
N = From SPT correlations
S = From s_u correlations
E = From expected geology

Table B-8. Soil Profile Data for I-405/SR-522 Site.

Depth (ft)	g (pcf)	PI	V_s (ft/sec)	V_s basis*	Model
0 - 10	130	0	400	N,S	Vucetic-Dobry
10 - 15	125	0	230	N,S	Vucetic-Dobry
15 - 25	125	0	700	N,S	Vucetic-Dobry
25 - 55	125	15	410	N,S	Vucetic-Dobry
55 - 75	125	0	1030	N,S	Vucetic-Dobry
75 - 80	125	7	750	N,S	Vucetic-Dobry
80 - 90	125	7	760	N,S	Vucetic-Dobry
90 - 110	125	7	770	N,S	Vucetic-Dobry
110 - 140	125	7	790	N,S	Vucetic-Dobry
140 - 185	125	7	810	S,E	Vucetic-Dobry
185 - 235	125	7	850	S,E	Vucetic-Dobry
235 - 335	125	7	900	S,E	Vucetic-Dobry
335 - 435	125	7	950	S,E	Vucetic-Dobry
435 - 485	125	7	990	S,E	Vucetic-Dobry
485 - 535	125	7	1030	S,E	Vucetic-Dobry
535 - 565	125	7	1040	S,E	Vucetic-Dobry
565 - 585	125	7	1050	S,E	Vucetic-Dobry
585 - 600	125	7	1060	S,E	Vucetic-Dobry
600 -	150	n.a.	2500	E	Rock

Groundwater level: 15 ft depth
Boring log depth: 140 ft

* V = From shear wave velocity measurements
N = From SPT correlations
S = From s_u correlations
E = From expected geology

Table B-9. Soil Profile Data for I-5/NE 99th Street Site.

Depth (ft)	g (pcf)	PI	V_s (ft/sec)	V_s basis*	Model
0 - 5	110	5	78	N,S	Vucetic-Dobry
5 - 10	110	5	400	N,S	Vucetic-Dobry
10 - 15	110	5	461	N,S	Vucetic-Dobry
15 - 20	110	5	514	N,S	Vucetic-Dobry
20 - 25	120	0	675	N,S	Vucetic-Dobry
25 - 35	120	0	720	S,E	Vucetic-Dobry
35 - 40	120	0	752	S,E	Vucetic-Dobry
40 - 70	125	20	720	S,E	Vucetic-Dobry
70 - 75	130	0	940	S,E	Vucetic-Dobry
75 - 80	130	0	970	S,E	Vucetic-Dobry
80 -	150	n.a.	2500	E	Rock

Groundwater level: 5 ft depth
Boring log depth: 80 ft

* V = From shear wave velocity measurements
N = From SPT correlations
S = From s_u correlations
E = From expected geology

Table B-10. Soil Profile Data for Kent Valley Site.

Depth (ft)	g (pcf)	PI	V_s (ft/sec)	V_s basis*	Model
0 - 10	125	10	610	V	Vucetic-Dobry
10 - 13	125	0	575	V	Vucetic-Dobry
13 - 28	125	0	630	V	Vucetic-Dobry
28 - 50	125	0	785	V	Vucetic-Dobry
50 - 55	125	0	880	N,E	Vucetic-Dobry
55 - 65	125	0	900	N,E	Vucetic-Dobry
65 - 85	125	0	1000	N,E	Vucetic-Dobry
85 - 115	125	0	1090	N,E	Vucetic-Dobry
115 - 165	125	0	1180	N,E	Vucetic-Dobry
165 - 225	125	0	1270	N,E	Vucetic-Dobry
225 - 300	125	0	1370	N,E	Vucetic-Dobry
300 - 400	125	0	1390	N,E	Vucetic-Dobry
400 -	150	n.a.	2500	E	Rock

Groundwater level: 10 ft depth
Boring log depth: 50 ft

* V = From shear wave velocity measurements
N = From SPT correlations
S = From s_u correlations
E = From expected geology

Table B-11. Soil Profile Data for Mercer Slough I Site.

Depth (ft)	g (pcf)	PI	V_s (ft/sec)	V_s basis*	Model
0 - 20	66.4	0	40	V	Vucetic-Dobry
20 - 30	66.4	0	60	V	Vucetic-Dobry
30 - 35	142	0	520	V	Vucetic-Dobry
35 - 40	142	0	630	V	Vucetic-Dobry
40 - 50	142	0	730	V	Vucetic-Dobry
50 - 70	142	0	880	N,E	Vucetic-Dobry
70 - 115	142	0	1030	N,E	Vucetic-Dobry
115 - 165	142	0	1190	N,E	Vucetic-Dobry
165 - 265	142	0	1360	N,E	Vucetic-Dobry
265 - 400	142	0	1520	N,E	Vucetic-Dobry
400 - 600	142	0	1690	N,E	Vucetic-Dobry
600 - 800	142	0	1880	N,E	Vucetic-Dobry
800-1000	142	0	2100	N,E	Vucetic-Dobry
1000 -	150	n.a.	2500	E	Rock

Groundwater level: 0 ft depth
Boring log depth: 100 ft

* V = From shear wave velocity measurements
N = From SPT correlations
S = From s_u correlations
E = From expected geology

Table B-12. Soil Profile Data for Mercer Slough II Site.

Depth (ft)	g (pcf)	PI	V_s (ft/sec)	V_s basis*	Model
0 - 20	66.4	0	40	V,S	Vucetic-Dobry
20 - 60	66.4	0	60	V,S	Vucetic-Dobry
60 - 100	107	20	310	V,S	Vucetic-Dobry
100 - 105	142	0	830	N,E	Vucetic-Dobry
105 - 110	142	0	880	N,E	Vucetic-Dobry
110 - 120	142	0	920	N,E	Vucetic-Dobry
120 - 140	142	0	1000	N,E	Vucetic-Dobry
140 - 185	142	0	1120	N,E	Vucetic-Dobry
185 - 240	142	0	1250	N,E	Vucetic-Dobry
240 - 340	142	0	1390	N,E	Vucetic-Dobry
340 - 440	142	0	1530	N,E	Vucetic-Dobry
440 - 600	142	0	1680	N,E	Vucetic-Dobry
600 - 800	142	0	1830	N,E	Vucetic-Dobry
800-1000	142	0	1960	N,E	Vucetic-Dobry
1000 -	150	n.a.	2500	E	Rock

Groundwater level: 0 ft depth
Boring log depth: 100 ft

* V = From shear wave velocity measurements
N = From SPT correlations
S = From s_u correlations
E = From expected geology

Table B-13. Soil Profile Data for Nooksack River Site.

Depth (ft)	g (pcf)	PI	V_s (ft/sec)	V_s basis*	Model
0 - 5	120	0	310	N,S	Vucetic-Dobry
5 - 20	120	0	640	N,S	Vucetic-Dobry
20 - 45	110	30	180	N,S	Vucetic-Dobry
45 - 130	110	30	360	N,S	Vucetic-Dobry
130 - 190	125	20	460	N,S	Vucetic-Dobry
190 - 195	125	0	1270	N,S	Vucetic-Dobry
195 - 205	125	0	1290	N,E	Vucetic-Dobry
205 - 225	125	0	1310	N,E	Vucetic-Dobry
225 - 255	125	0	1360	N,E	Vucetic-Dobry
255 - 315	125	0	1430	N,E	Vucetic-Dobry
315 - 400	125	0	1520	N,E	Vucetic-Dobry
400 - 500	125	0	1620	N,E	Vucetic-Dobry
500 - 600	125	0	1700	N,E	Vucetic-Dobry
600 - 700	125	0	1780	N,E	Vucetic-Dobry
700 - 800	125	0	1850	N,E	Vucetic-Dobry
800 - 900	125	0	1910	N,E	Vucetic-Dobry
900 -	150	n.a.	2500	E	Rock

Groundwater level: 0 ft depth
Boring log depth: 200 ft

* V = From shear wave velocity measurements
N = From SPT correlations
S = From s_u correlations
E = From expected geology

Table B-14. Soil Profile Data for North Ferndale Site.

Depth (ft)	g (pcf)	PI	V_s (ft/sec)	V_s basis*	Model
0 - 5	130	0	420	N,S	Vucetic-Dobry
5 - 10	130	0	580	N,S	Vucetic-Dobry
10 - 15	130	0	630	N,S	Vucetic-Dobry
15 - 50	110	15	330	N,S	Vucetic-Dobry
50 - 75	125	7	390	N,S	Vucetic-Dobry
75 - 100	140	0	1260	N,S	Vucetic-Dobry
100 - 105	140	0	1310	N,E	Vucetic-Dobry
105 - 115	140	0	1320	N,E	Vucetic-Dobry
115 - 135	140	0	1360	N,E	Vucetic-Dobry
135 - 165	140	0	1420	N,E	Vucetic-Dobry
165 - 215	140	0	1510	N,E	Vucetic-Dobry
215 - 300	140	0	1630	N,E	Vucetic-Dobry
300 - 400	140	0	1750	N,E	Vucetic-Dobry
400 -	150	n.a.	2500	E	Rock

Groundwater level: 10 ft depth
Boring log depth: 100 ft

* V = From shear wave velocity measurements
N = From SPT correlations
S = From s_u correlations
E = From expected geology

Table B-15. Soil Profile Data for Yakima Site.

Depth (ft)	g (pcf)	PI	V_s (ft/sec)	V_s basis*	Model
0 - 5	135	0	560	N	Vucetic-Dobry
5 - 15	135	0	720	N	Vucetic-Dobry
15 - 35	135	0	890	N	Vucetic-Dobry
35 - 50	150	0	1060	N	Vucetic-Dobry
50 - 70	150	0	1120	N	Vucetic-Dobry
70 -	150	n.a.	2500	E	Rock

Groundwater level: 35 ft depth
Boring log depth: 70 ft

* V = From shear wave velocity measurements
N = From SPT correlations
S = From s_u correlations
E = From expected geology

APPENDIX C

COMPUTED GROUND SURFACE RESPONSE SPECTRA: EQUIVALENT LINEAR

Alaskan Way Viaduct 1

Spectral Accelerations (M=8.0)

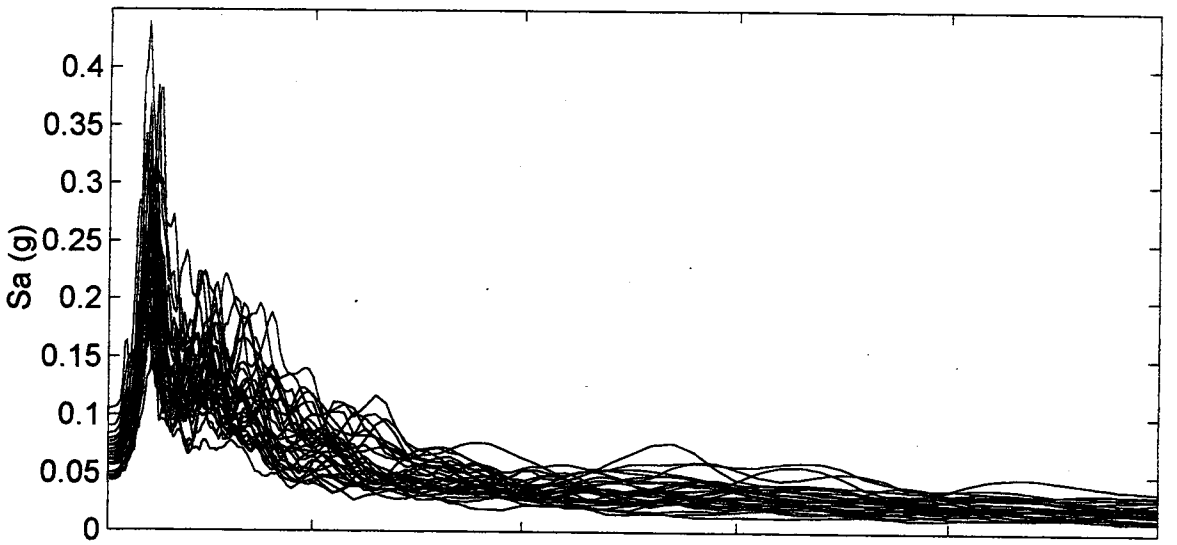

Mean and Mean +/- One Standard Deviation

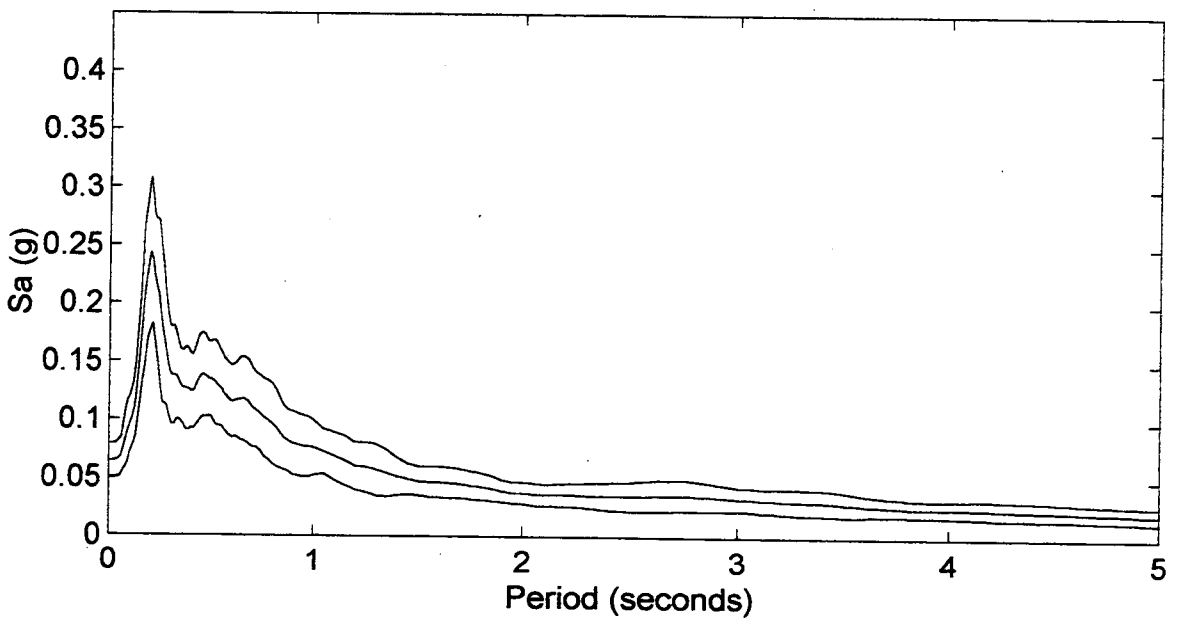

Alaskan Way Viaduct 2

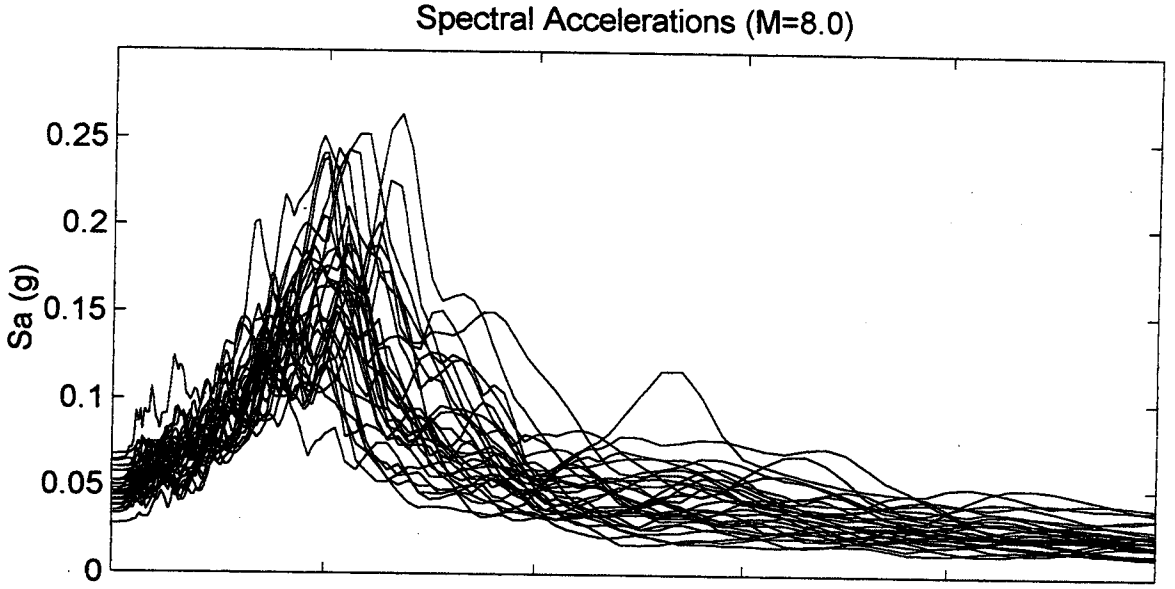

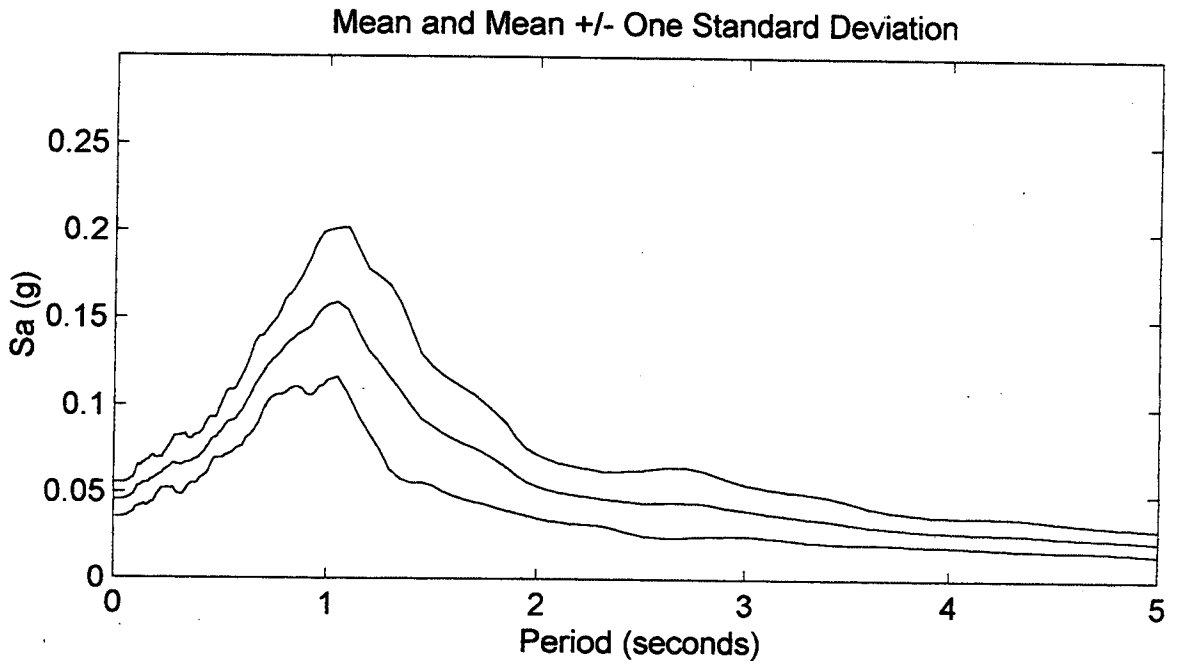

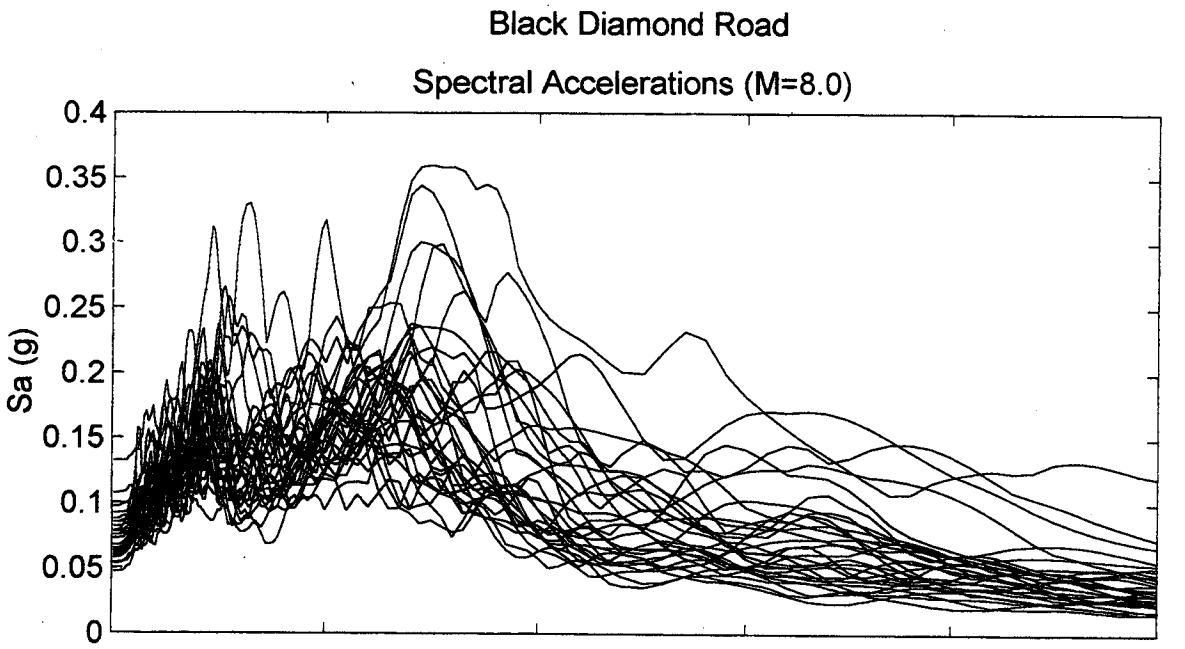
Black Diamond Road
Spectral Accelerations (M=8.0)
Sa (g)
0.4
0.35
0.3
0.25
0.2
0.15
0.1
0.05
0

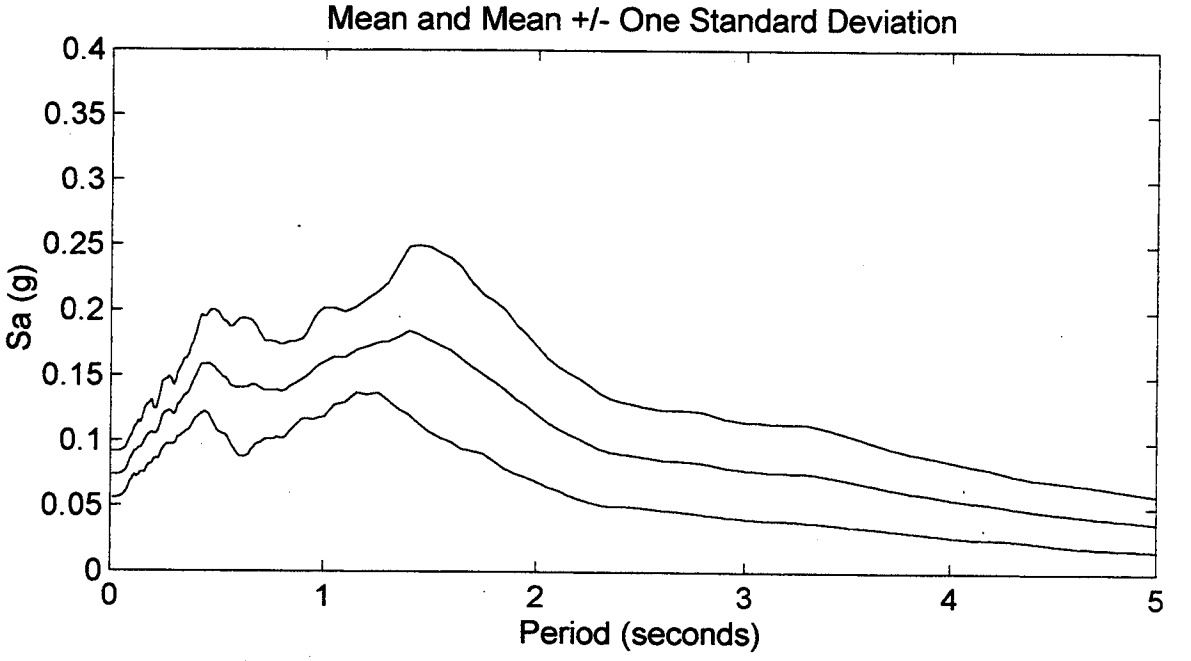
Mean and Mean +/- One Standard Deviation
Sa (g)
0.4
0.35
0.3
0.25
0.2
0.15
0.1
0.05
0
0
1
2
3
4
5
Period (seconds)

Bone River

Spectral Accelerations (M=8.0)

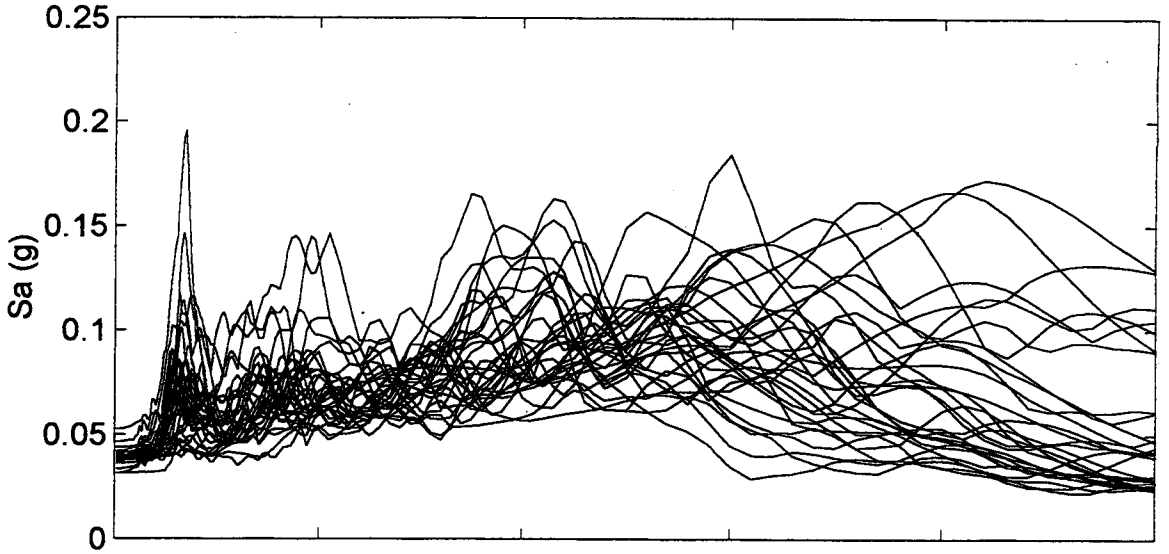

Mean and Mean +/- One Standard Deviation

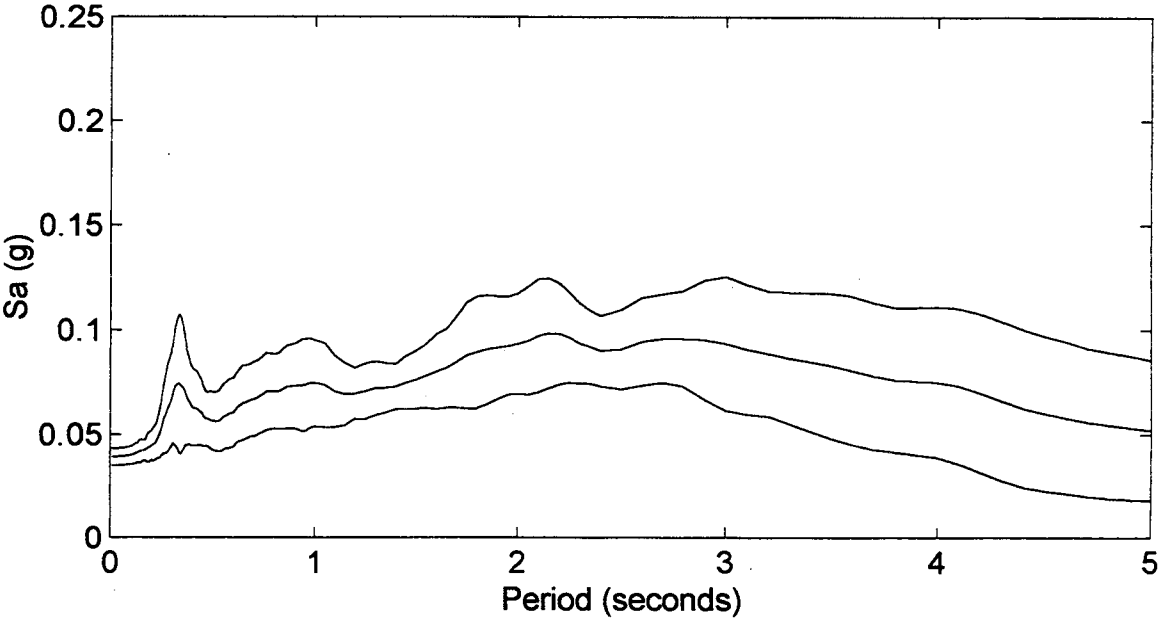

Capitol Boulevard

Spectral Accelerations (M=8.0)

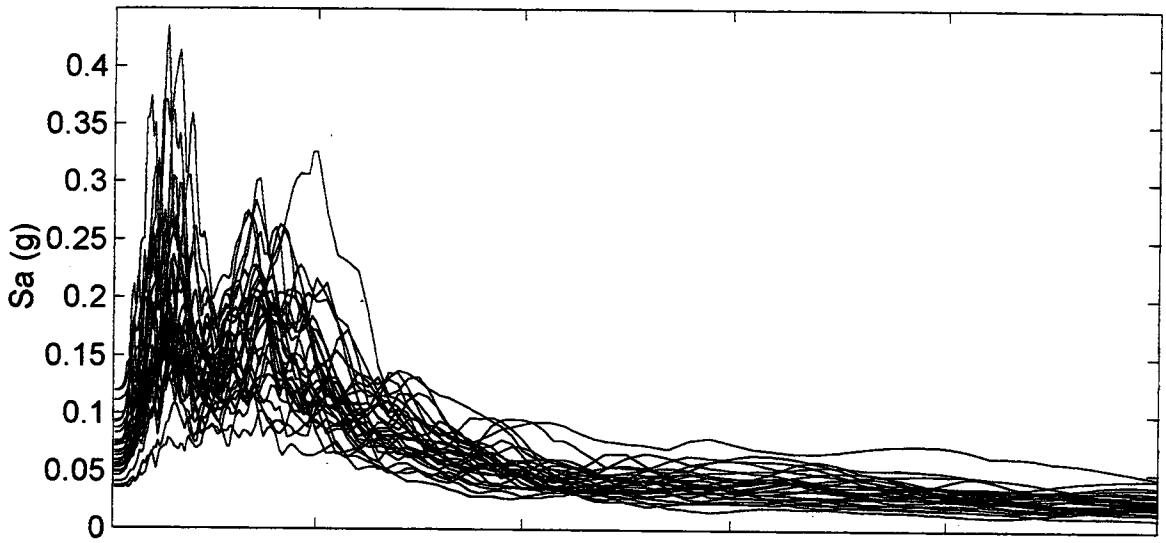

Mean and Mean +/- One Standard Deviation

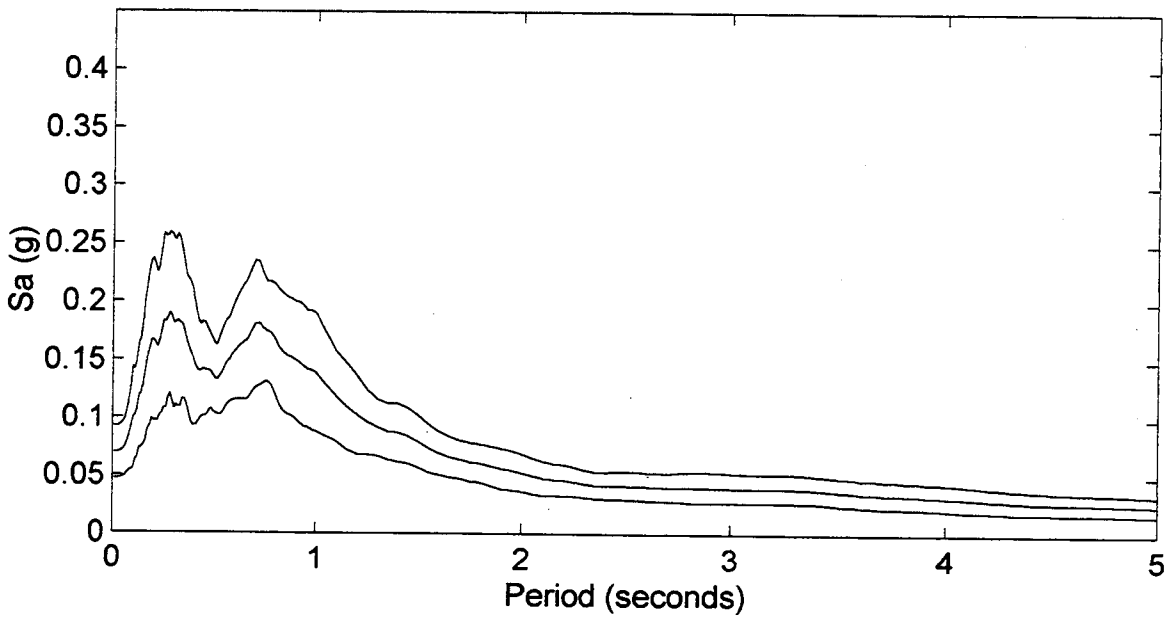

Coldwater Creek

Spectral Accelerations (M=8.0)

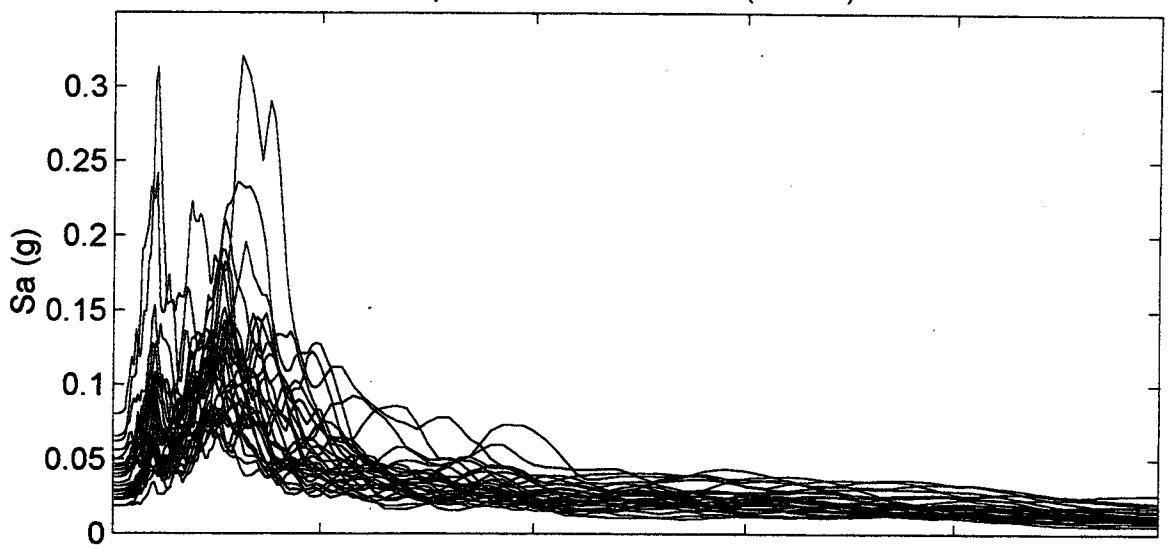

Mean and Mean +/- One Standard Deviation

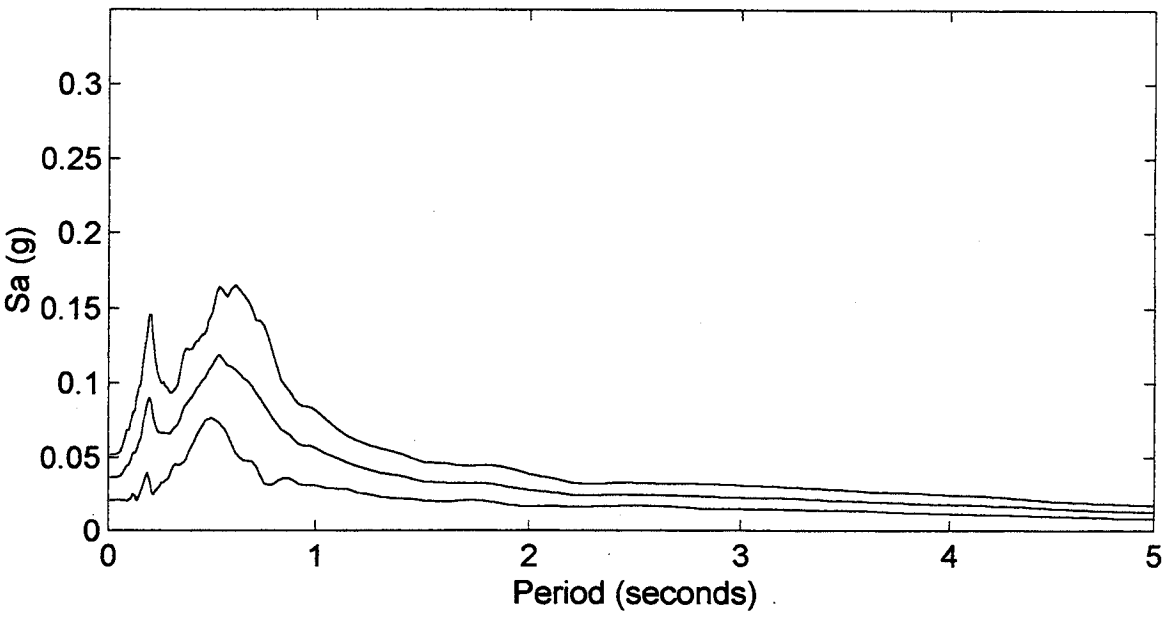

I-5/NE 99th Street

Spectral Accelerations (M=8.0)

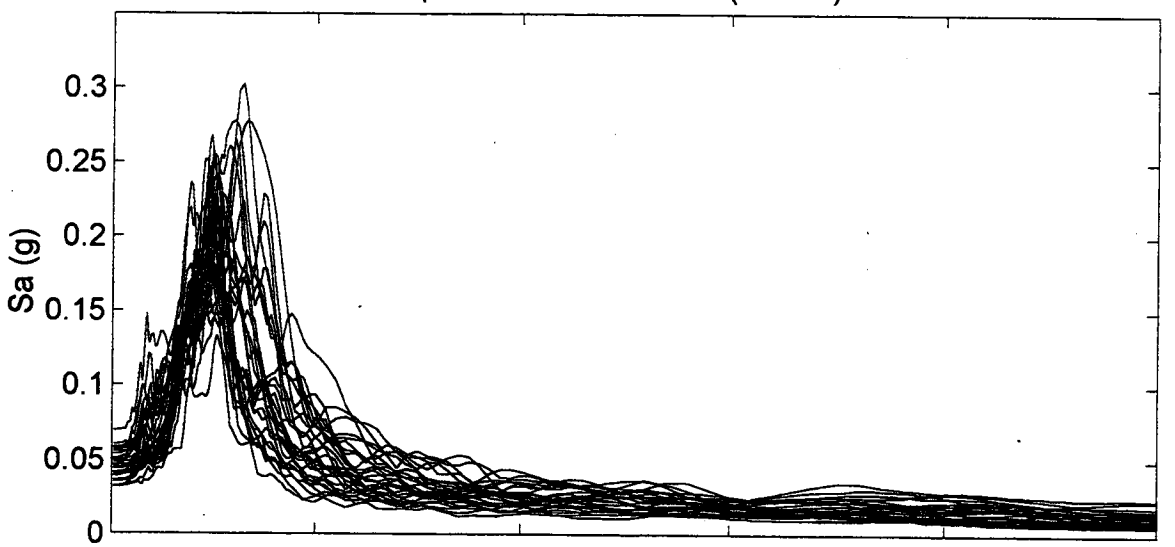

Mean and Mean +/- One Standard Deviation

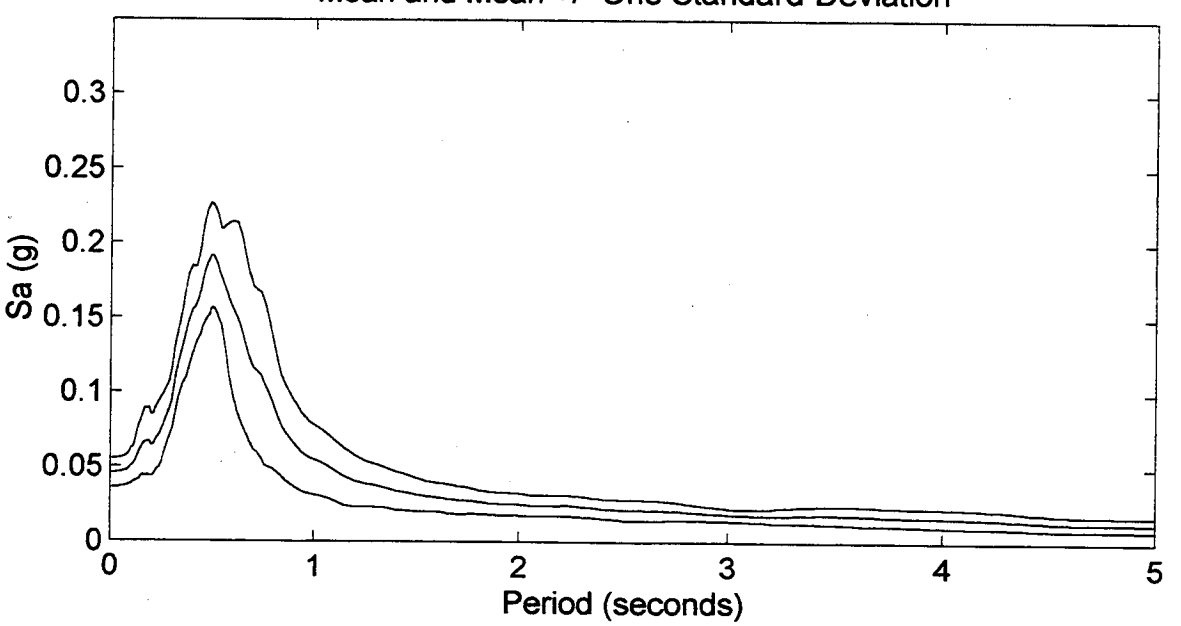

I-405/SR-522

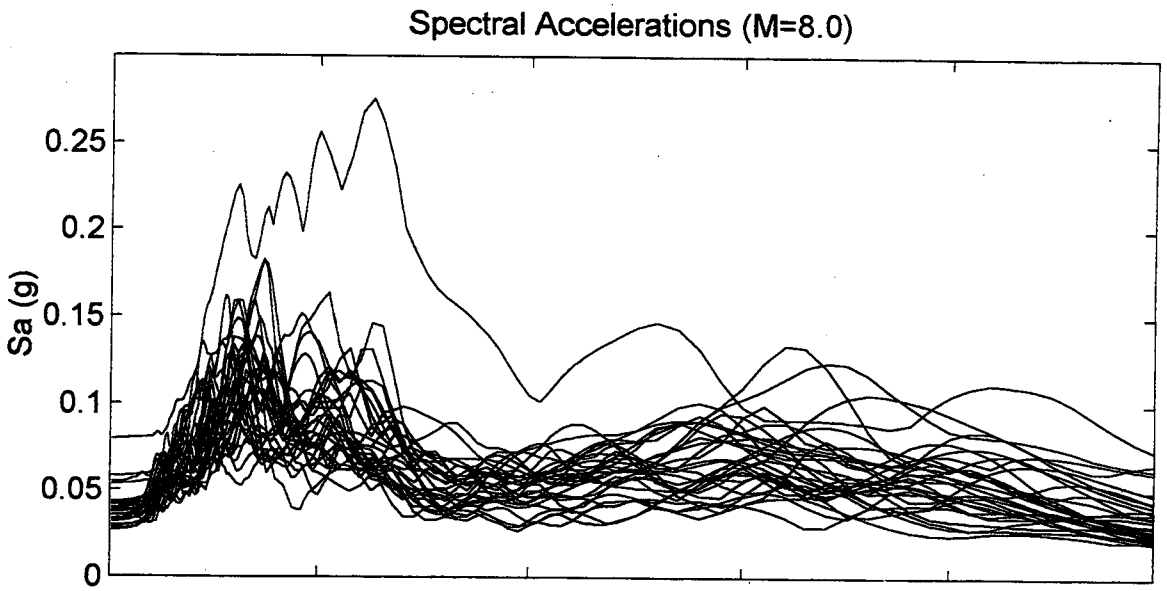
Spectral Accelerations (M=8.0)
Sa (g)
0.25
0.2
0.15
0.1
0.05
0

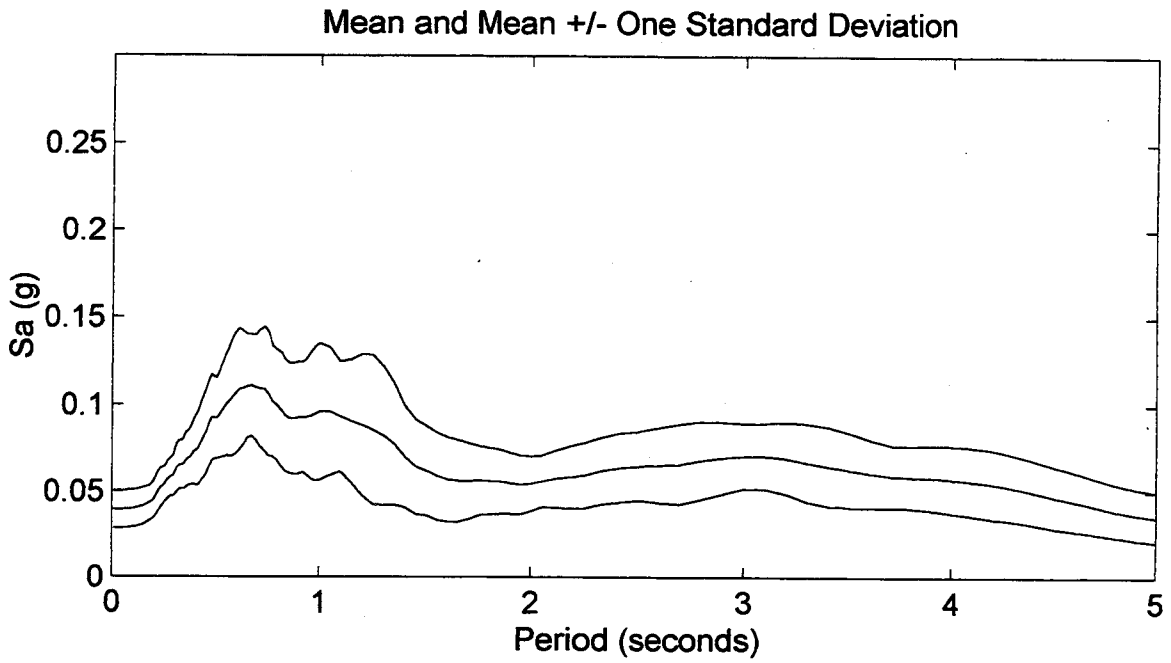
Mean and Mean +/- One Standard Deviation
Sa (g)
0.25
0.2
0.15
0.1
0.05
0
0
1
2
3
4
5
Period (seconds)

Kent Valley

Spectral Accelerations (M=8.0)

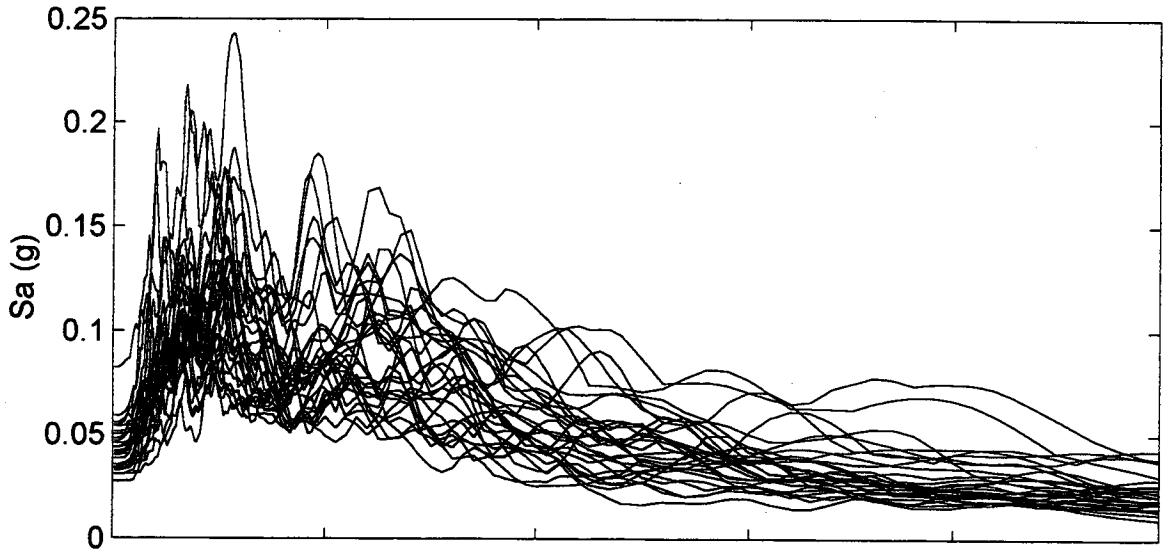

Mean and Mean +/- One Standard Deviation

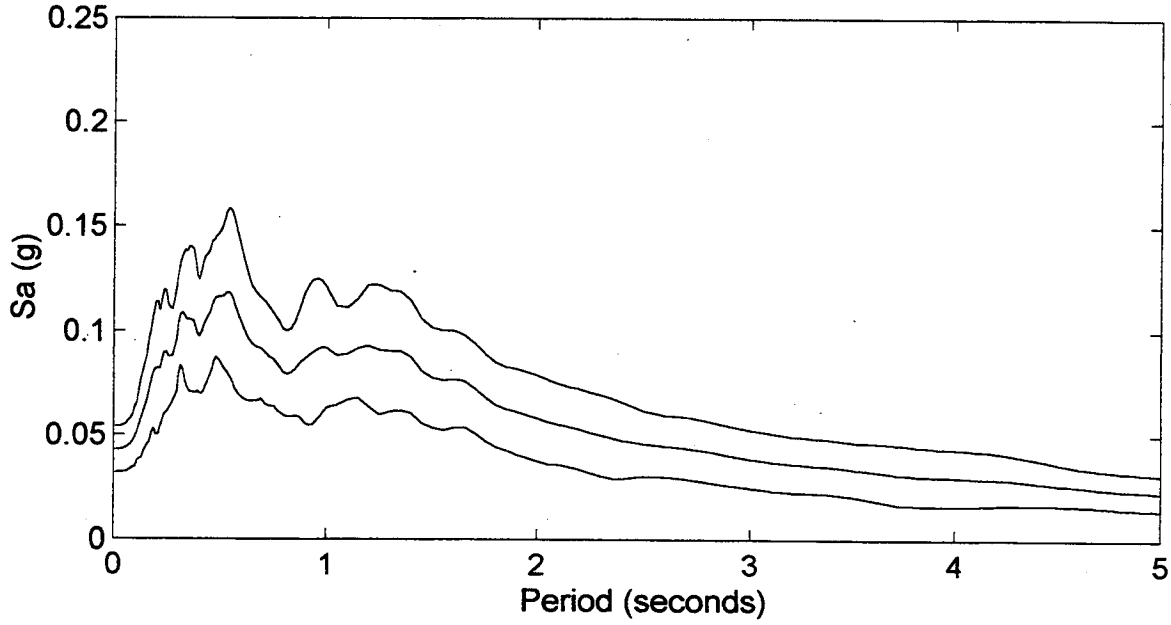

Mercer Slough 1

Spectral Accelerations (M=8.0)

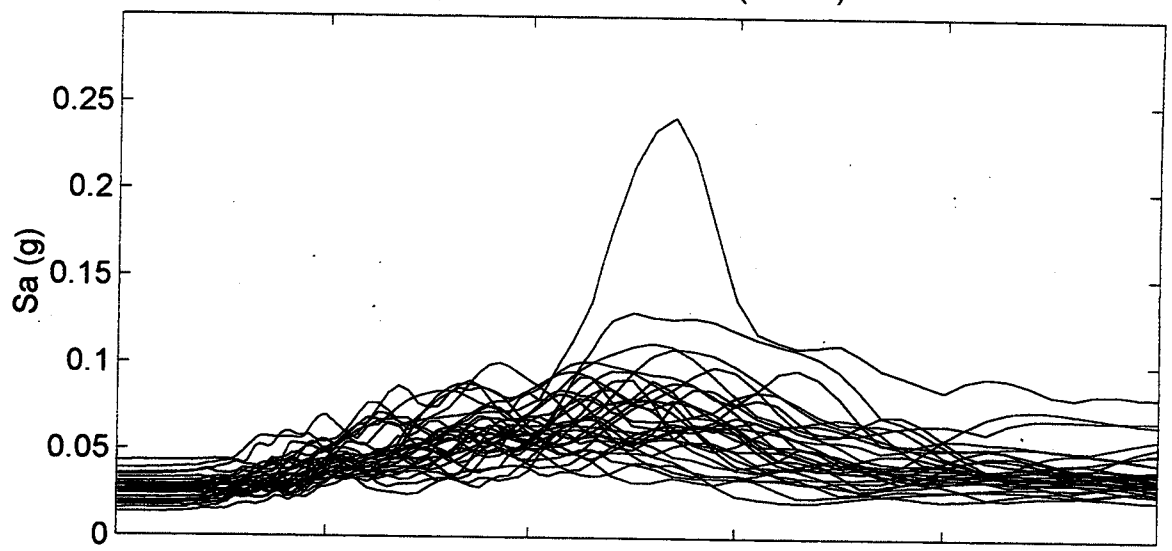

Mean and Mean +/- One Standard Deviation

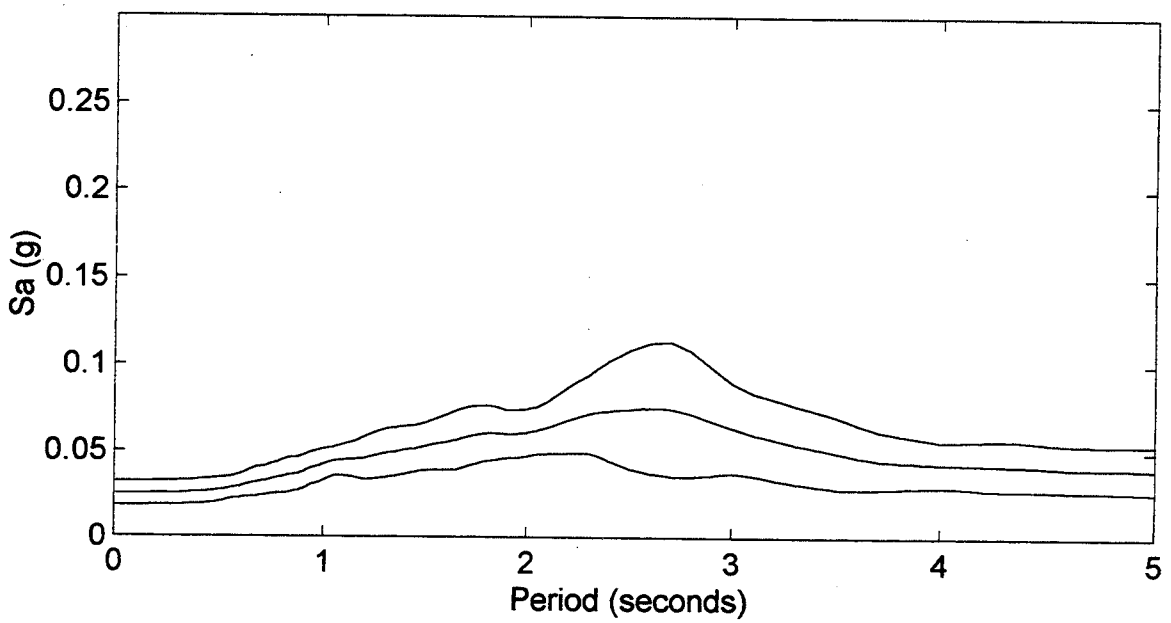

Mercer Slough 2

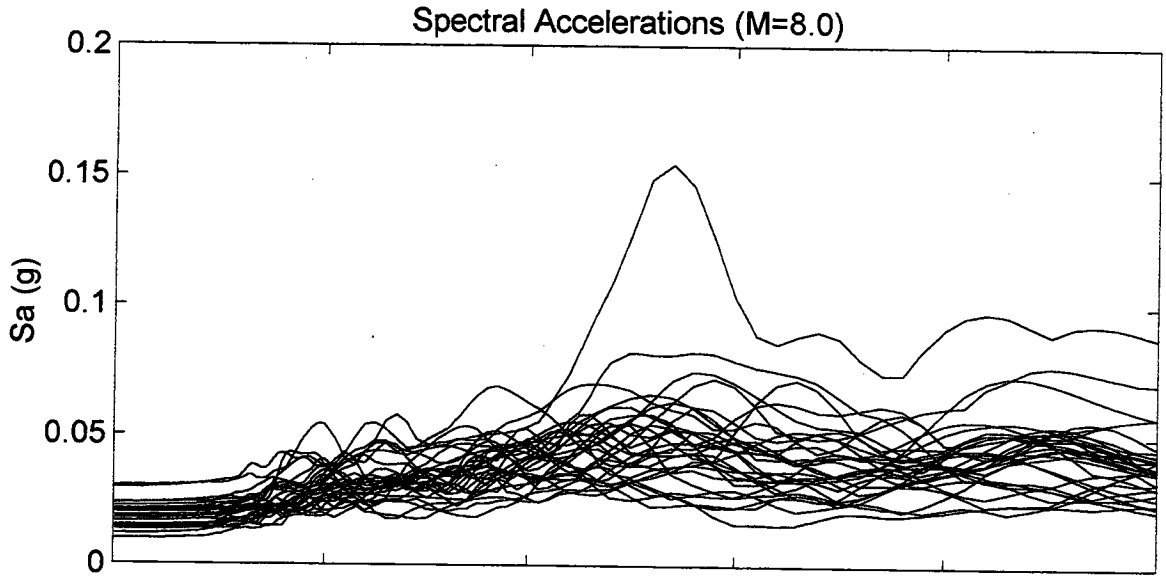

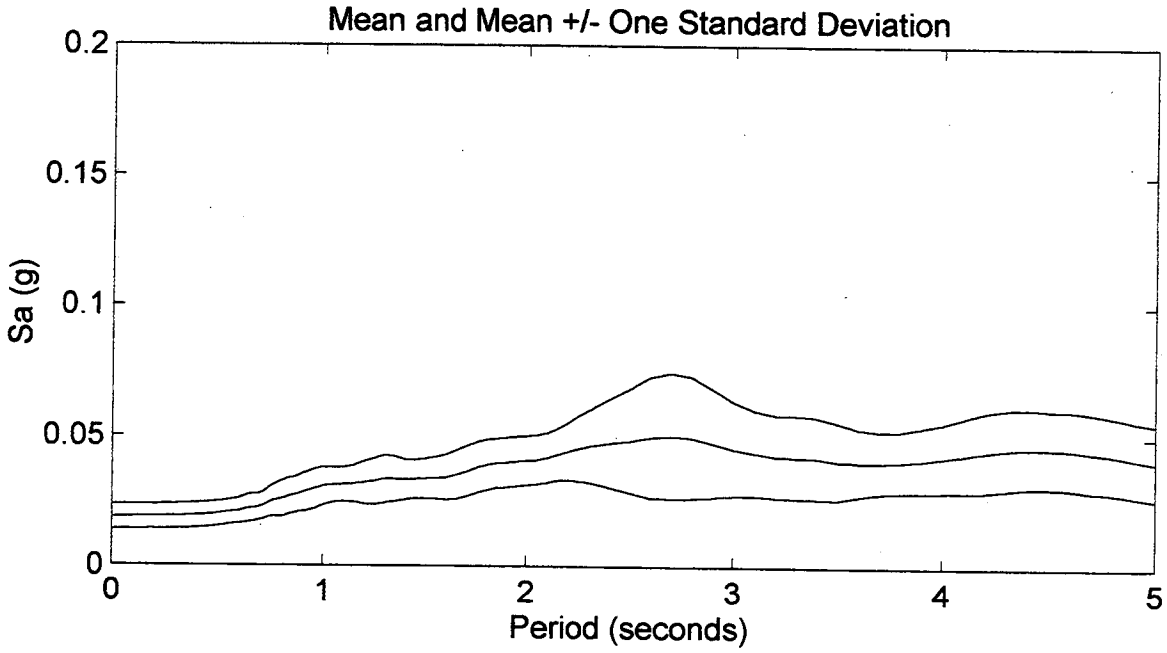

Nooksack River

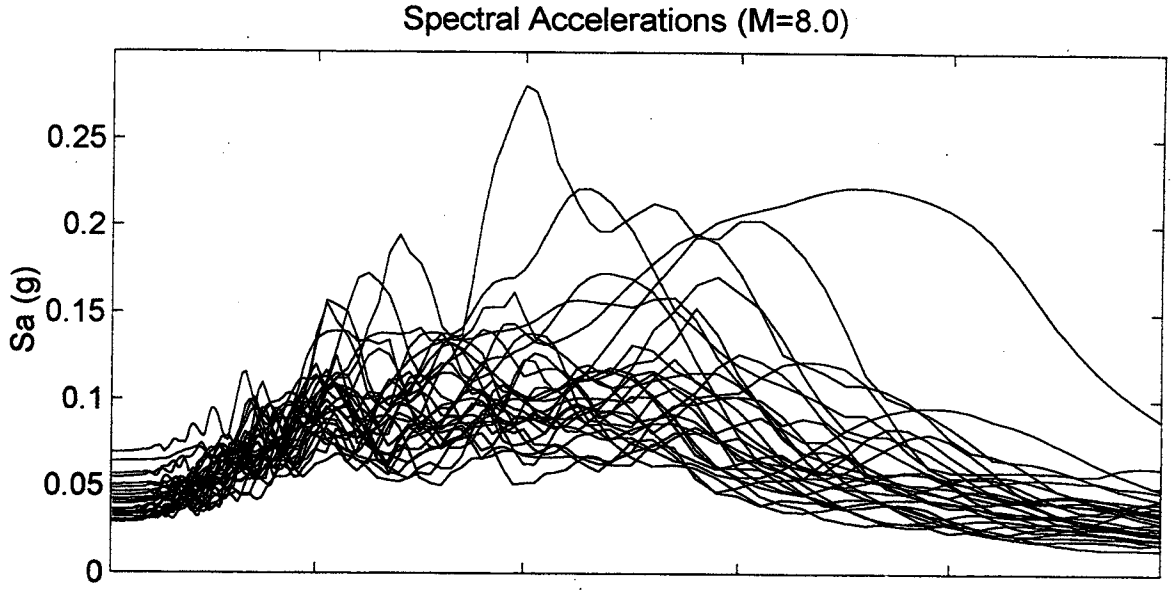

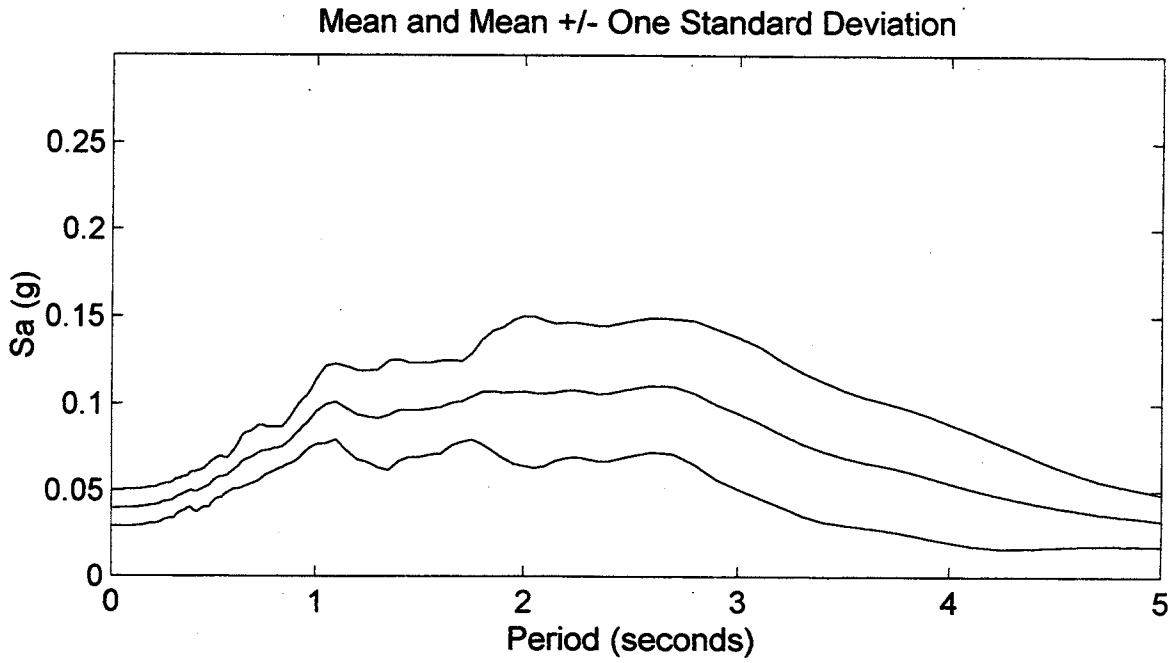

North Ferndale

Spectral Accelerations (M=8.0)

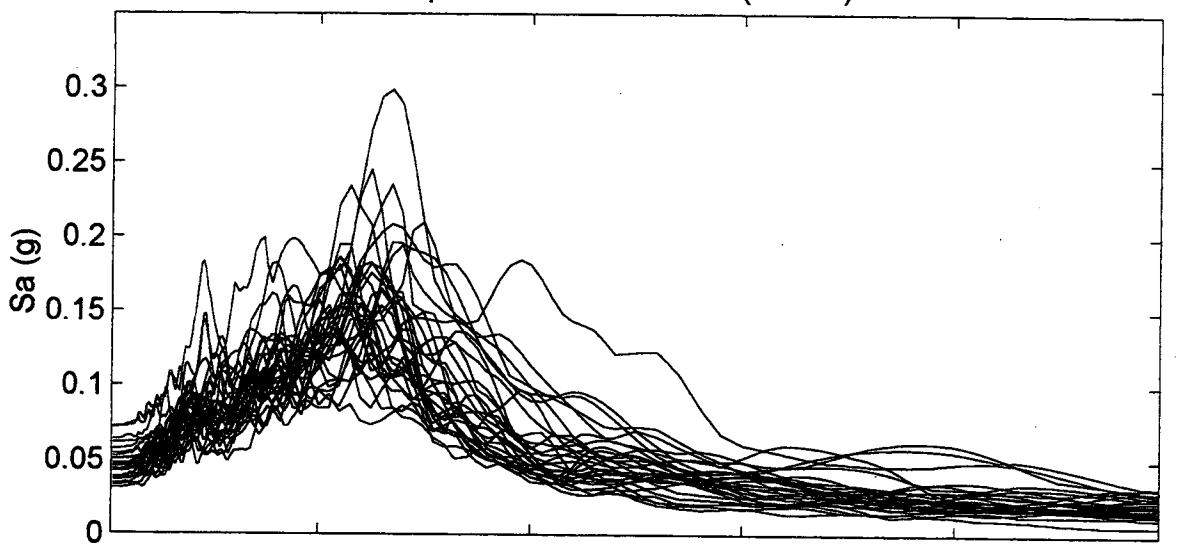

Mean and Mean +/- One Standard Deviation

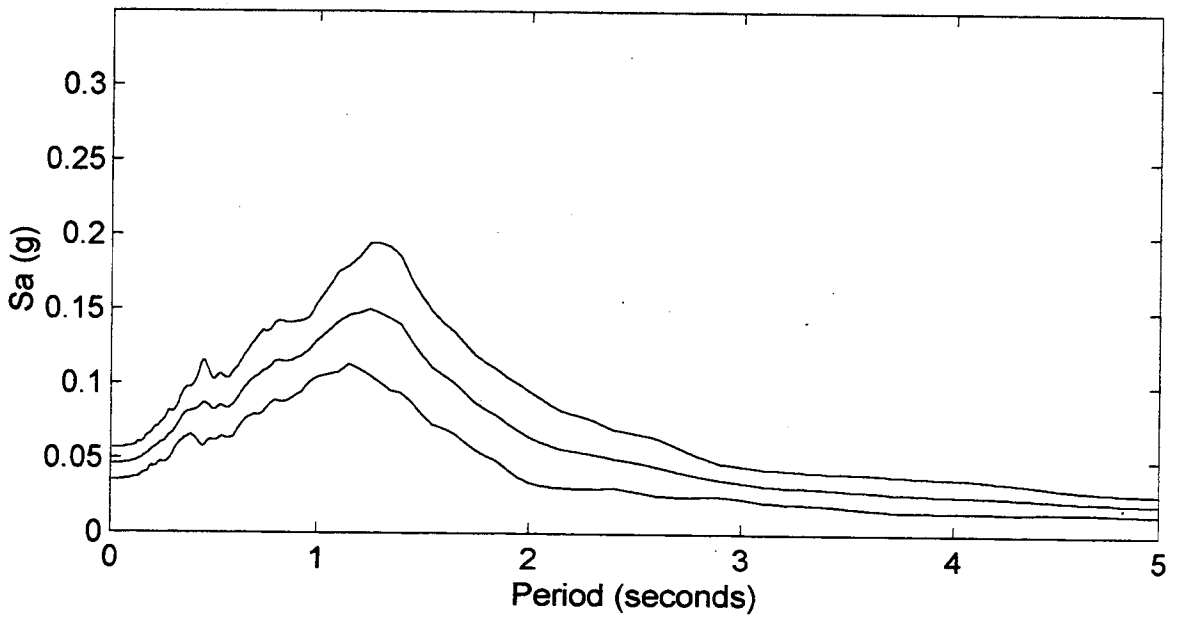

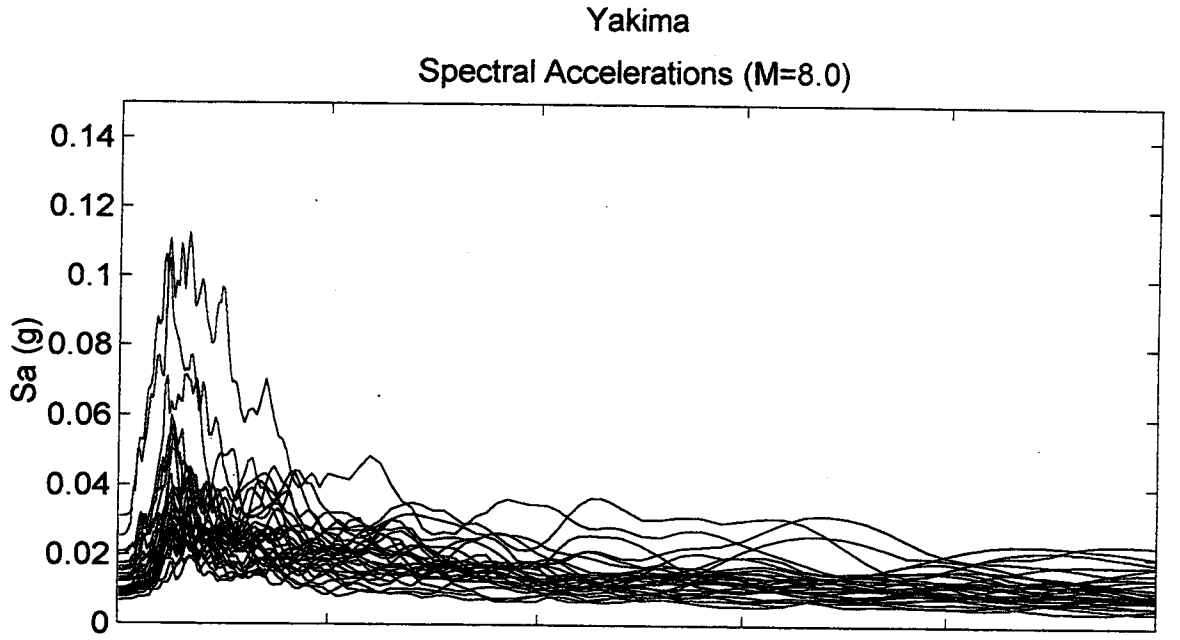
Yakima
Spectral Accelerations (M=8.0)
Sa (g)
0.14
0.12
0.1
0.08
0.06
0.04
0.02
0

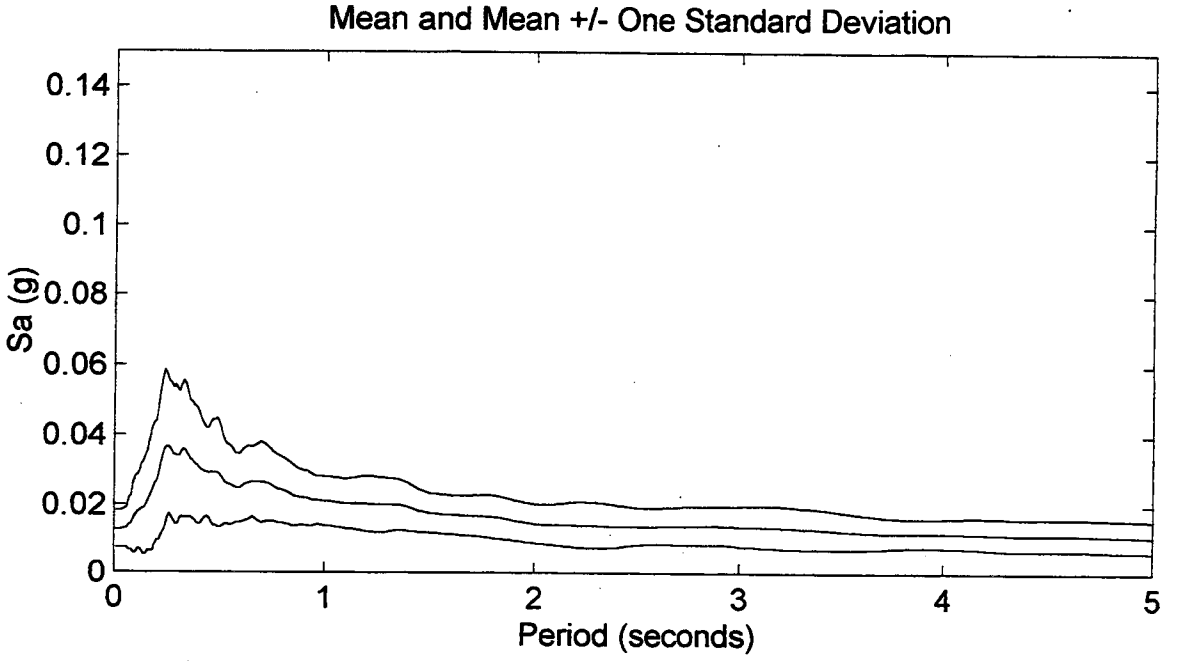
Mean and Mean +/- One Standard Deviation
Sa (g)
0.14
0.12
0.1
0.08
0.06
0.04
0.02
0
0
1
2
3
4
5
Period (seconds)

Andresen Road

Spectral Accelerations (M=8.5)

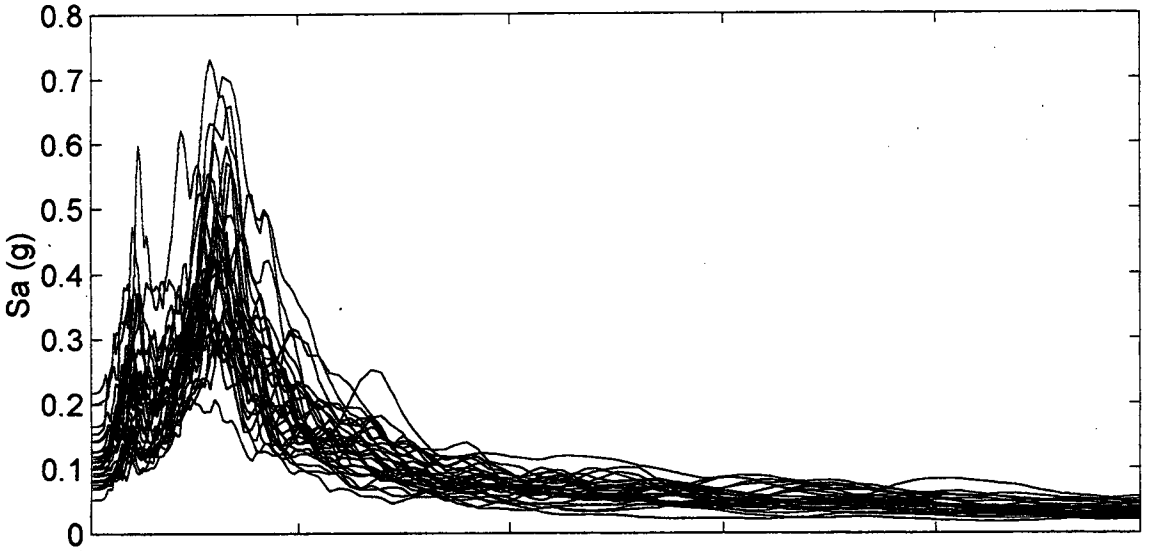

Mean and Mean +/- One Standard Deviation

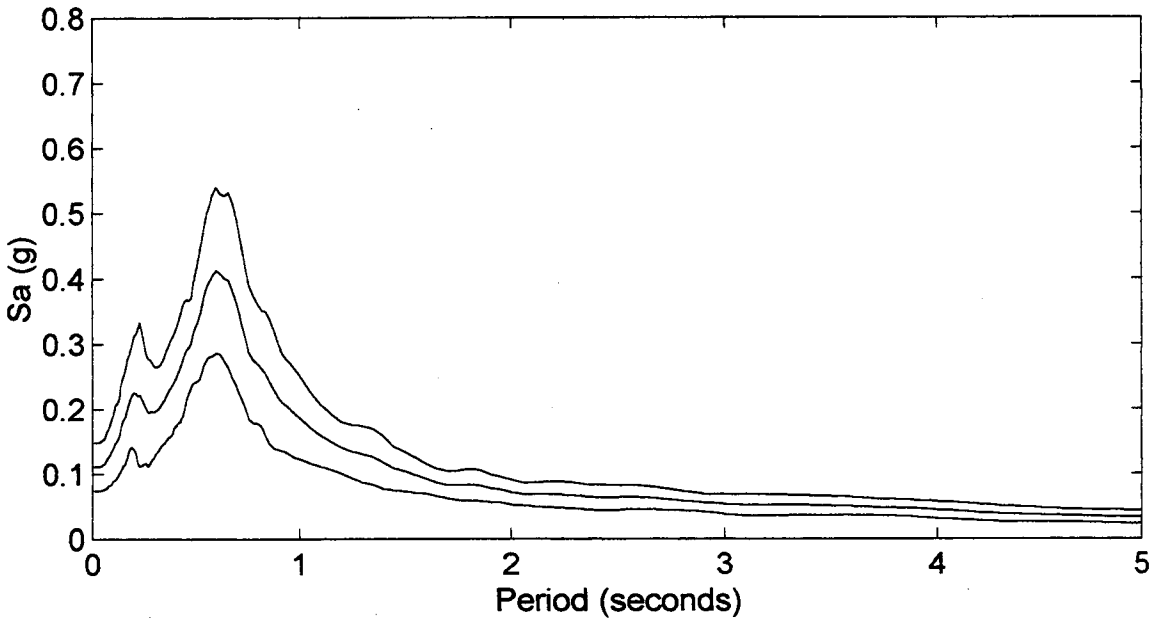

Alaskan Way Viaduct 1

Spectral Accelerations (M=8.5)

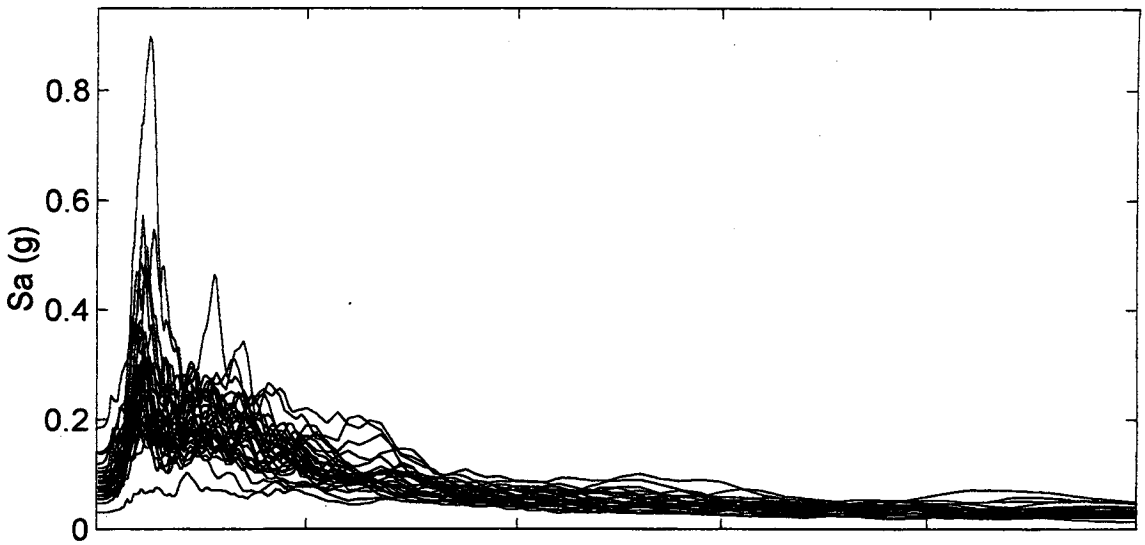

Mean and Mean +/- One Standard Deviation

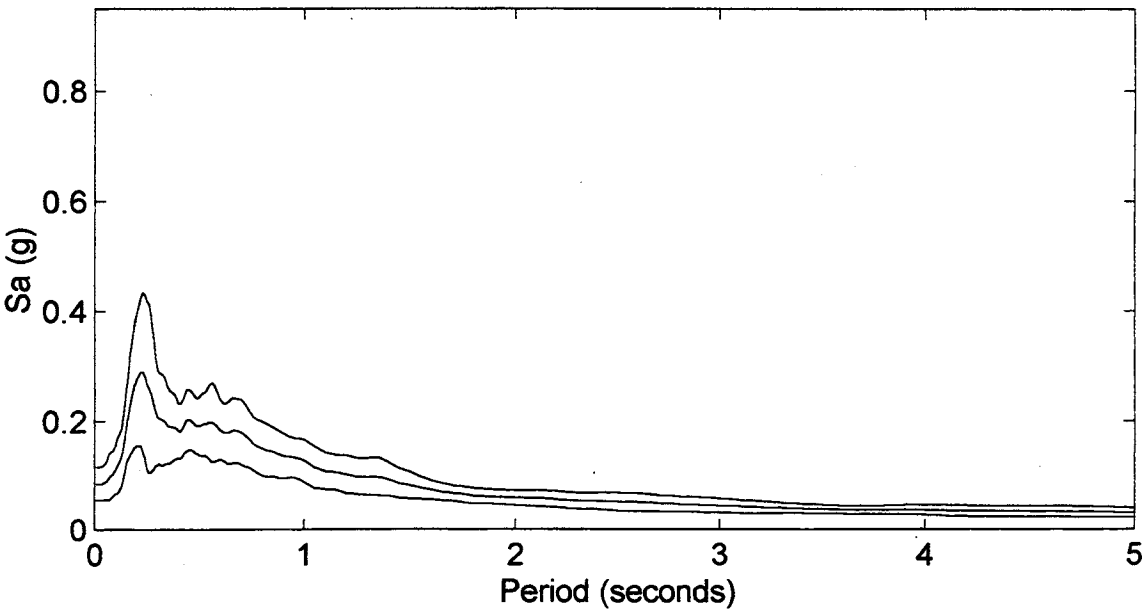

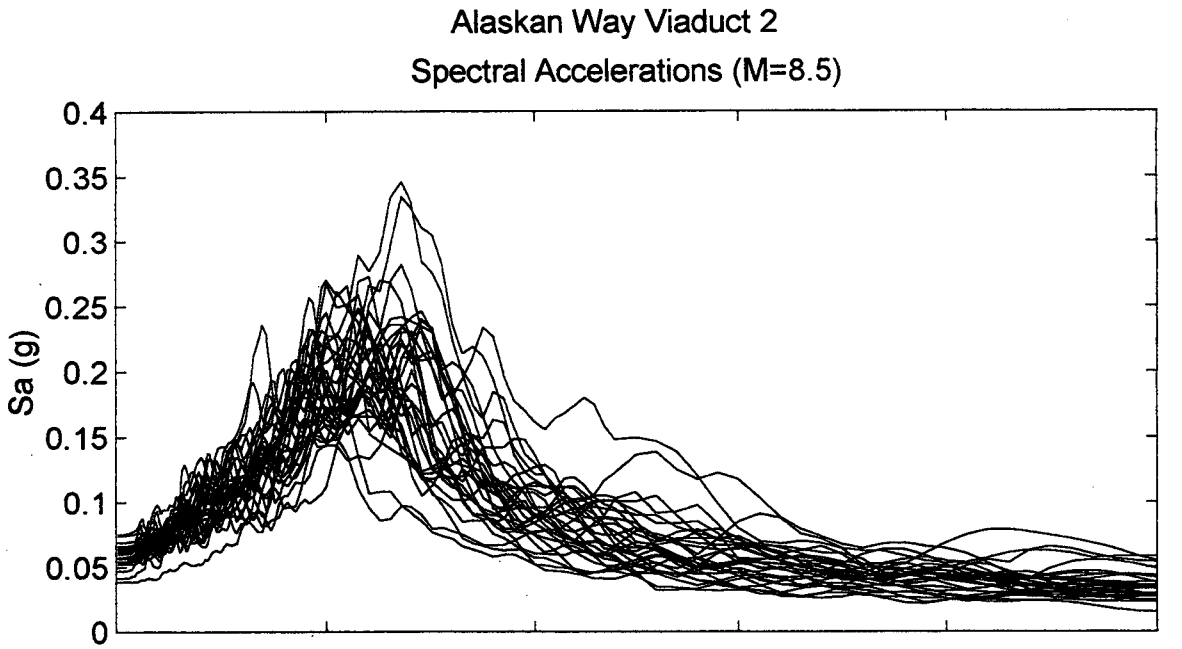
Alaskan Way Viaduct 2
Spectral Accelerations (M=8.5)
Sa (g)
0.4
0.35
0.3
0.25
0.2
0.15
0.1
0.05
0

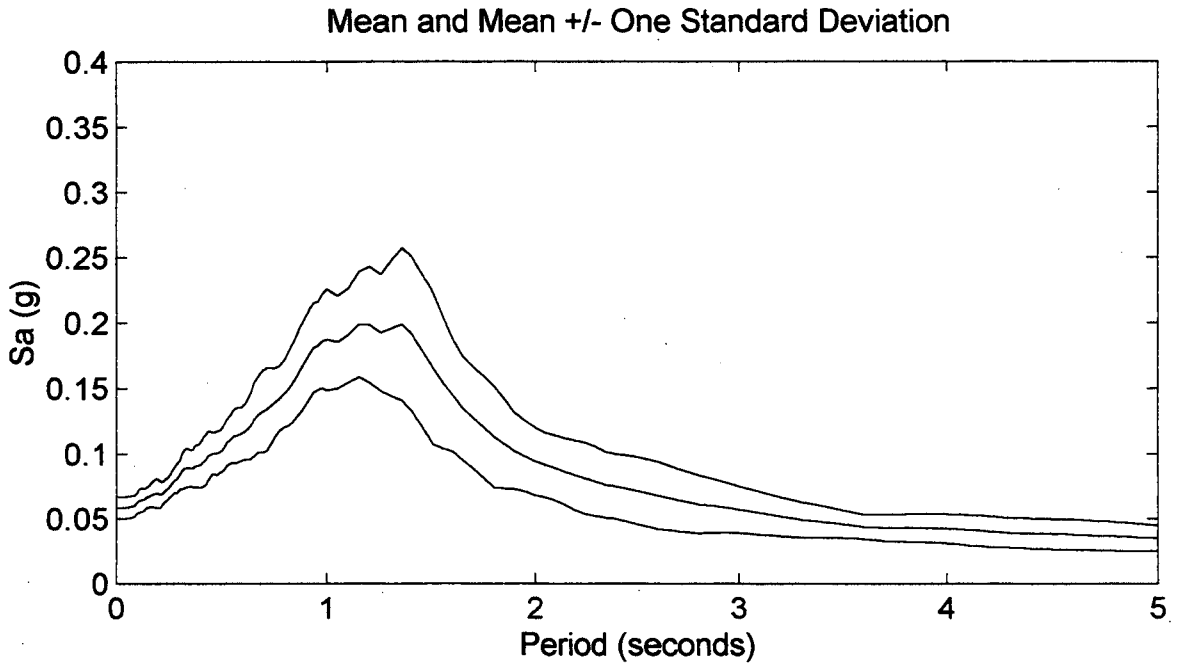
Mean and Mean +/- One Standard Deviation
Sa (g)
0.4
0.35
0.3
0.25
0.2
0.15
0.1
0.05
0
0
1
2
3
4
5
Period (seconds)

Black Diamond Road

Spectral Accelerations (M=8.5)

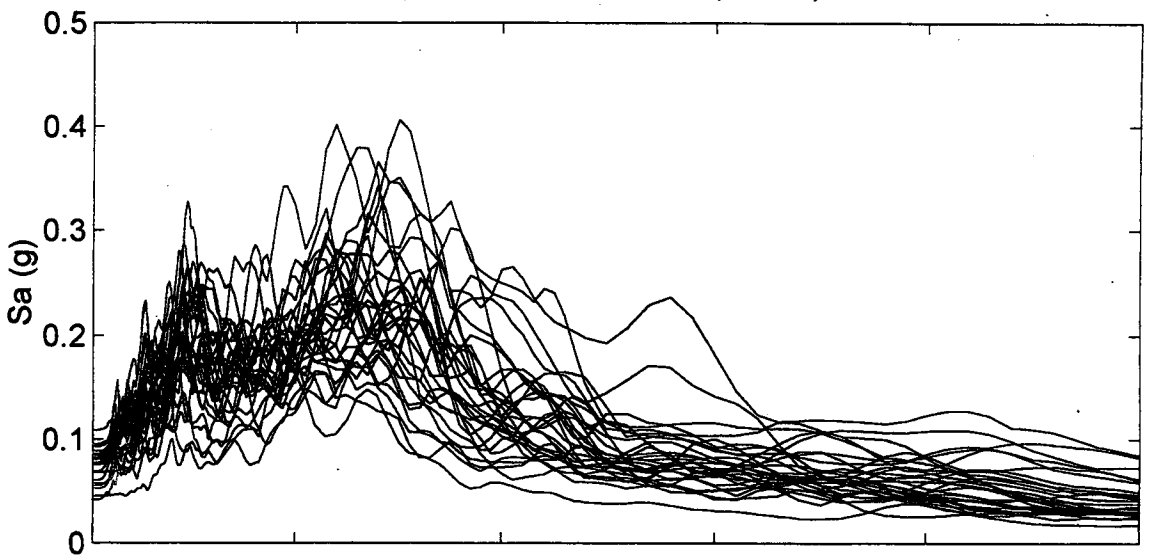

Mean and Mean +/- One Standard Deviation

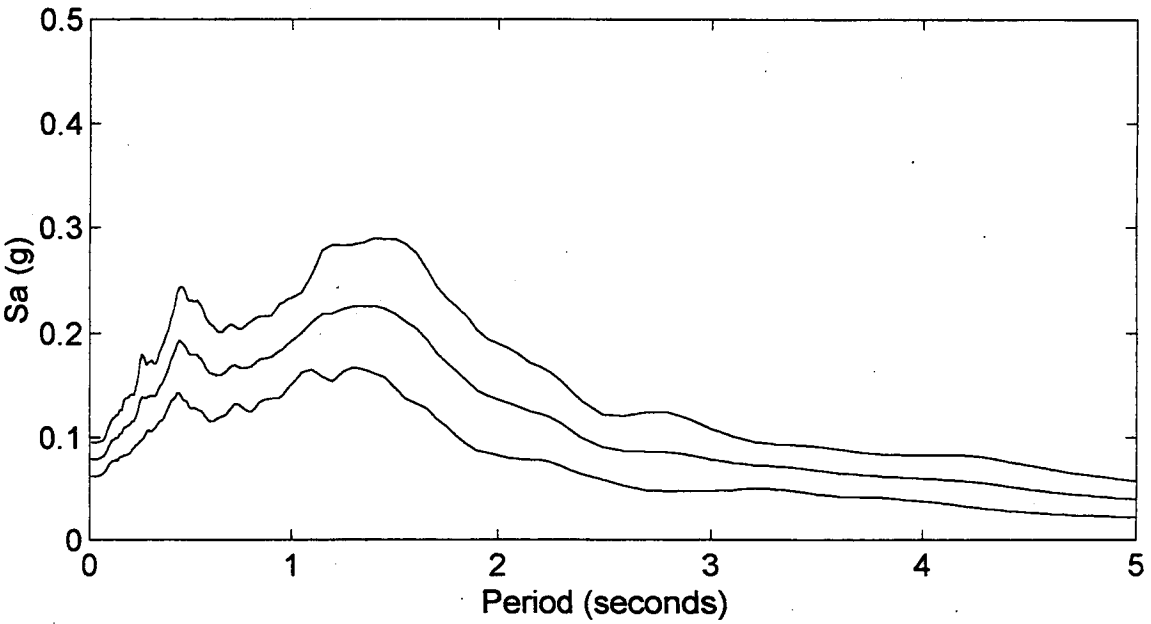

Bone River

Spectral Accelerations (M=8.5)

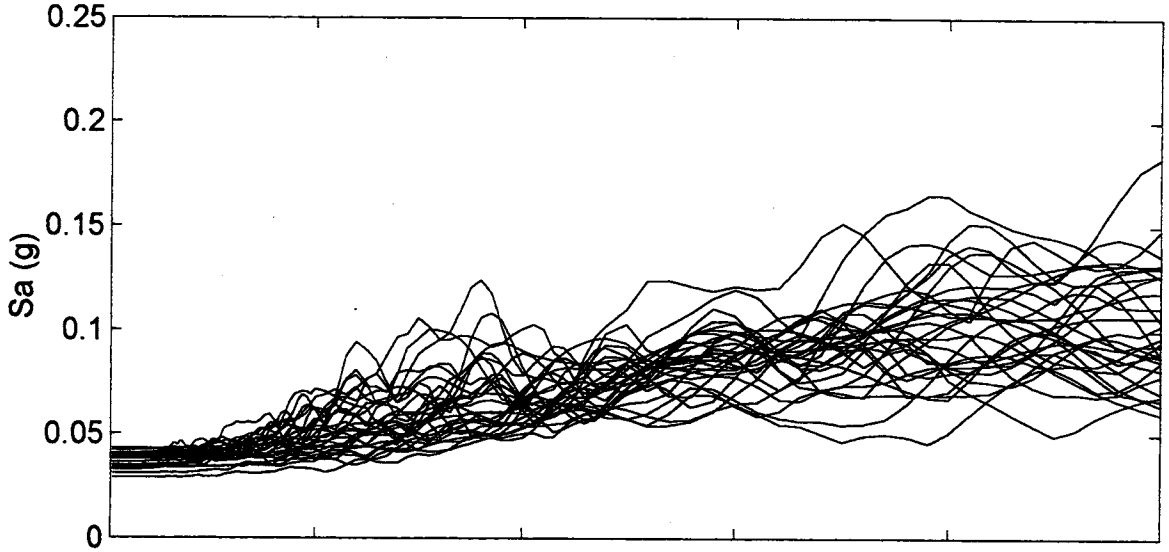

Mean and Mean +/- One Standard Deviation

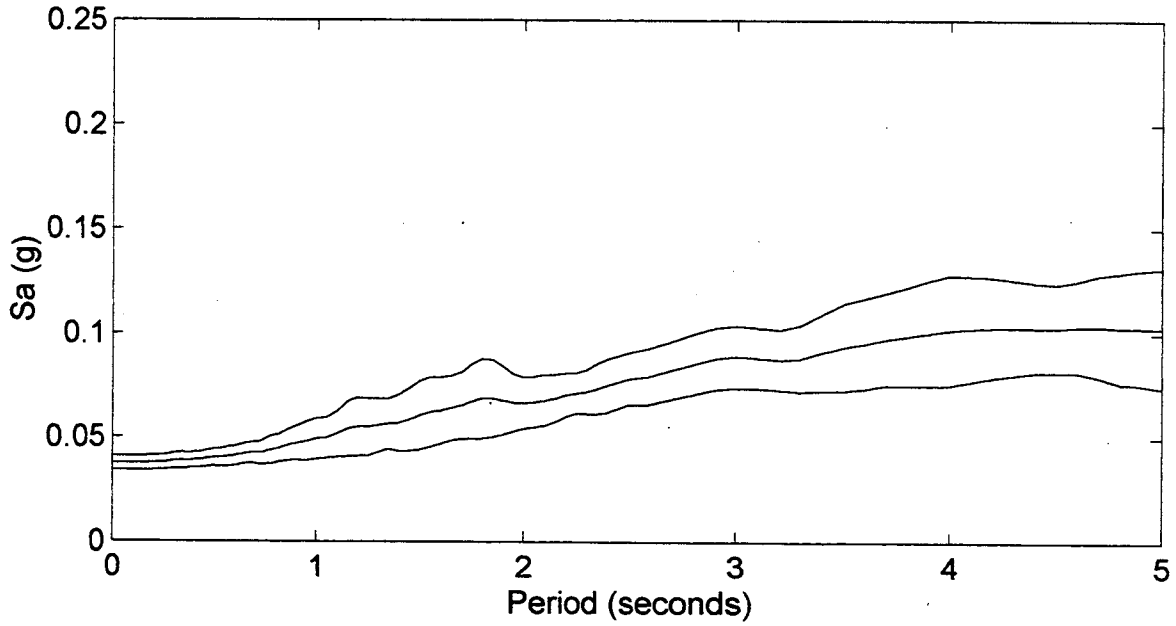

Capitol Boulevard

Spectral Accelerations (M=8.5)

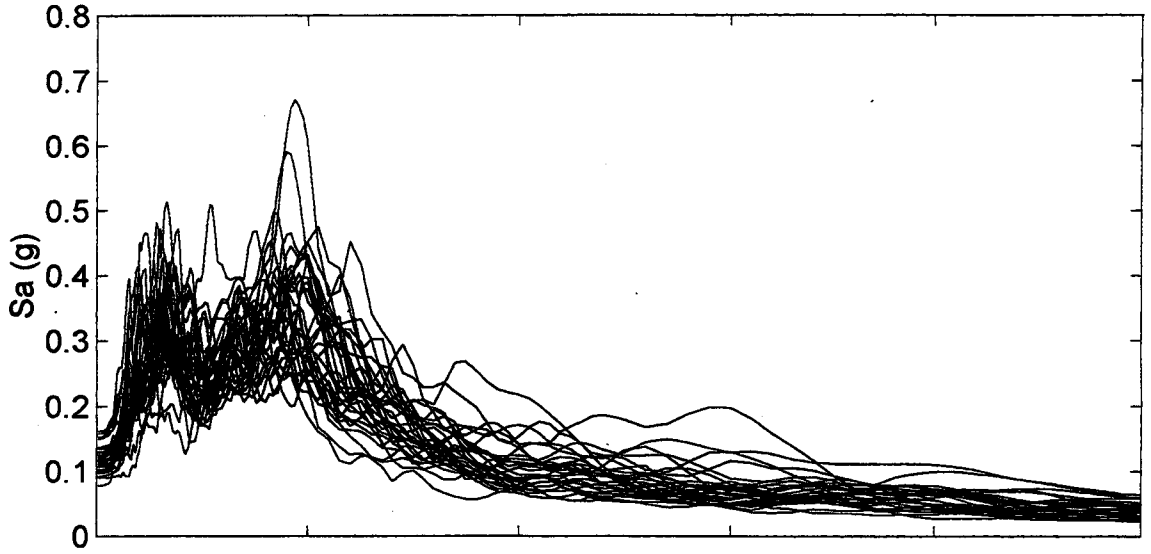

Mean and Mean +/- One Standard Deviation

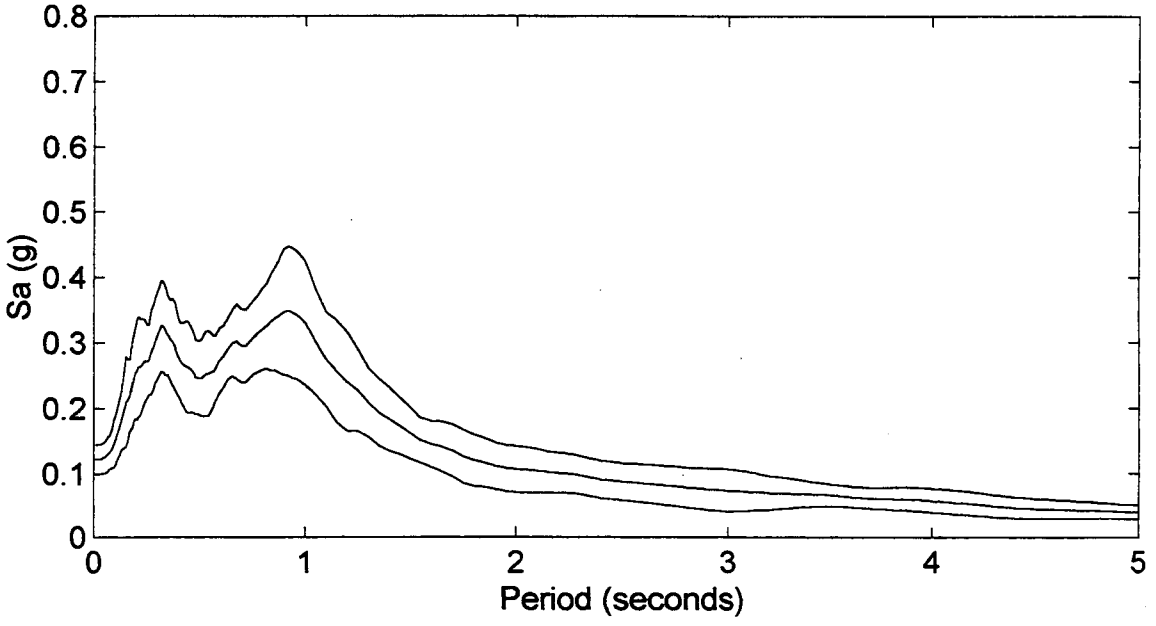

Coldwater Creek

Spectral Accelerations (M=8.5)

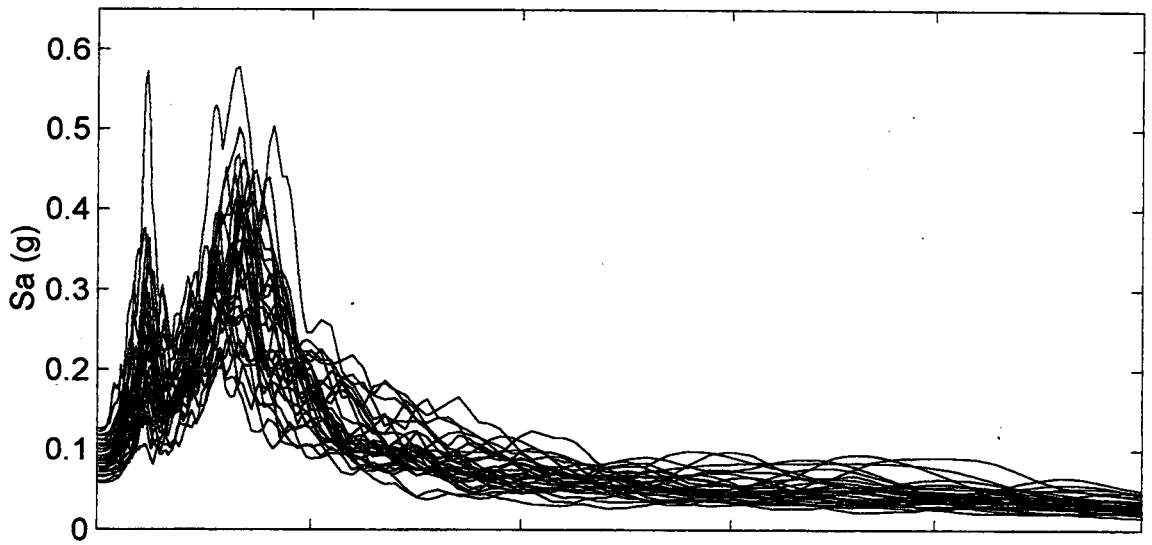

Mean and Mean +/- One Standard Deviation

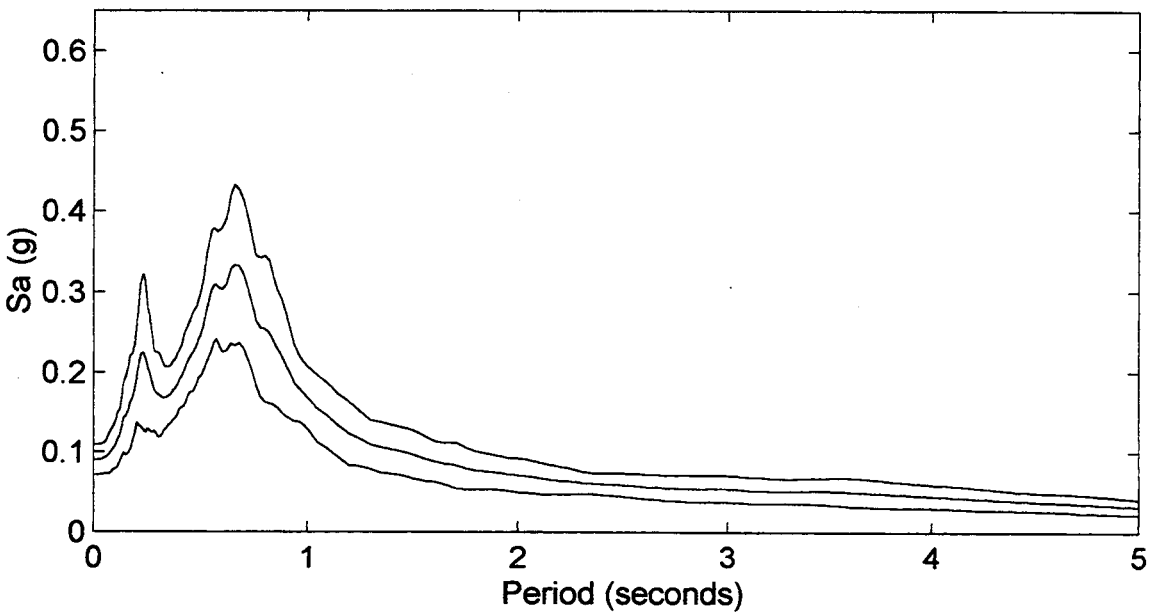

I-5/NE 99th Street

Spectral Accelerations (M=8.5)

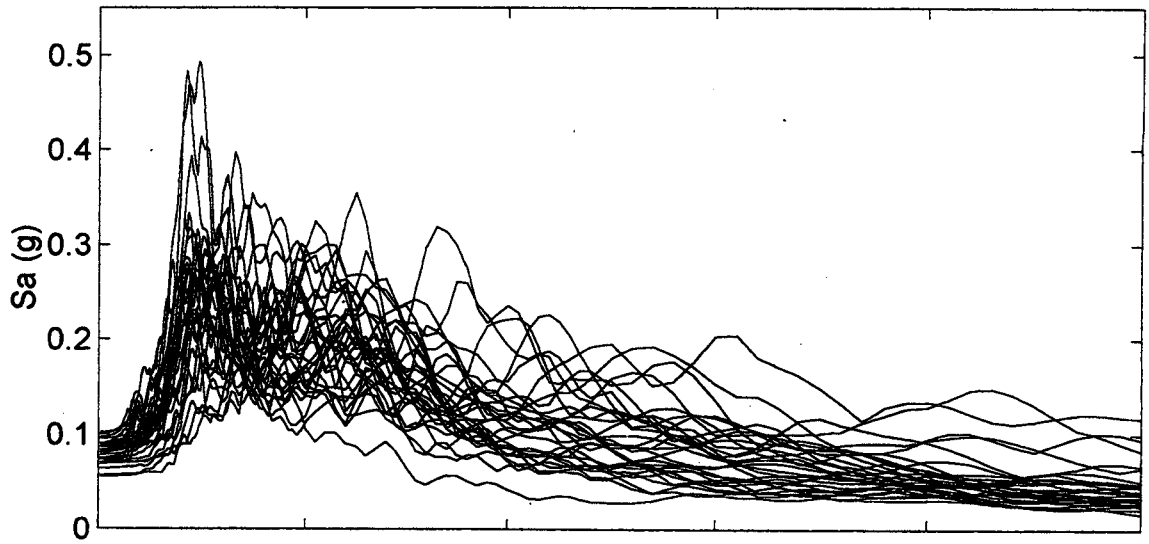

Mean and Mean +/- One Standard Deviation

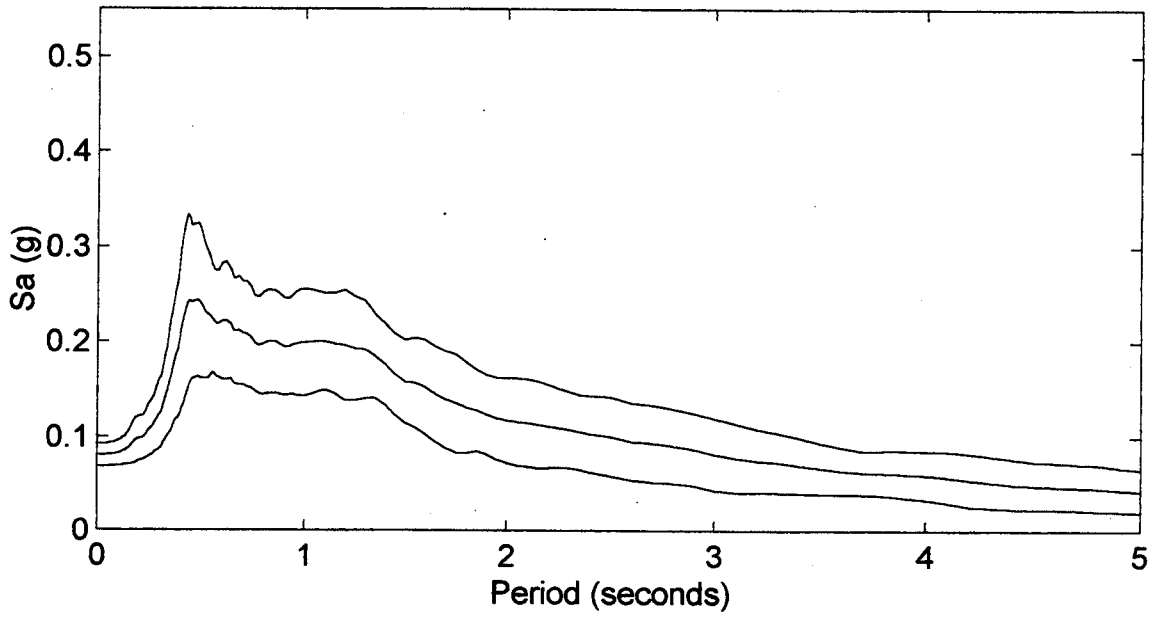

I-405/SR-522

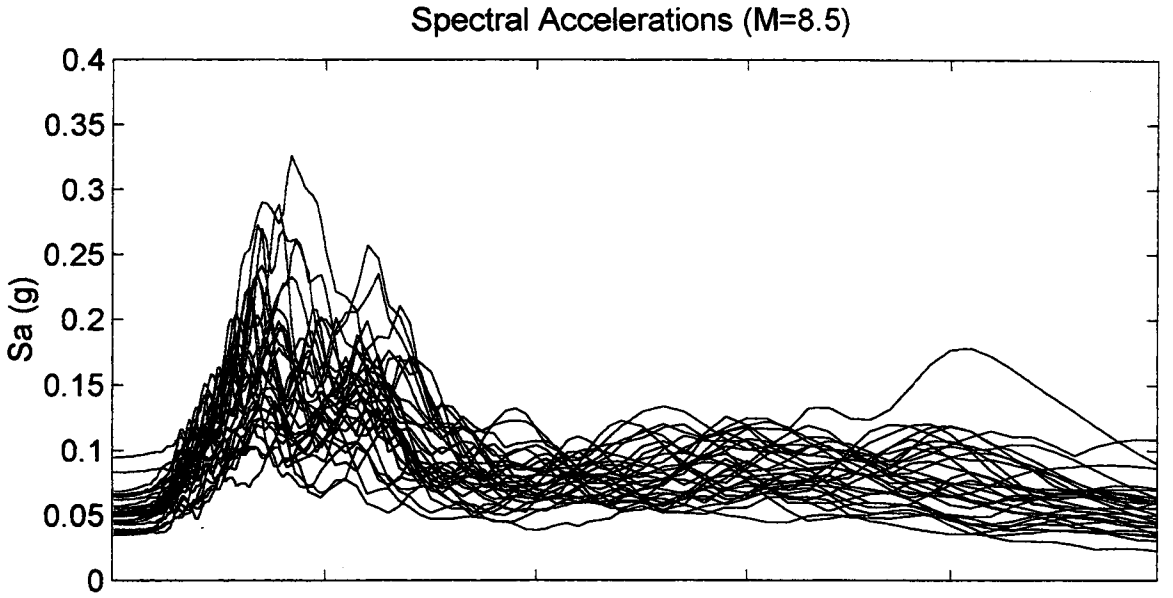
Spectral Accelerations (M=8.5)
Sa (g)
0.4
0.35
0.3
0.25
0.2
0.15
0.1
0.05
0

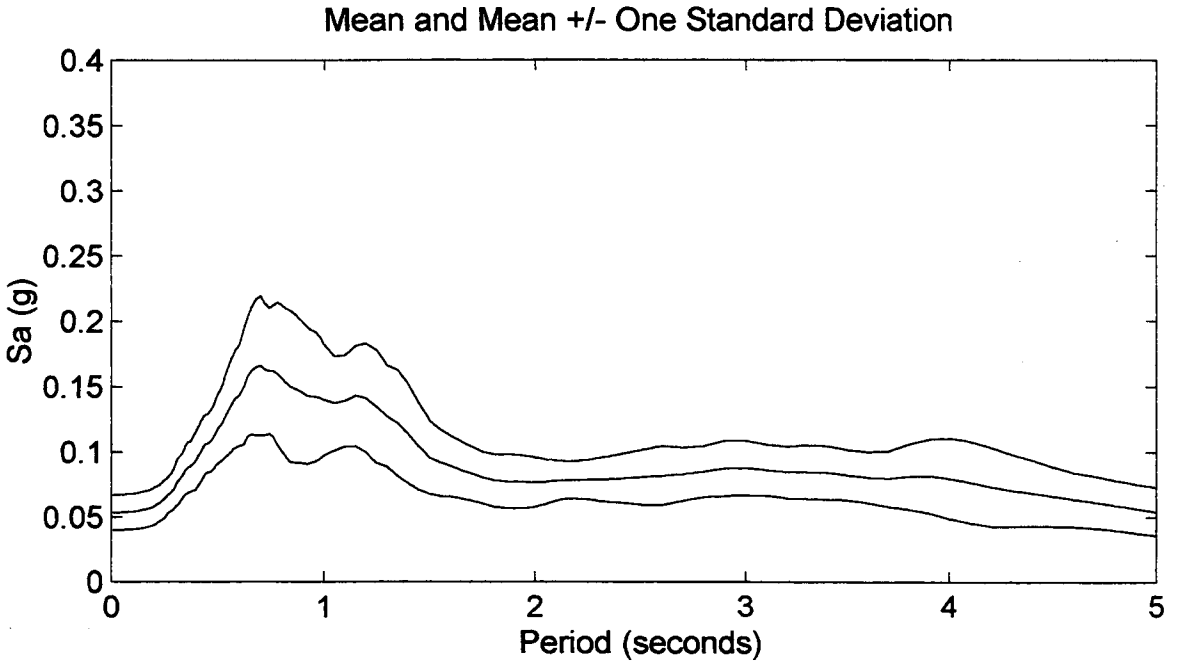
Mean and Mean +/- One Standard Deviation
Sa (g)
0.4
0.35
0.3
0.25
0.2
0.15
0.1
0.05
0
0
1
2
3
4
5
Period (seconds)

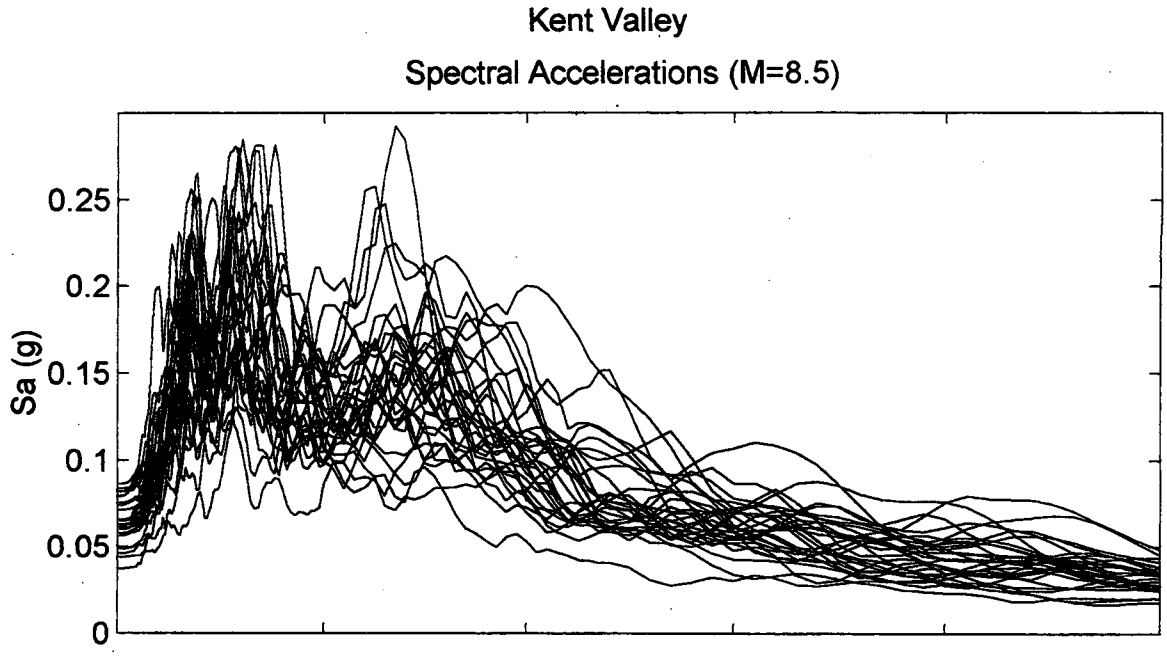
Kent Valley
Spectral Accelerations (M=8.5)
Sa (g)
0.25
0.2
0.15
0.1
0.05
0

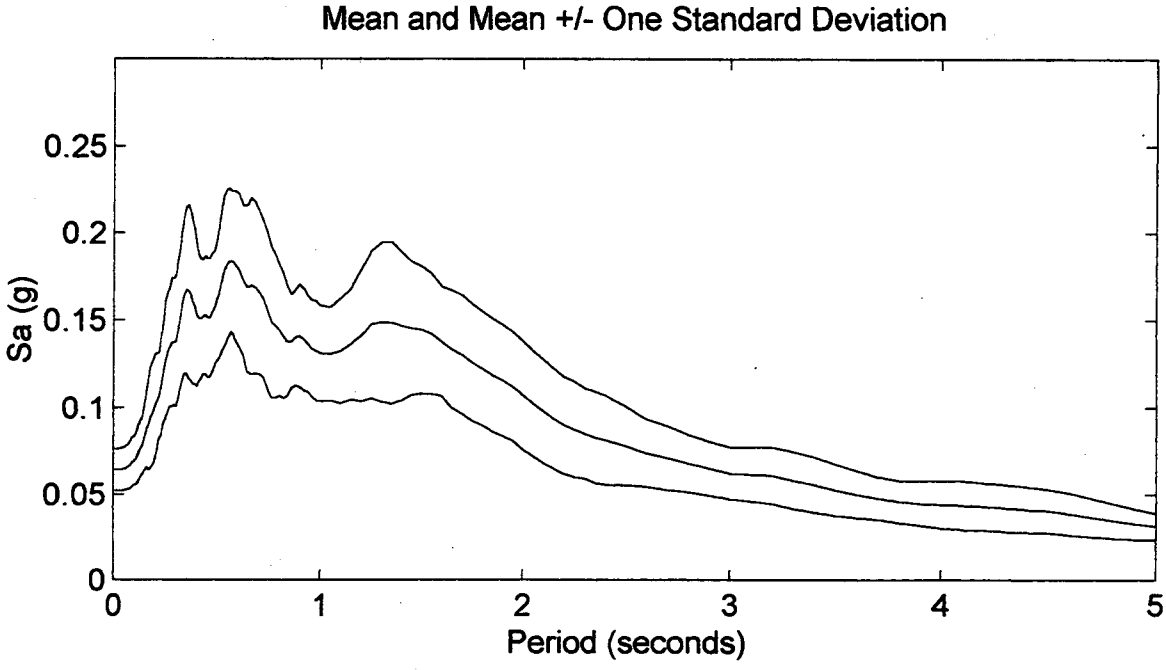
Mean and Mean +/- One Standard Deviation
Sa (g)
0.25
0.2
0.15
0.1
0.05
0
0
1
2
3
4
5
Period (seconds)

Mercer Slough 1

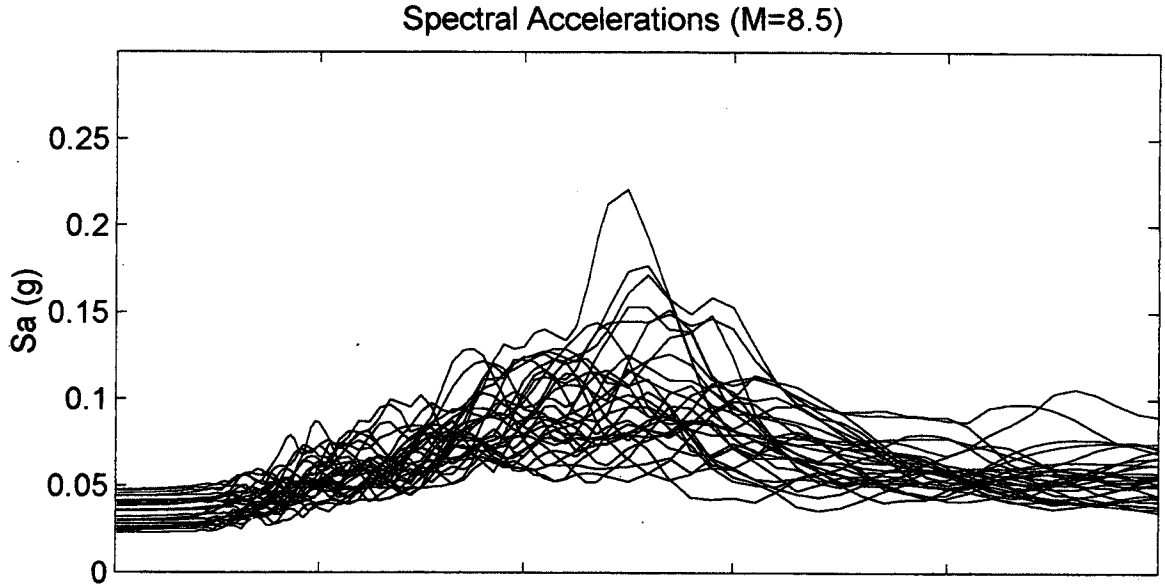

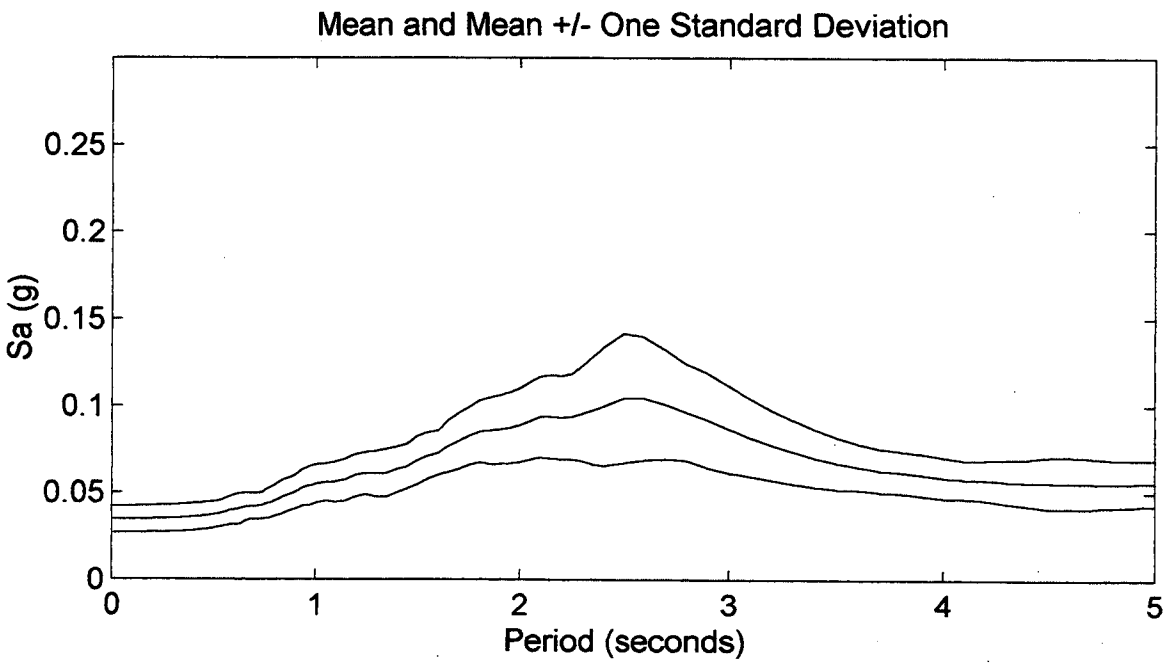

Mercer Slough 2

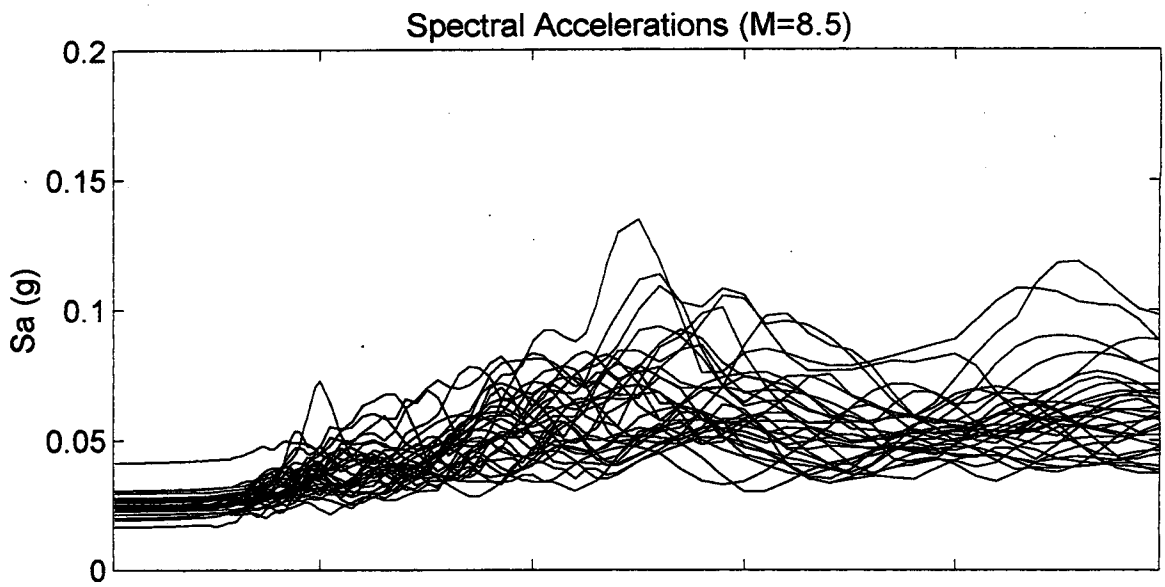

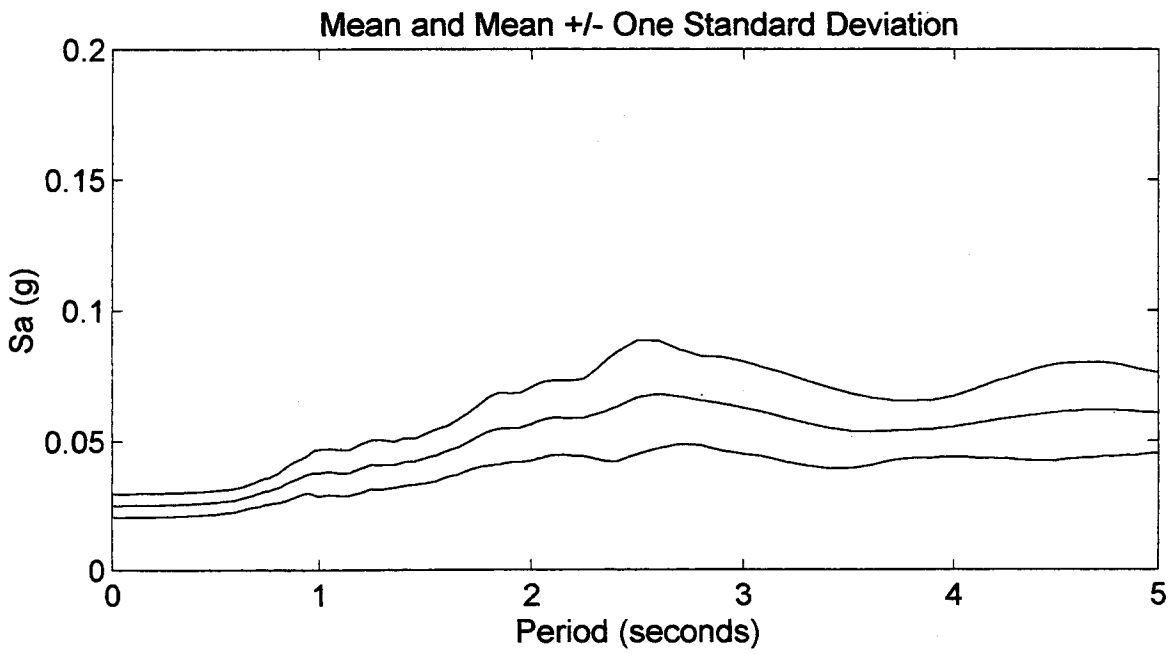

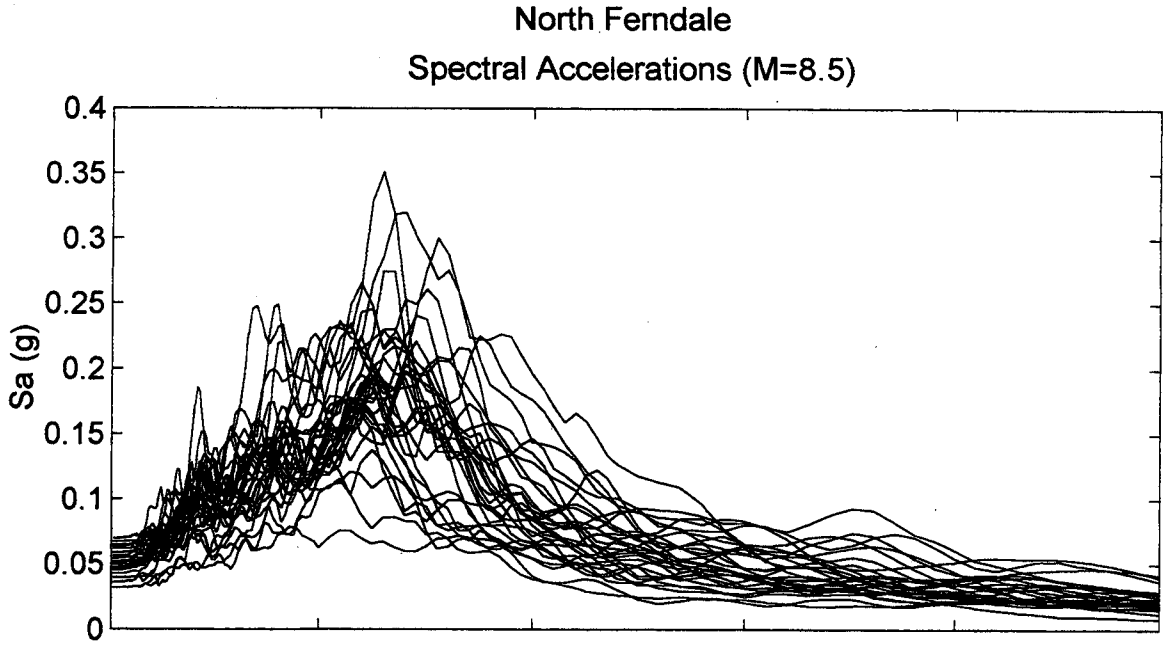
North Ferndale
Spectral Accelerations (M=8.5)
Sa (g)
0.4
0.35
0.3
0.25
0.2
0.15
0.1
0.05
0

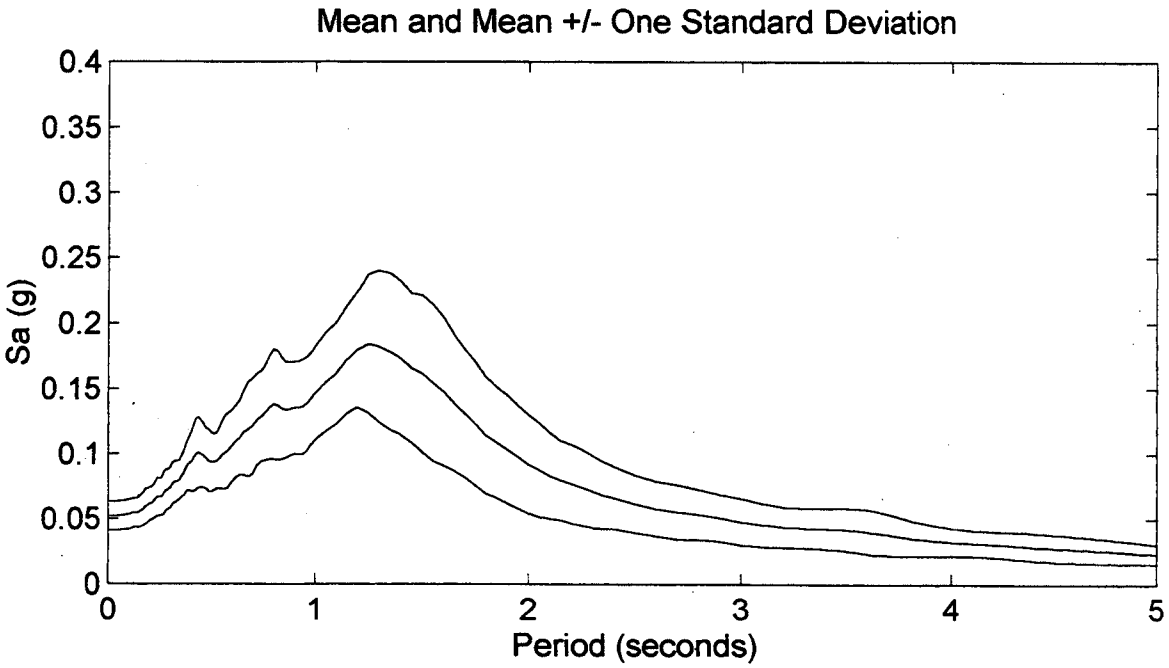
Mean and Mean +/- One Standard Deviation
Sa (g)
0.4
0.35
0.3
0.25
0.2
0.15
0.1
0.05
0
0
1
2
3
4
5
Period (seconds)

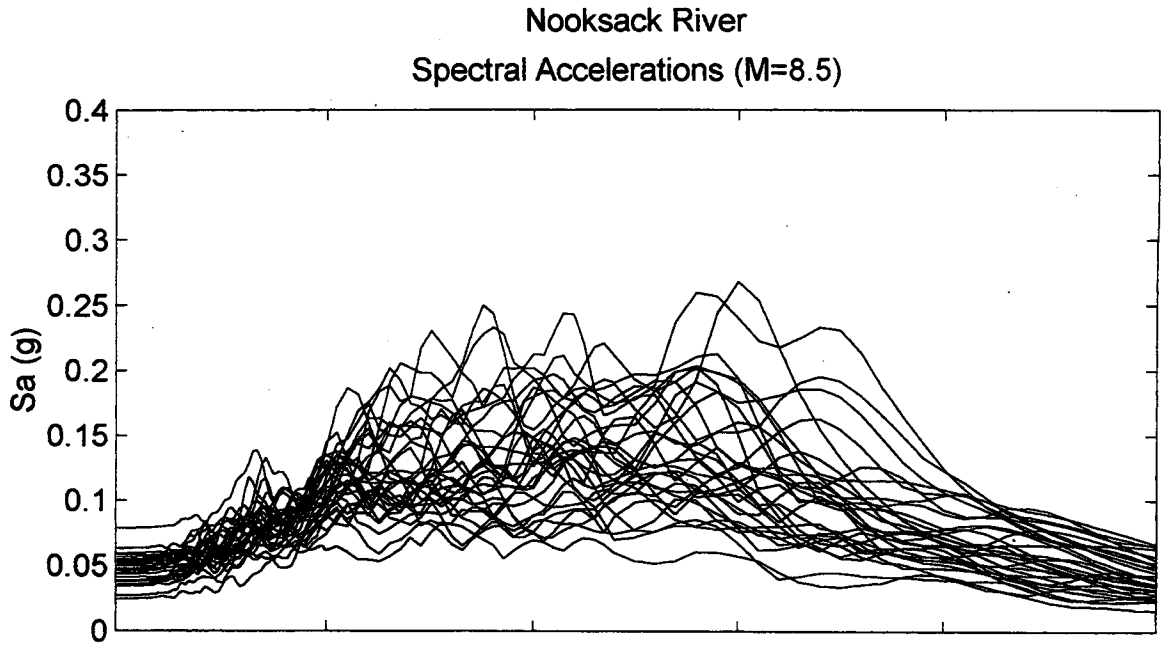
Nooksack River
Spectral Accelerations (M=8.5)
Sa (g)
0.4
0.35
0.3
0.25
0.2
0.15
0.1
0.05
0

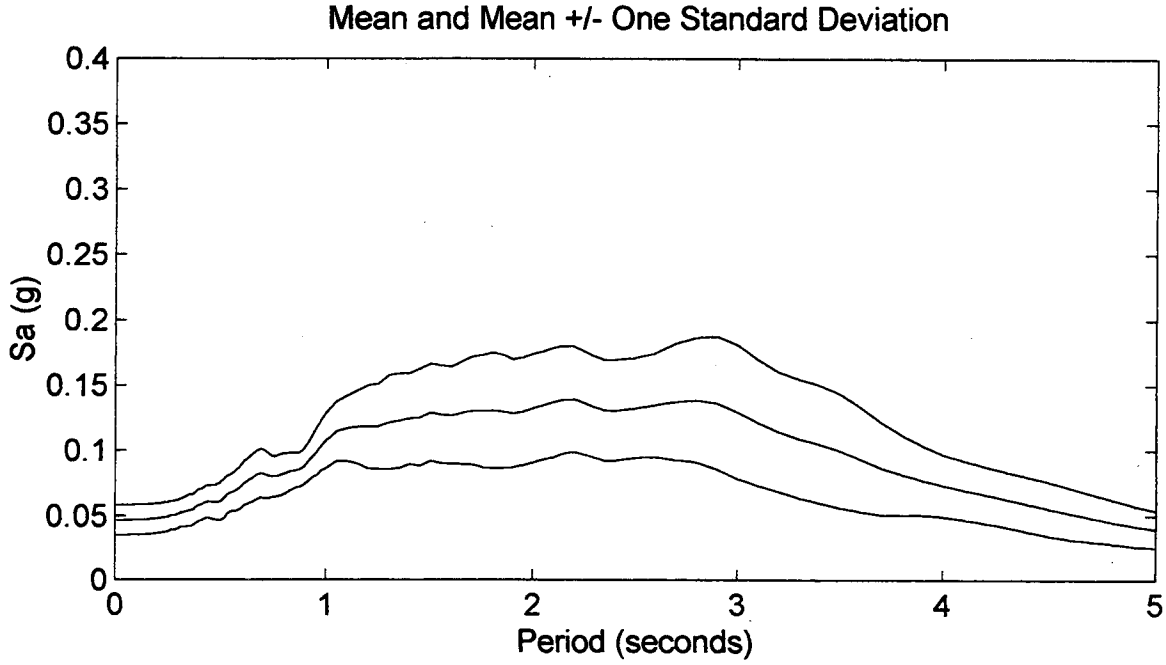
Mean and Mean +/- One Standard Deviation
Sa (g)
0.4
0.35
0.3
0.25
0.2
0.15
0.1
0.05
0
0
1
2
3
4
5
Period (seconds)

Yakima

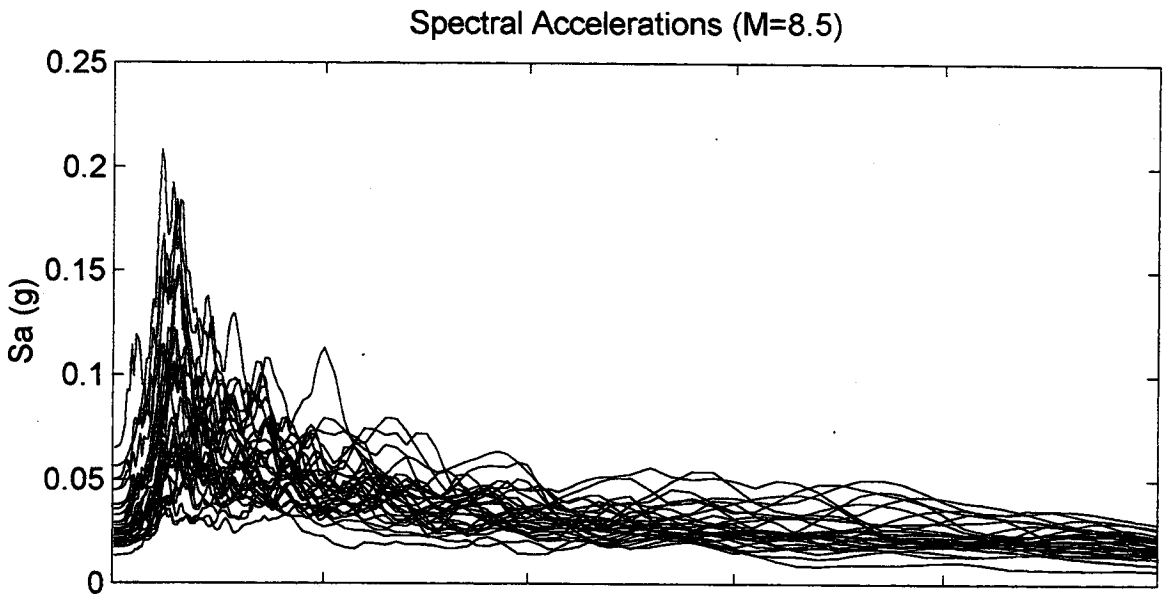
Spectral Accelerations (M=8.5)
0.25
0.2
0.15
0.1
0.05
0
Sa (g)

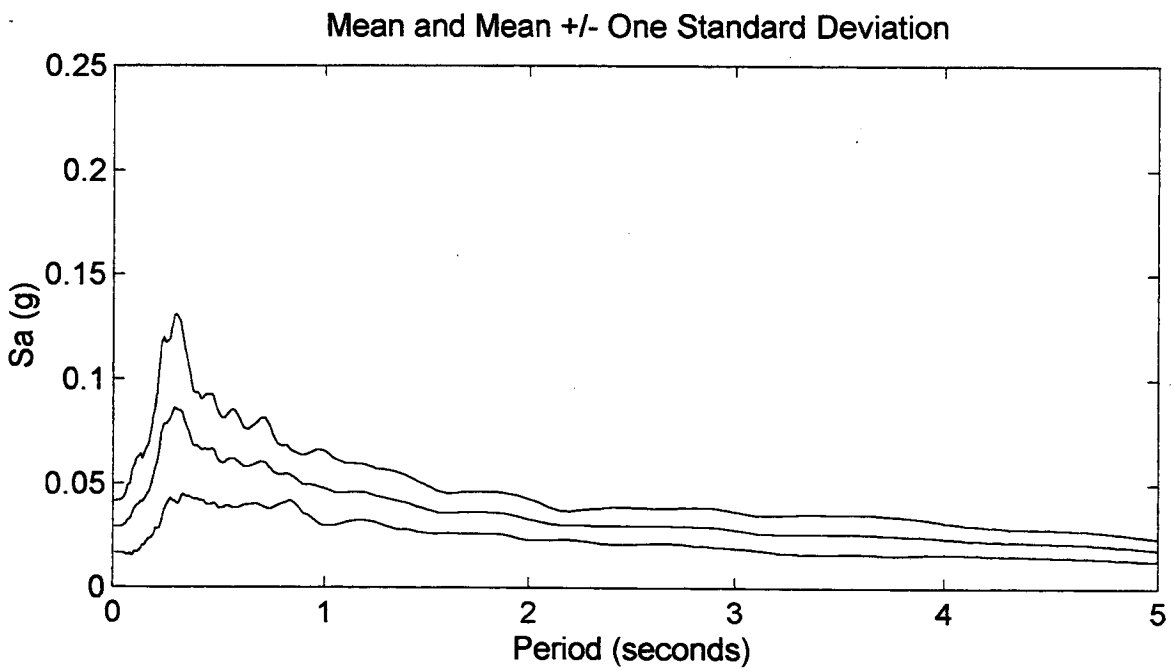
Mean and Mean +/- One Standard Deviation
0.25
0.2
0.15
0.1
0.05
0
Sa (g)
0
1
2
3
4
5
Period (seconds)

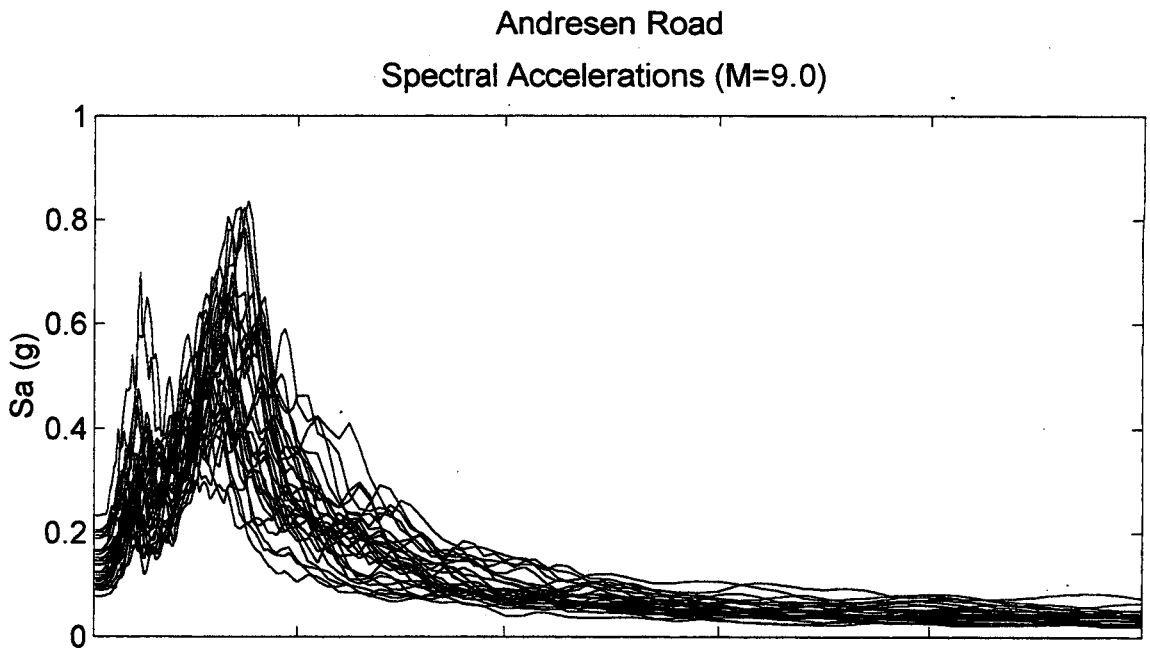
Andresen Road
Spectral Accelerations (M=9.0)
Sa (g)
0
0.2
0.4
0.6
0.8
1

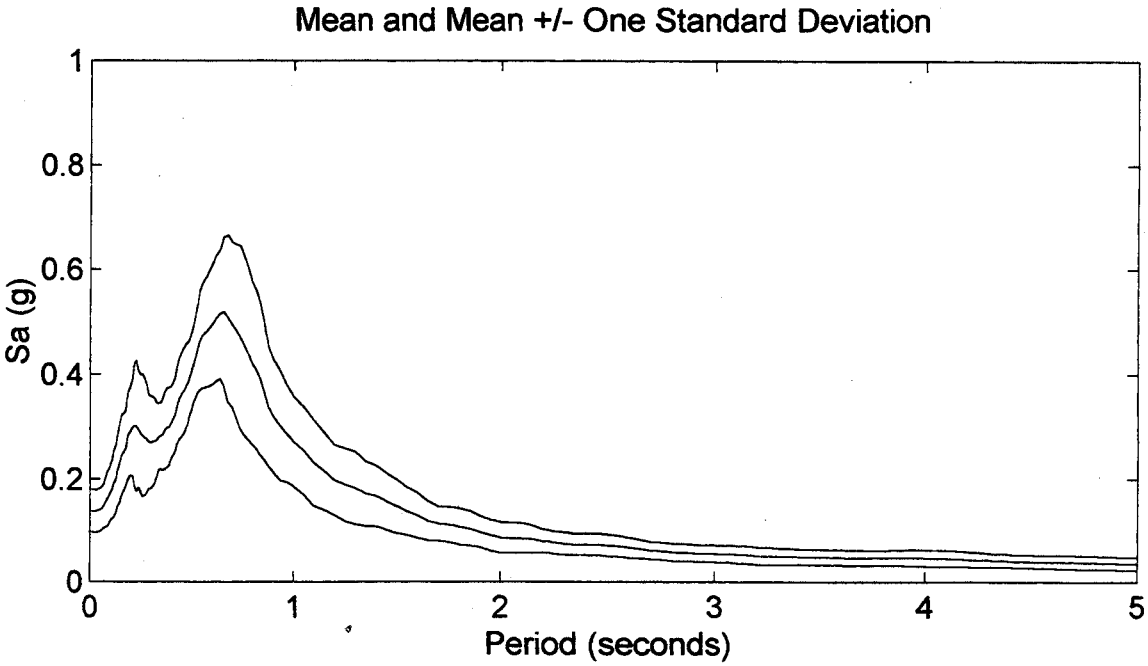
Mean and Mean +/- One Standard Deviation
Sa (g)
0
0.2
0.4
0.6
0.8
1
0
1
2
3
4
5
Period (seconds)

Alaskan Way Viaduct 1

Spectral Accelerations (M=9.0)

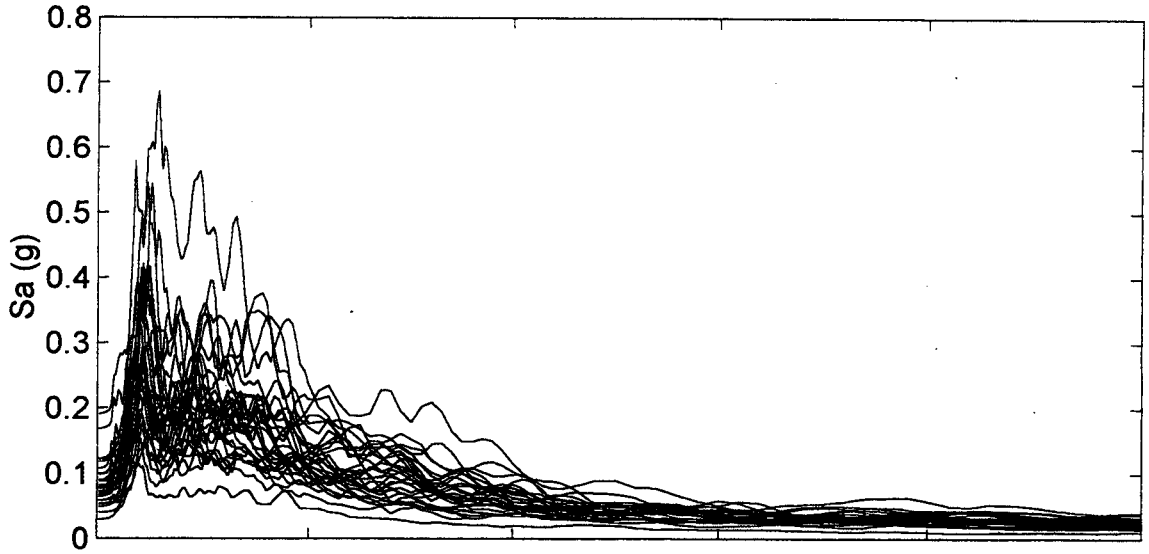

Mean and Mean +/- One Standard Deviation

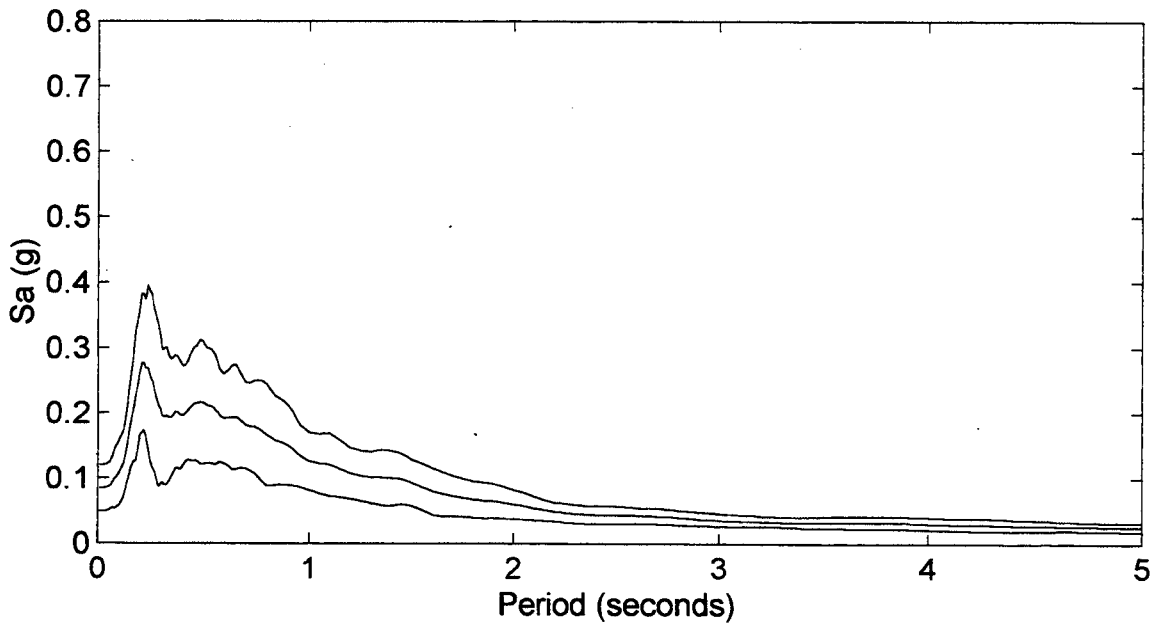

Alaskan Way Viaduct 2

Spectral Accelerations (M=9.0)

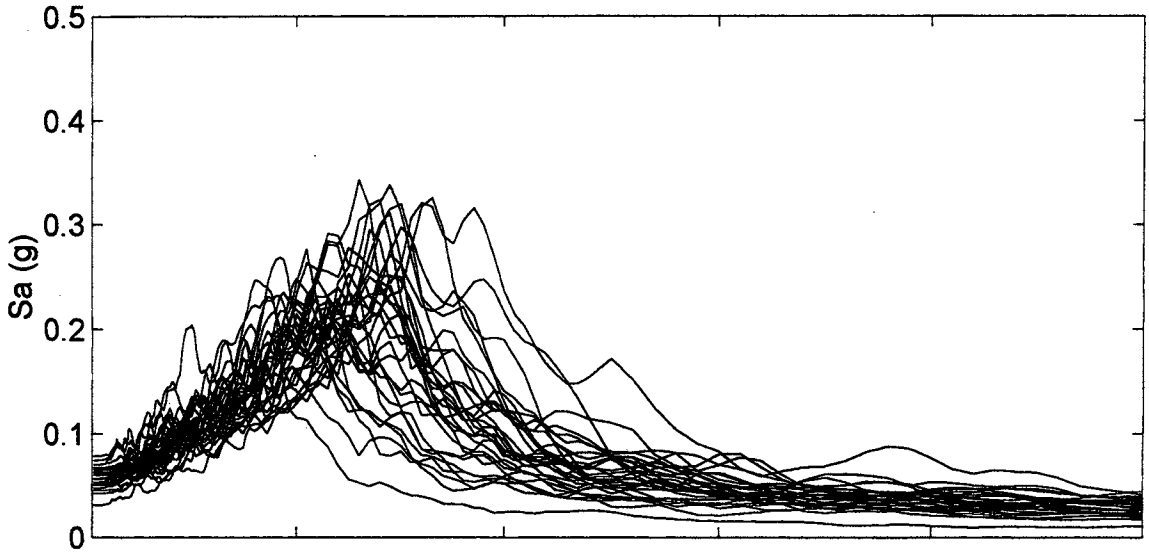

Mean and Mean +/- One Standard Deviation

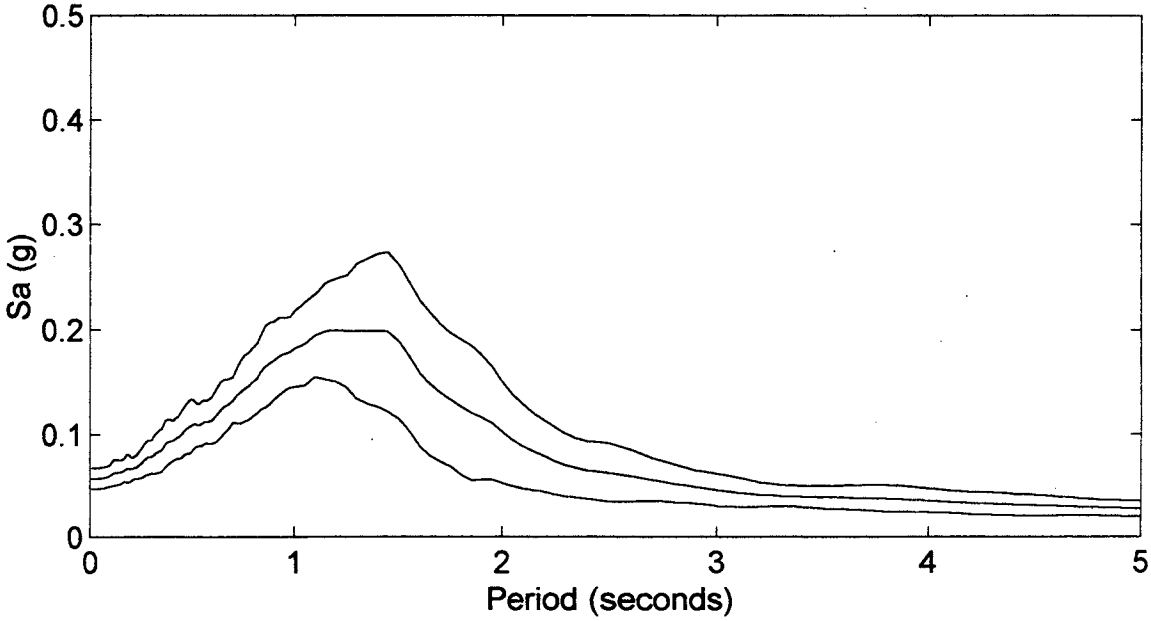

Black Diamond Road

Spectral Accelerations (M=9.0)

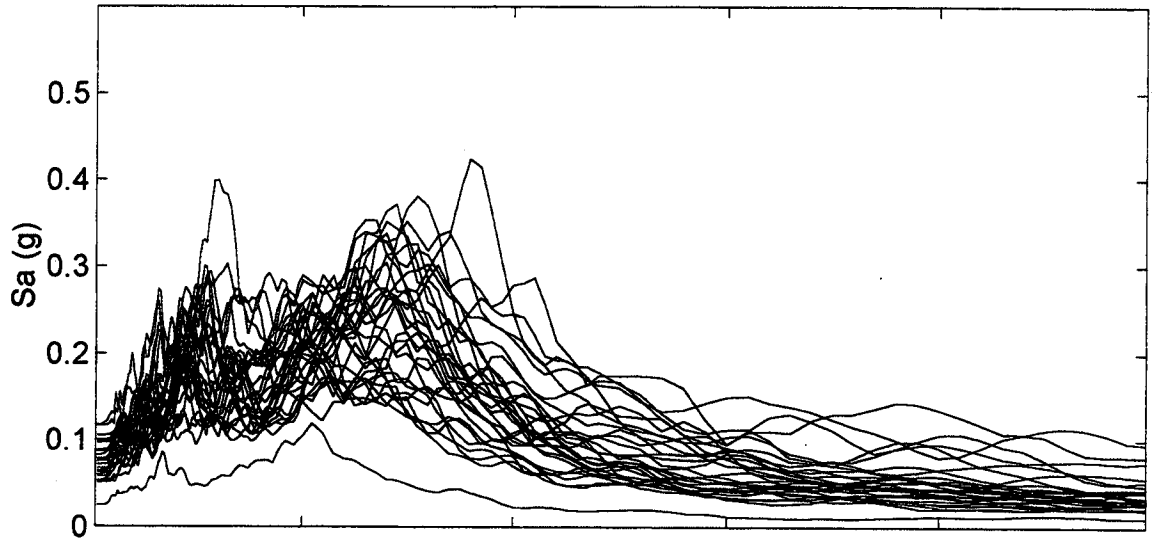

Mean and Mean +/- One Standard Deviation

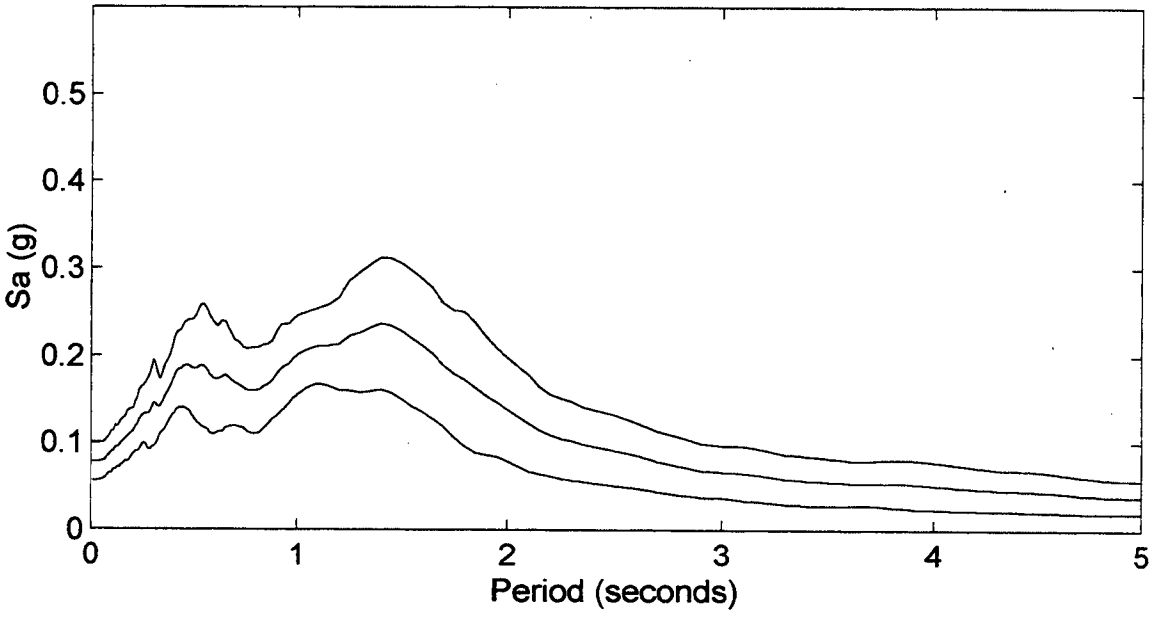

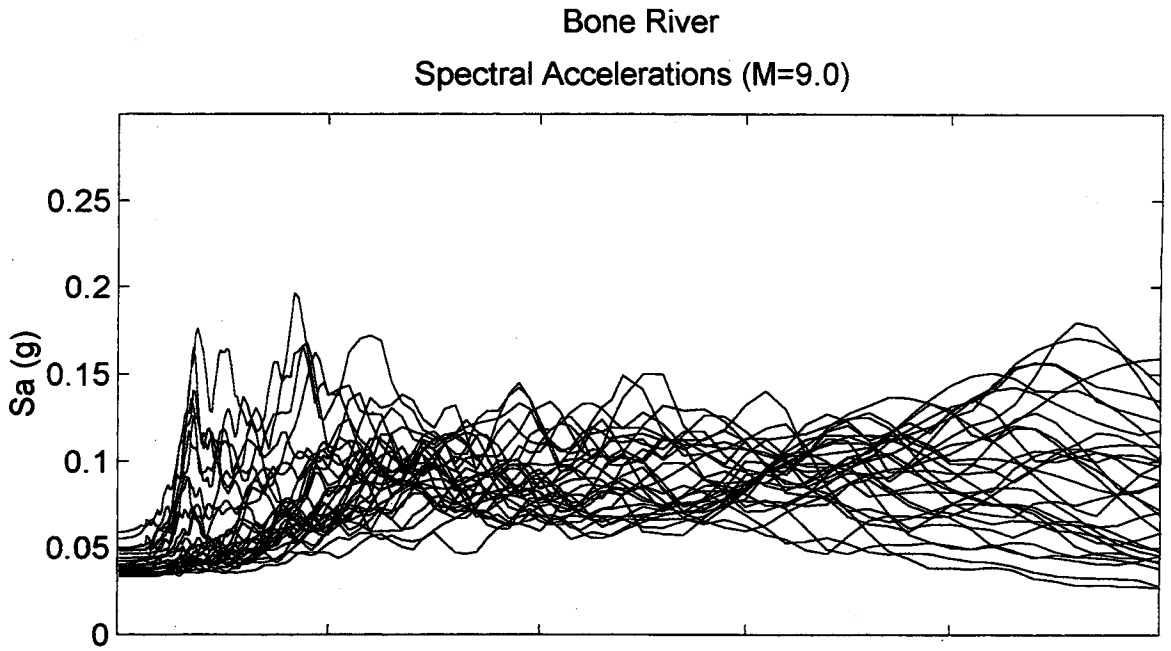
Bone River
Spectral Accelerations (M=9.0)
Sa (g)
0.25
0.2
0.15
0.1
0.05
0

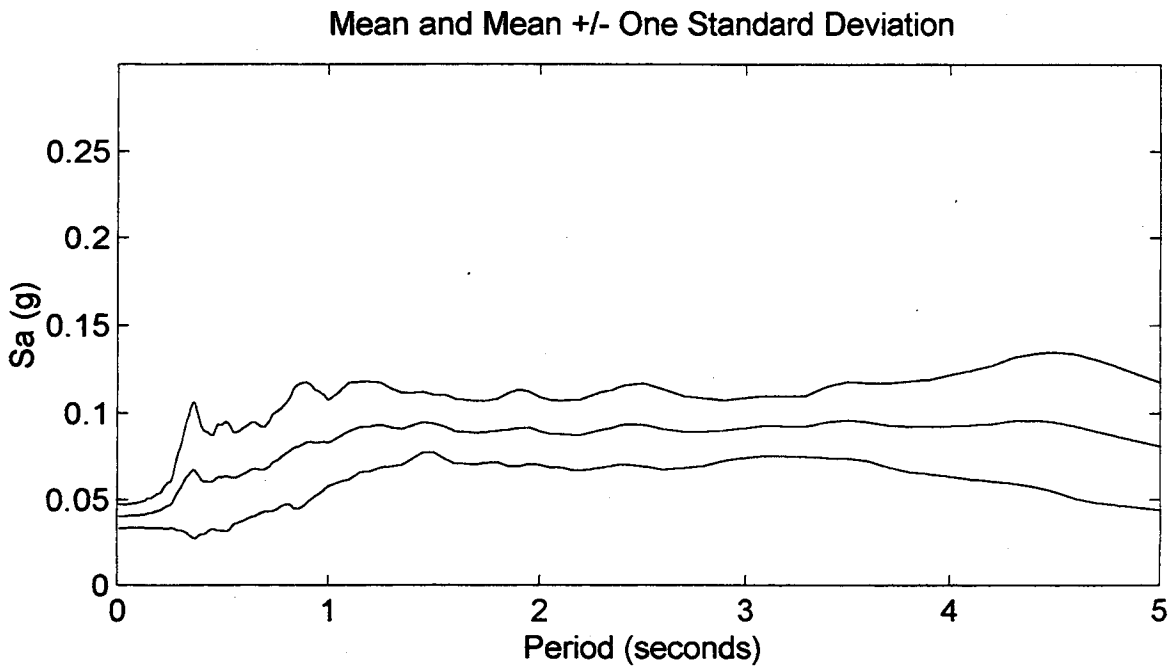
Mean and Mean +/- One Standard Deviation
Sa (g)
0.25
0.2
0.15
0.1
0.05
0
0
1
2
3
4
5
Period (seconds)

Capitol Boulevard

Spectral Accelerations (M=9.0)

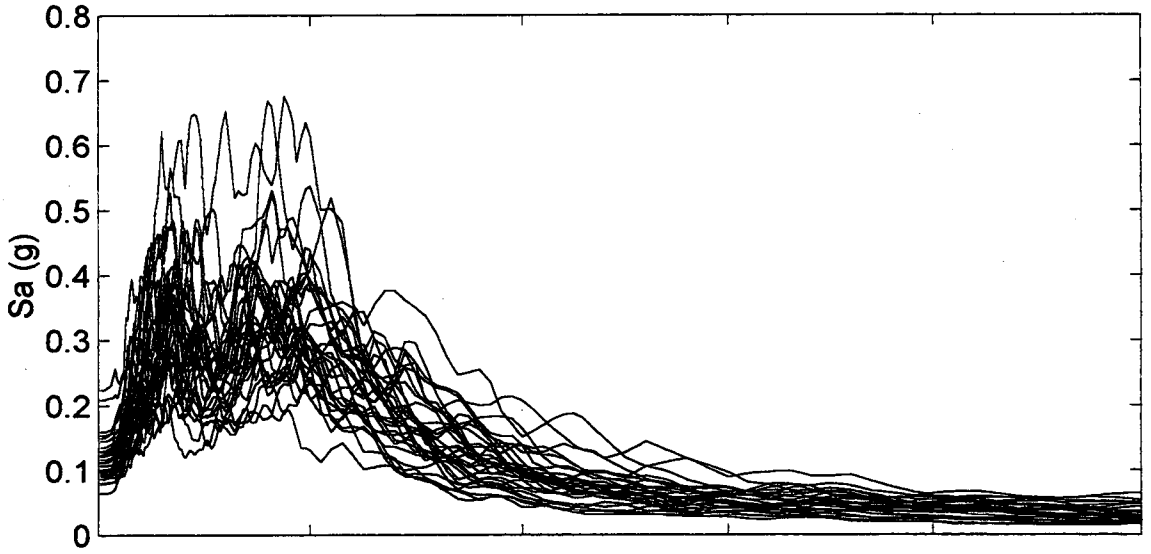

Mean and Mean +/- One Standard Deviation

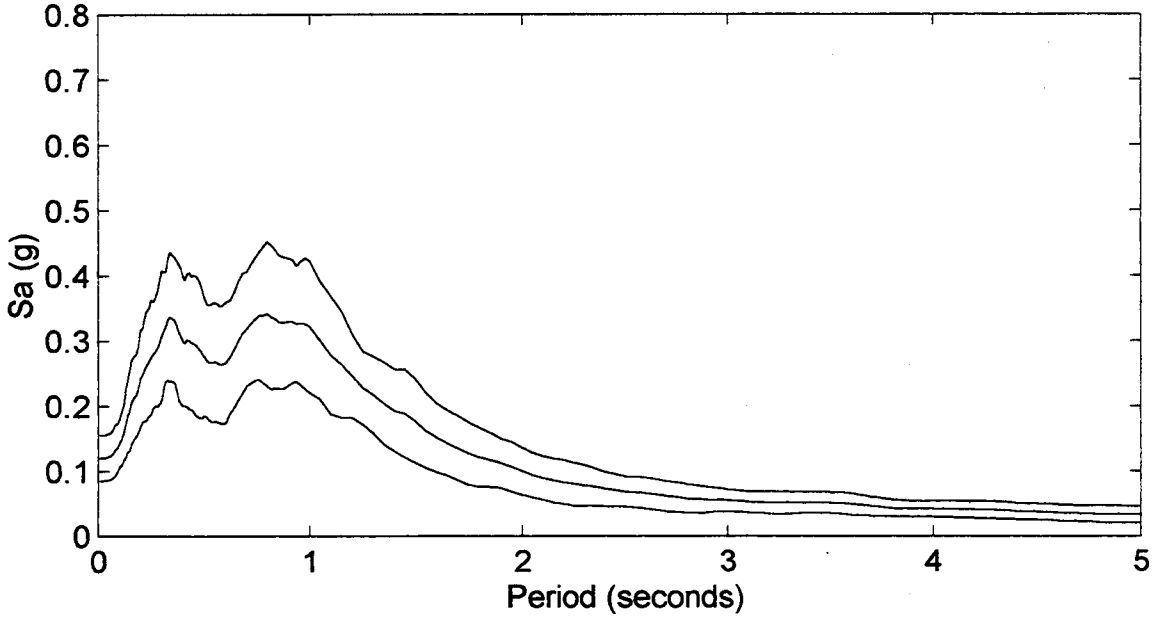

Coldwater Creek

Spectral Accelerations (M=9.0)

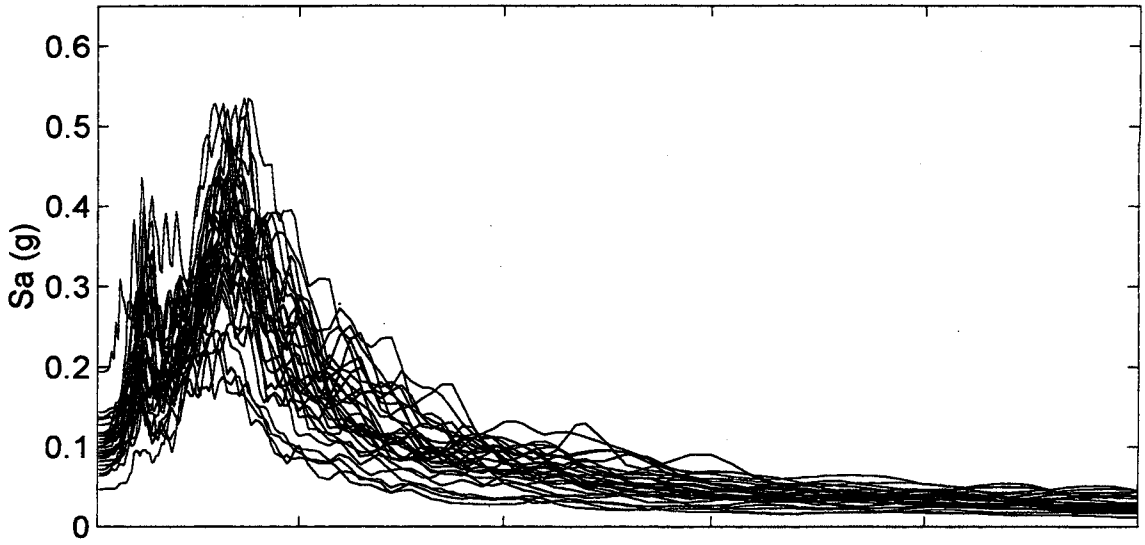

Mean and Mean +/- One Standard Deviation

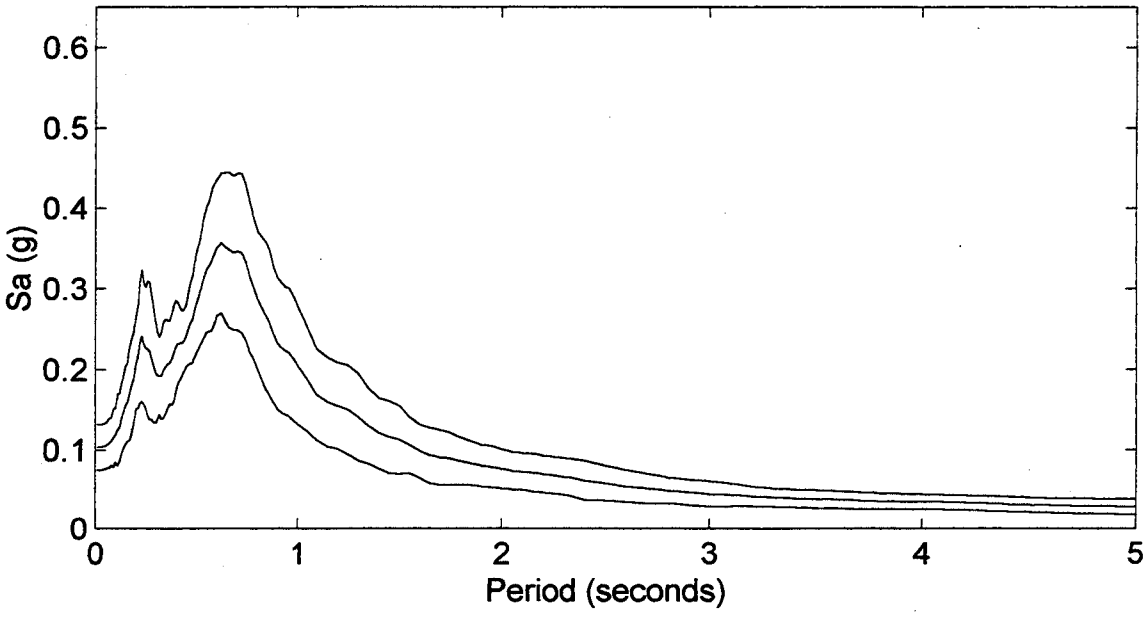

I-5/NE 99th Street

Spectral Accelerations (M=9.0)

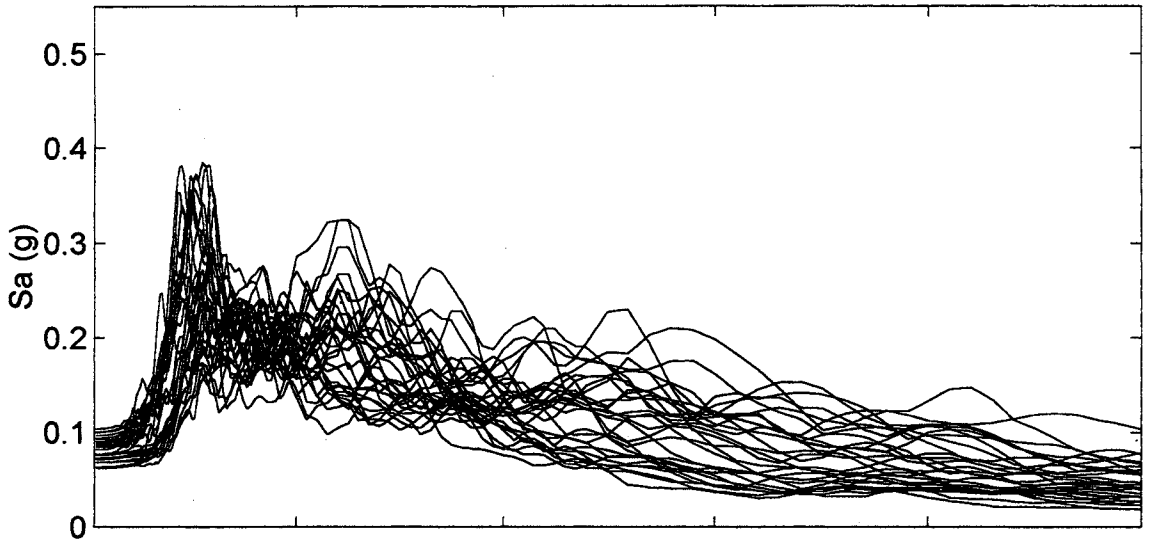

Mean and Mean +/- One Standard Deviation

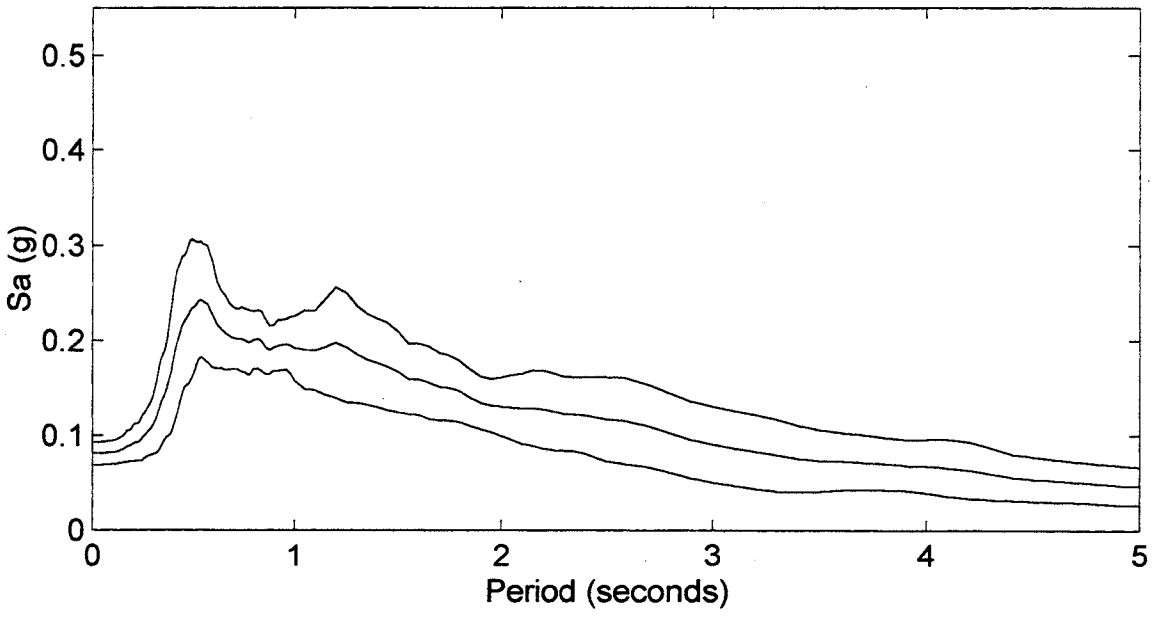

I-405/SR-522

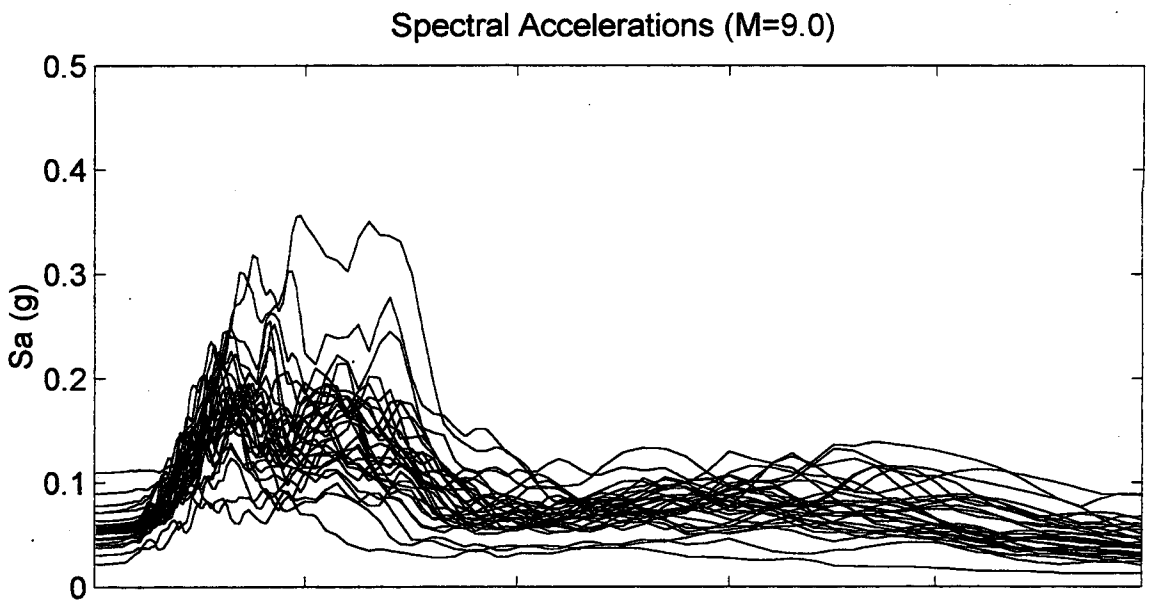
Spectral Accelerations (M=9.0)
Sa (g)
0.5
0.4
0.3
0.2
0.1
0

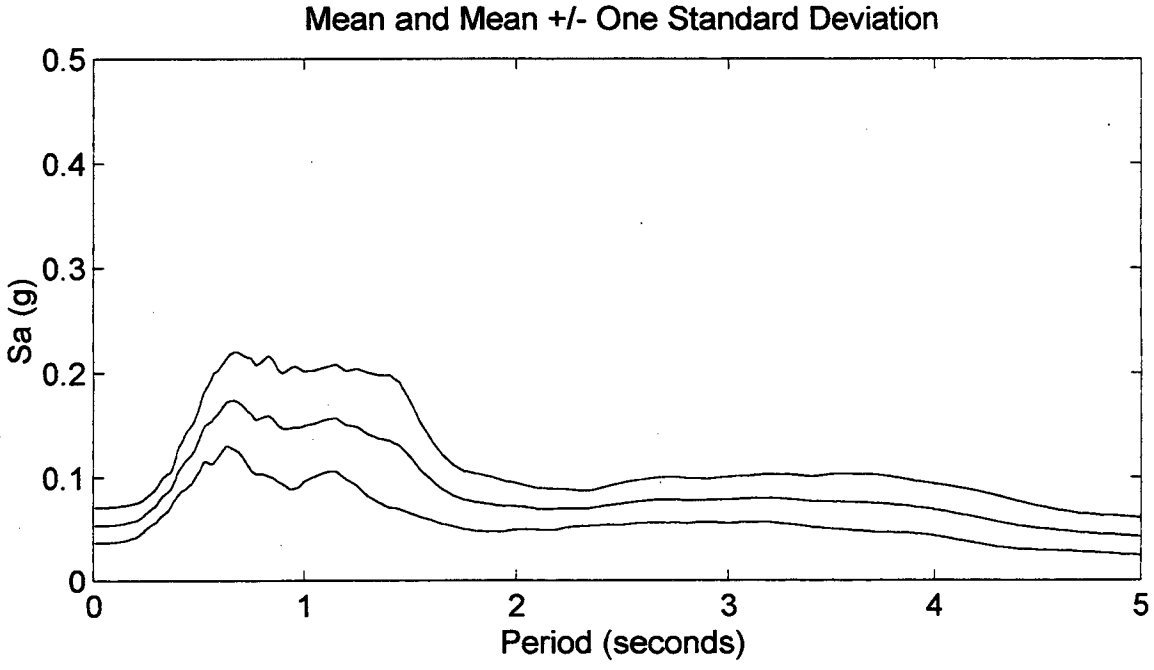
Mean and Mean +/- One Standard Deviation
Sa (g)
0.5
0.4
0.3
0.2
0.1
0
0
1
2
3
4
5
Period (seconds)

Kent Valley

Spectral Accelerations (M=9.0)

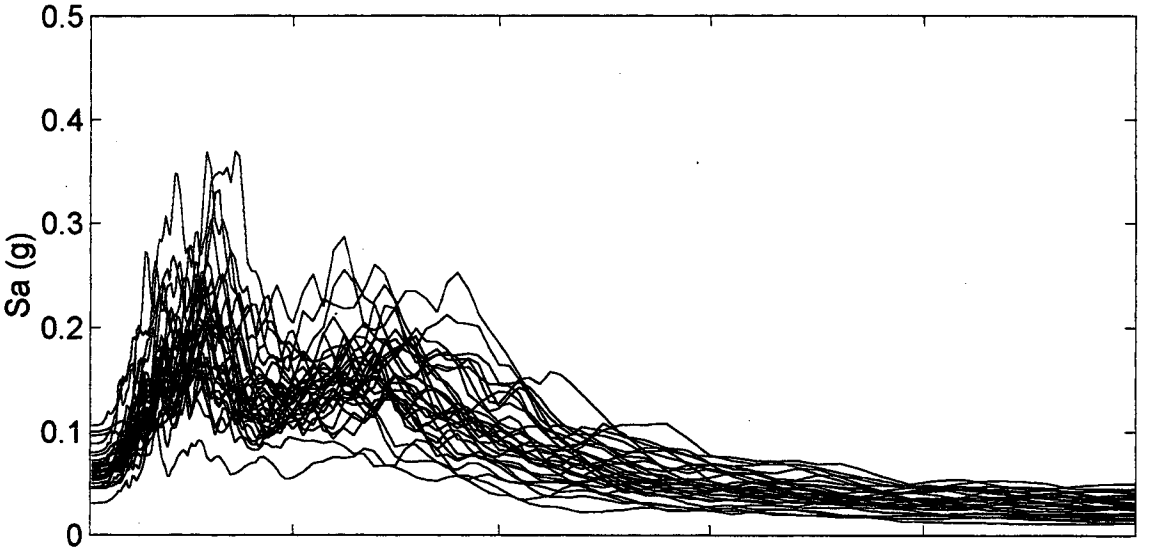

Mean and Mean +/- One Standard Deviation

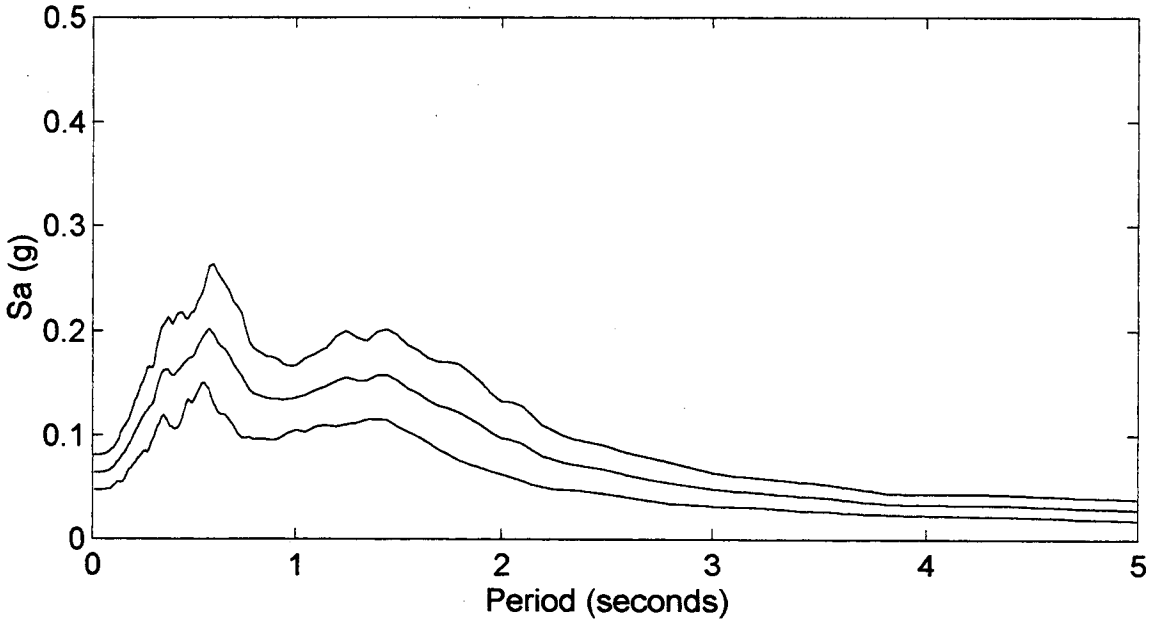

Mercer Slough 1

Spectral Accelerations (M=9.0)

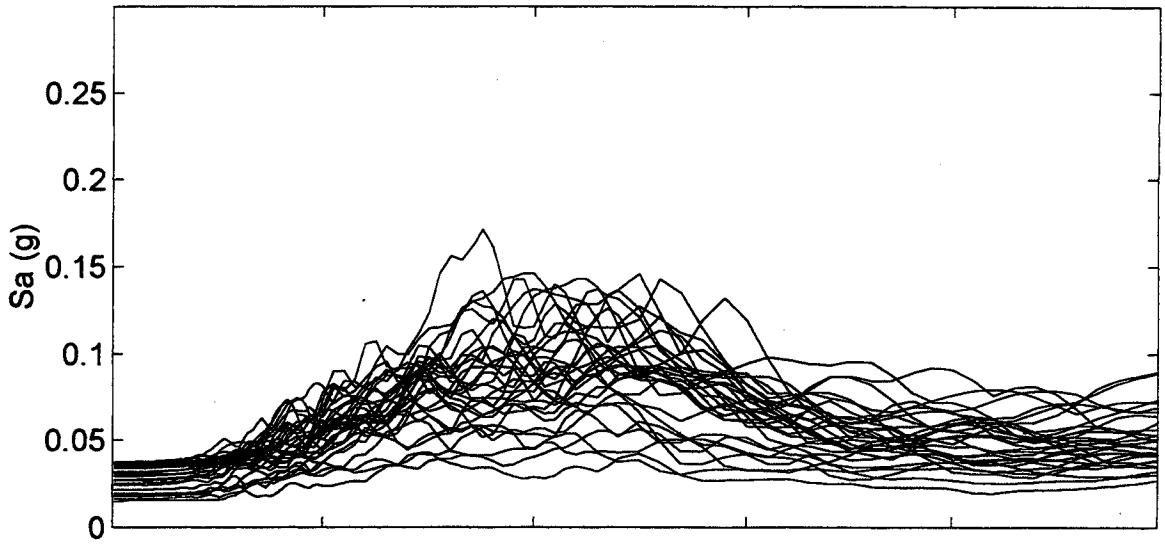

Mean and Mean +/- One Standard Deviation

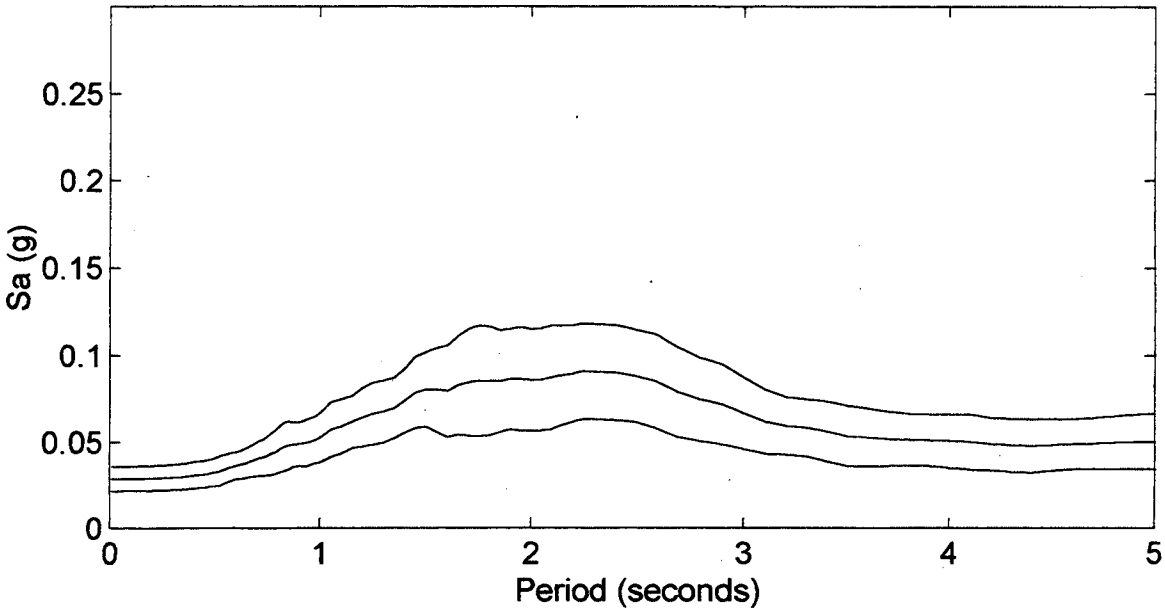

Mercer Slough 2

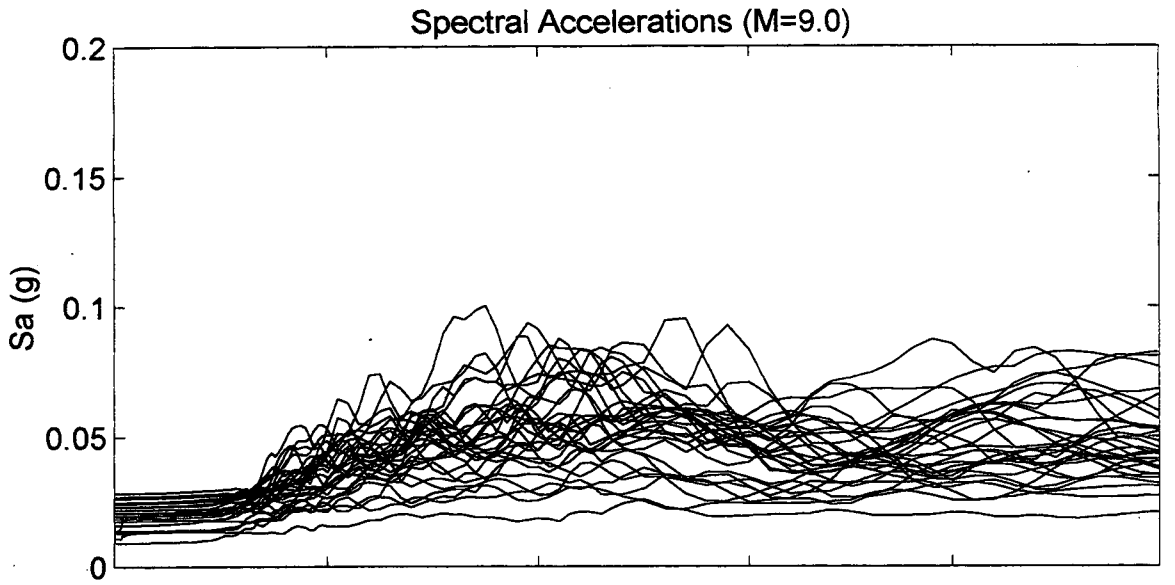

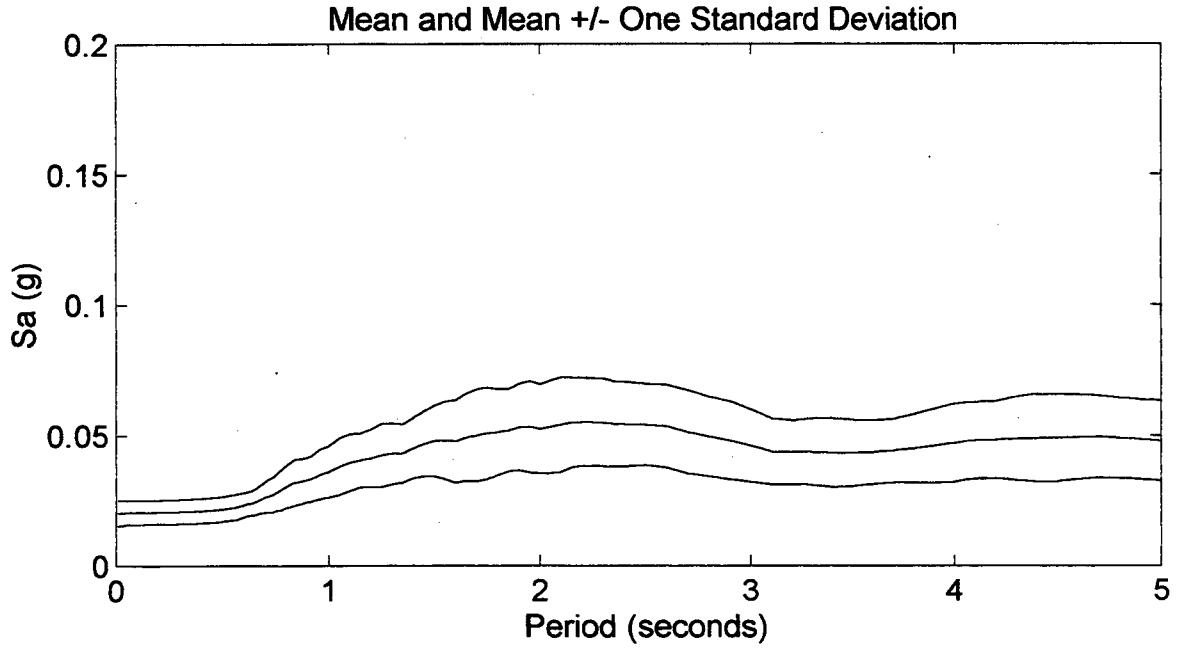

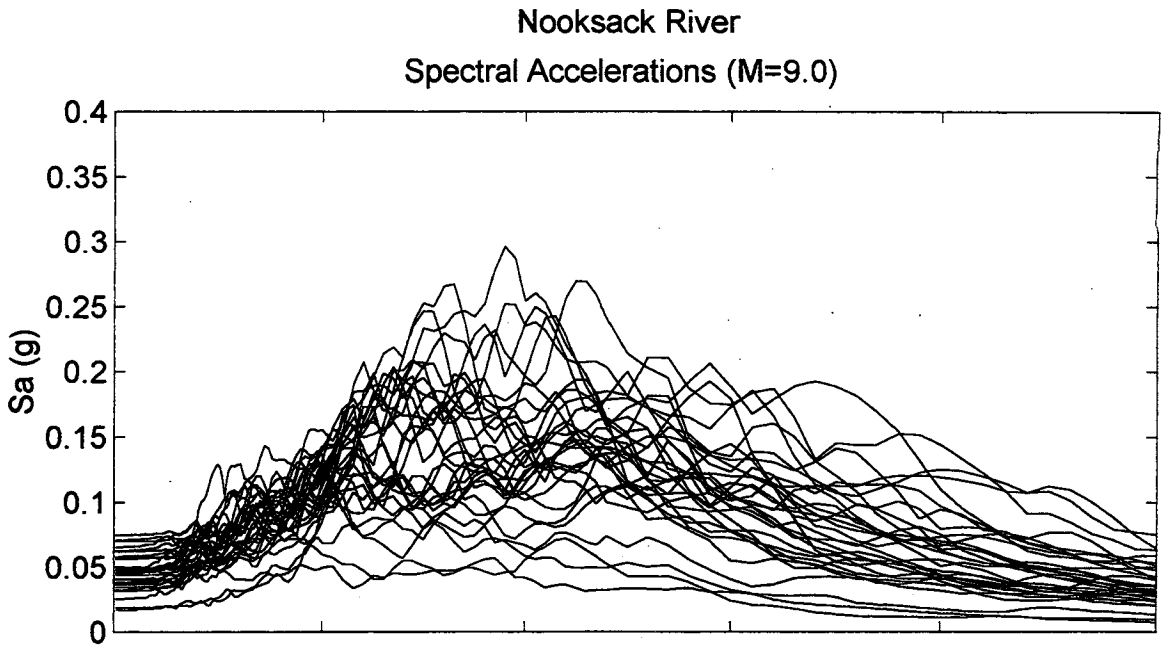
Nooksack River
Spectral Accelerations (M=9.0)
Sa (g)
0.4
0.35
0.3
0.25
0.2
0.15
0.1
0.05
0

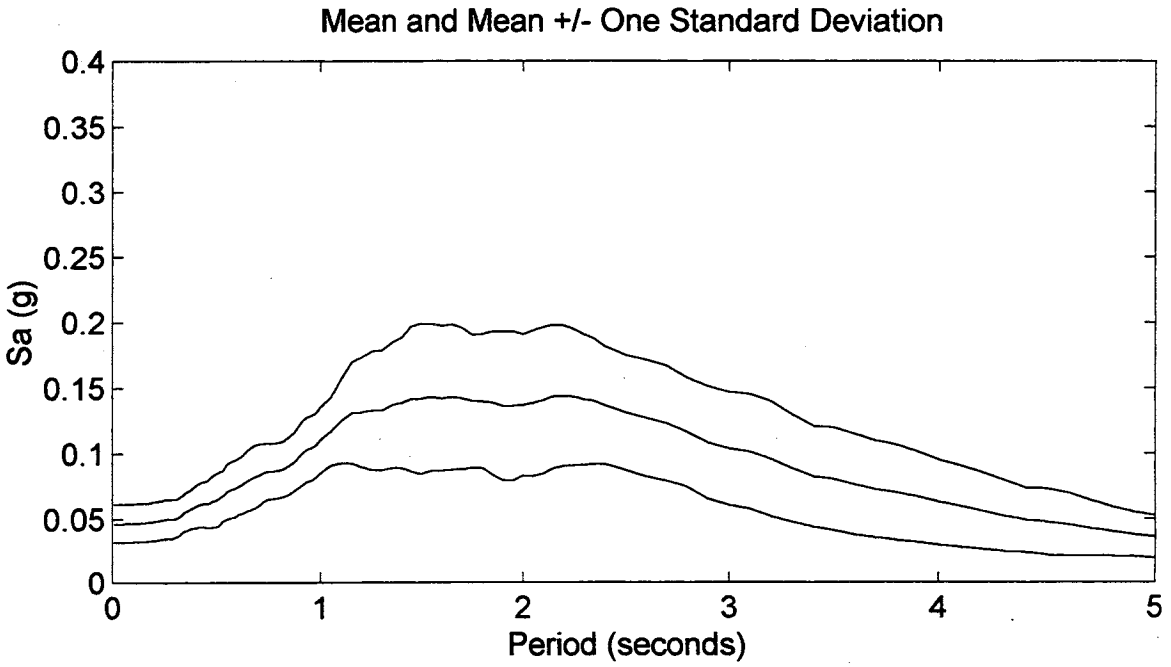
Mean and Mean +/- One Standard Deviation
Sa (g)
0.4
0.35
0.3
0.25
0.2
0.15
0.1
0.05
0
0
1
2
3
4
5
Period (seconds)

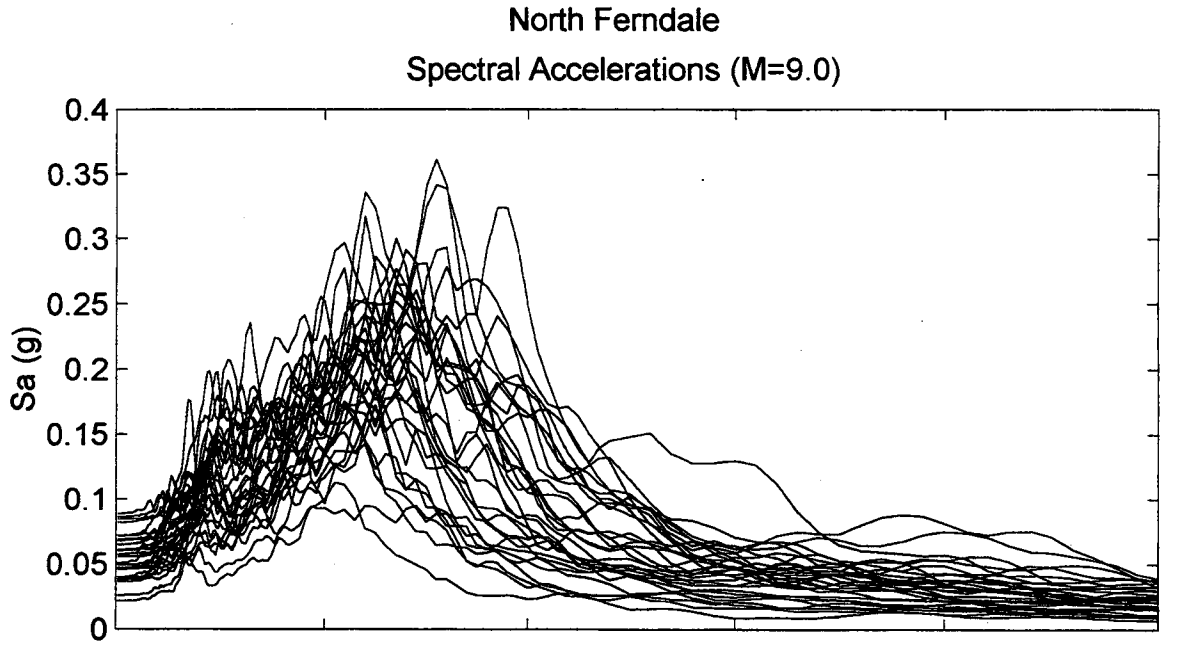
North Ferndale
Spectral Accelerations (M=9.0)
Sa (g)
0.4
0.35
0.3
0.25
0.2
0.15
0.1
0.05
0

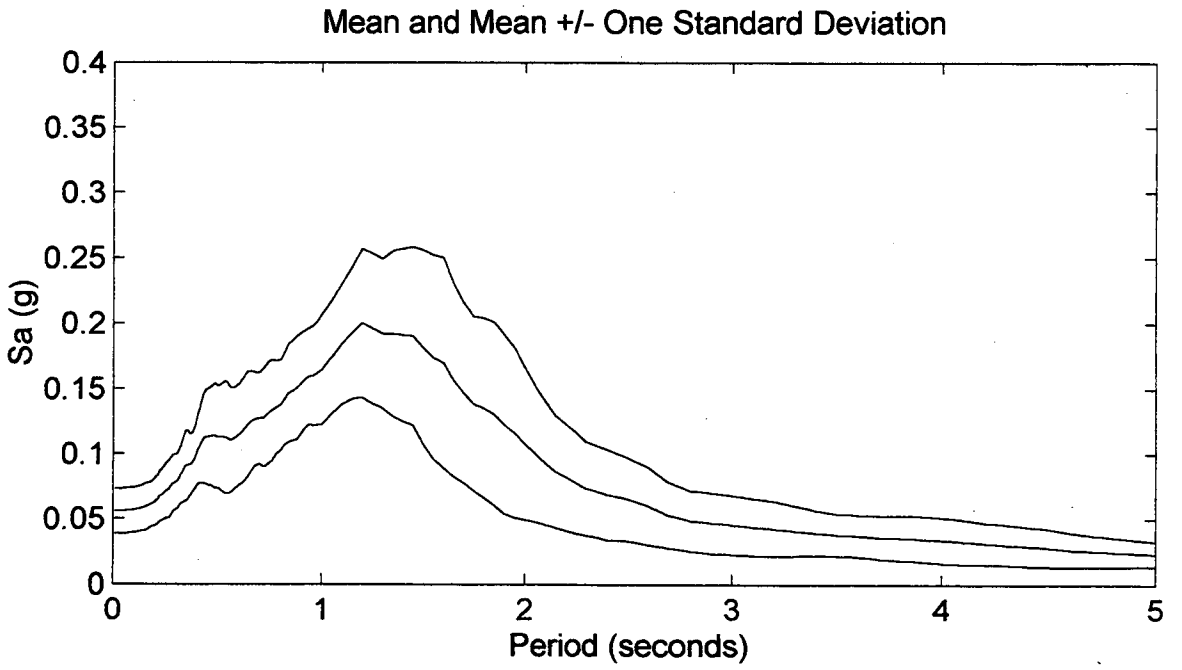
Mean and Mean +/- One Standard Deviation
Sa (g)
0.4
0.35
0.3
0.25
0.2
0.15
0.1
0.05
0
0
1
2
3
4
5
Period (seconds)

Yakima

Spectral Accelerations (M=9.0)

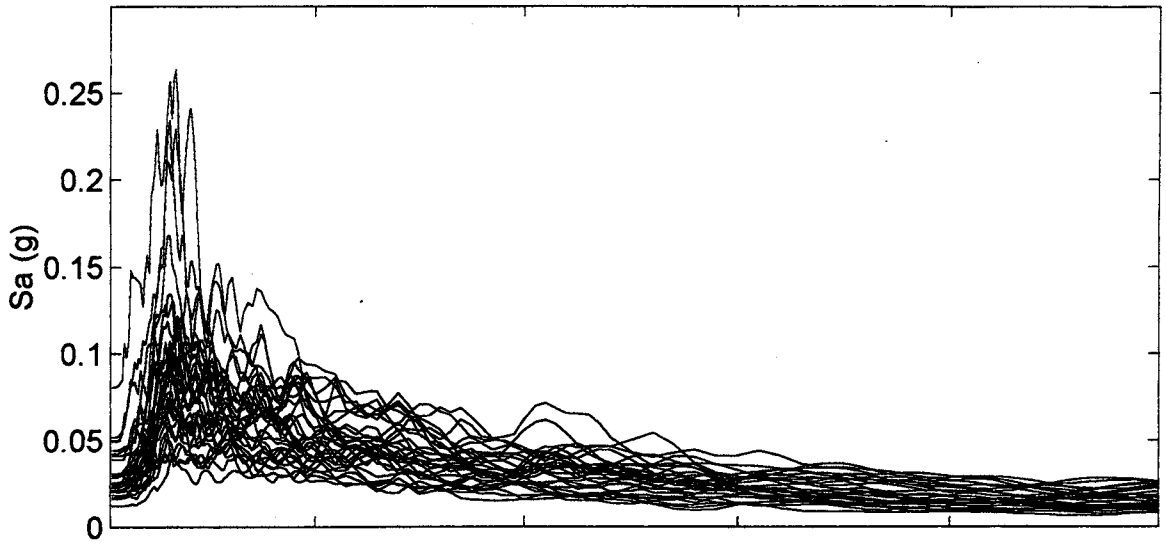

Mean and Mean +/- One Standard Deviation

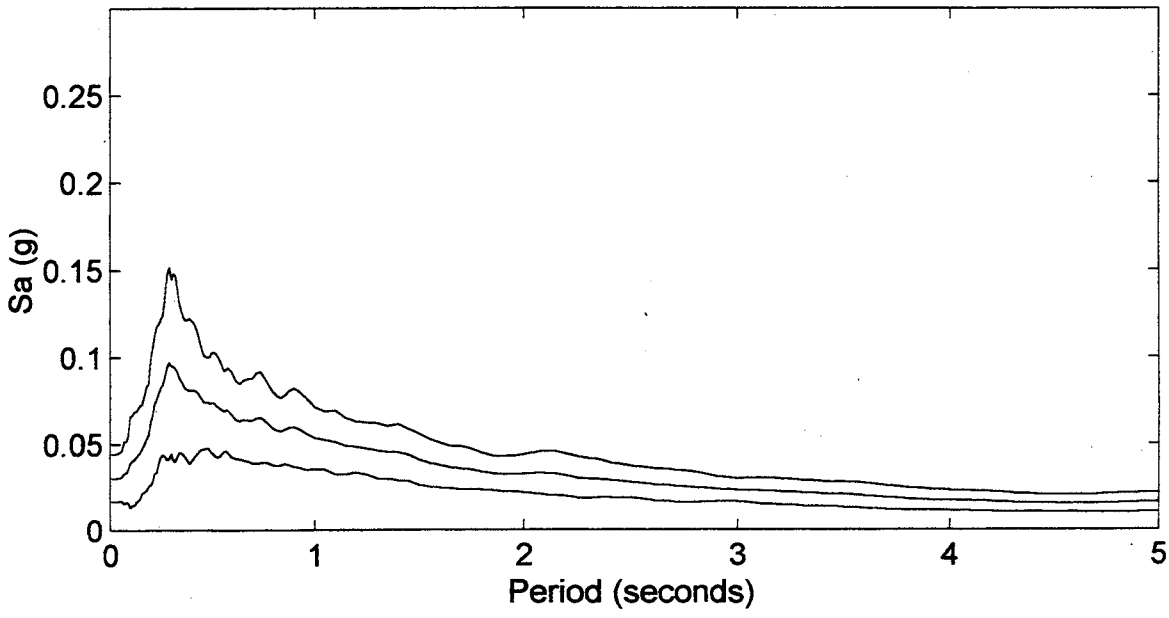

APPENDIX D

COMPUTED GROUND SURFACE RESPONSE SPECTRA: NONLINEAR

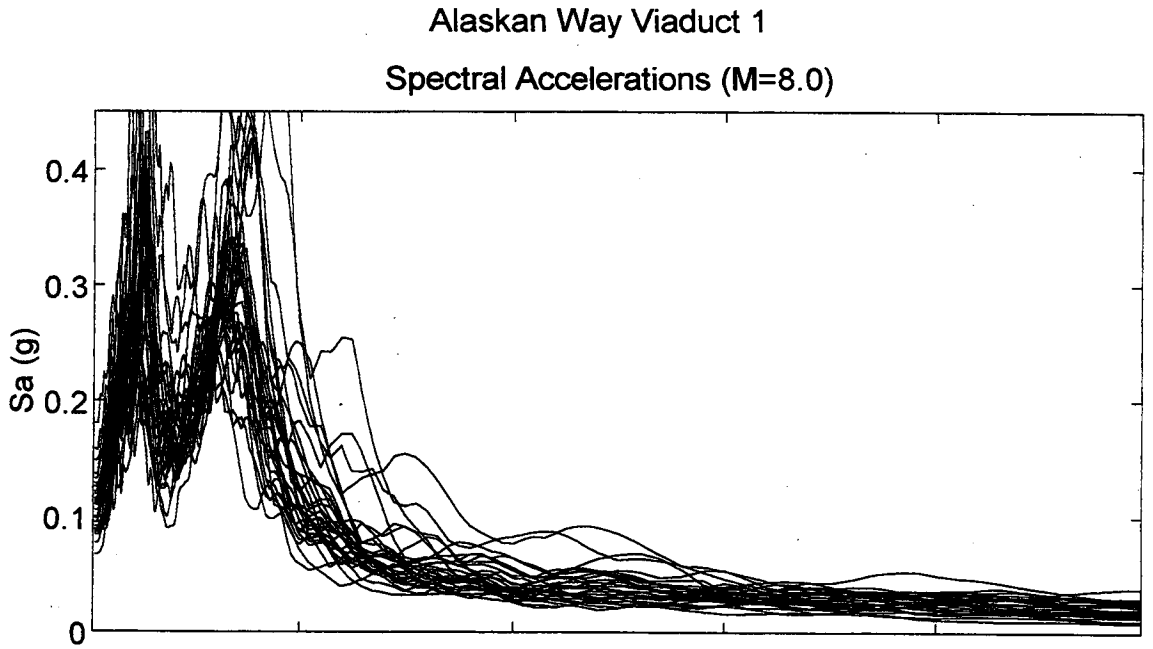
Alaskan Way Viaduct 1
Spectral Accelerations (M=8.0)
Sa (g)
0.4
0.3
0.2
0.1
0

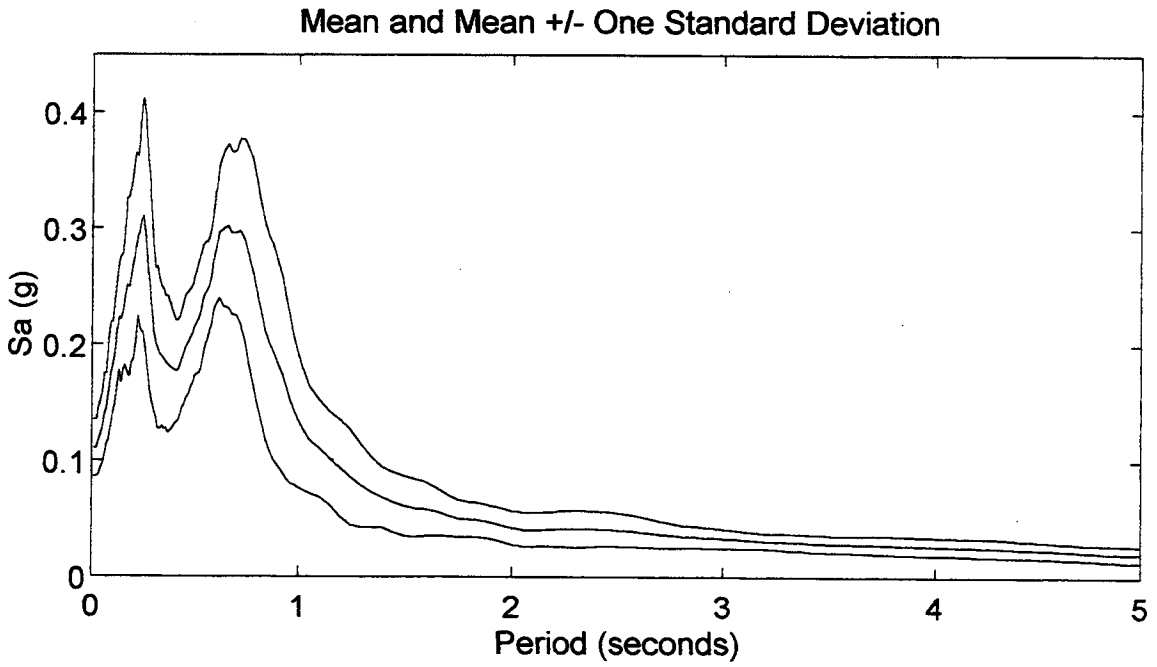
Mean and Mean +/- One Standard Deviation
Sa (g)
0.4
0.3
0.2
0.1
0
0
1
2
3
4
5
Period (seconds)

Alaskan Way Viaduct 1

Spectral Accelerations (M=8.5)

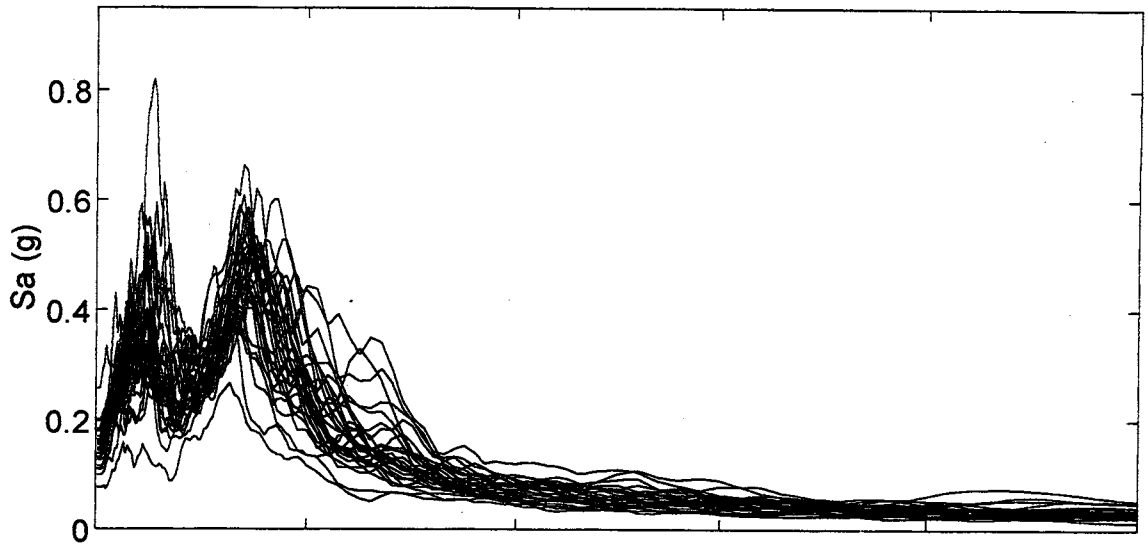

Mean and Mean +/- One Standard Deviation

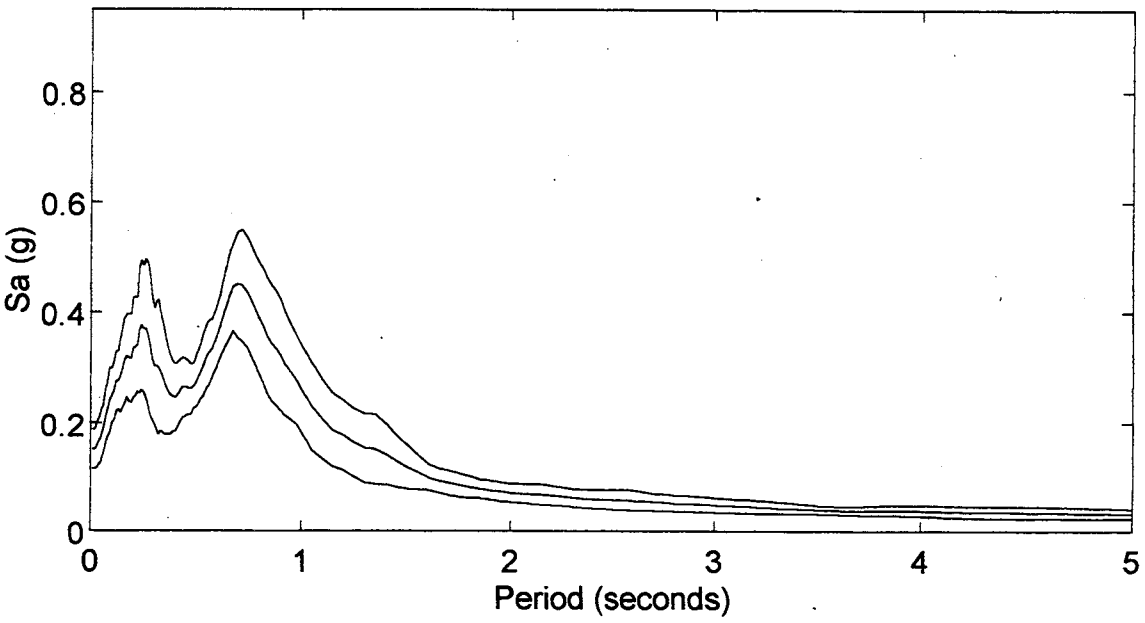

Alaskan Way Viaduct 1

Spectral Accelerations (M=9.0)

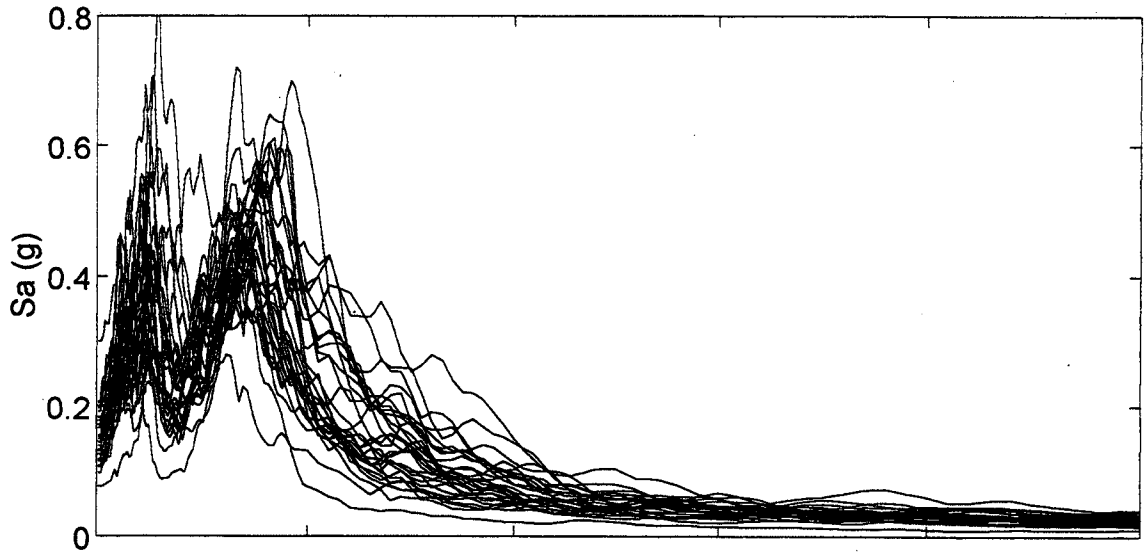

Mean and Mean +/- One Standard Deviation

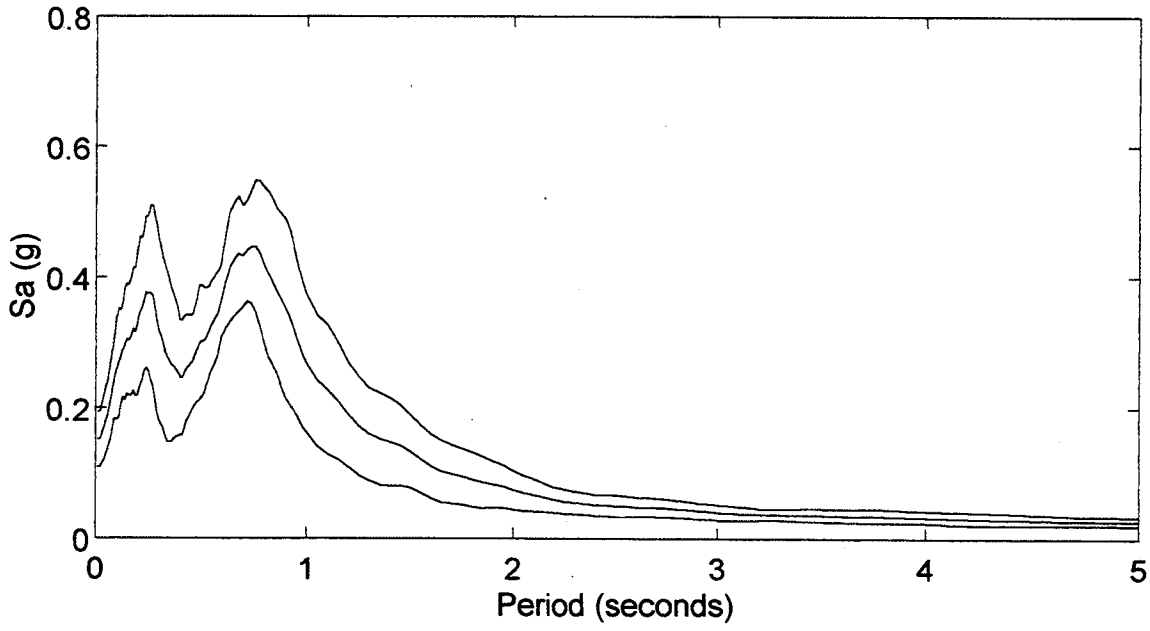

Alaskan Way Viaduct 2

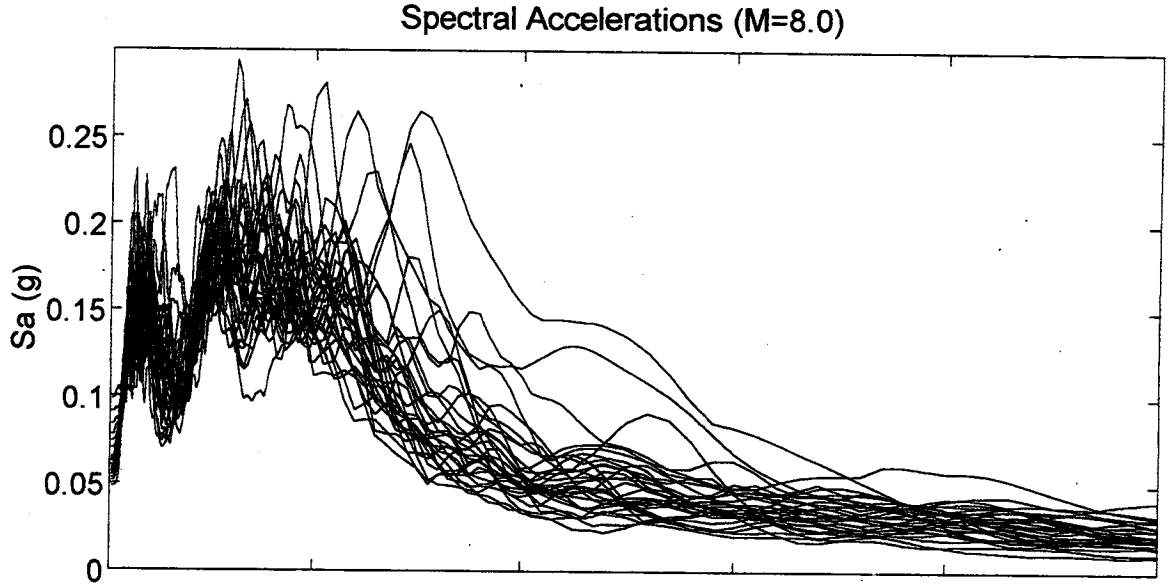

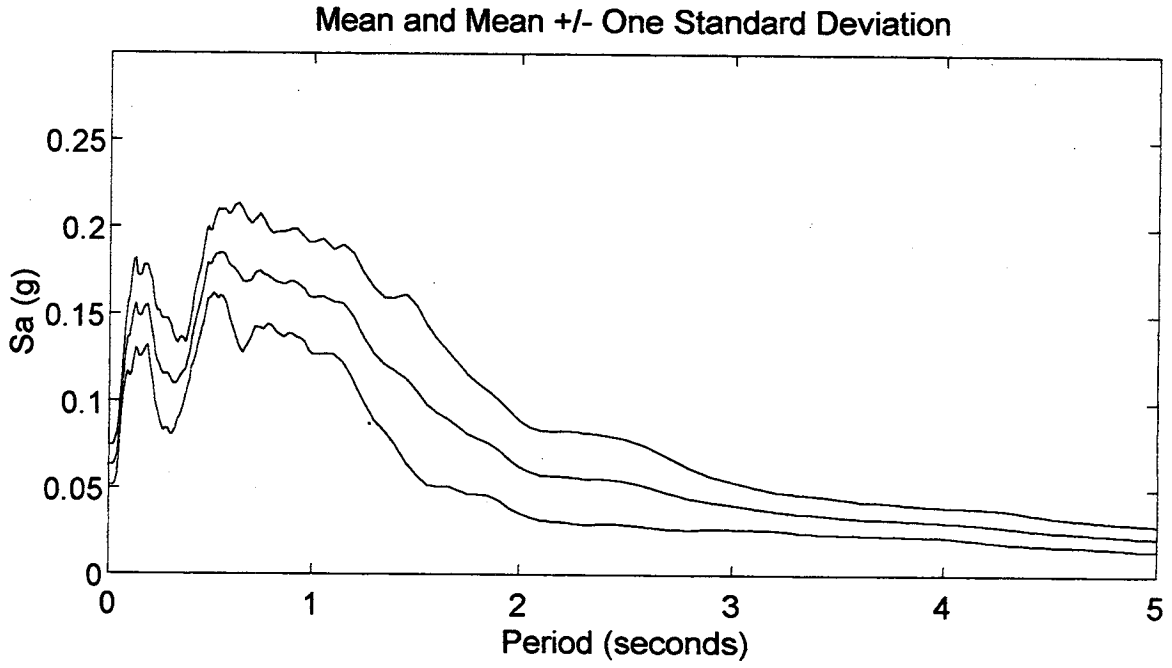

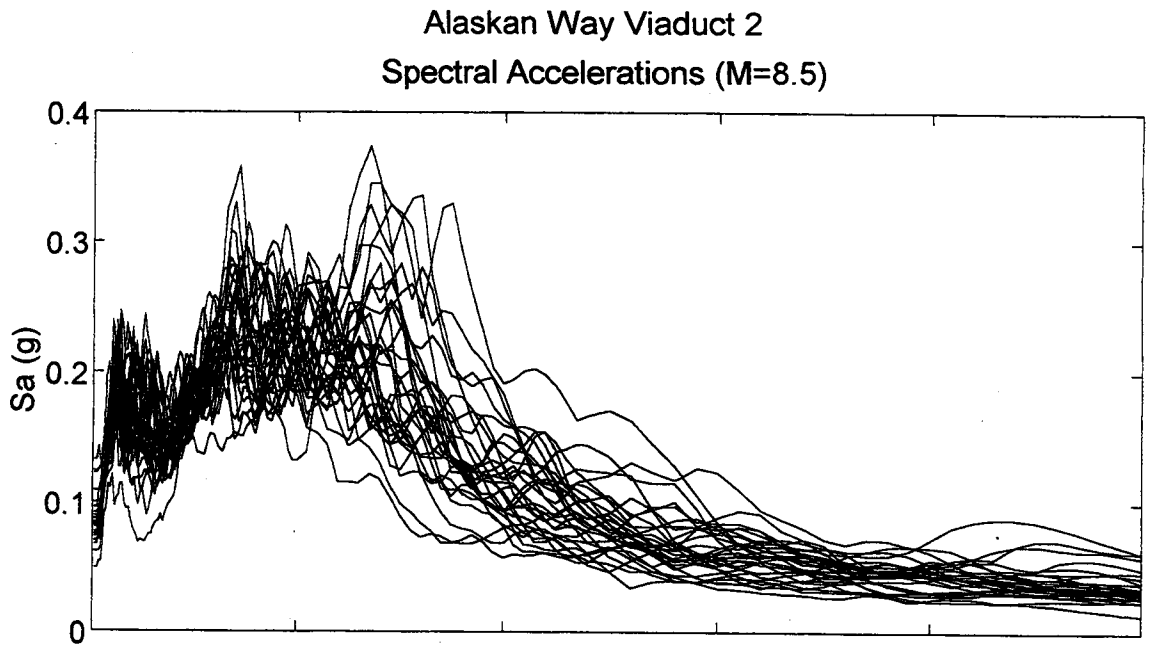
Alaskan Way Viaduct 2
Spectral Accelerations (M=8.5)
Sa (g)
0.4
0.3
0.2
0.1
0

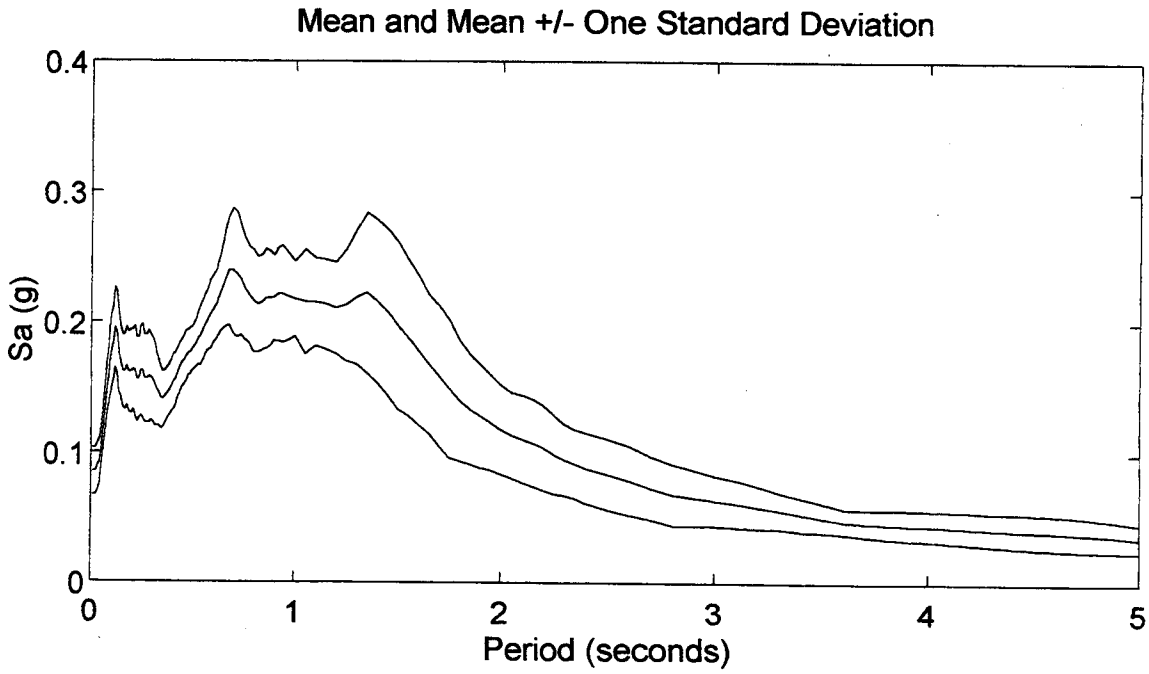
Mean and Mean +/- One Standard Deviation
Sa (g)
0.4
0.3
0.2
0.1
0
0
1
2
3
4
5
Period (seconds)

Alaskan Way Viaduct 2

Spectral Accelerations (M=9.0)

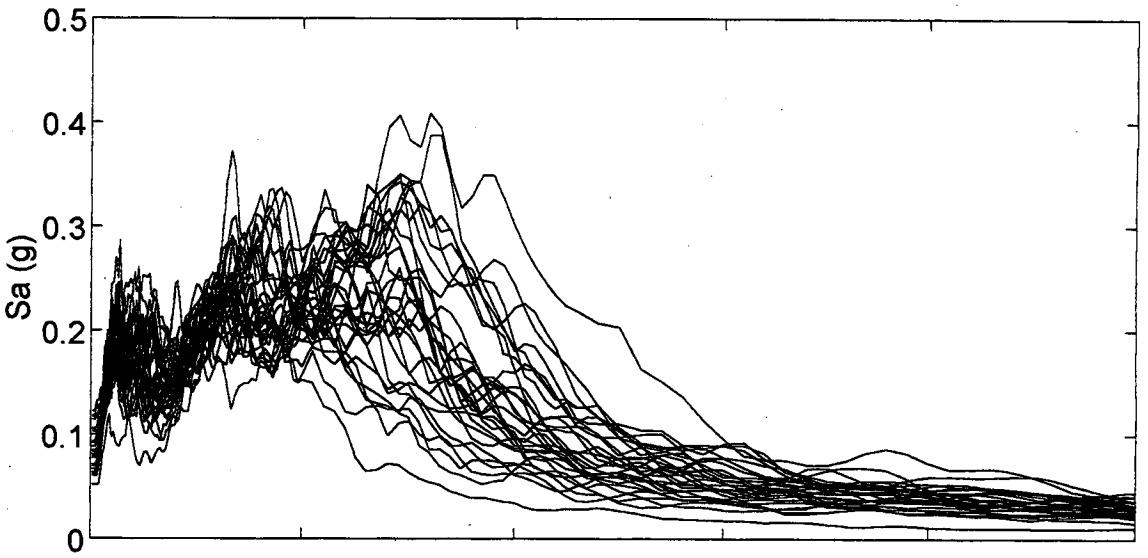

Mean and Mean +/- One Standard Deviation

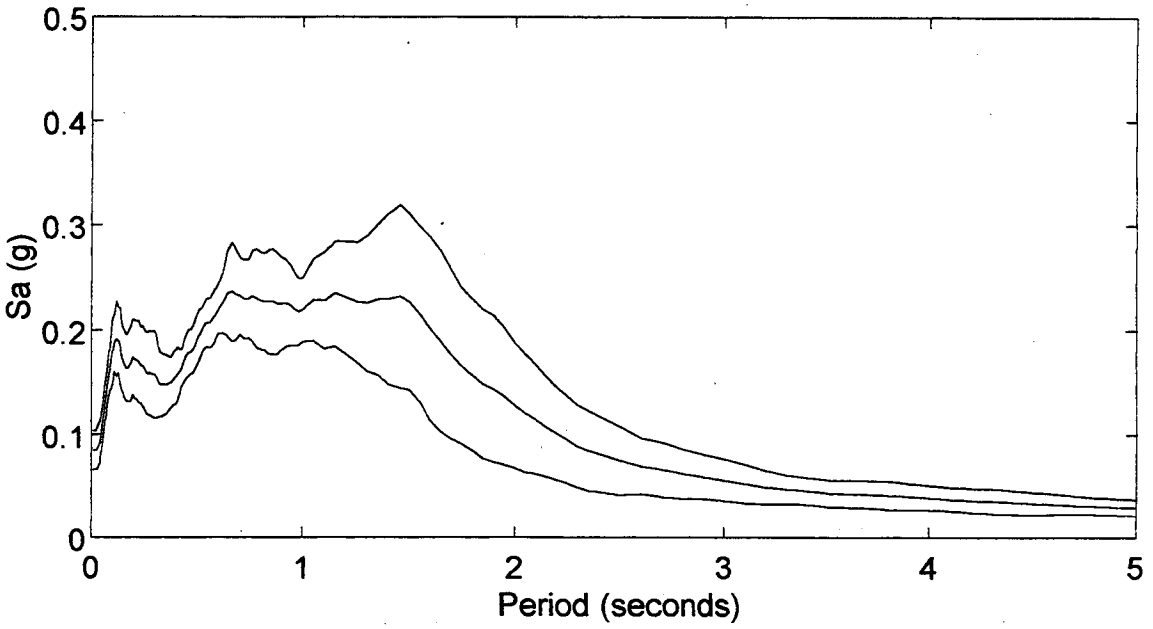

Andresen Road

Spectral Accelerations (M=8.0)

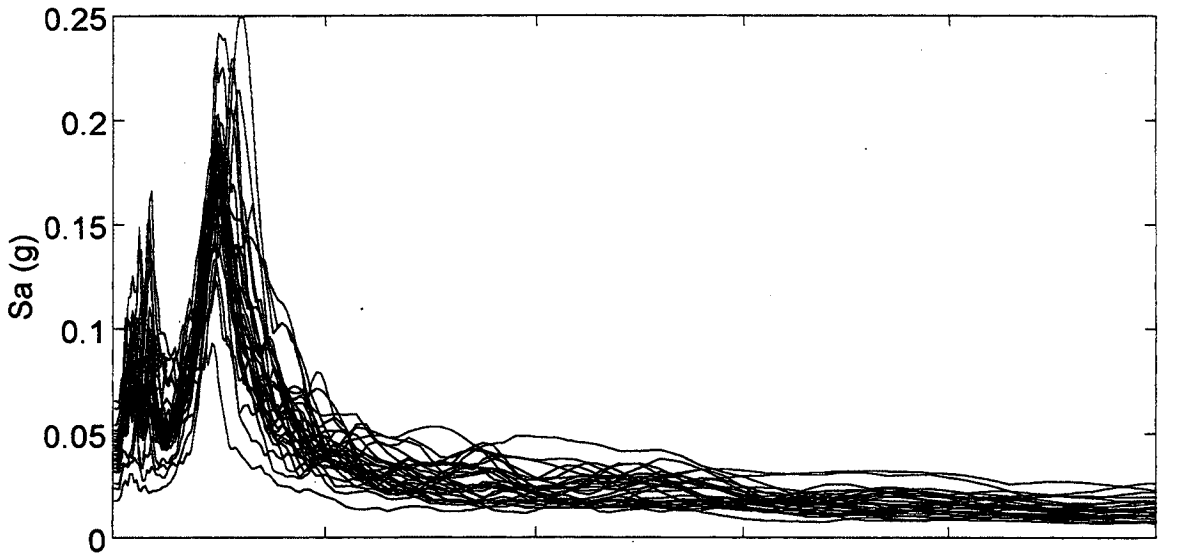

Mean and Mean +/- One Standard Deviation

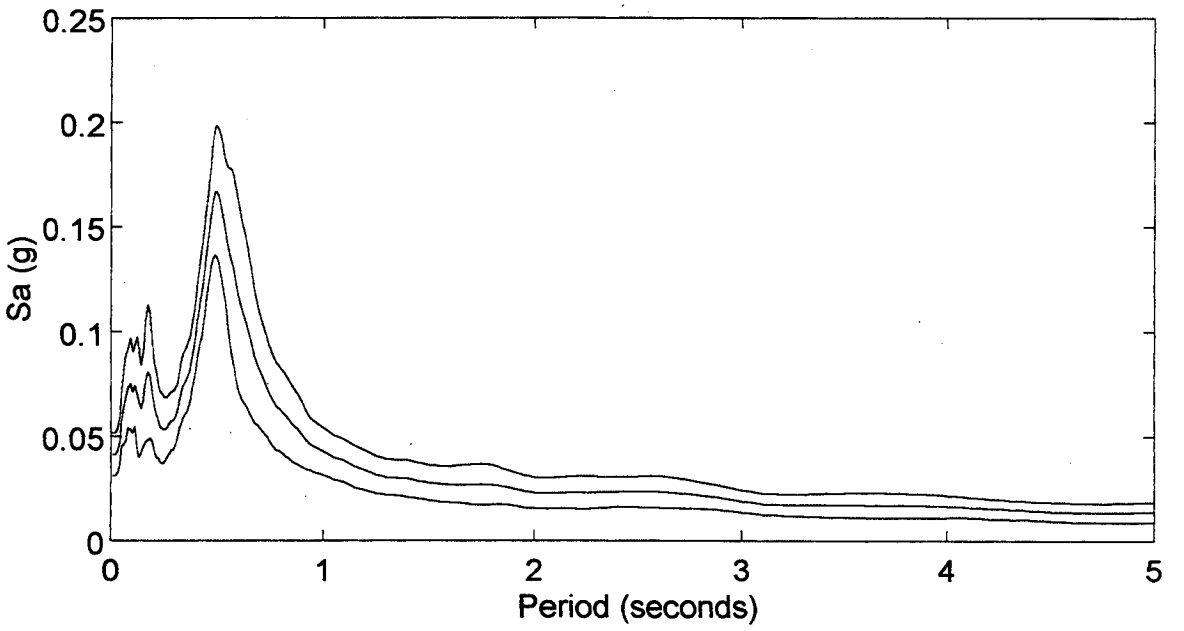

Andresen Road

Spectral Accelerations (M=8.5)

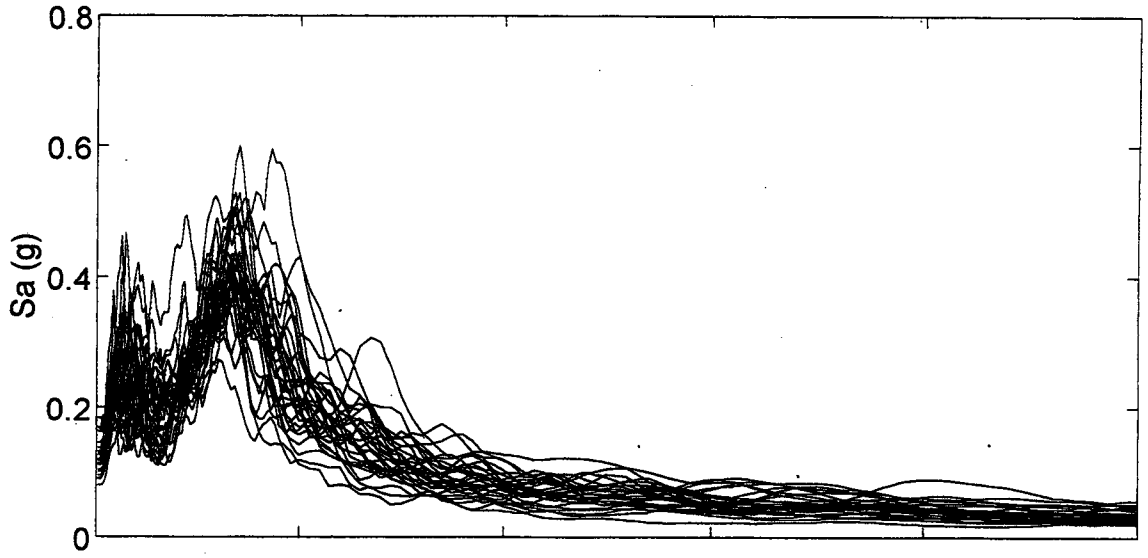

Mean and Mean +/- One Standard Deviation

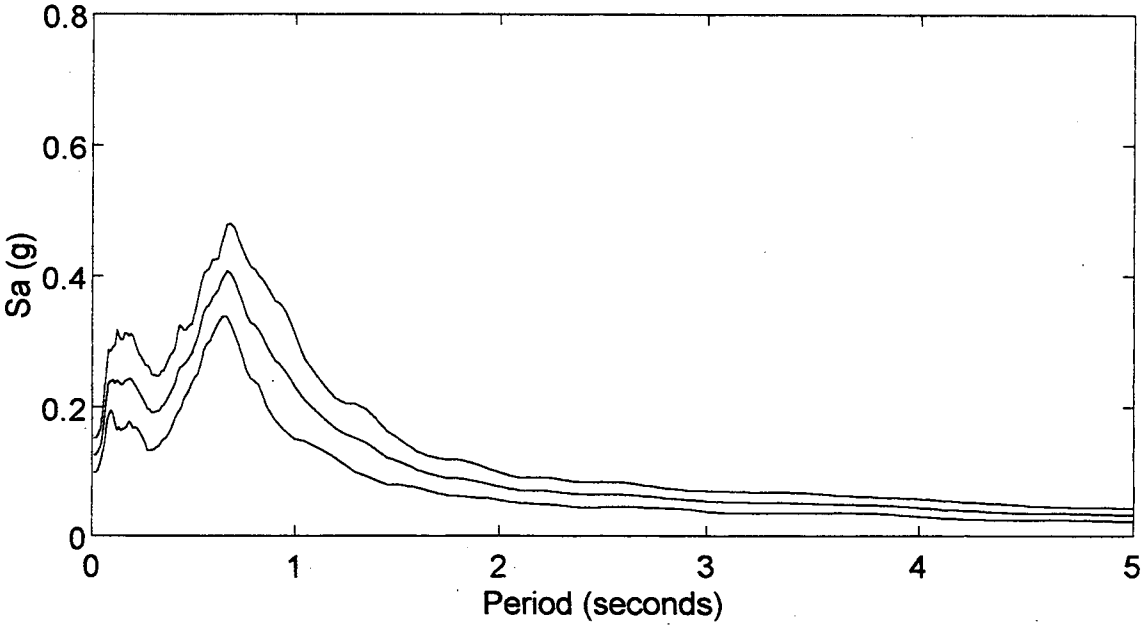

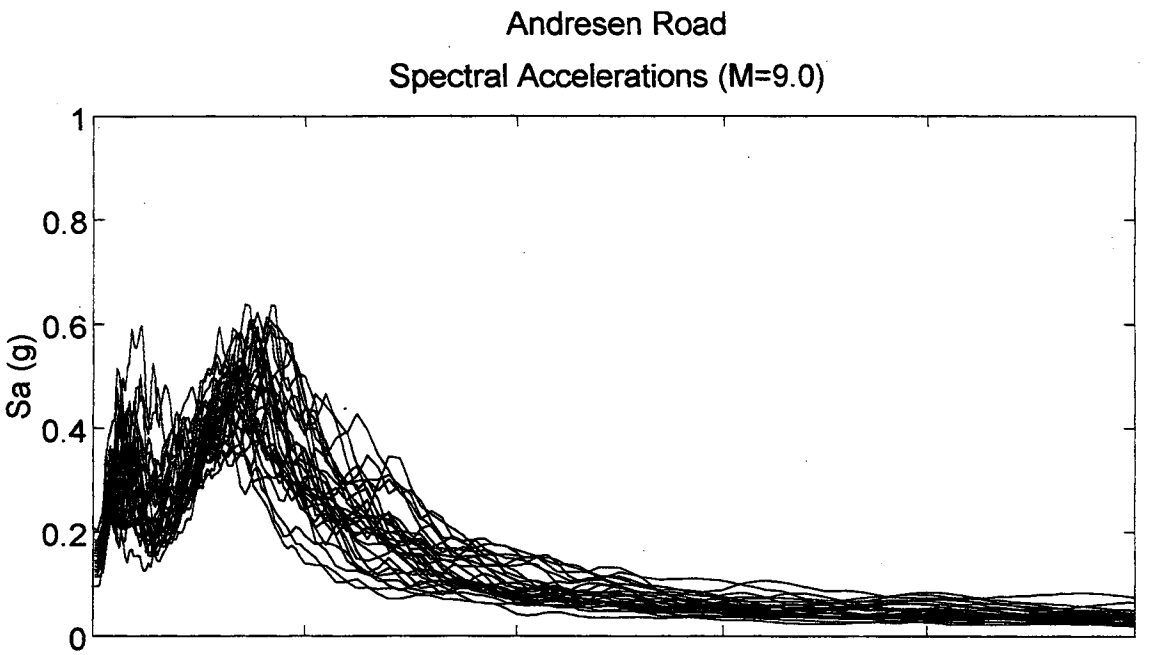
Andresen Road
Spectral Accelerations (M=9.0)
Sa (g)
0
0.2
0.4
0.6
0.8
1

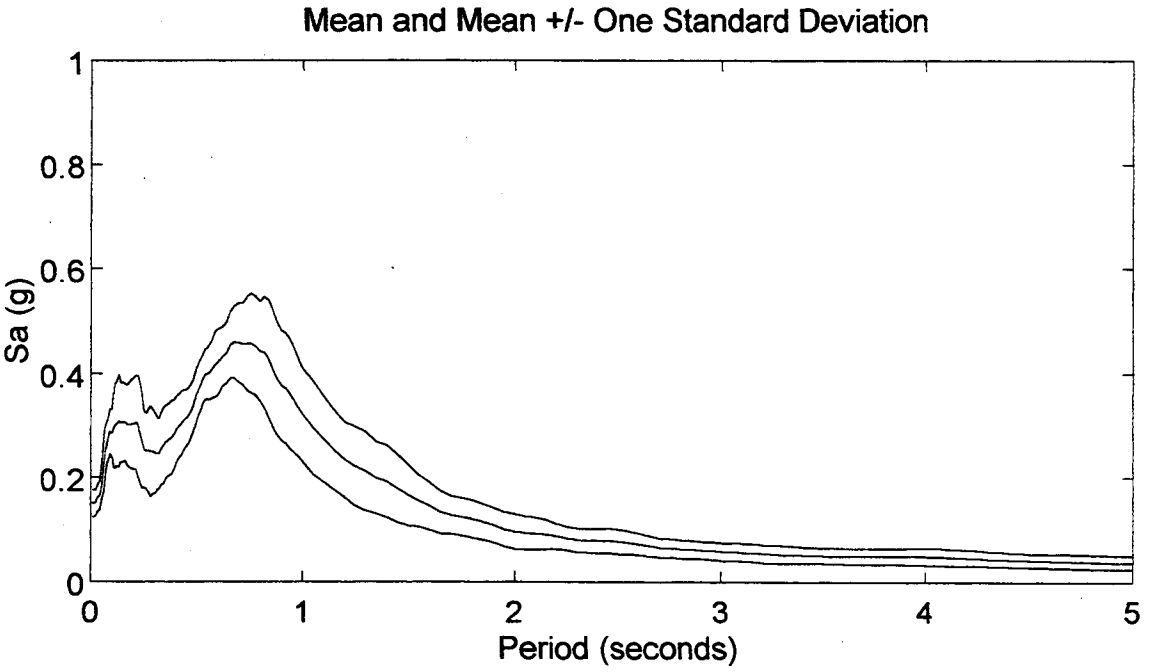
Mean and Mean +/- One Standard Deviation
Sa (g)
0
0.2
0.4
0.6
0.8
1
0
1
2
3
4
5
Period (seconds)

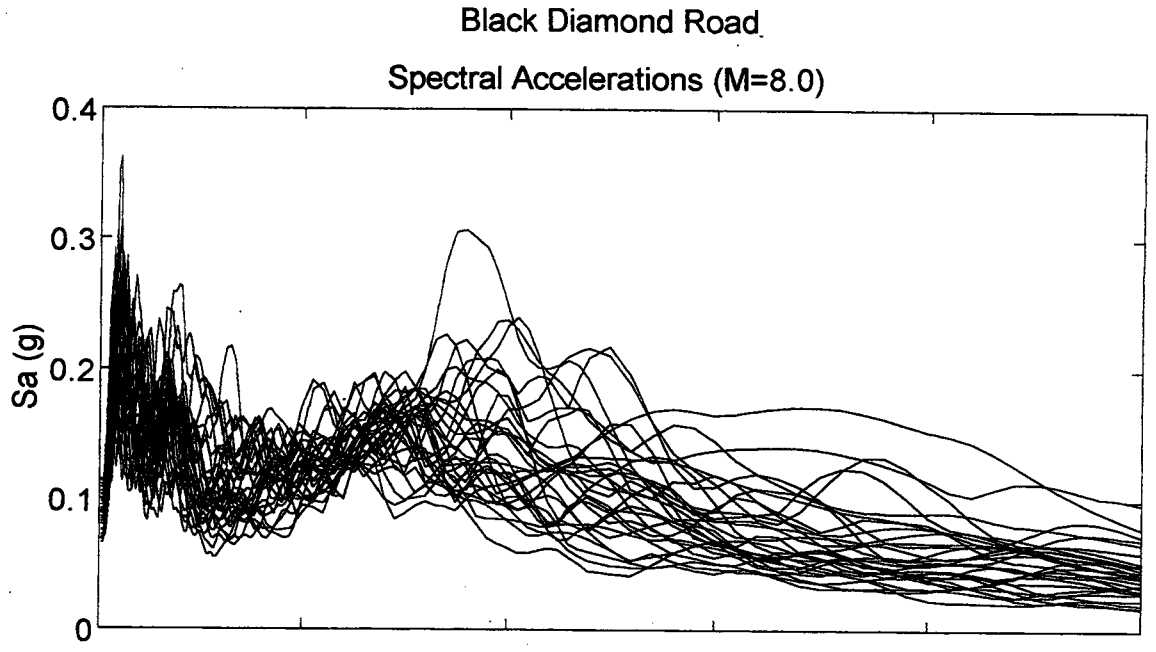
Black Diamond Road
Spectral Accelerations (M=8.0)
Sa (g)
0.4
0.3
0.2
0.1
0

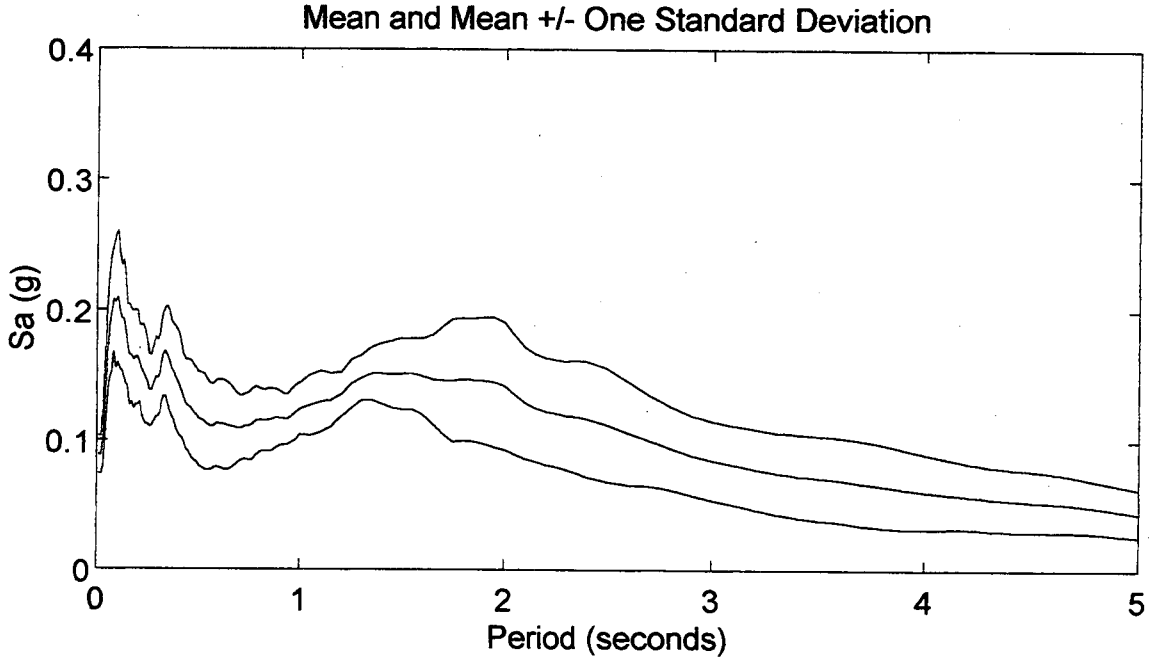
Mean and Mean +/- One Standard Deviation
Sa (g)
0.4
0.3
0.2
0.1
0
0
1
2
3
4
5
Period (seconds)

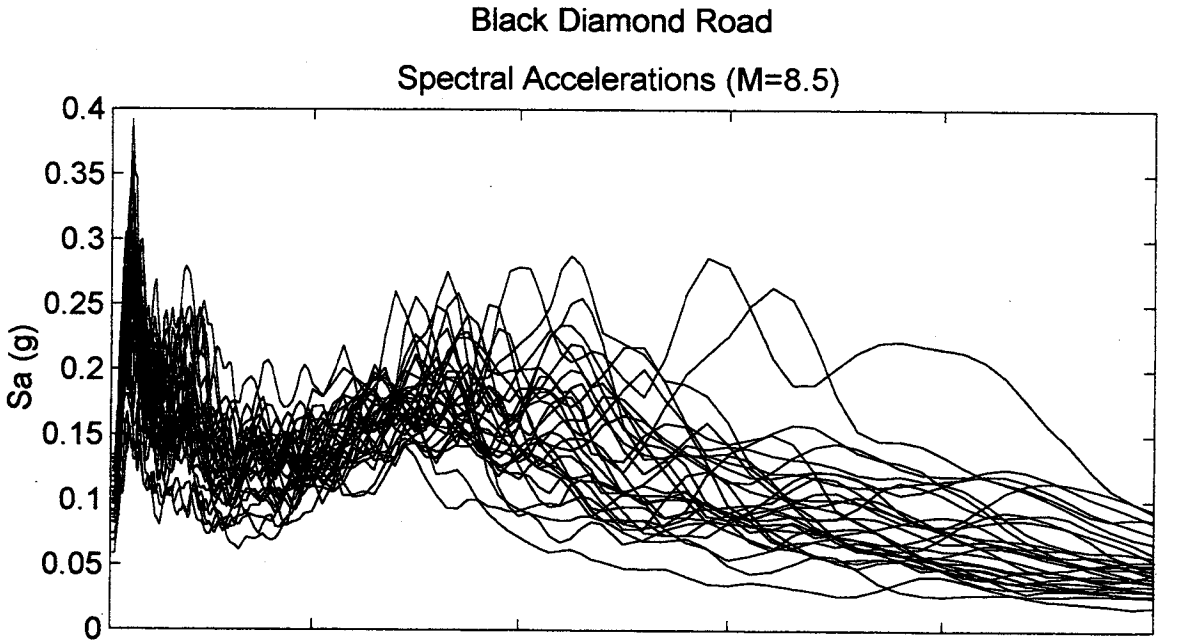
Black Diamond Road
Spectral Accelerations (M=8.5)
Sa (g)
0.4
0.35
0.3
0.25
0.2
0.15
0.1
0.05
0

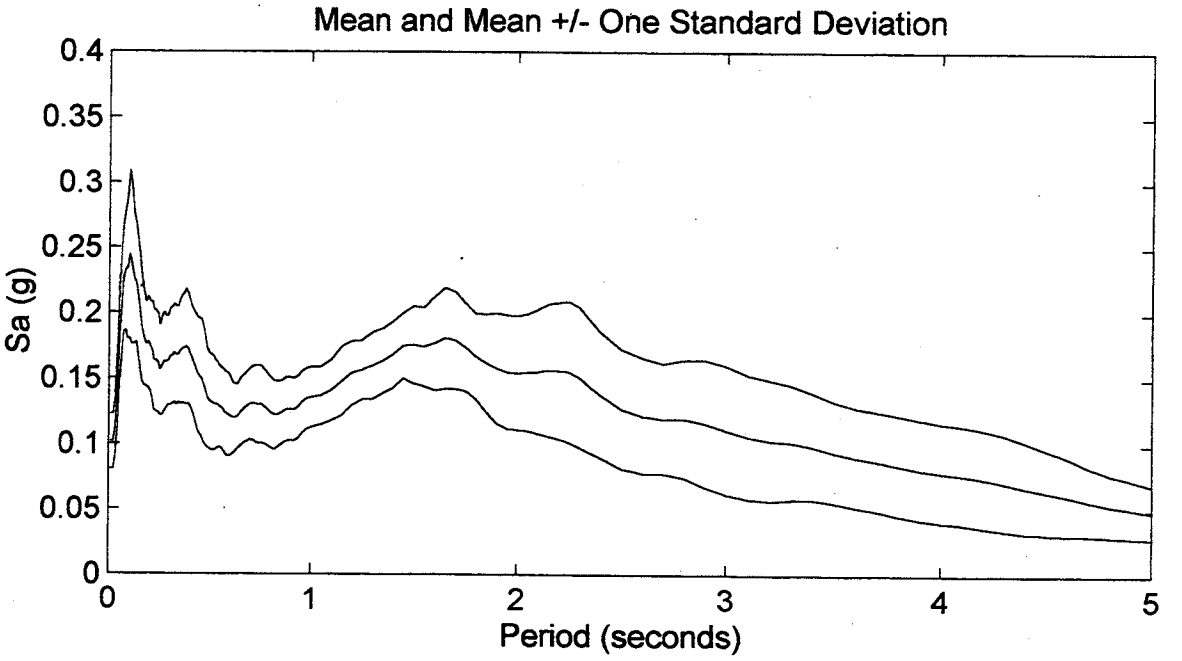
Mean and Mean +/- One Standard Deviation
Sa (g)
0.4
0.35
0.3
0.25
0.2
0.15
0.1
0.05
0
0
1
2
3
4
5
Period (seconds)

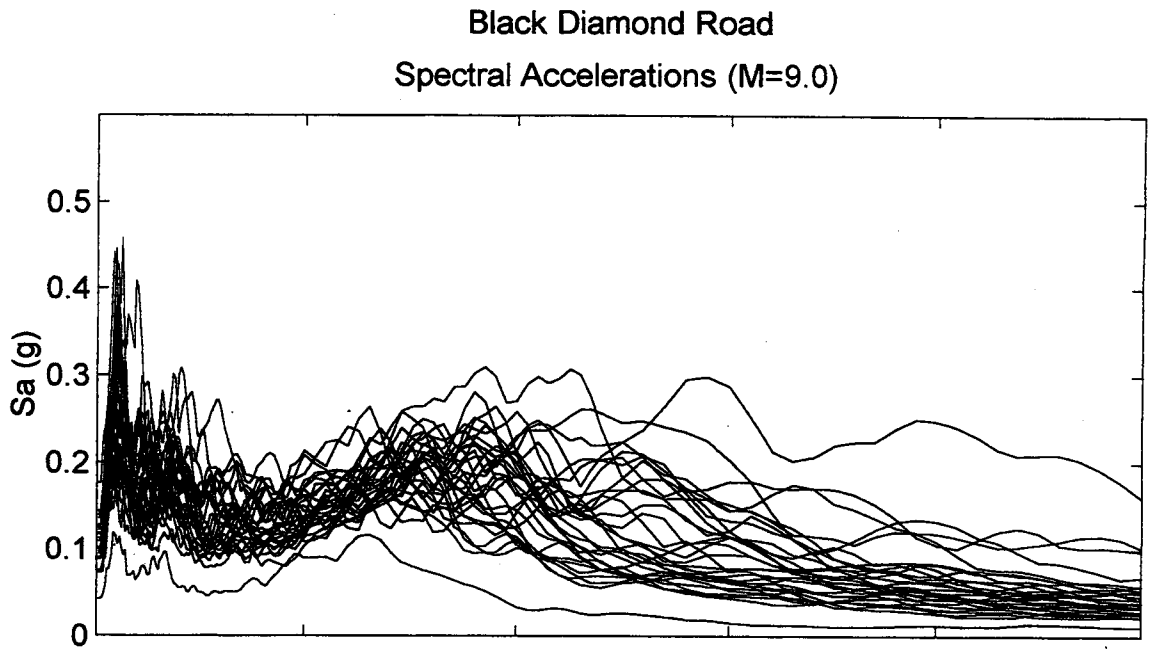
Black Diamond Road
Spectral Accelerations (M=9.0)
Sa (g)
0.5
0.4
0.3
0.2
0.1
0

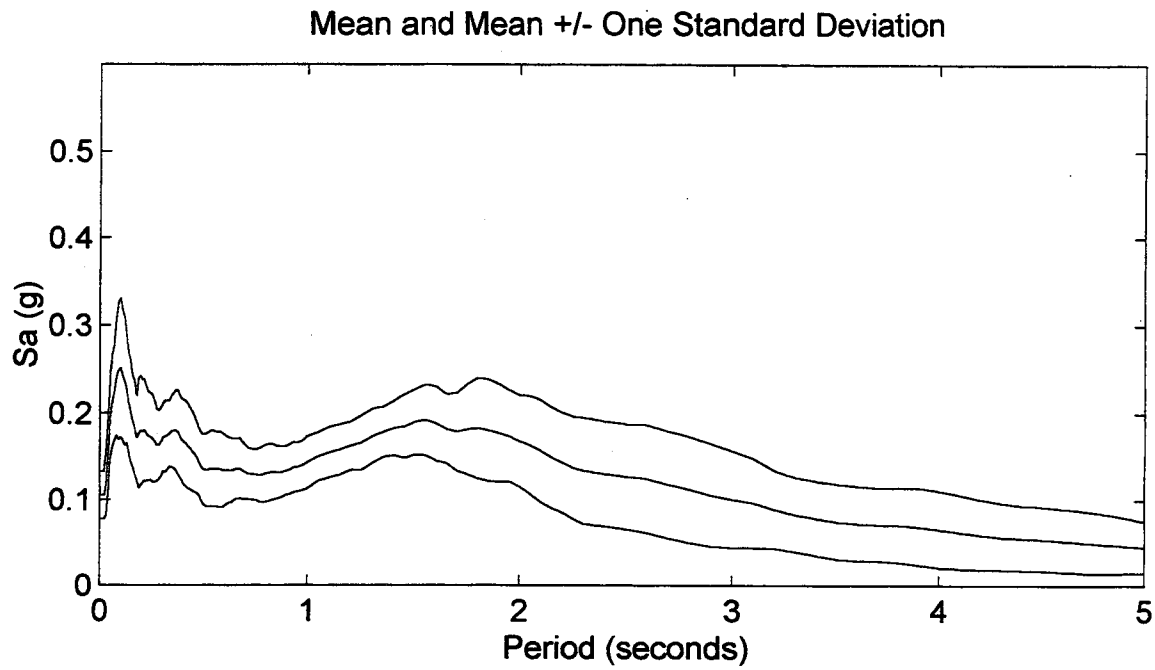
Mean and Mean +/- One Standard Deviation
Sa (g)
0.5
0.4
0.3
0.2
0.1
0
0
1
2
3
4
5
Period (seconds)

Bone River

Spectral Accelerations (M=8.0)

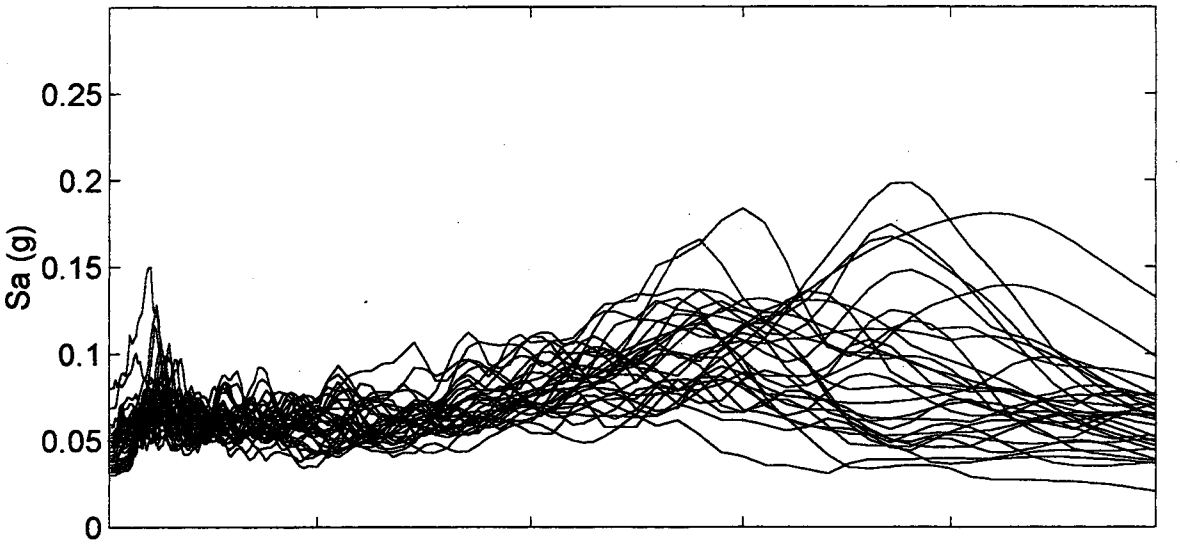

Mean and Mean +/- One Standard Deviation

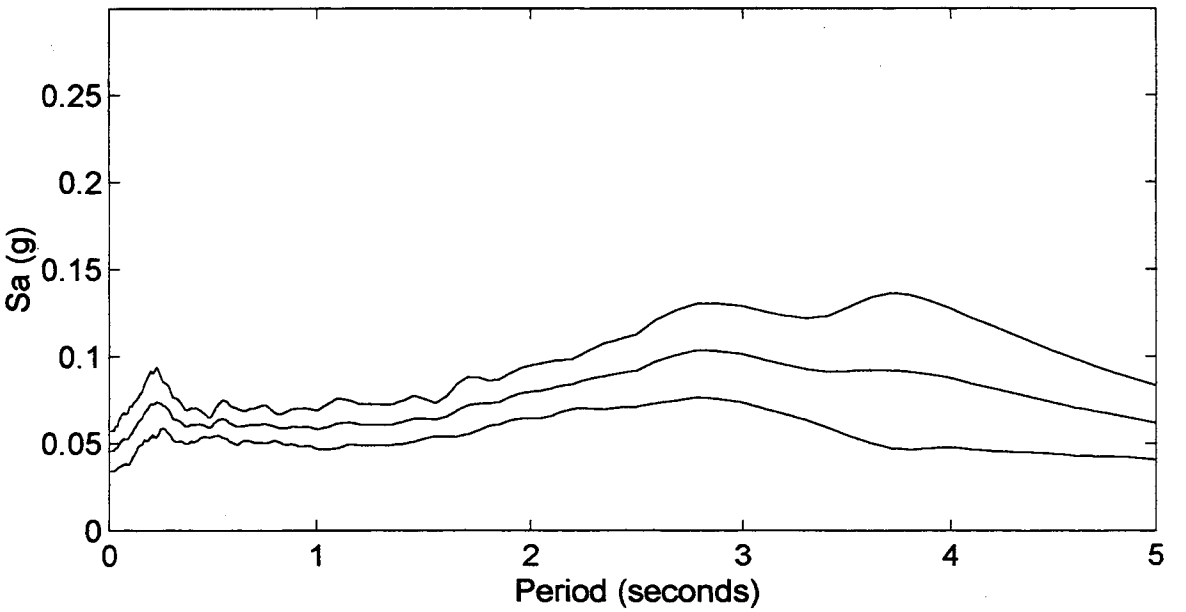

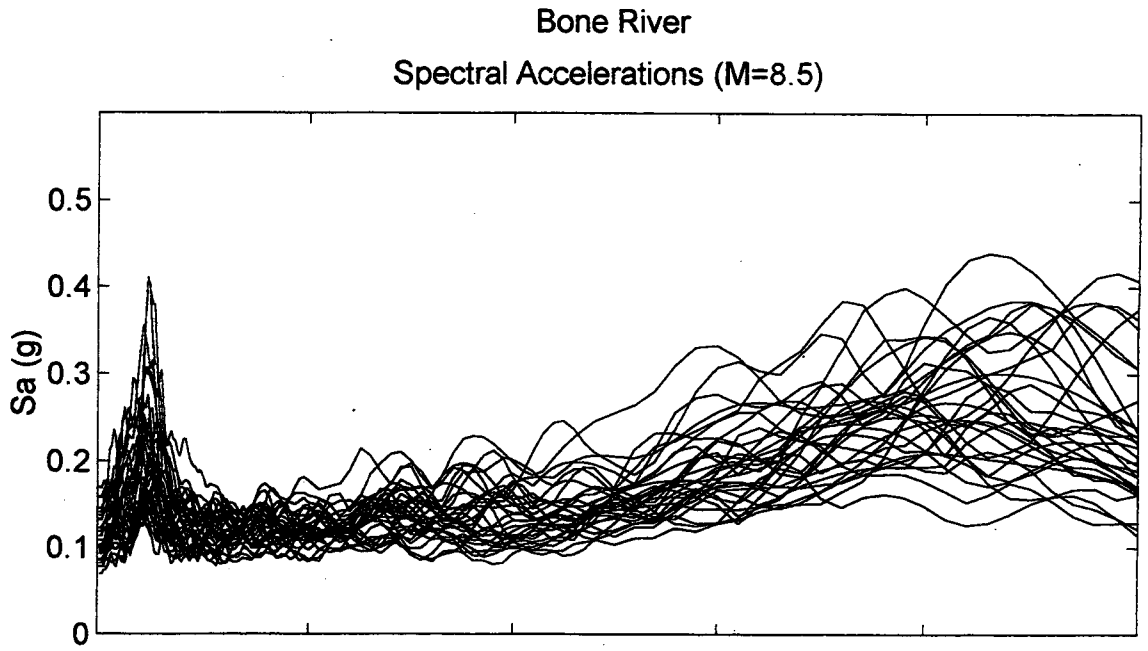
Bone River
Spectral Accelerations (M=8.5)
Sa (g)
0.5
0.4
0.3
0.2
0.1
0

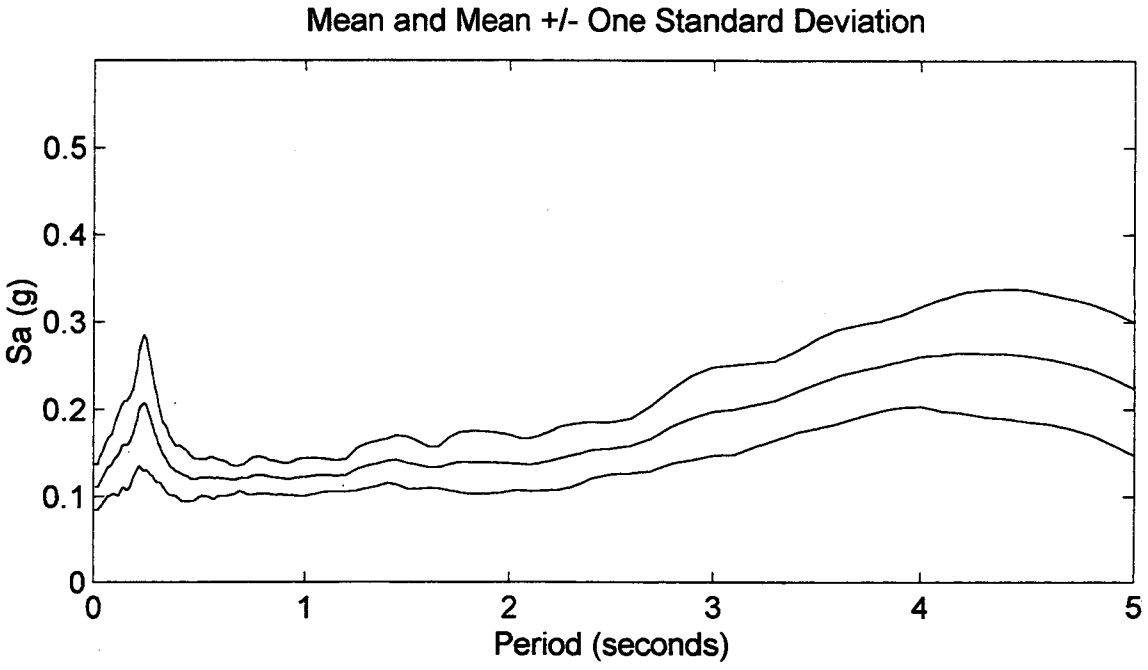
Mean and Mean +/- One Standard Deviation
Sa (g)
0.5
0.4
0.3
0.2
0.1
0
0
1
2
3
4
5
Period (seconds)

Bone River

Spectral Accelerations (M=9.0)

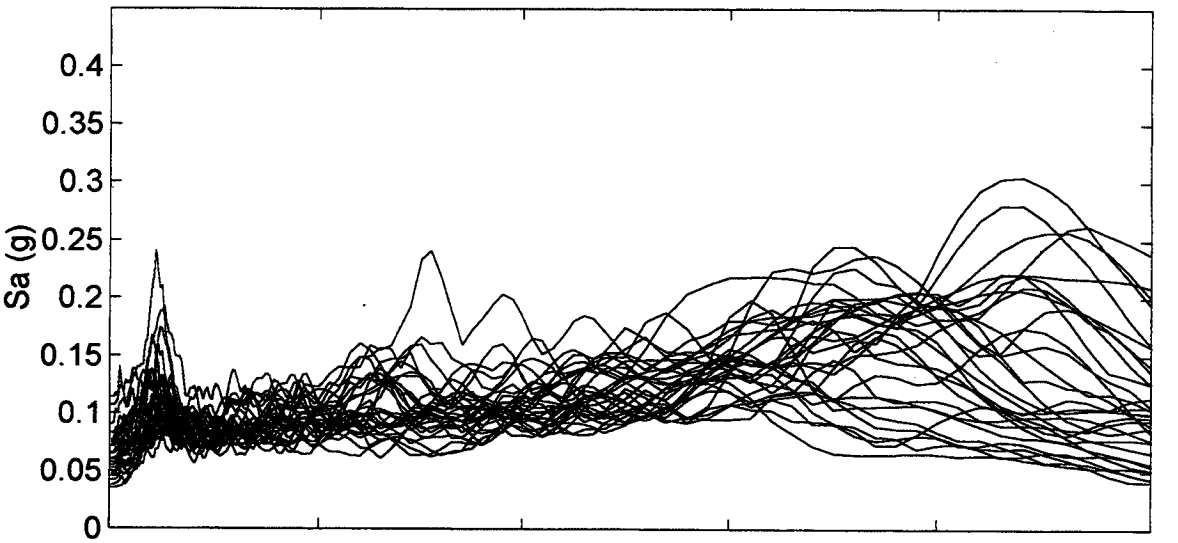

Mean and Mean +/- One Standard Deviation

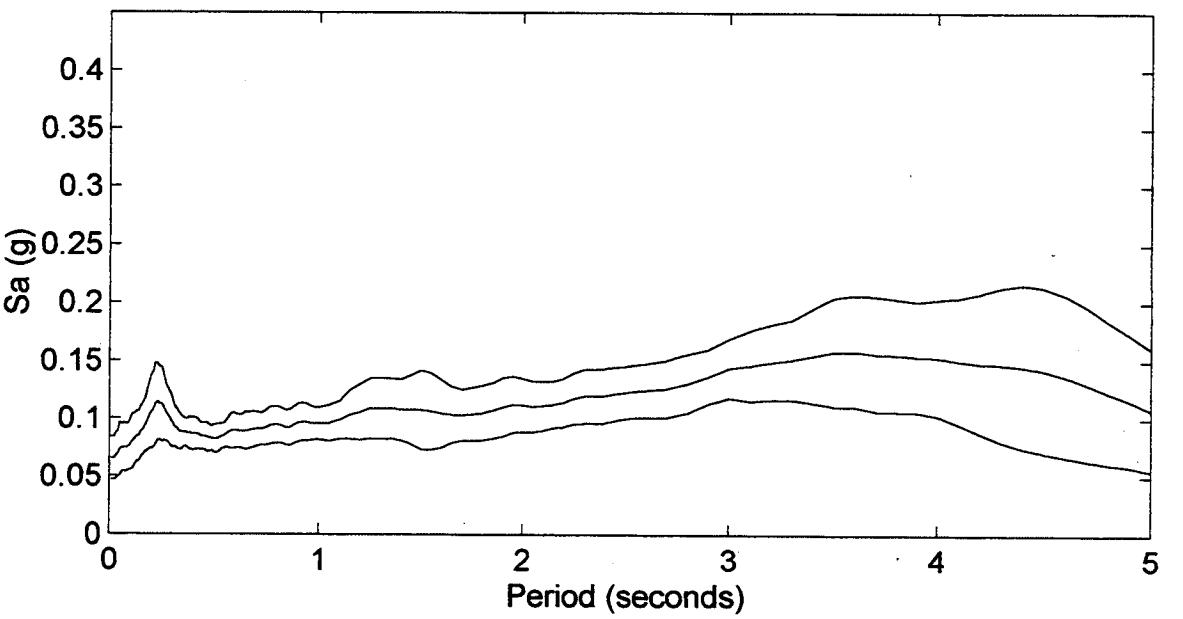

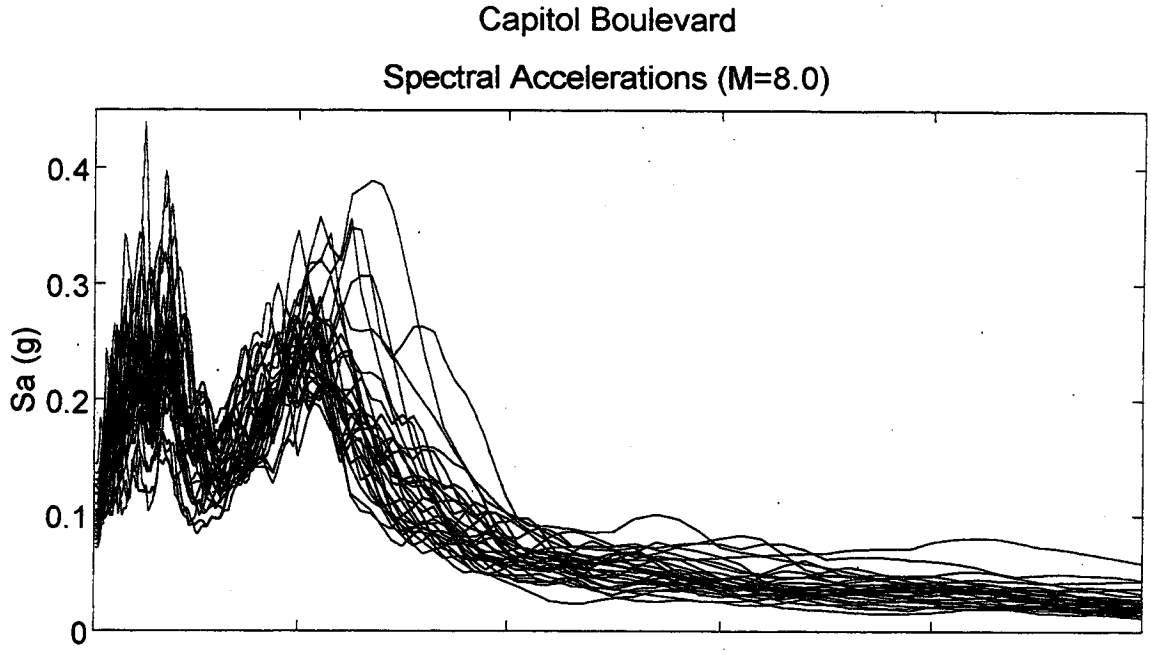
Capitol Boulevard
Spectral Accelerations (M=8.0)
Sa (g)
0.4
0.3
0.2
0.1
0

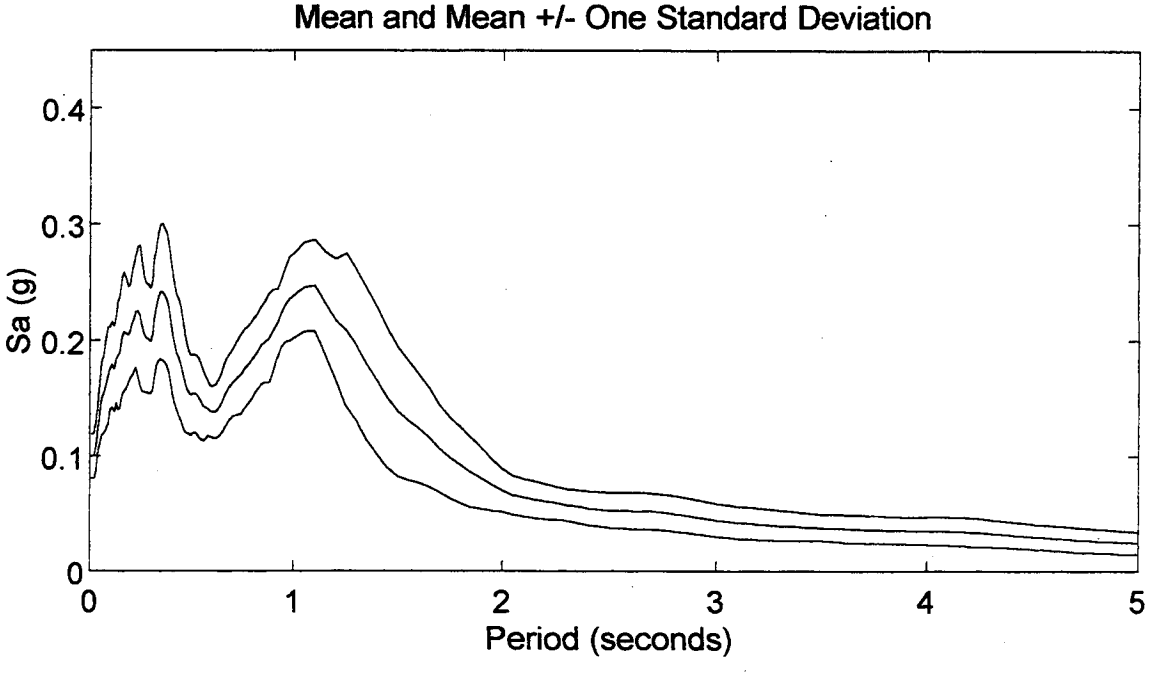
Mean and Mean +/- One Standard Deviation
Sa (g)
0.4
0.3
0.2
0.1
0
0
1
2
3
4
5
Period (seconds)

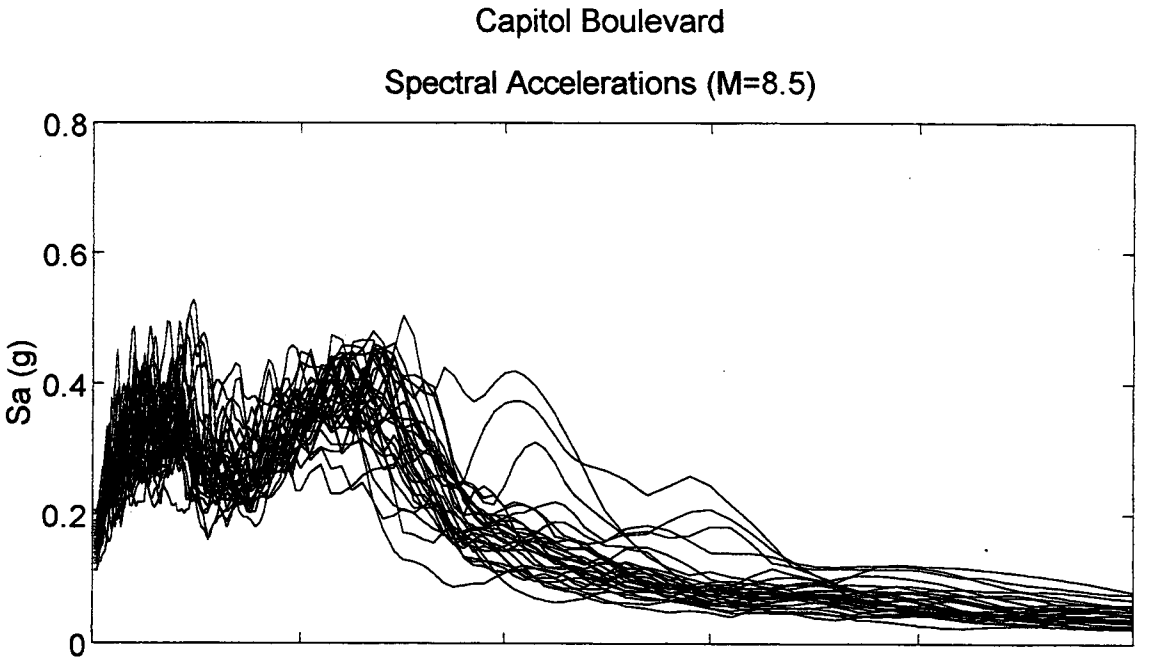
Capitol Boulevard
Spectral Accelerations (M=8.5)
Sa (g)
0.8
0.6
0.4
0.2
0

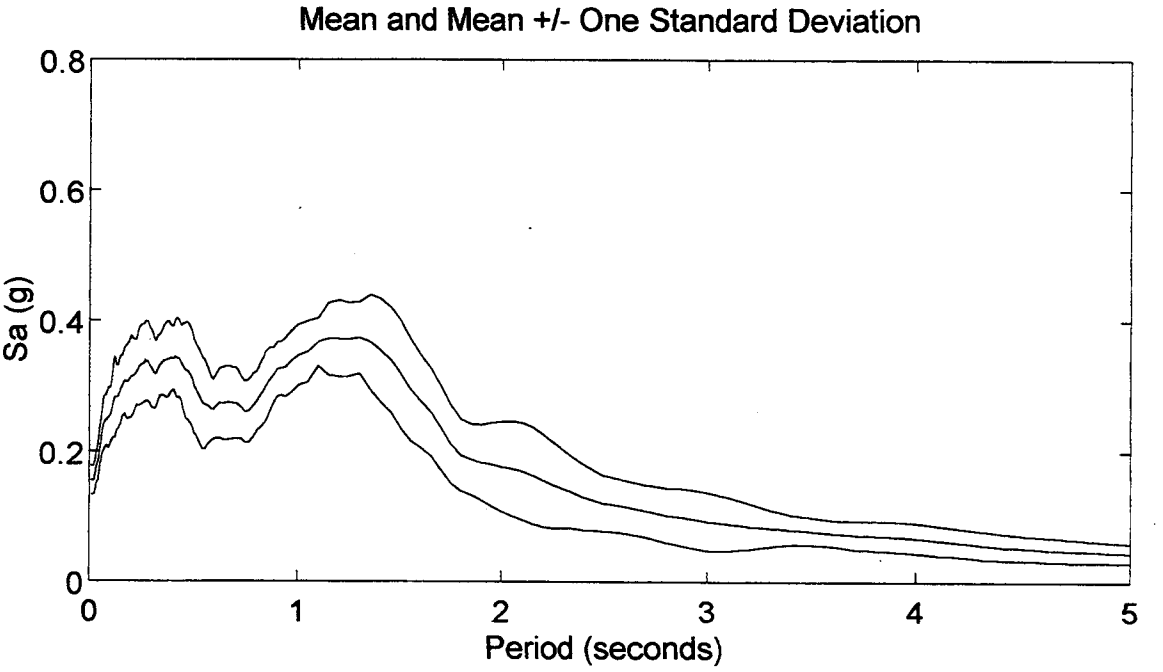
Mean and Mean +/- One Standard Deviation
Sa (g)
0.8
0.6
0.4
0.2
0
0
1
2
3
4
5
Period (seconds)

Capitol Boulevard

Spectral Accelerations (M=9.0)

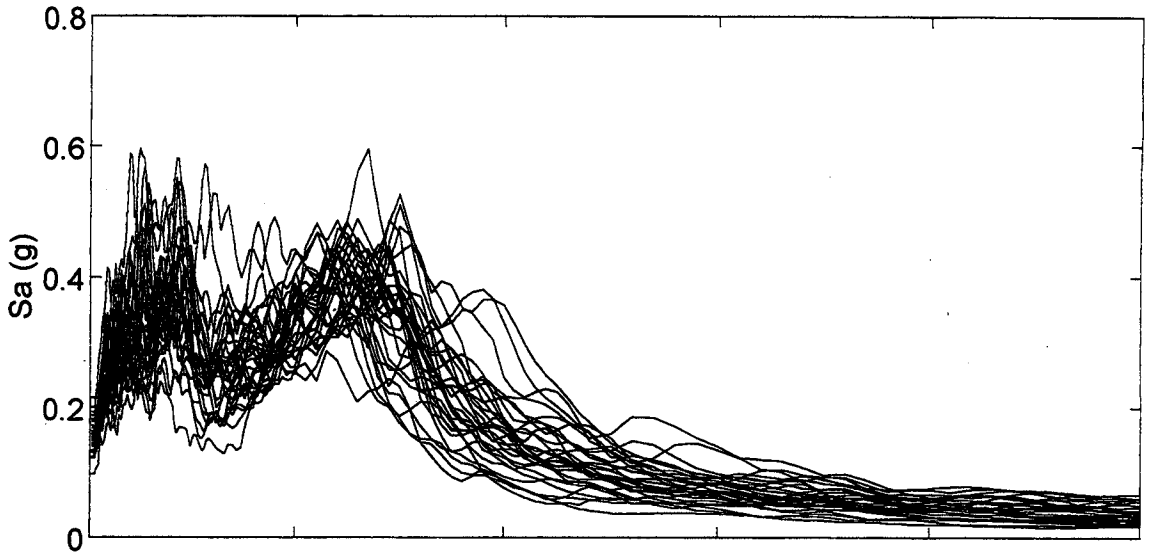

Mean and Mean +/- One Standard Deviation

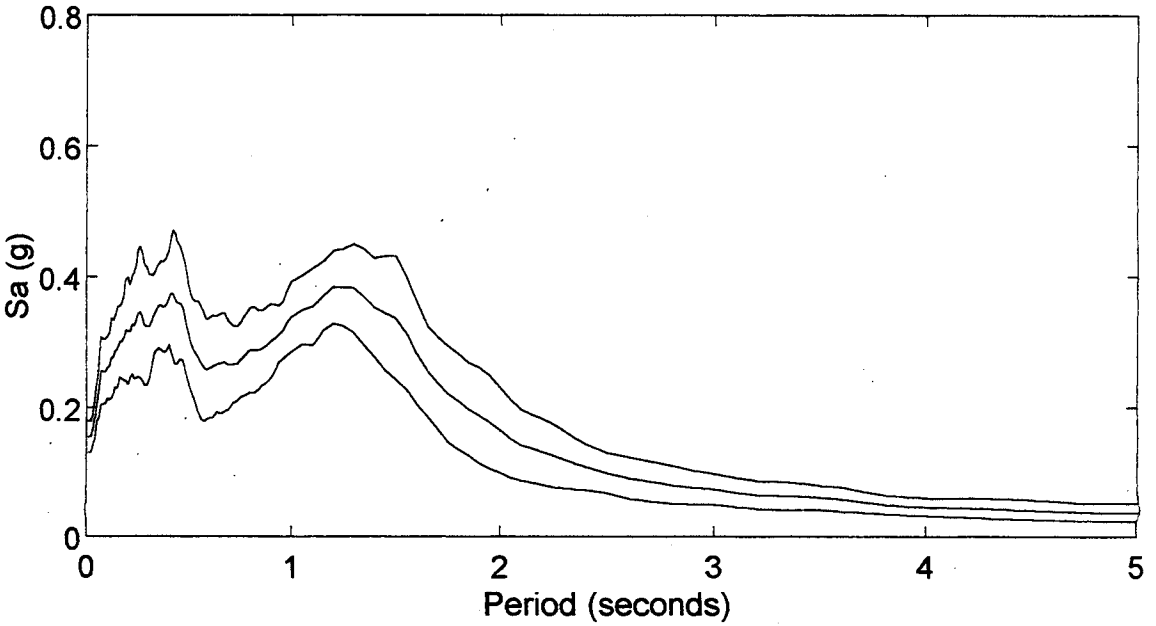

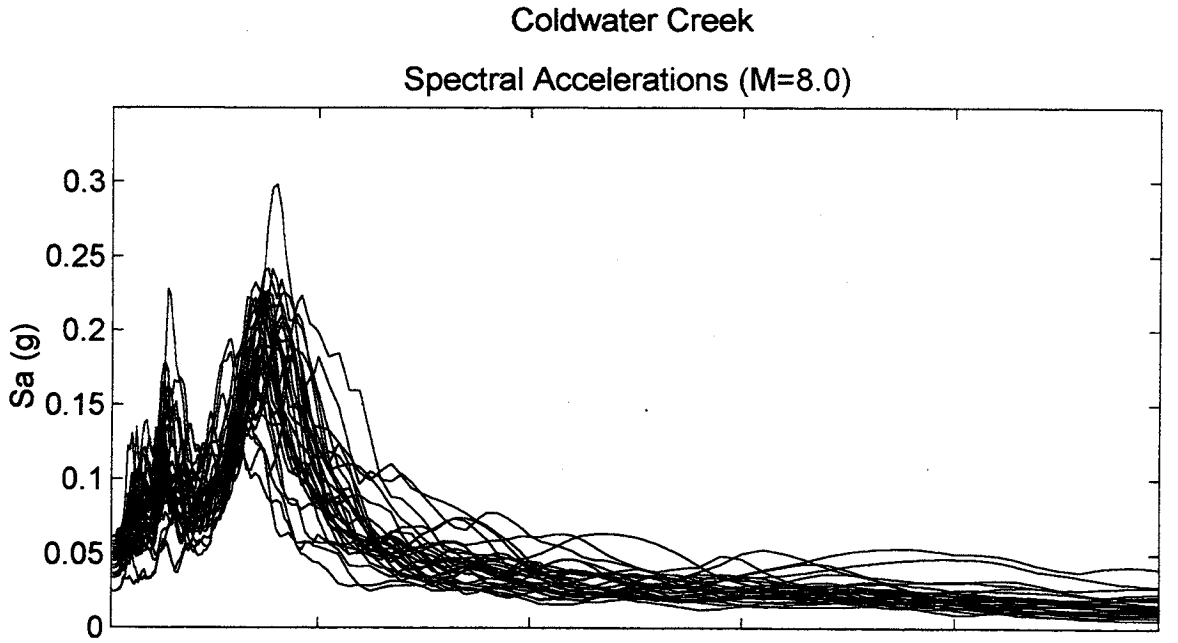
Coldwater Creek
Spectral Accelerations (M=8.0)
Sa (g)
0.3
0.25
0.2
0.15
0.1
0.05
0

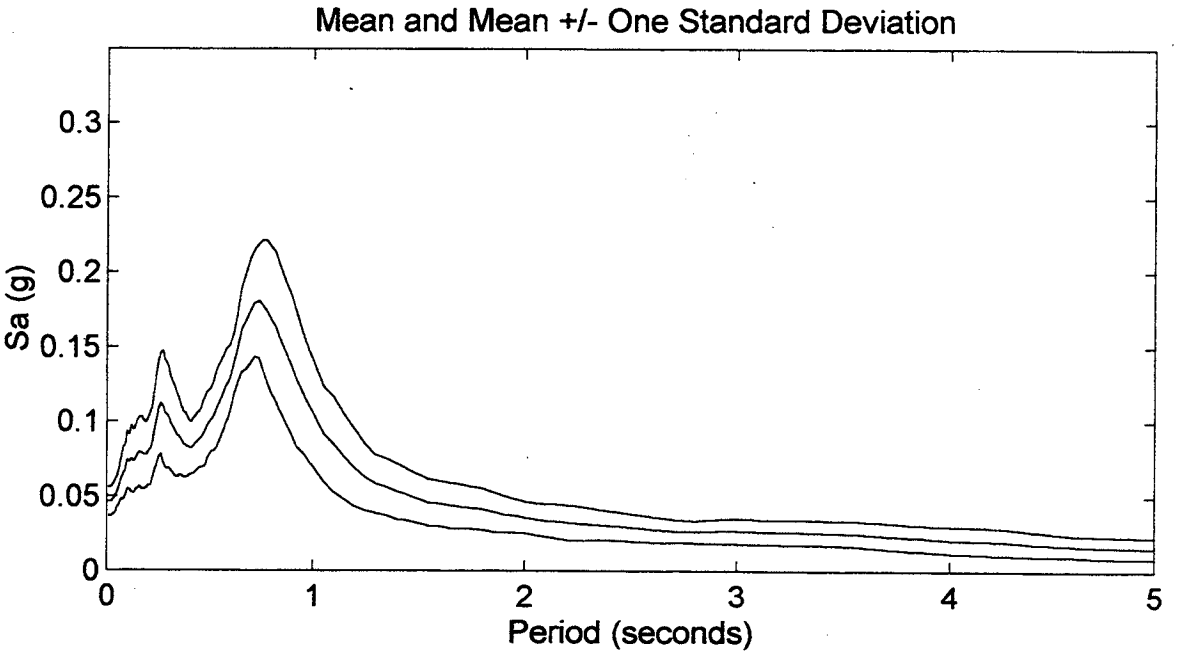
Mean and Mean +/- One Standard Deviation
Sa (g)
0.3
0.25
0.2
0.15
0.1
0.05
0
0
1
2
3
4
5
Period (seconds)

Coldwater Creek

Spectral Accelerations (M=8.5)

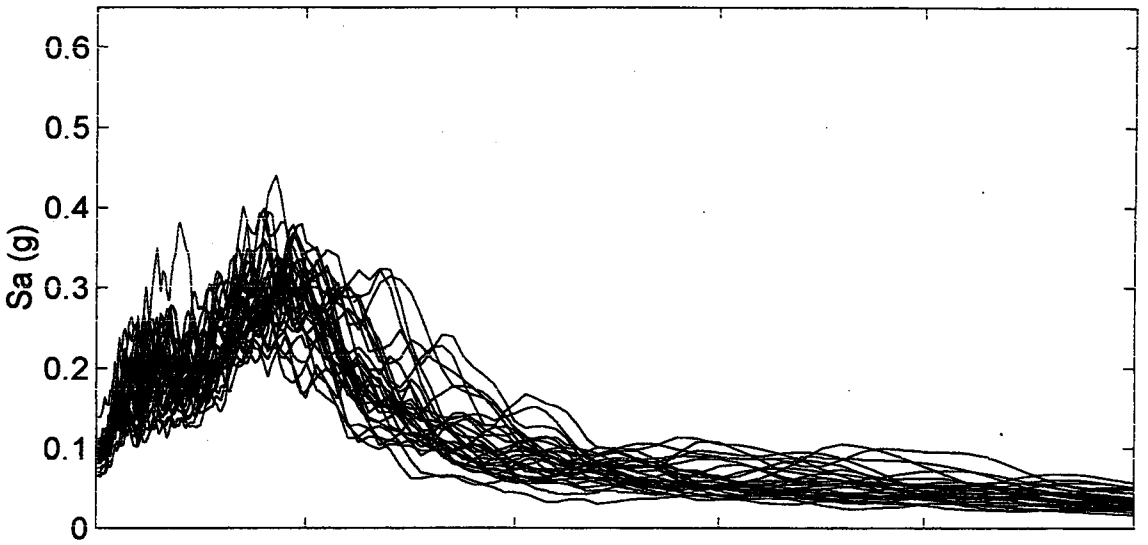

Mean and Mean +/- One Standard Deviation

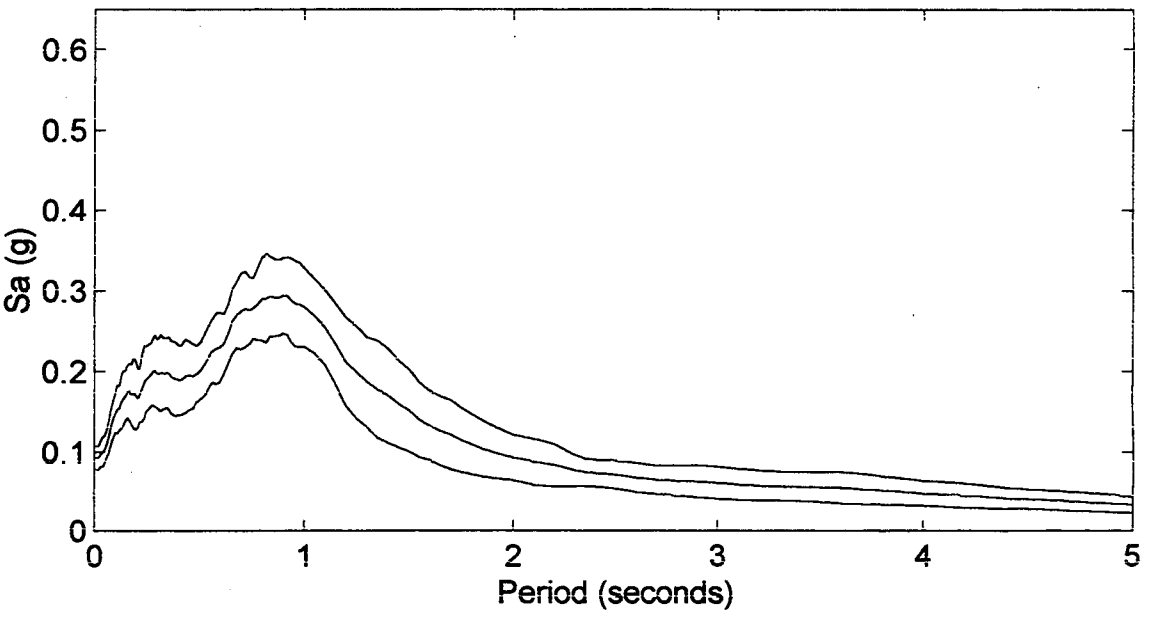

Coldwater Creek

Spectral Accelerations (M=9.0)

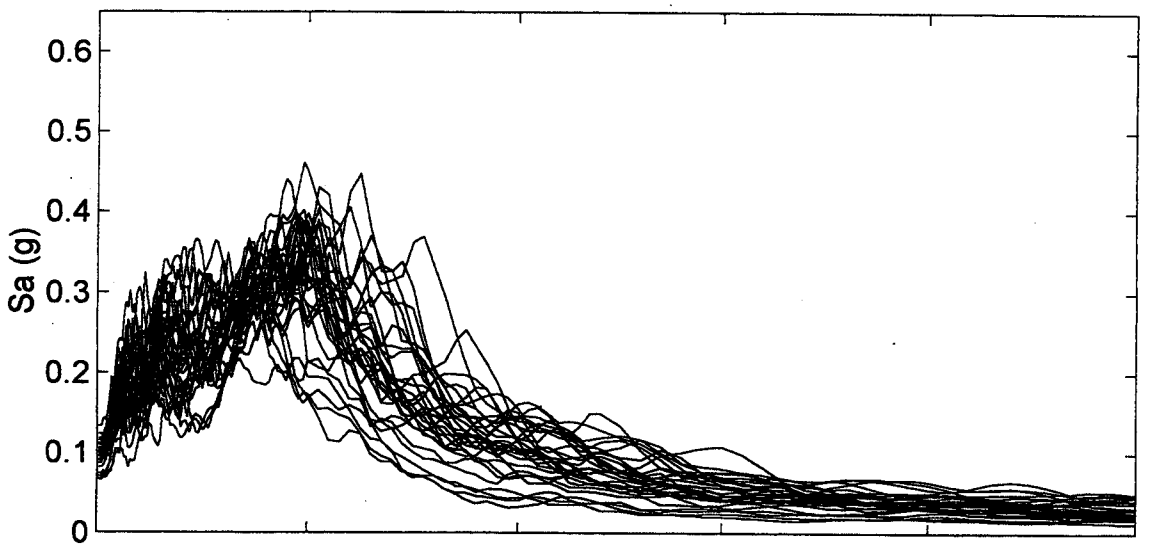

Mean and Mean +/- One Standard Deviation

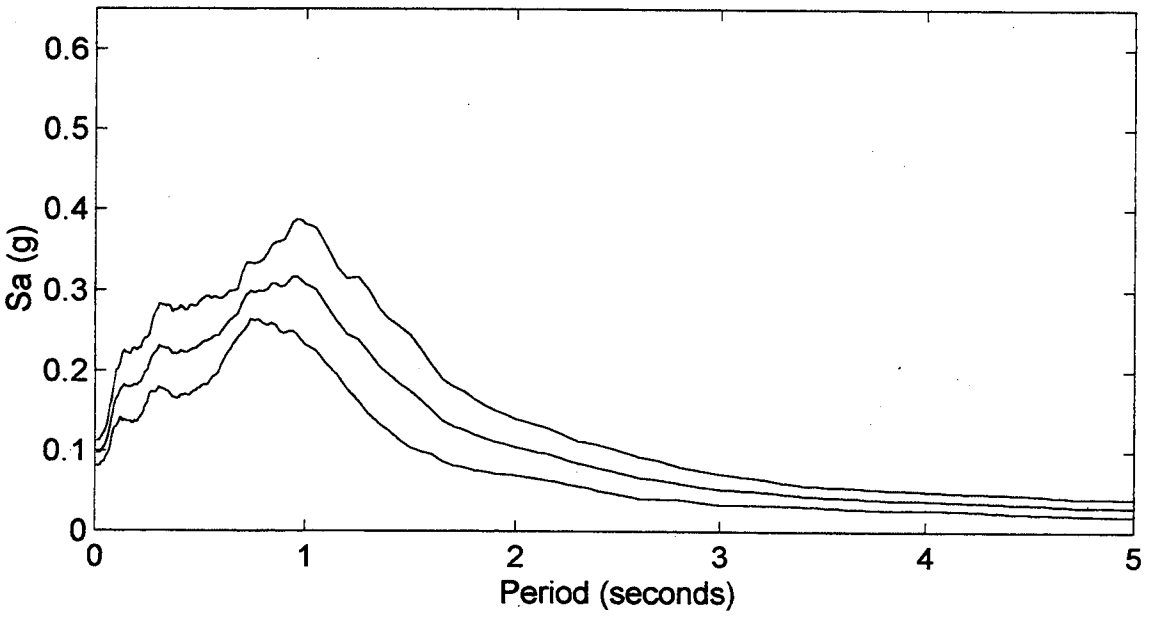

I-5/NE 99th Street

Spectral Accelerations (M=8.0)

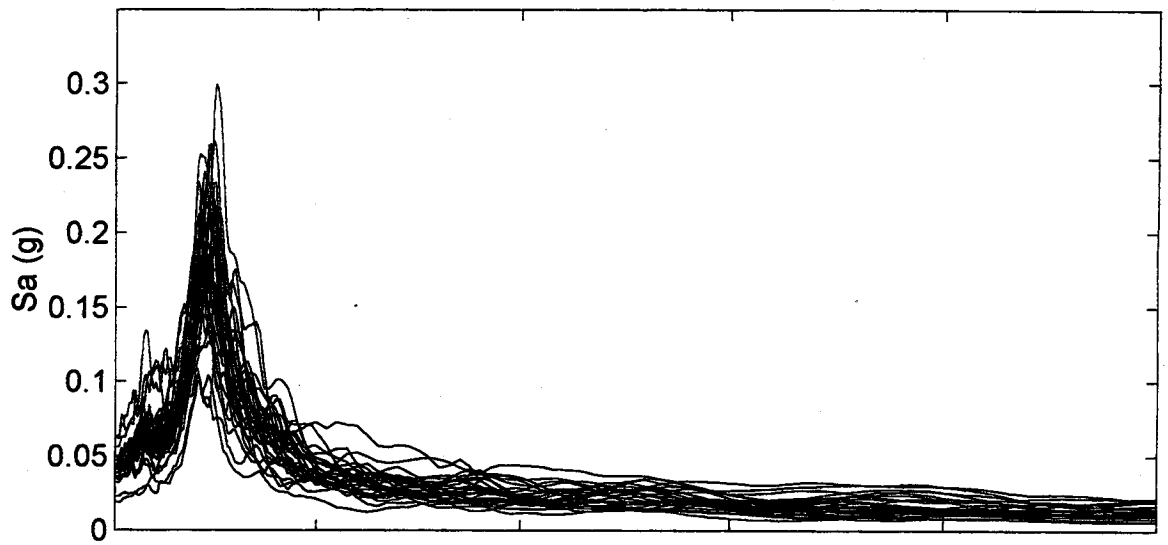

Mean and Mean +/- One Standard Deviation

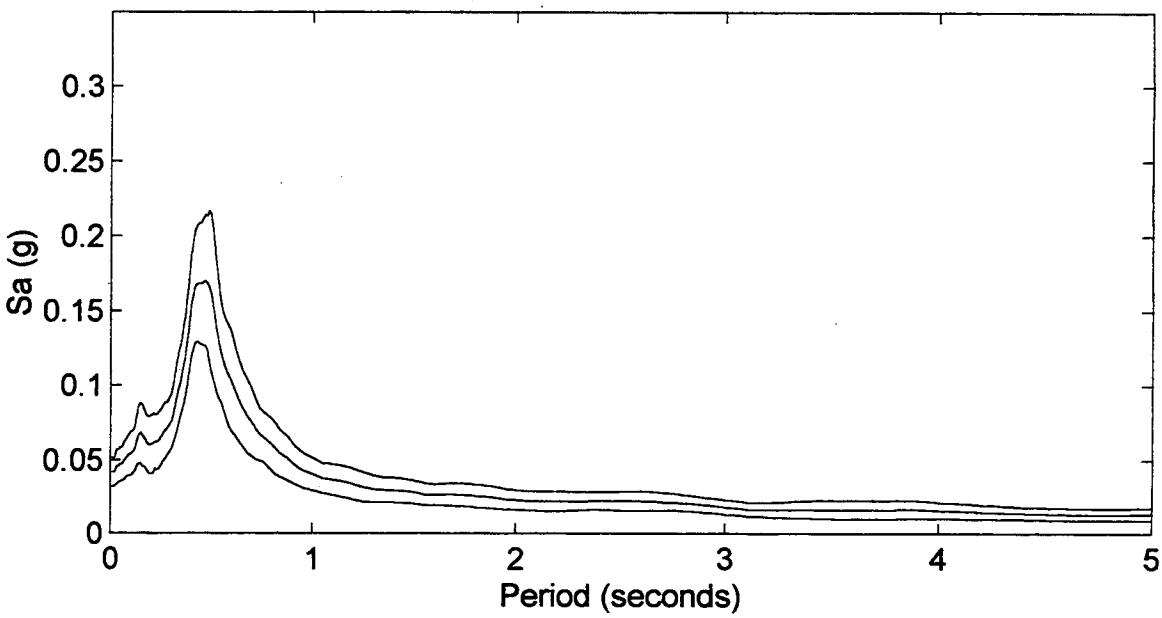

I-5/NE 99th Street

Spectral Accelerations (M=8.5)

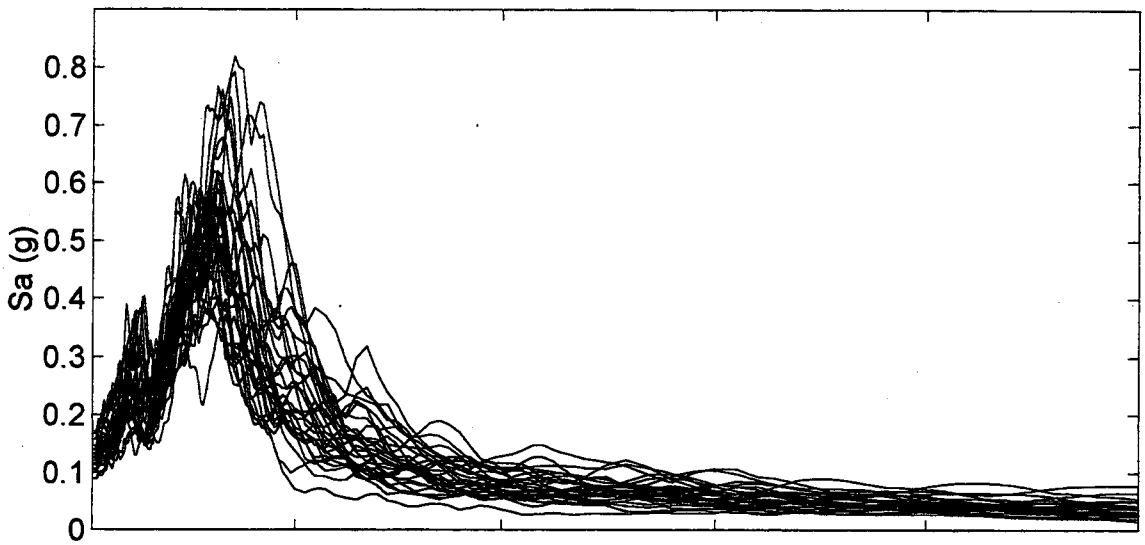

Mean and Mean +/- One Standard Deviation

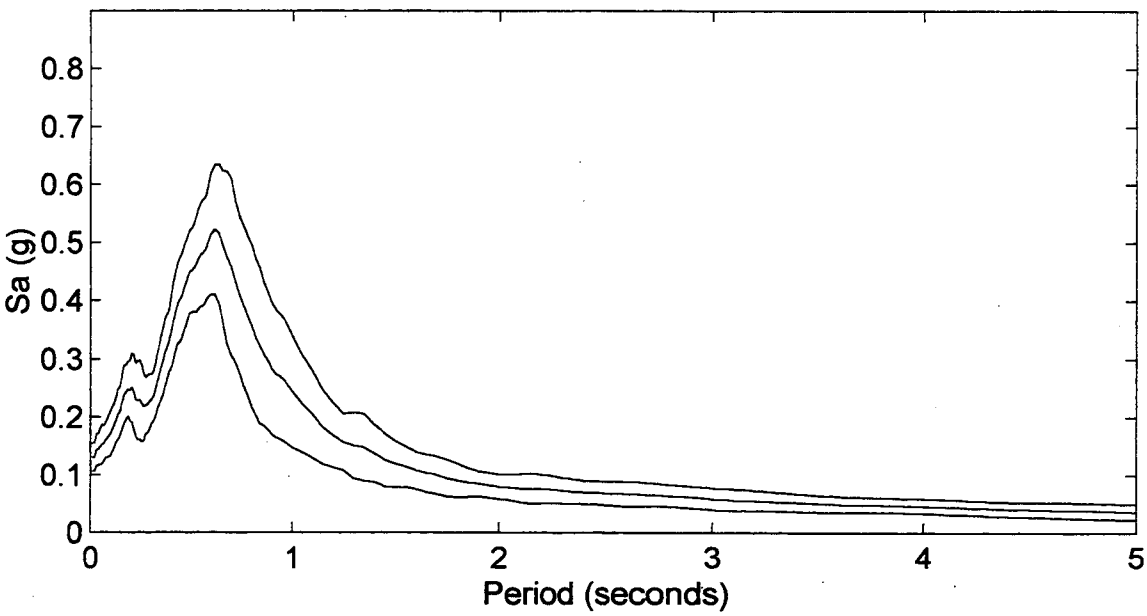

I-5/NE 99th Street

Spectral Accelerations (M=9.0)

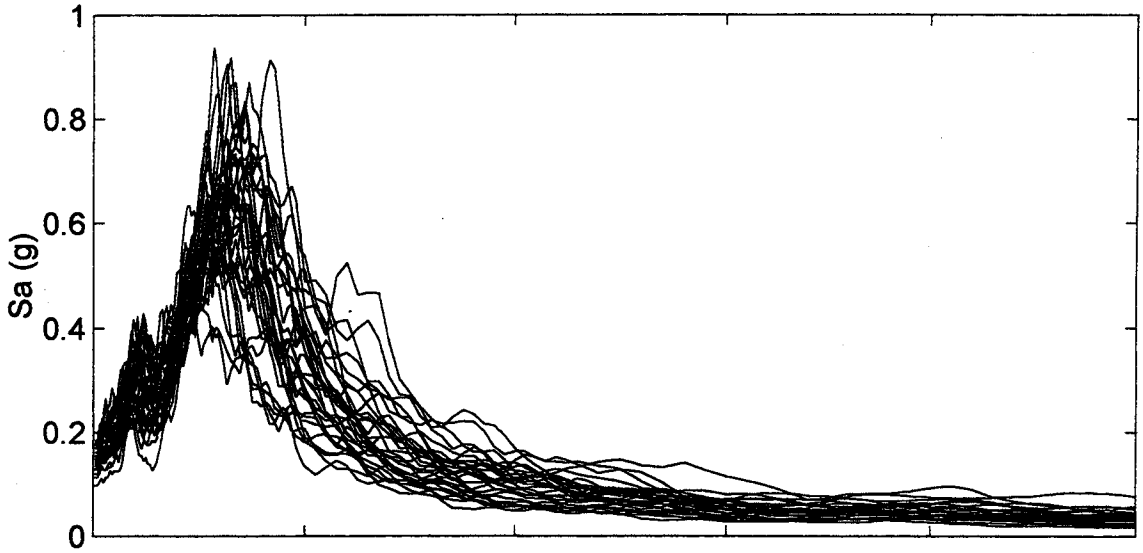

Mean and Mean +/- One Standard Deviation

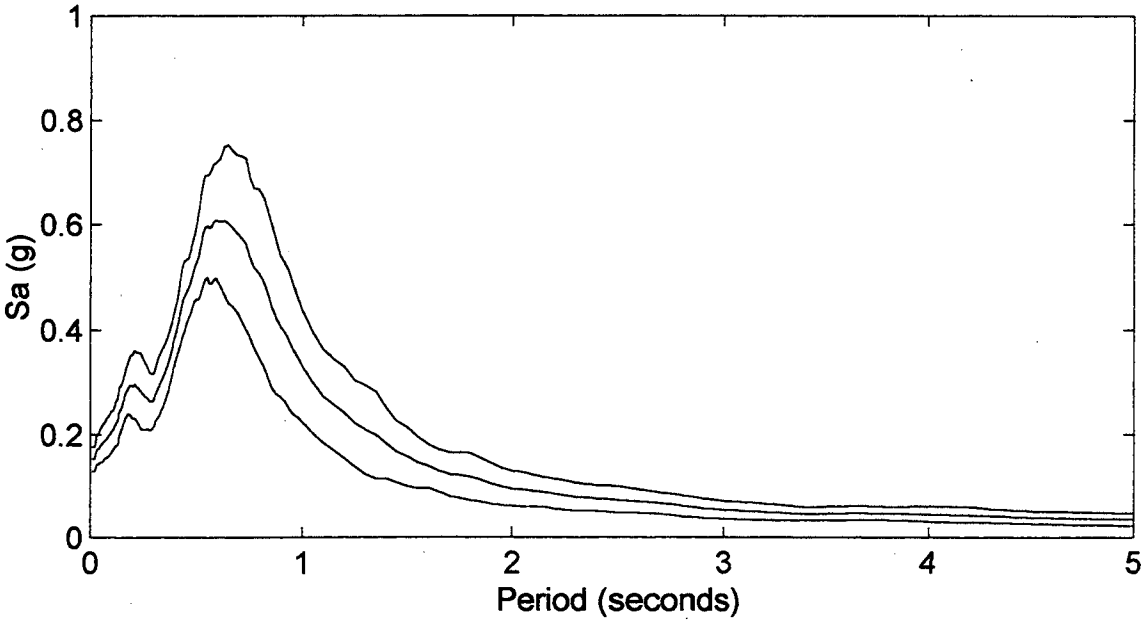

I-405/SR-522

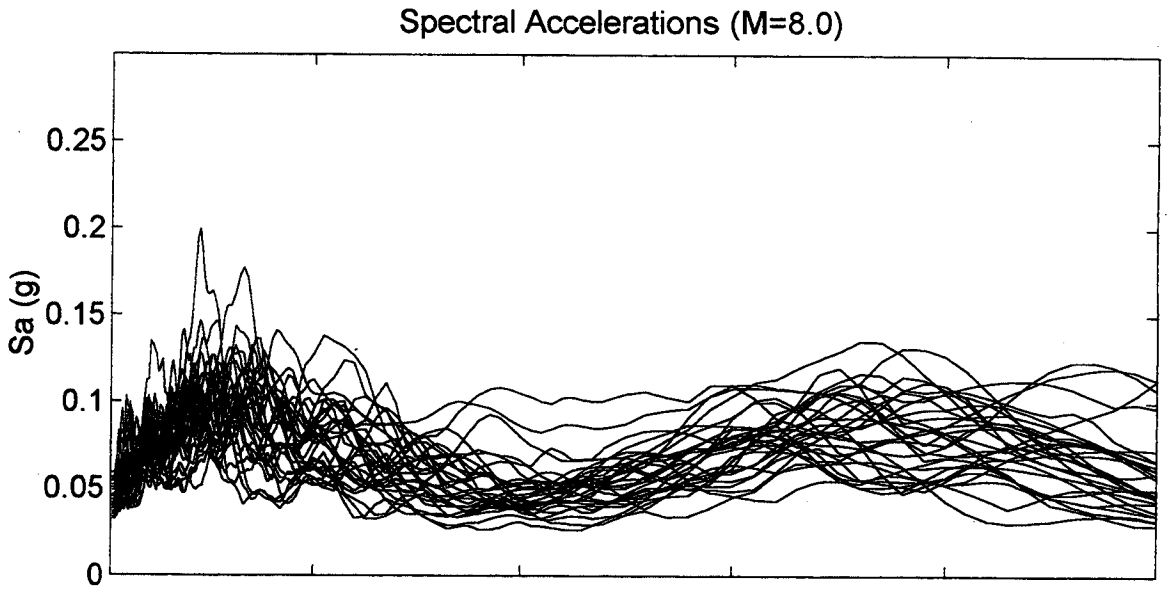
Spectral Accelerations (M=8.0)
Sa (g)
0.25
0.2
0.15
0.1
0.05
0

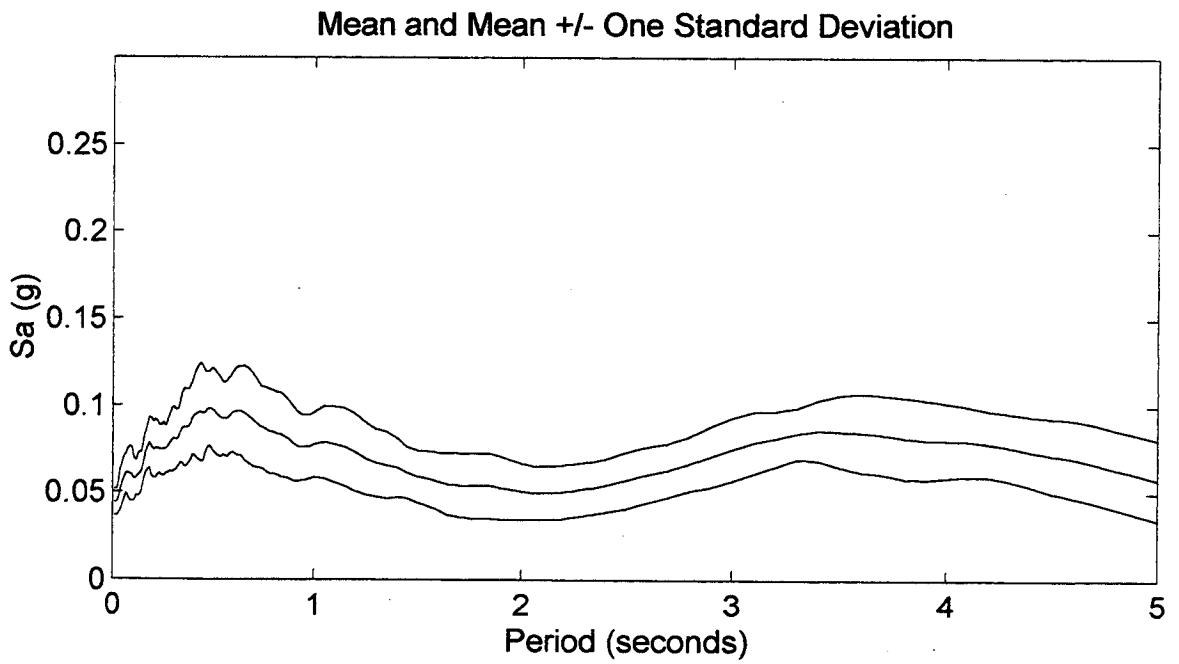
Mean and Mean +/- One Standard Deviation
Sa (g)
0.25
0.2
0.15
0.1
0.05
0
0
1
2
3
4
5
Period (seconds)

I-405/SR-522

Spectral Accelerations (M=8.5)

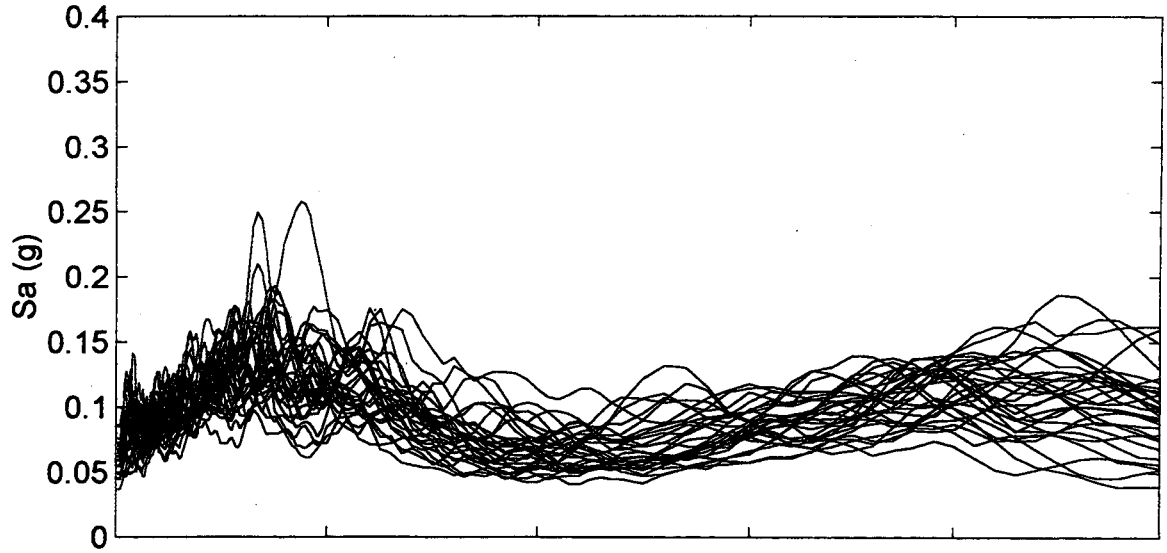

Mean and Mean +/- One Standard Deviation

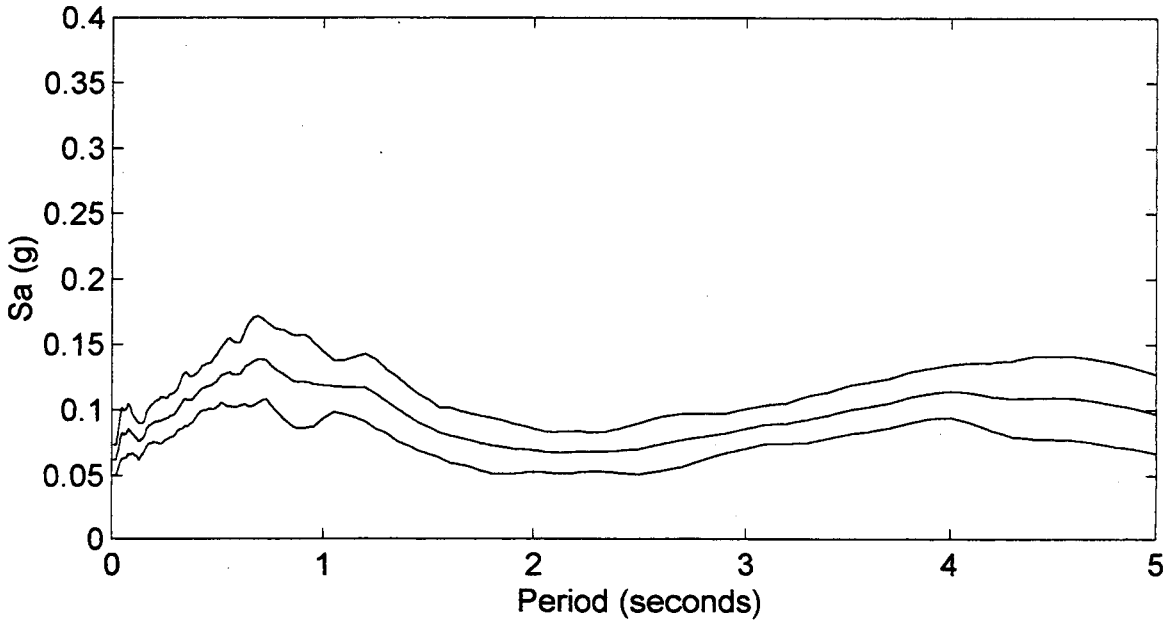

I-405/SR-522

Spectral Accelerations (M=9.0)

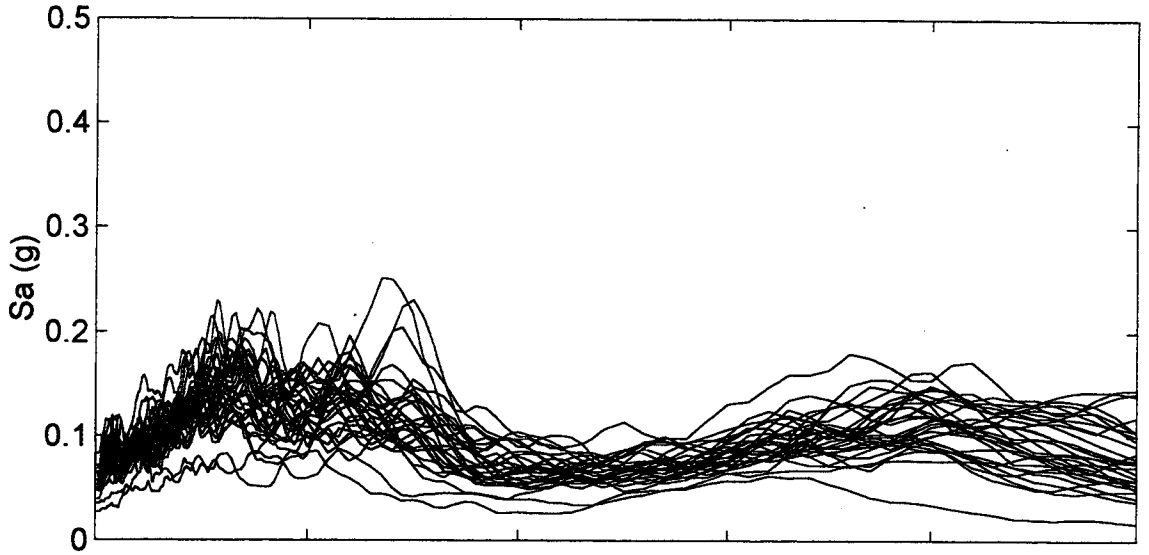

Mean and Mean +/- One Standard Deviation

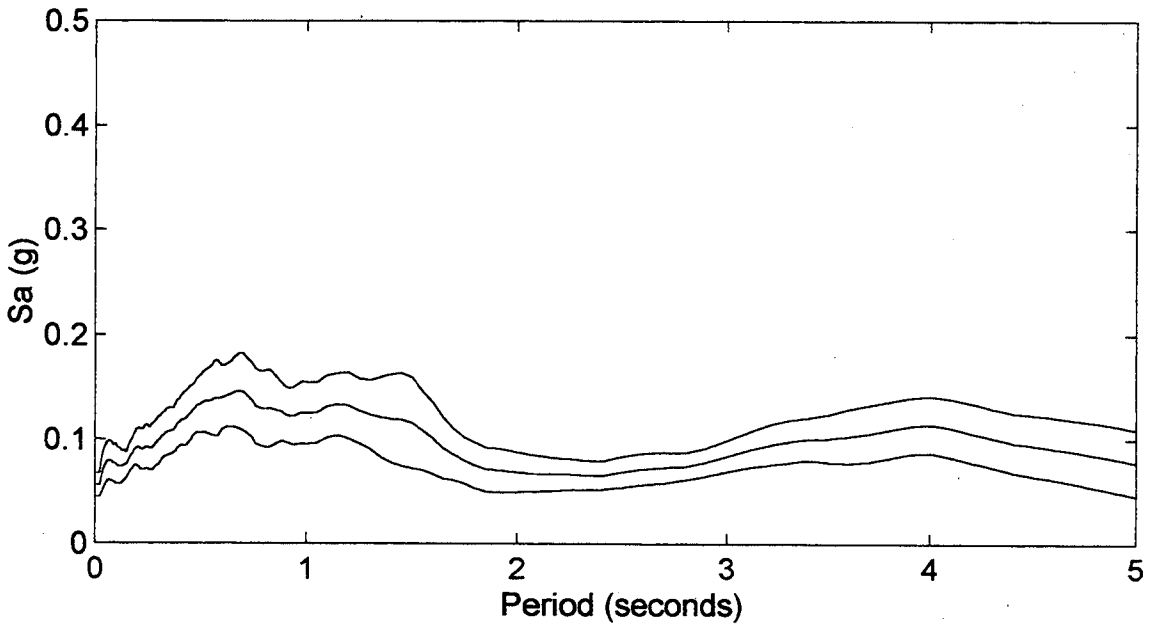

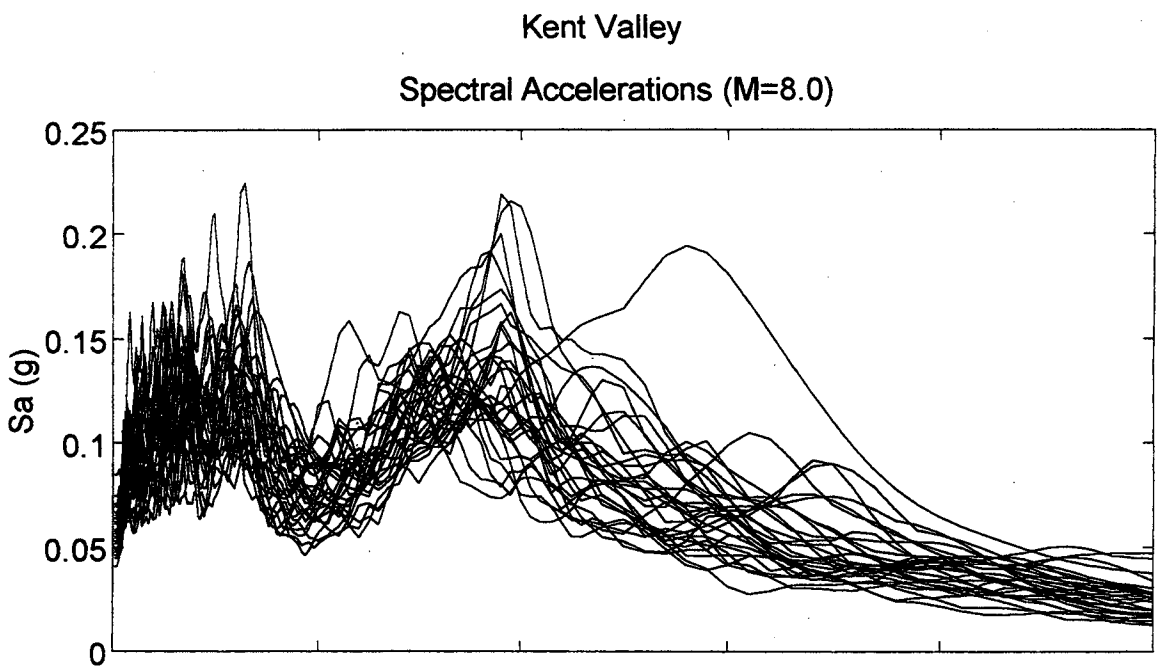
Kent Valley
Spectral Accelerations (M=8.0)
Sa (g)
0.25
0.2
0.15
0.1
0.05
0

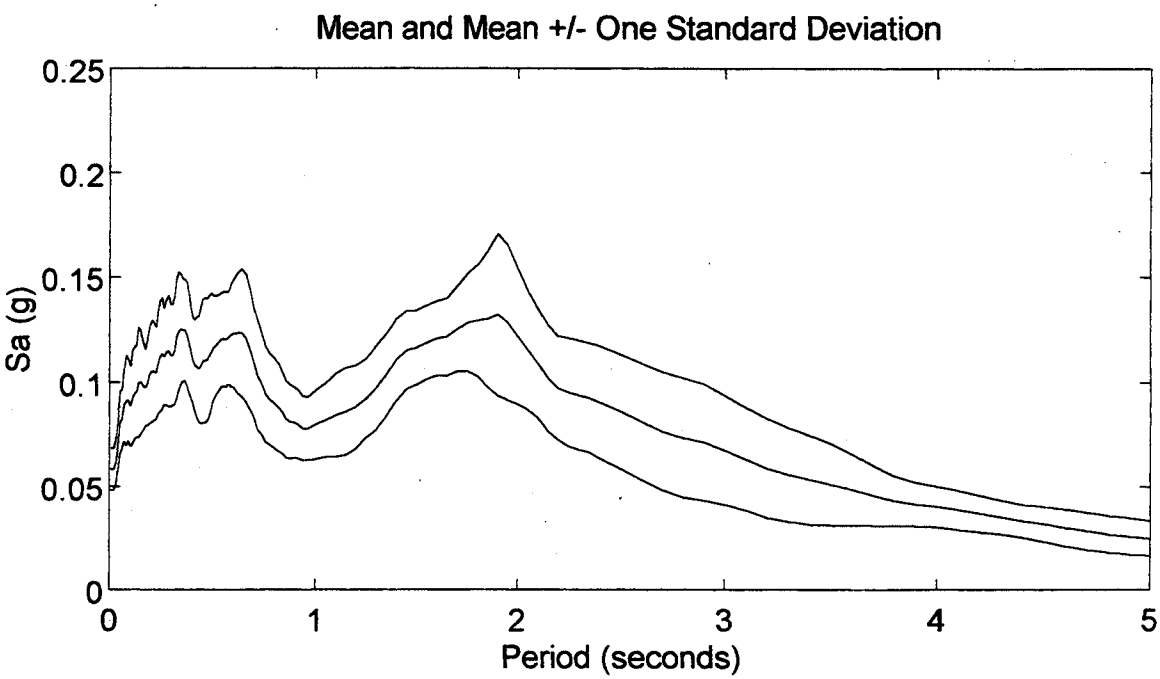
Mean and Mean +/- One Standard Deviation
Sa (g)
0.25
0.2
0.15
0.1
0.05
0
0
1
2
3
4
5
Period (seconds)

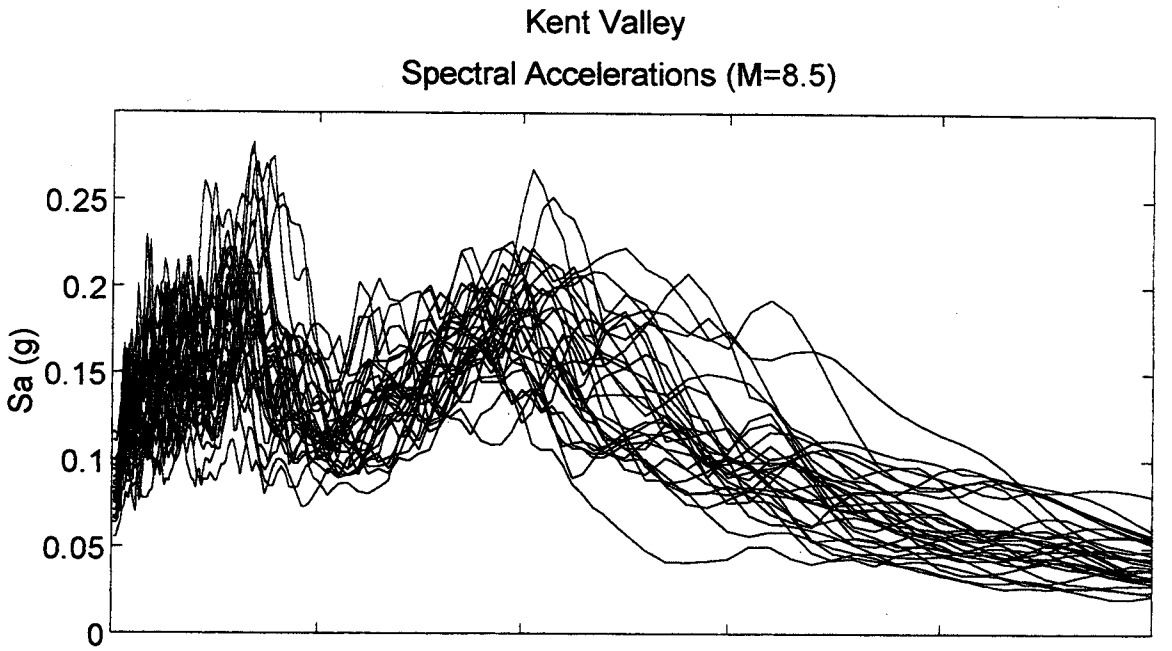
Kent Valley
Spectral Accelerations (M=8.5)
Sa (g)
0.25
0.2
0.15
0.1
0.05
0

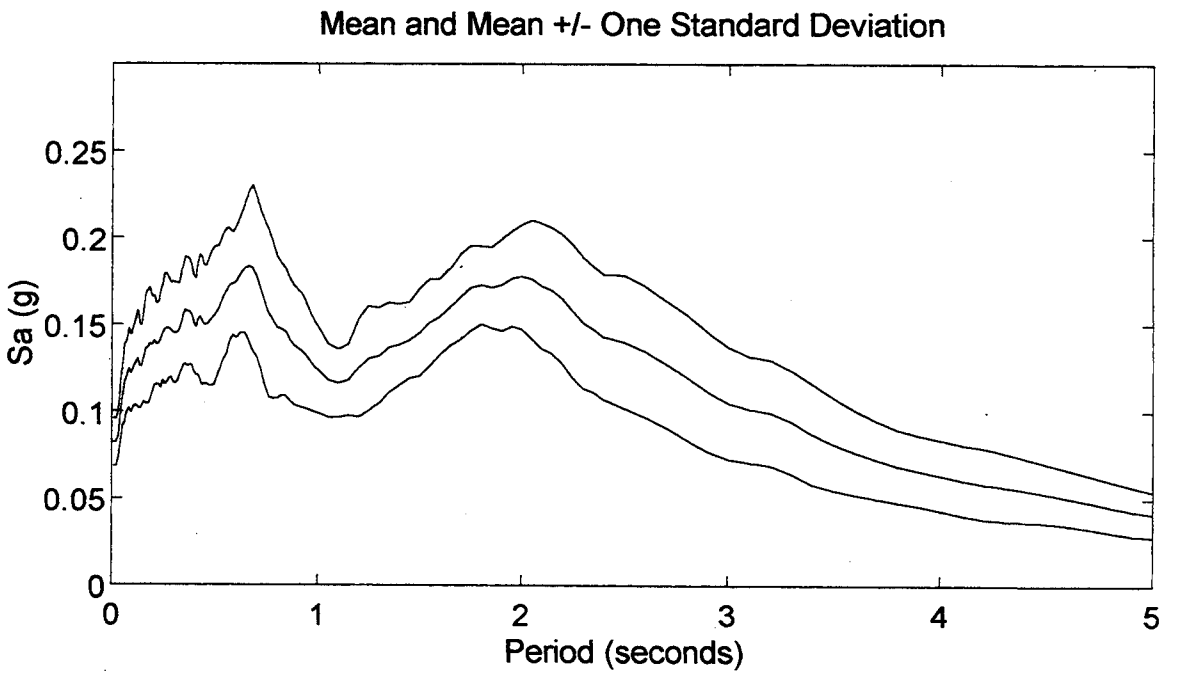
Mean and Mean +/- One Standard Deviation
Sa (g)
0.25
0.2
0.15
0.1
0.05
0
0
1
2
3
4
5
Period (seconds)

Kent Valley

Spectral Accelerations (M=9.0)

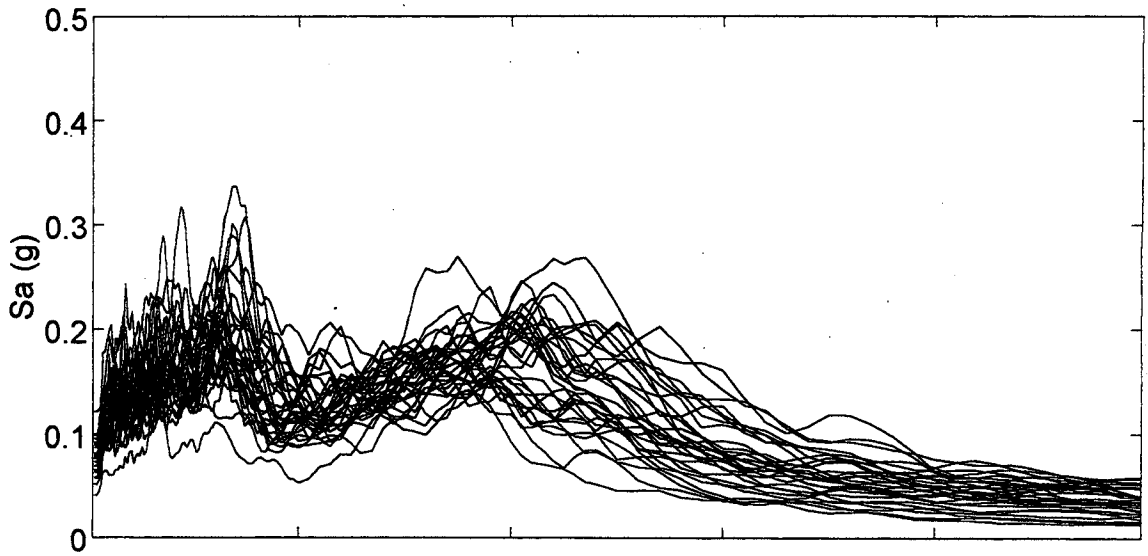

Mean and Mean +/- One Standard Deviation

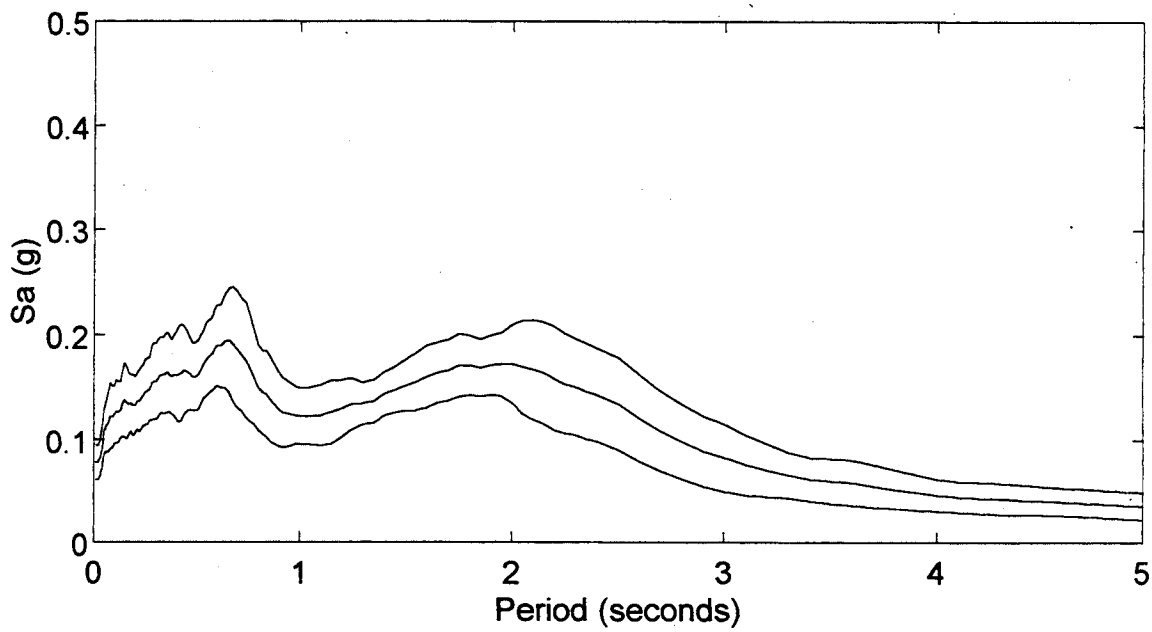

Mercer Slough 1

Spectral Accelerations (M=8.0)

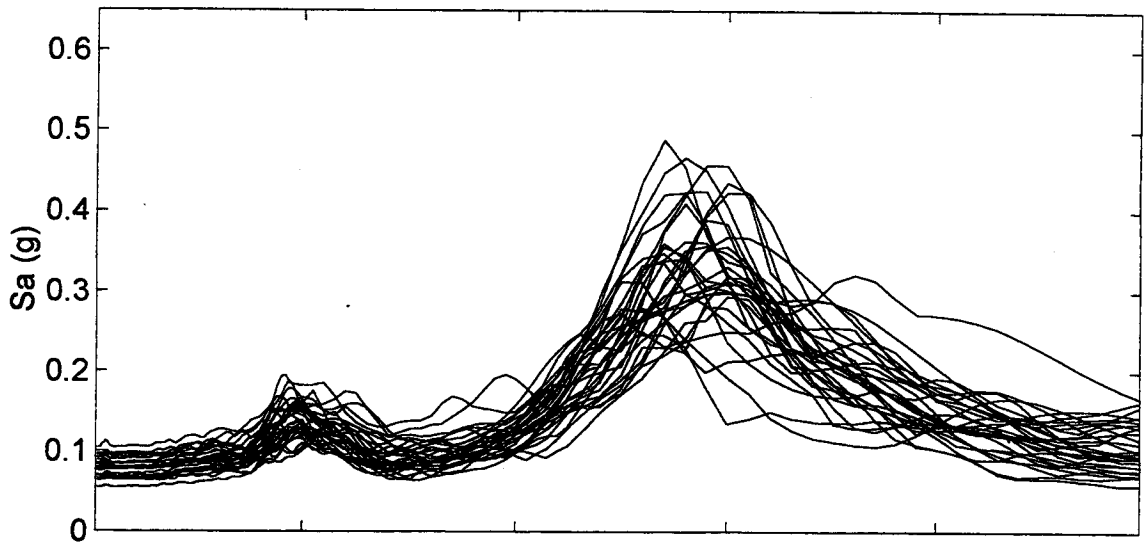

Mean and Mean +/- One Standard Deviation

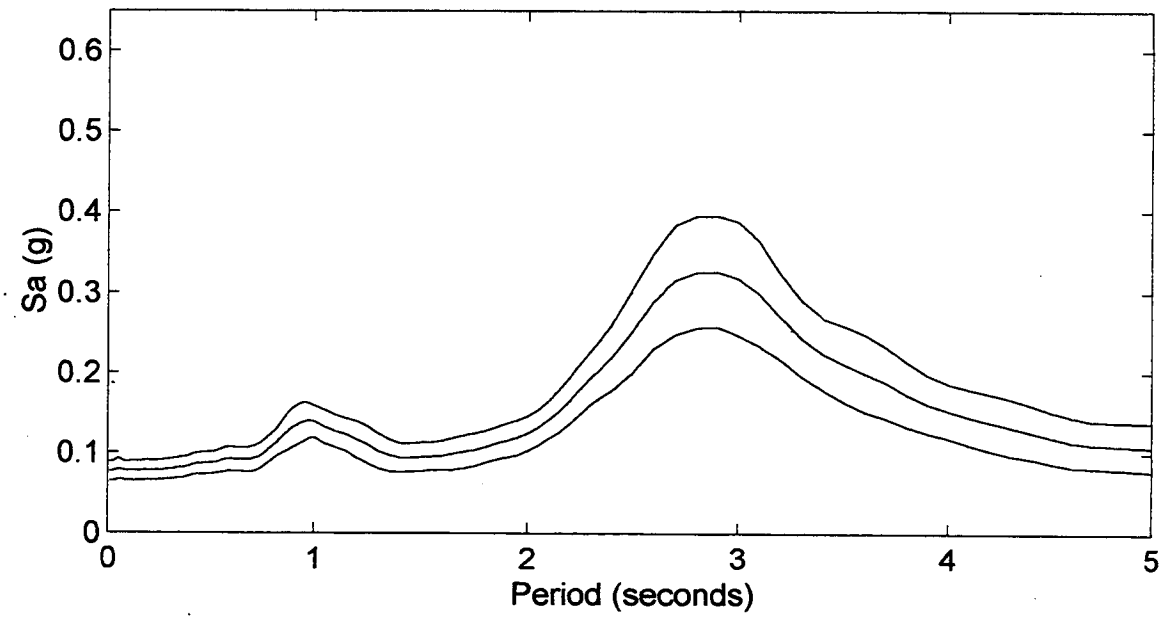

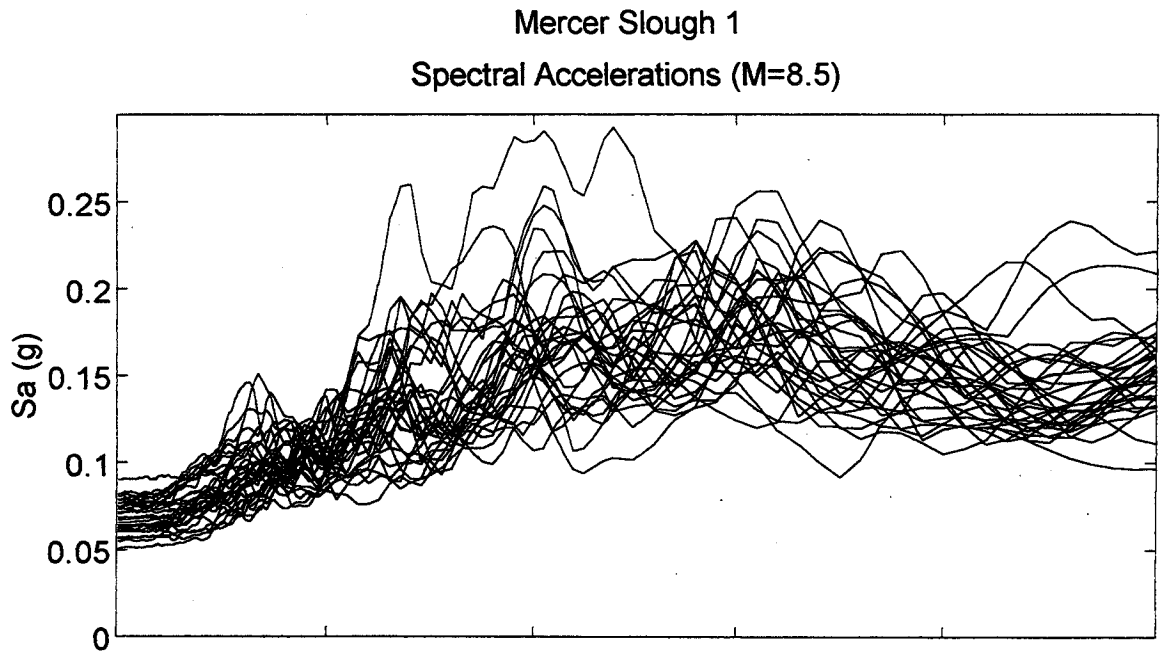
Mercer Slough 1
Spectral Accelerations (M=8.5)
Sa (g)
0.25
0.2
0.15
0.1
0.05
0

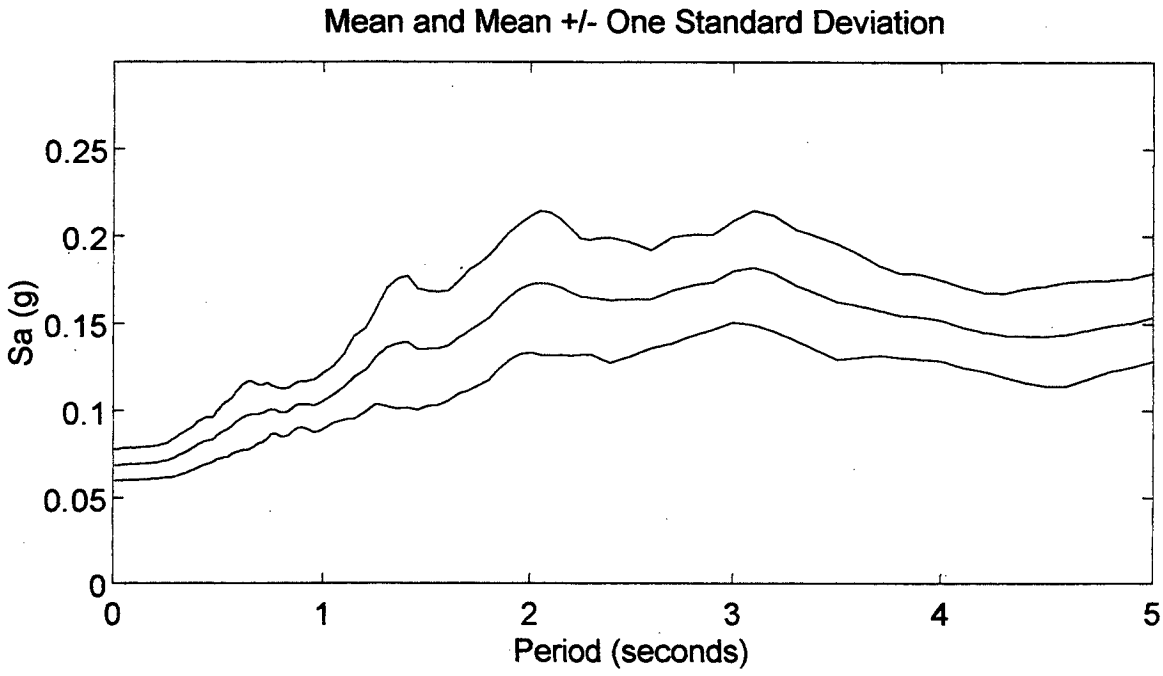
Mean and Mean +/- One Standard Deviation
Sa (g)
0.25
0.2
0.15
0.1
0.05
0
0
1
2
3
4
5
Period (seconds)

Mercer Slough 1

Spectral Accelerations (M=9.0)

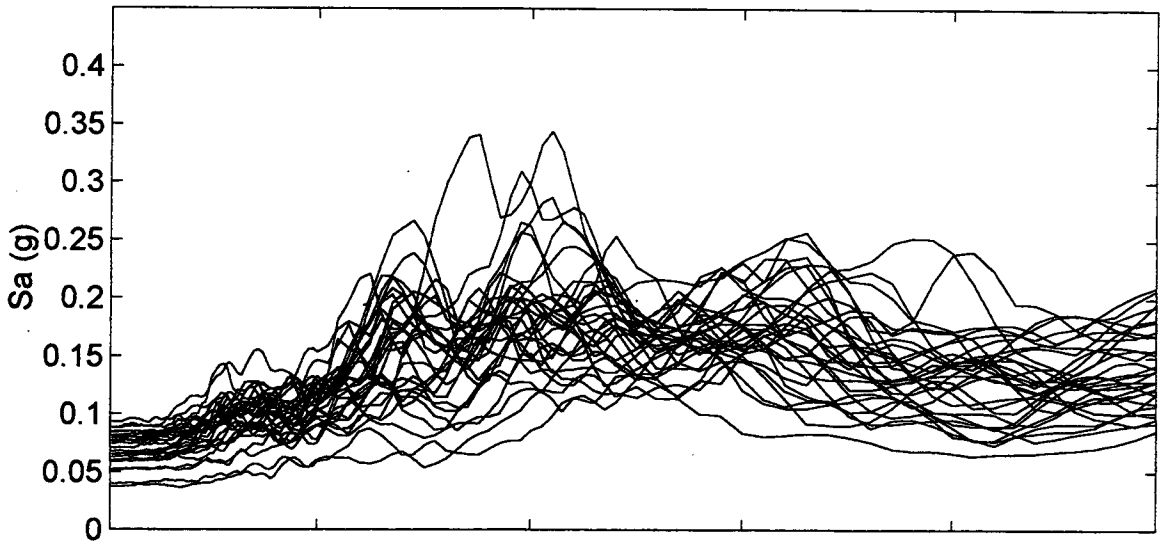

Mean and Mean +/- One Standard Deviation

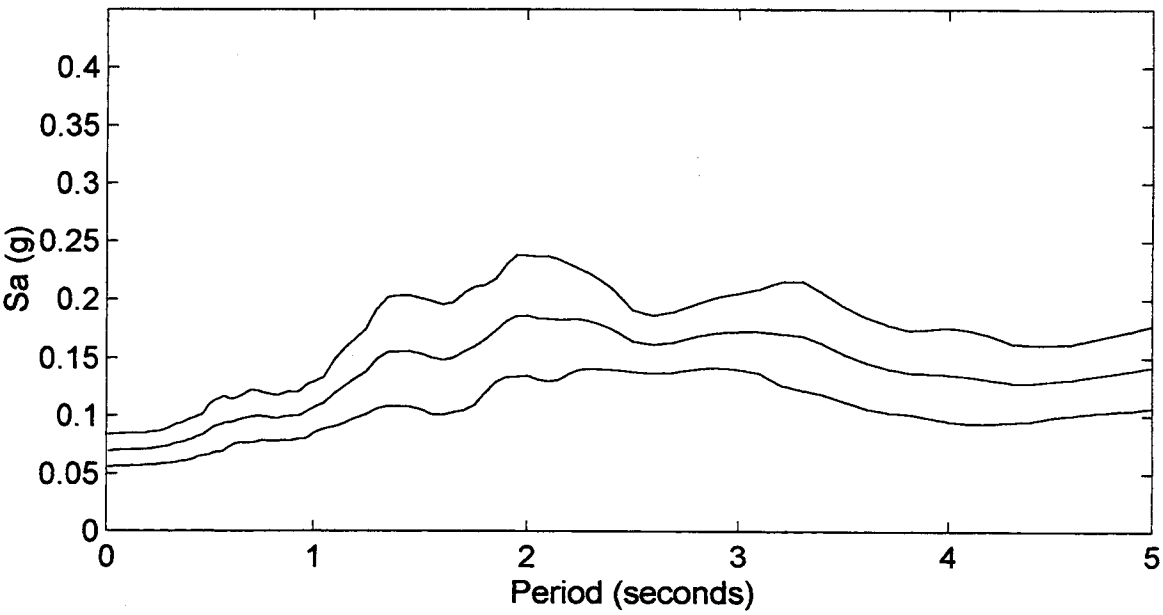

Mercer Slough 2

Spectral Accelerations (M=8.0)

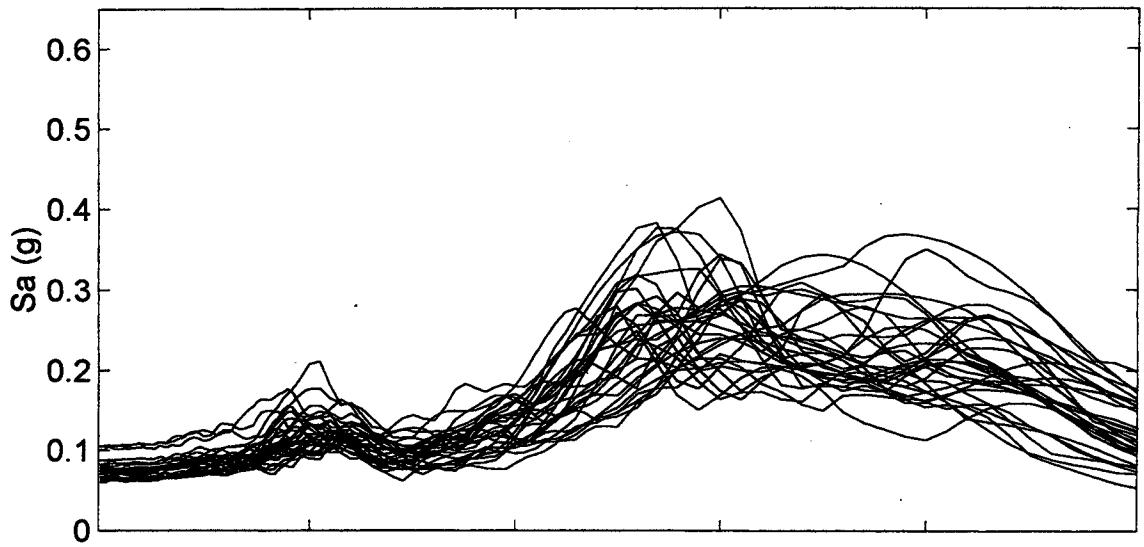

Mean and Mean +/- One Standard Deviation

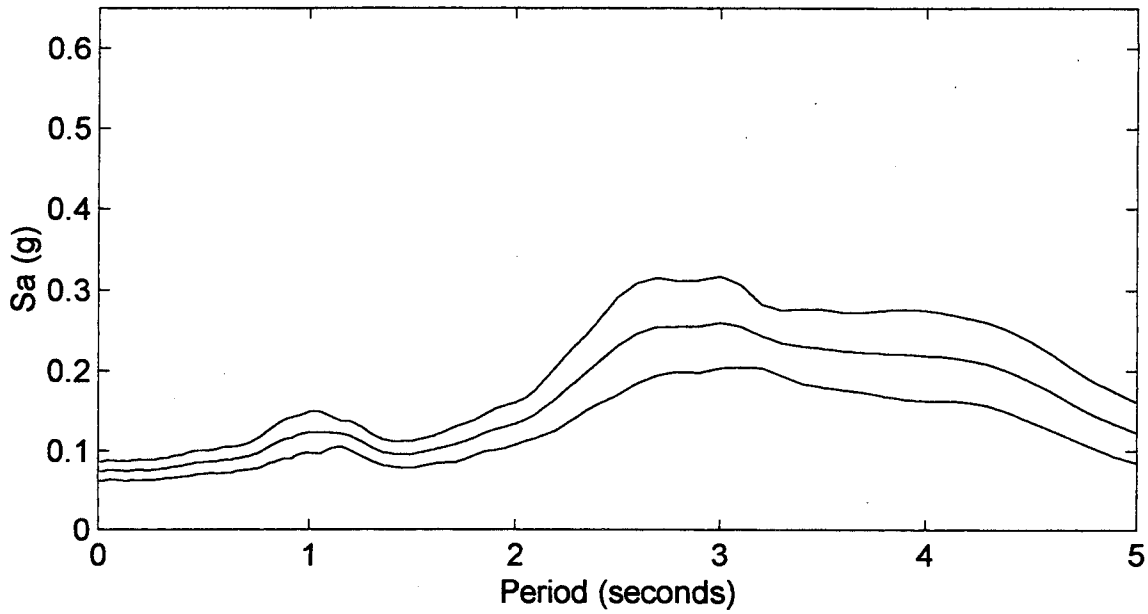

Mercer Slough 2

Spectral Accelerations (M=8.5)

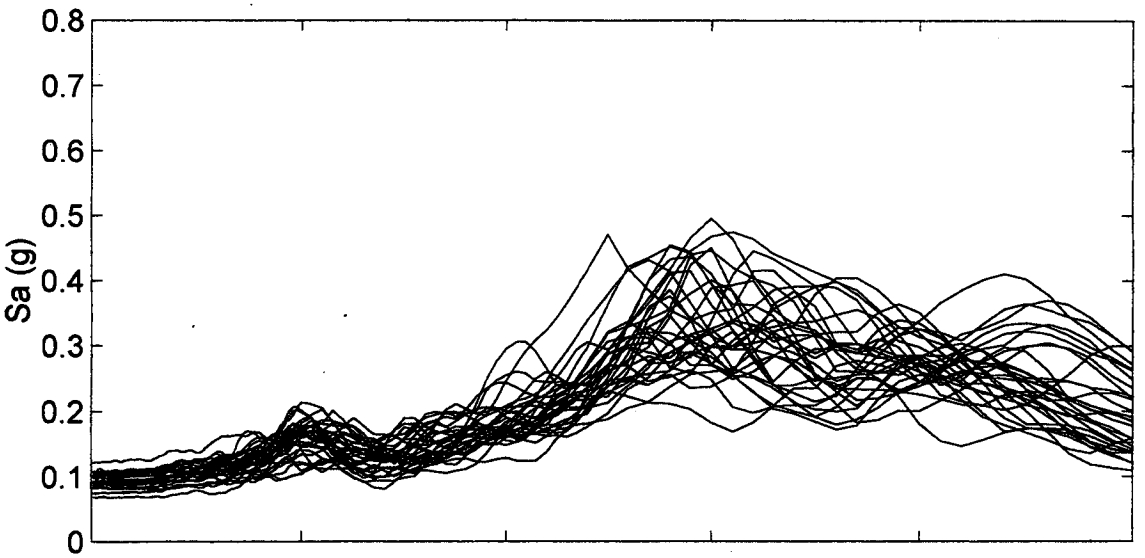

Mean and Mean +/- One Standard Deviation

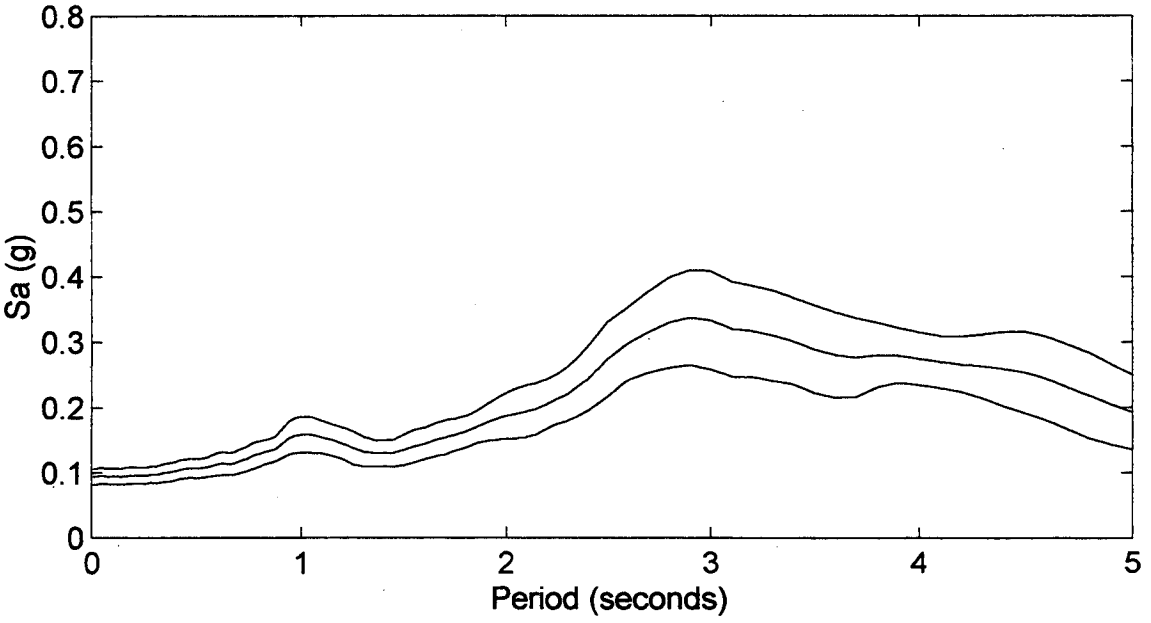

Mercer Slough 2

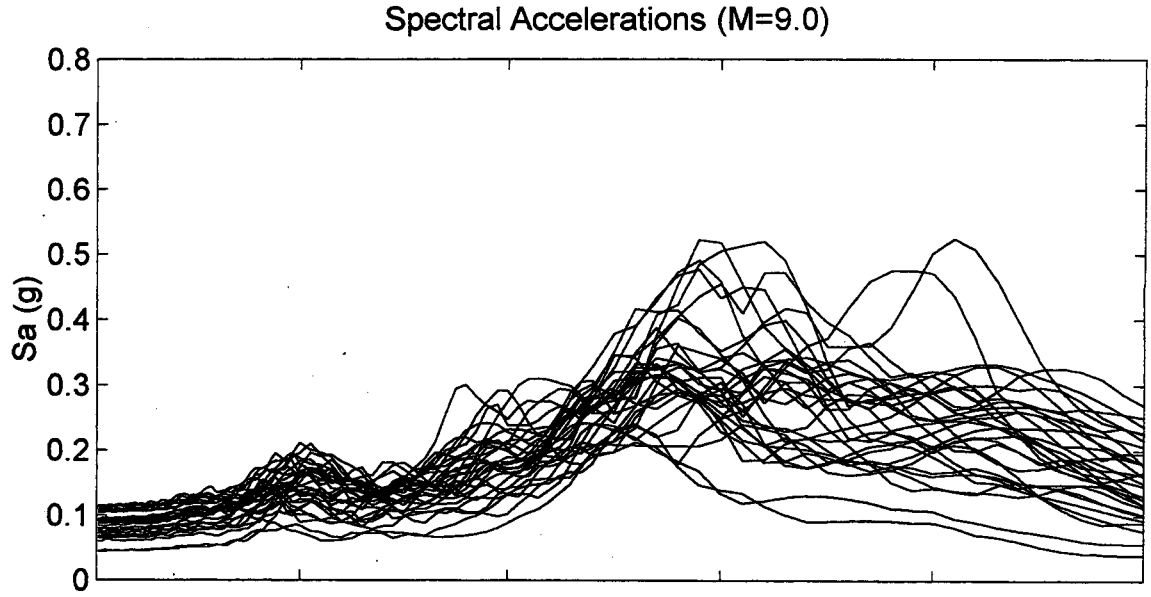

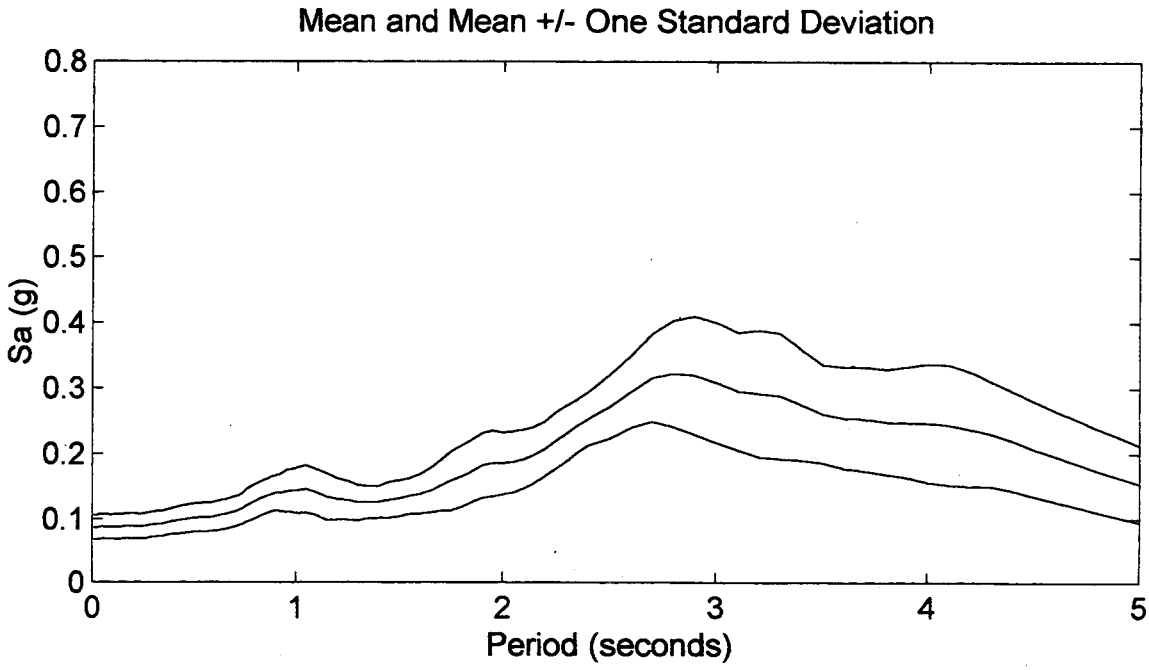

Nooksack River

Spectral Accelerations (M=8.0)

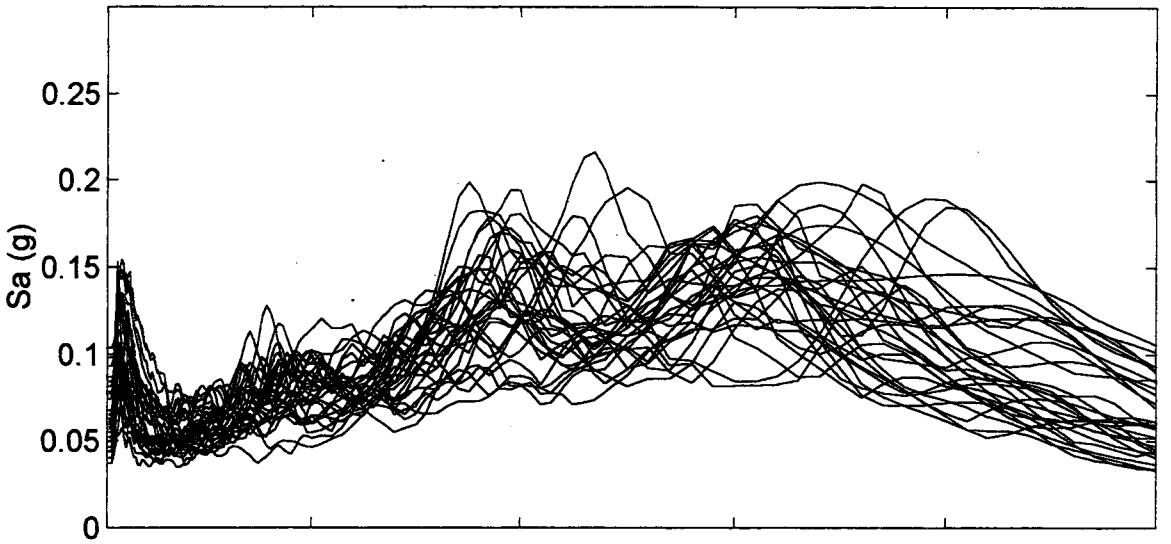

Mean and Mean +/- One Standard Deviation

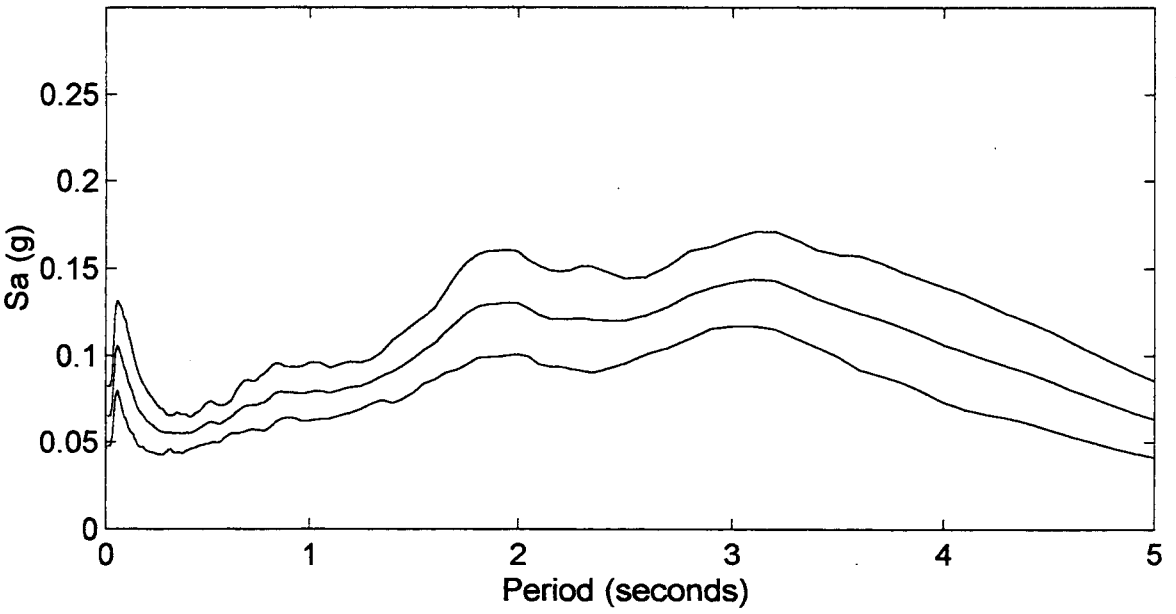

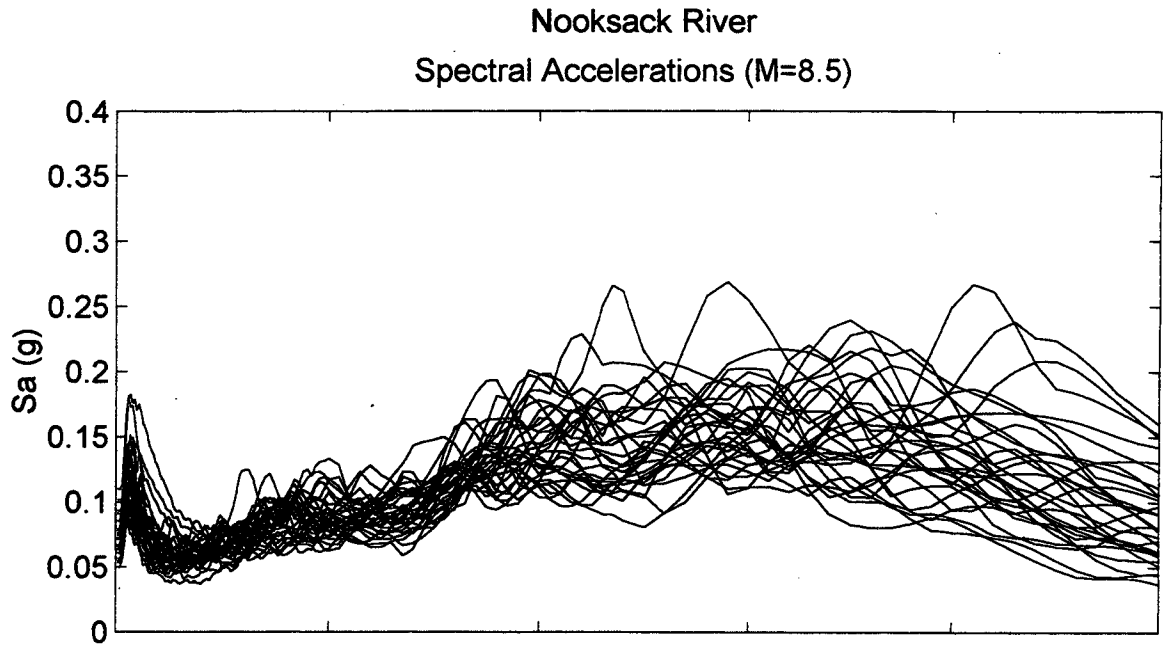
Nooksack River
Spectral Accelerations (M=8.5)
Sa (g)
0.4
0.35
0.3
0.25
0.2
0.15
0.1
0.05
0

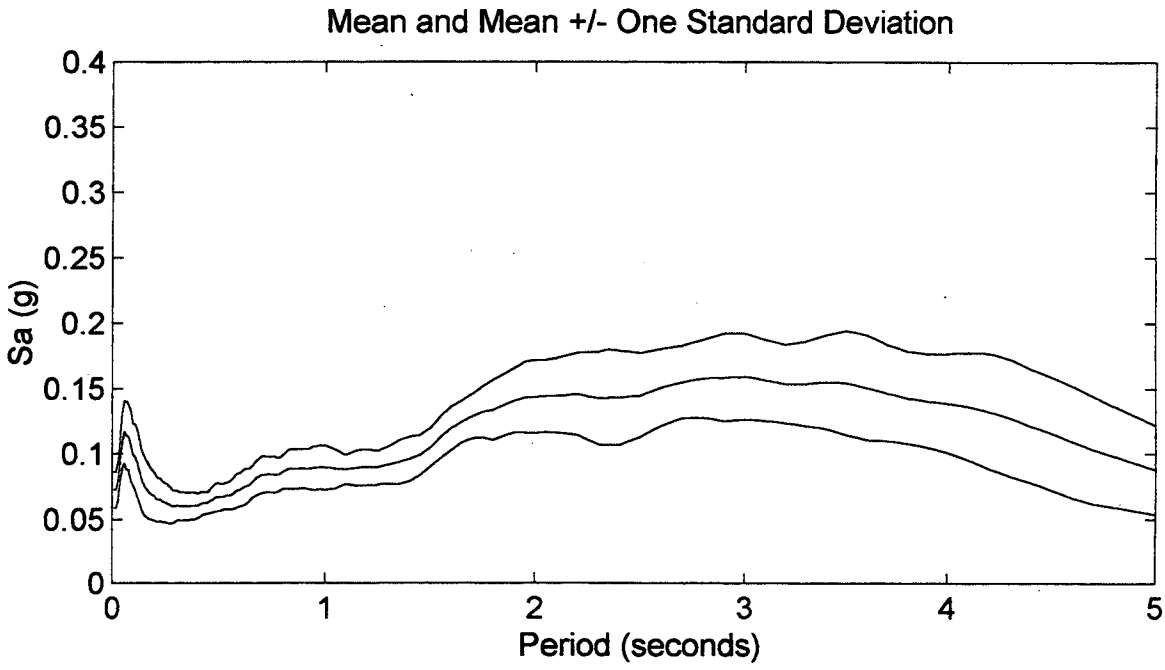
Mean and Mean +/- One Standard Deviation
Sa (g)
0.4
0.35
0.3
0.25
0.2
0.15
0.1
0.05
0
0
1
2
3
4
5
Period (seconds)

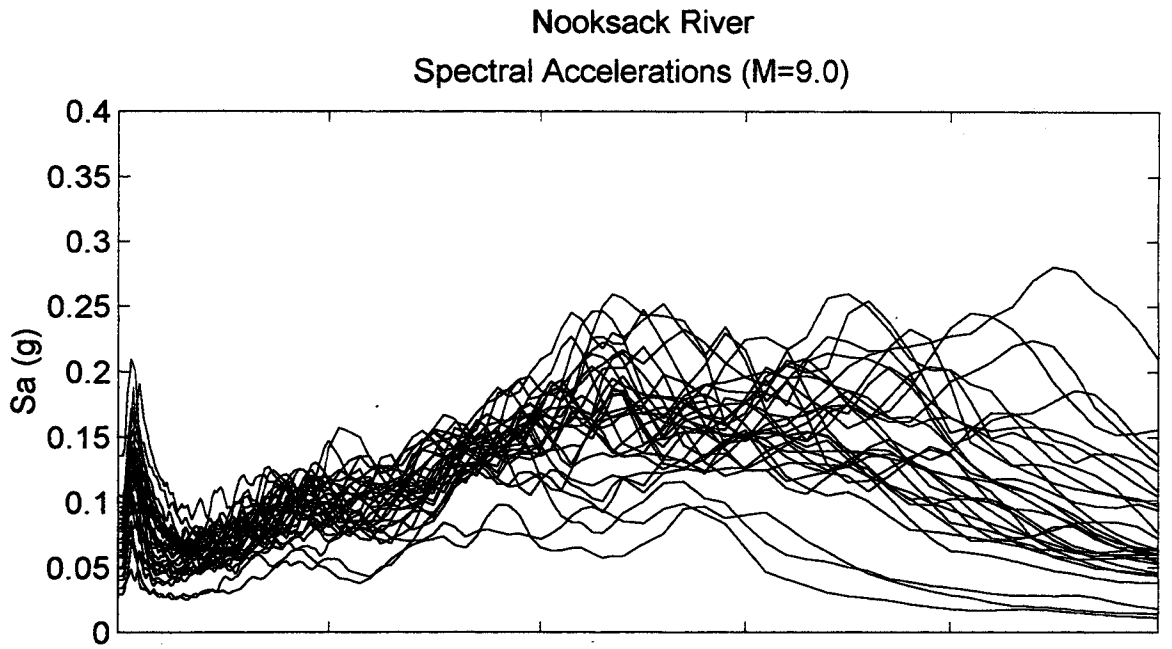
Nooksack River
Spectral Accelerations (M=9.0)
Sa (g)
0.4
0.35
0.3
0.25
0.2
0.15
0.1
0.05
0

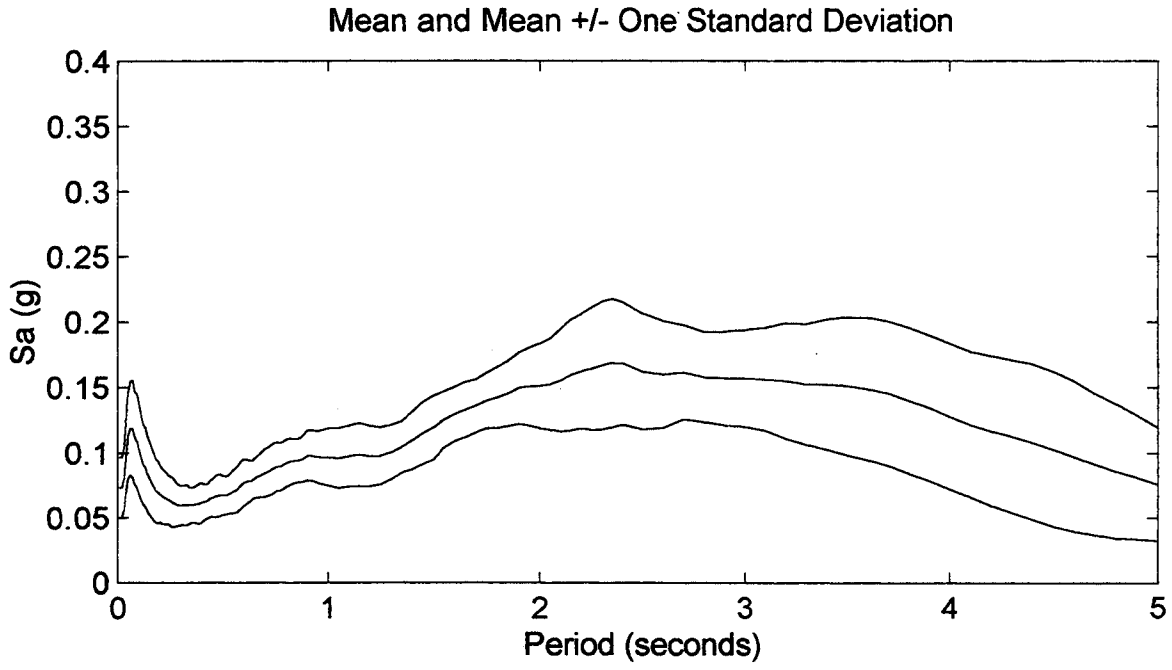
Mean and Mean +/- One Standard Deviation
Sa (g)
0.4
0.35
0.3
0.25
0.2
0.15
0.1
0.05
0
0
1
2
3
4
5
Period (seconds)

North Ferndale

Spectral Accelerations (M=8.0)

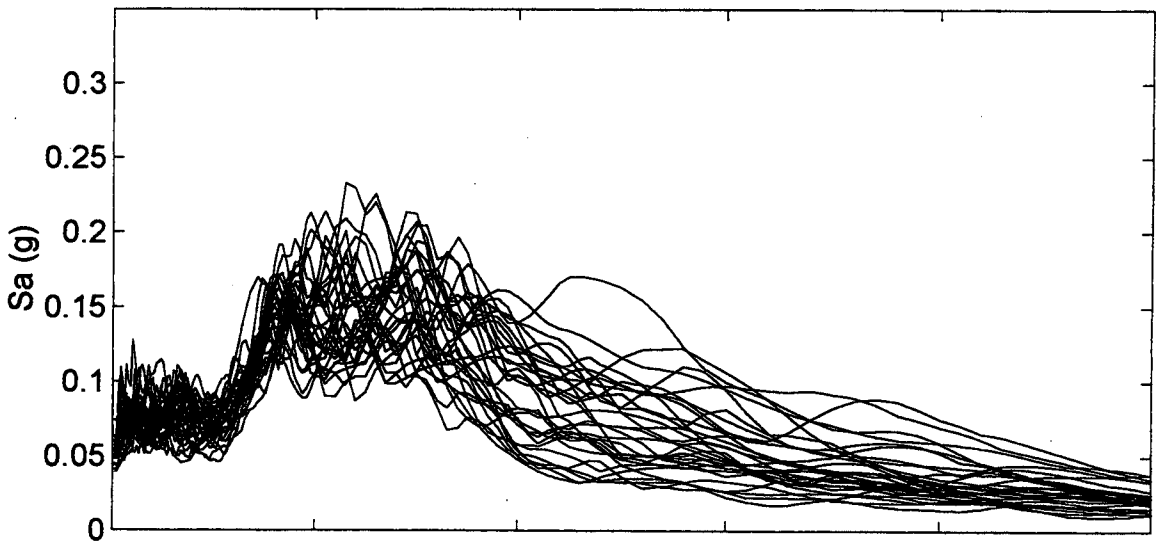

Mean and Mean +/- One Standard Deviation

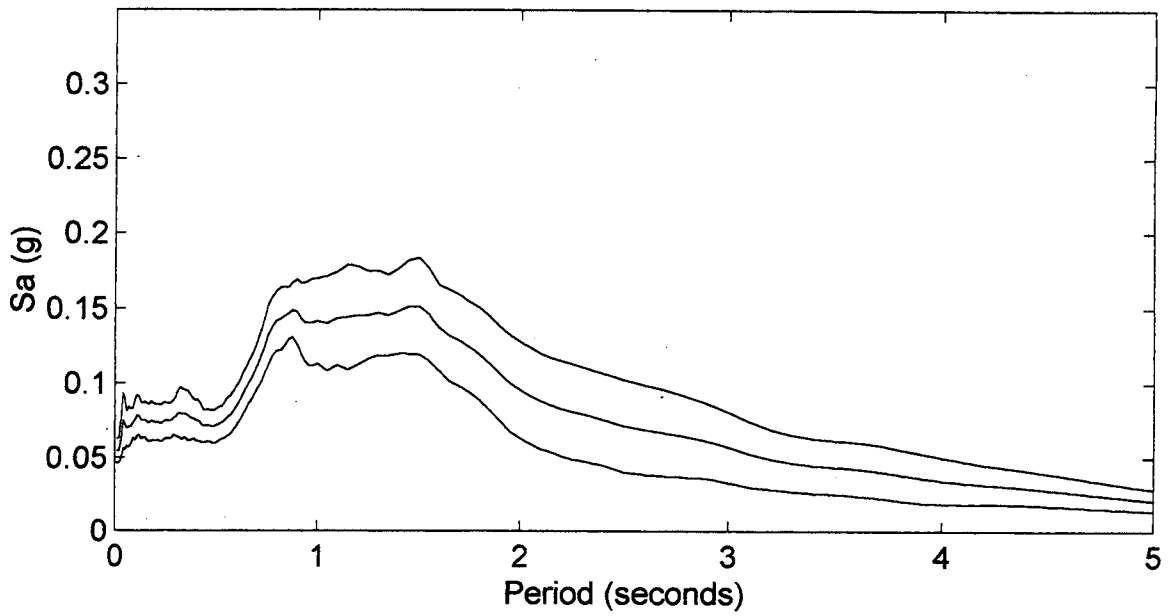

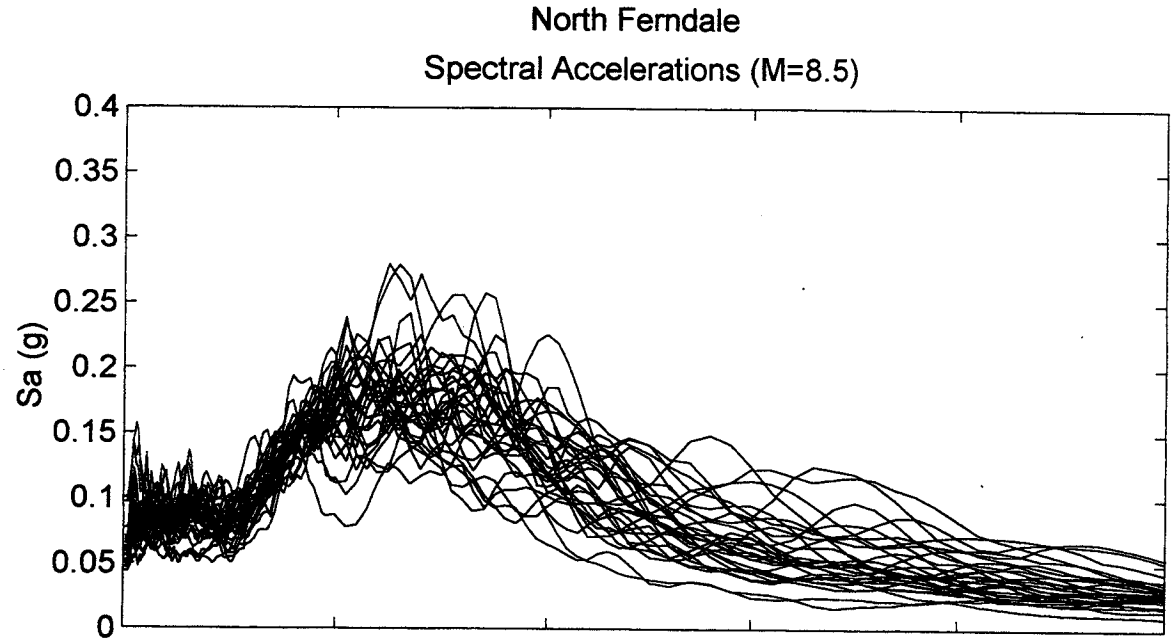
North Ferndale
Spectral Accelerations (M=8.5)
Sa (g)
0.4
0.35
0.3
0.25
0.2
0.15
0.1
0.05
0

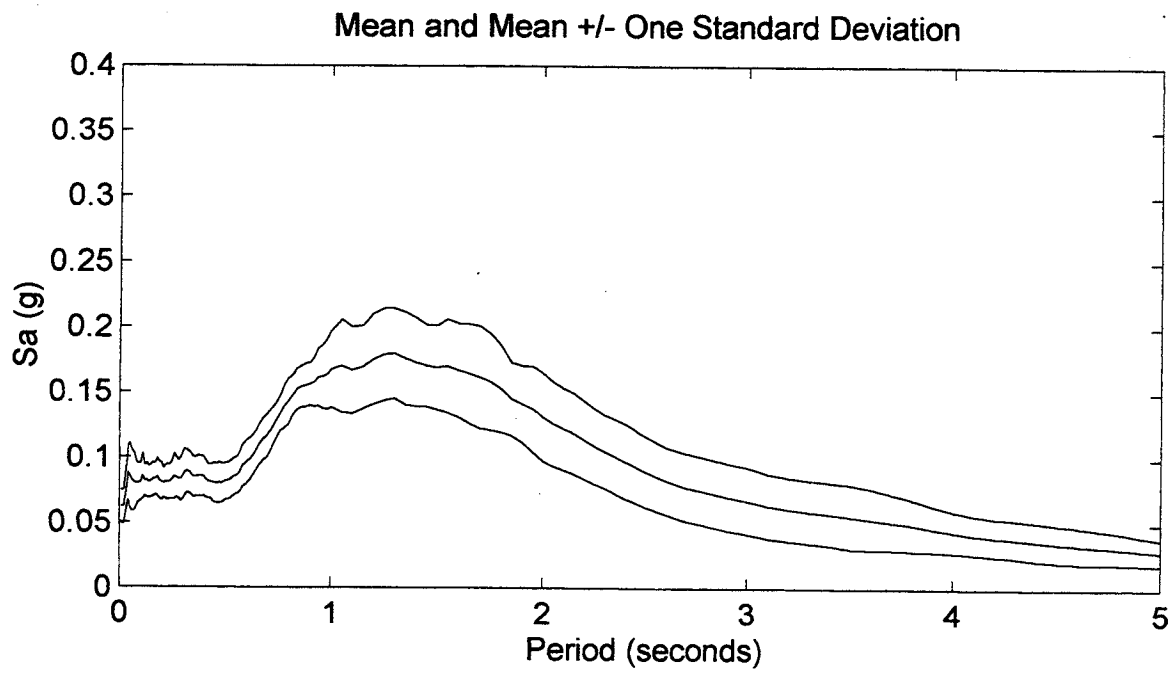
Mean and Mean +/- One Standard Deviation
Sa (g)
0.4
0.35
0.3
0.25
0.2
0.15
0.1
0.05
0
0
1
2
3
4
5
Period (seconds)

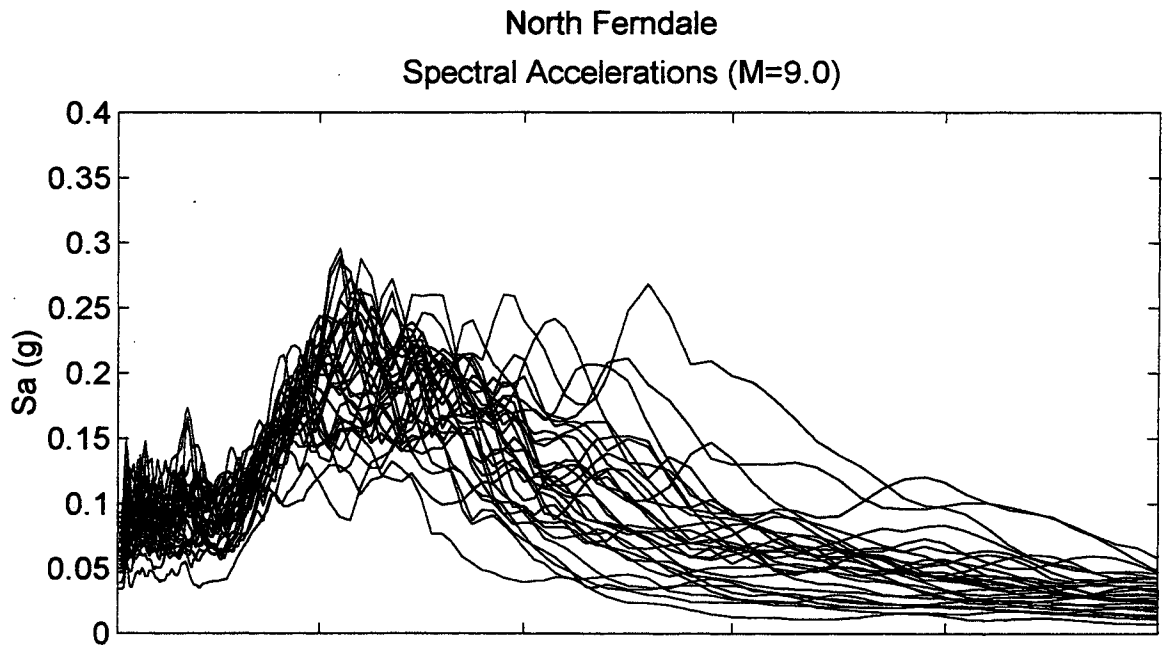
North Ferndale
Spectral Accelerations (M=9.0)
Sa (g)
0.4
0.35
0.3
0.25
0.2
0.15
0.1
0.05
0

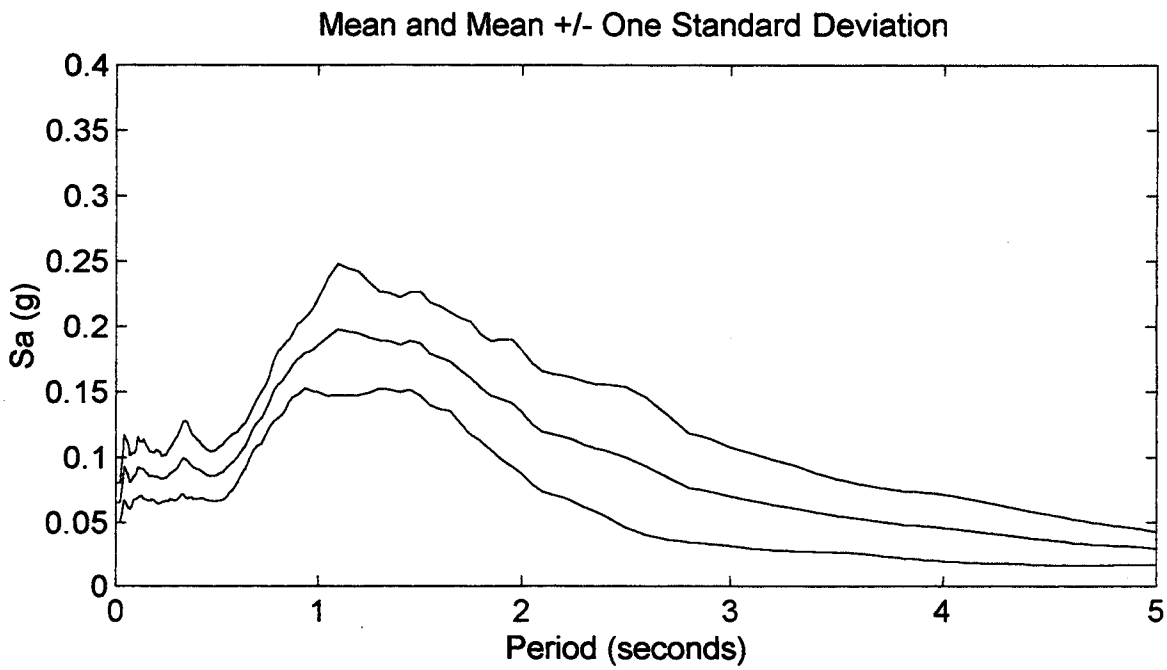
Mean and Mean +/- One Standard Deviation
Sa (g)
0.4
0.35
0.3
0.25
0.2
0.15
0.1
0.05
0
0
1
2
3
4
5
Period (seconds)

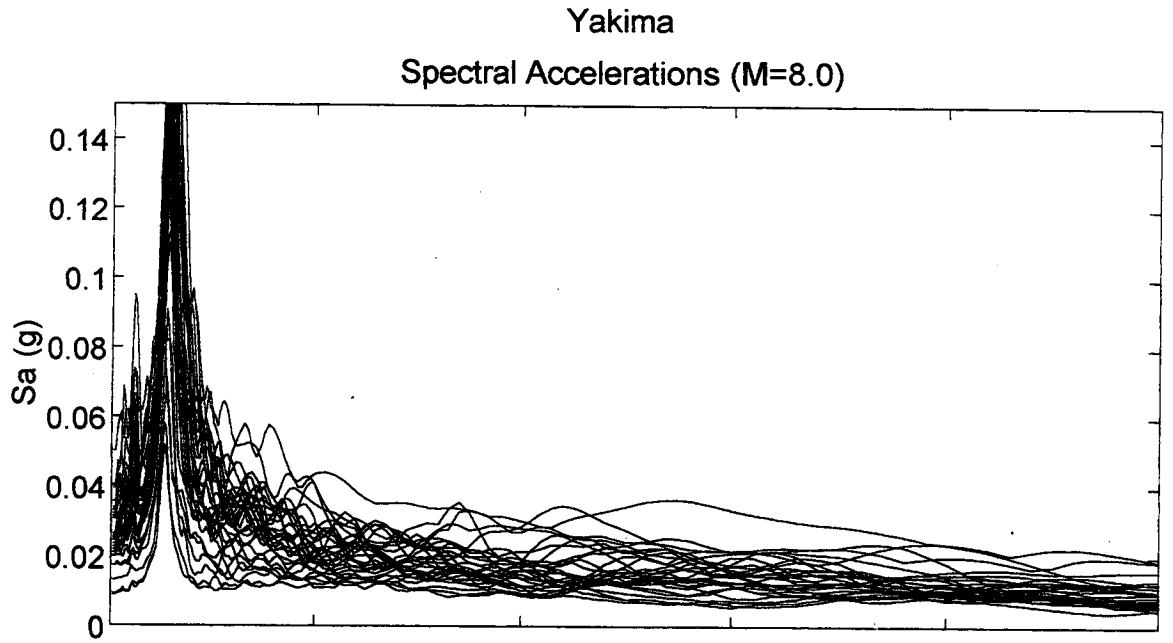
Yakima
Spectral Accelerations (M=8.0)
Sa (g)
0.14
0.12
0.1
0.08
0.06
0.04
0.02
0

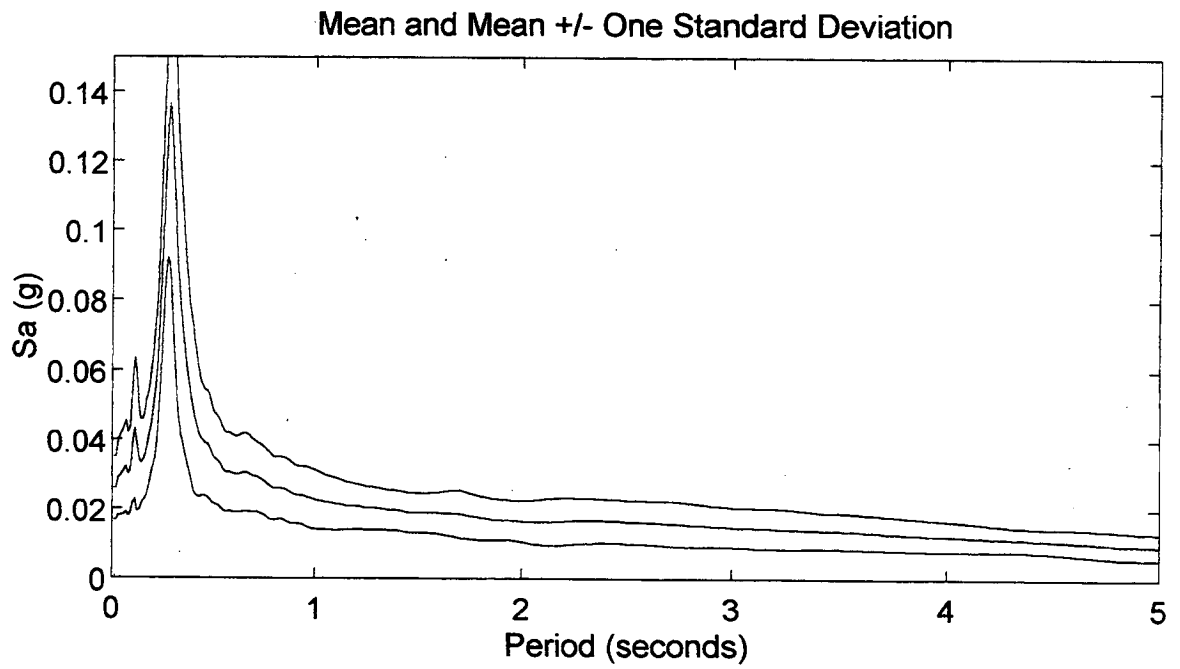
Mean and Mean +/- One Standard Deviation
Sa (g)
0.14
0.12
0.1
0.08
0.06
0.04
0.02
0
0
1
2
3
4
5
Period (seconds)

Yakima

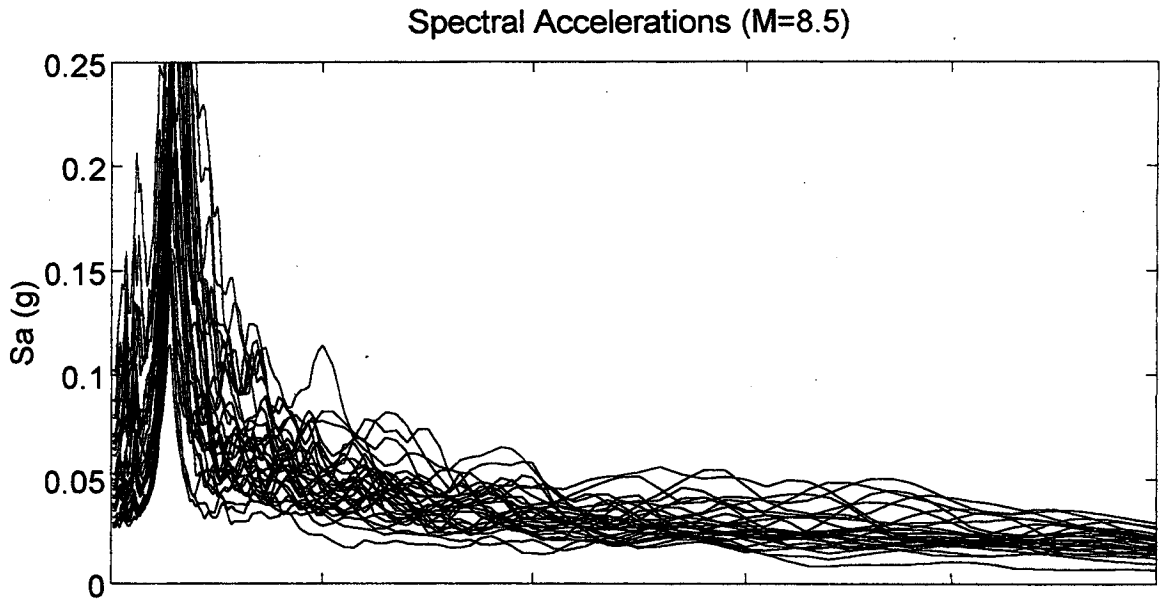
Spectral Accelerations (M=8.5)
Sa (g)
0.25
0.2
0.15
0.1
0.05
0

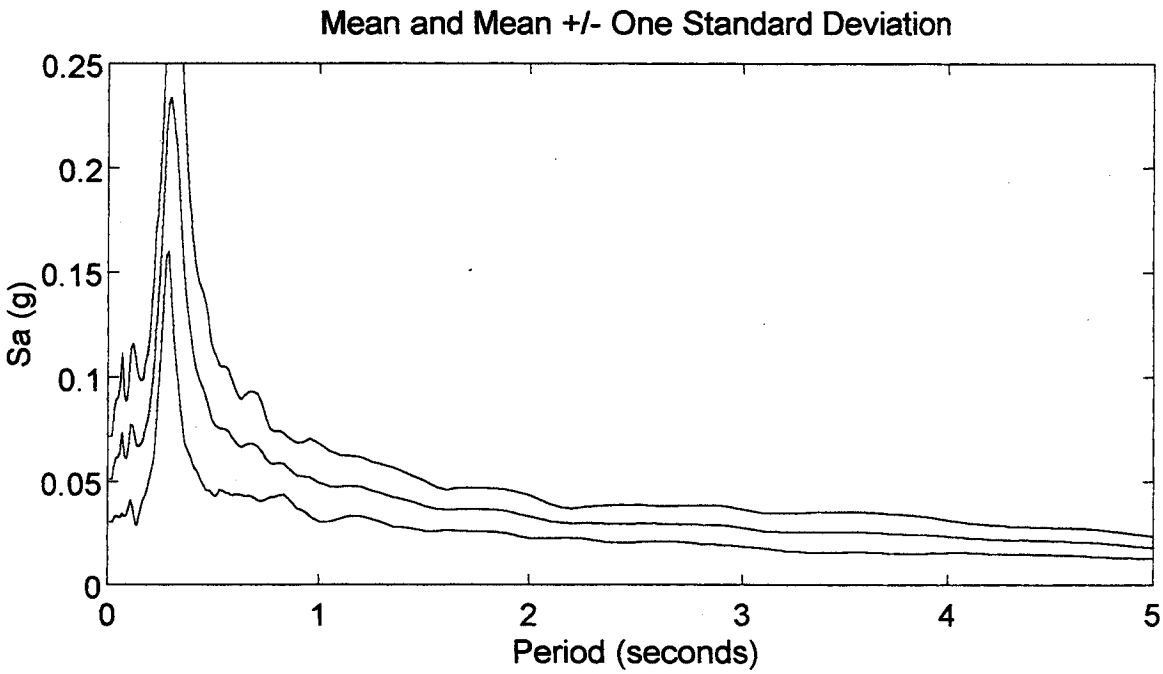
Mean and Mean +/- One Standard Deviation
Sa (g)
0.25
0.2
0.15
0.1
0.05
0
0
1
2
3
4
5
Period (seconds)

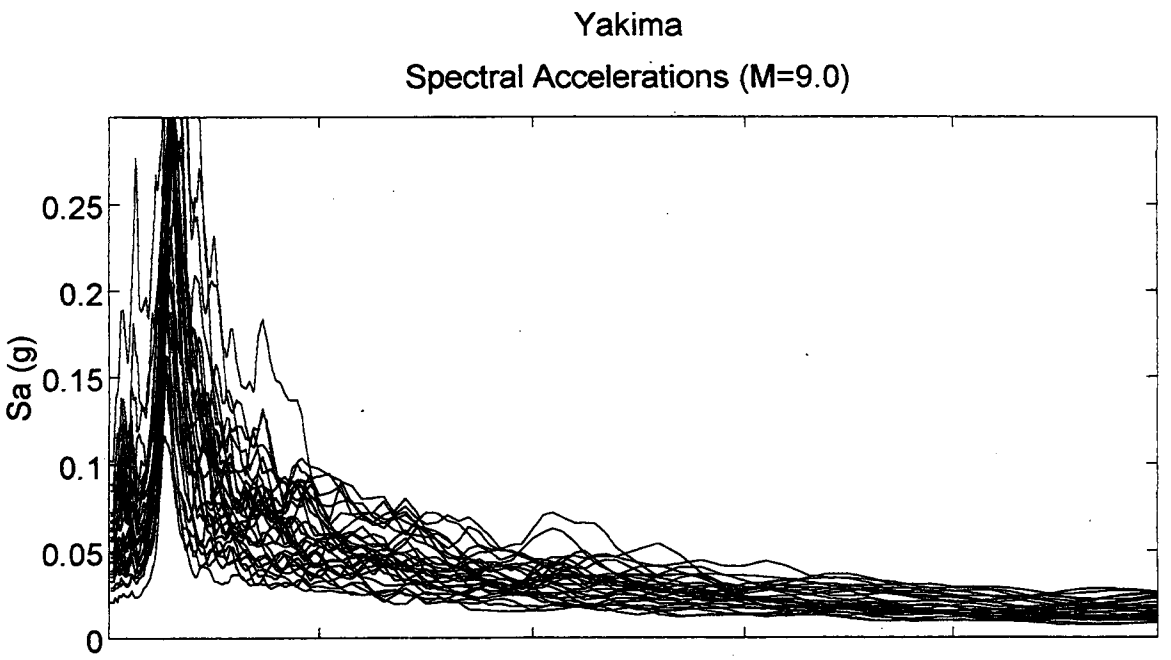
Yakima
Spectral Accelerations (M=9.0)
Sa (g)
0.25
0.2
0.15
0.1
0.05
0

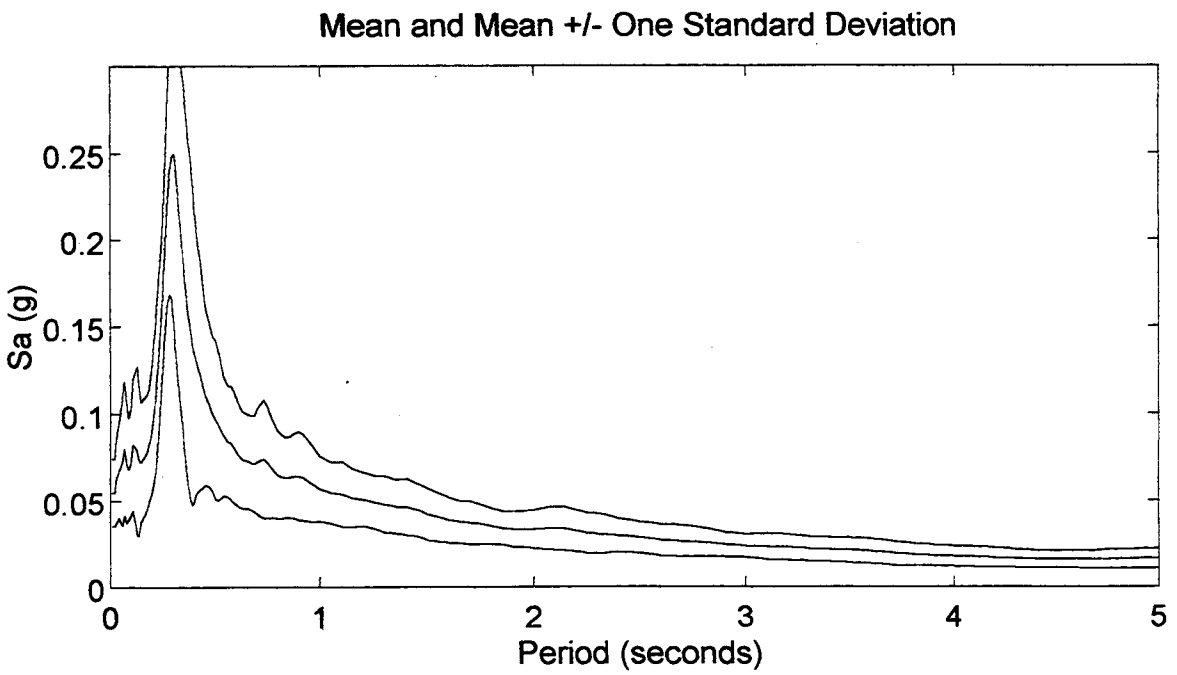
Mean and Mean +/- One Standard Deviation
Sa (g)
0.25
0.2
0.15
0.1
0.05
0
0
1
2
3
4
5
Period (seconds)